UNIVERSITY OF HAWAII LIBRARY

ADVANCES IN PHYSICS

A QUARTERLY SUPPLEMENT
of the
PHILOSOPHICAL MAGAZINE

EDITOR
PROFESSOR B. H. FLOWERS, M.A., D.Sc.

CONSULTANT EDITOR
PROFESSOR N. F. MOTT, M.A., D.Sc., F.R.S.

EDITORIAL BOARD
SIR LAWRENCE BRAGG, O.B.E., M.C., M.A., D.Sc., F.R.S.
SIR GEORGE THOMSON, M.A., D.Sc., F.R.S.
PROFESSOR A. M. TYNDALL, C.B.E., D.Sc., F.R.S.

VOLUME 9 JANUARY 1960 NUMBER 33

PRICE per part **20***s.*
PRICE per annum **£3 15***s.* **0***d.* post free

PRINTED AND PUBLISHED BY TAYLOR & FRANCIS LTD
RED LION COURT, FLEET ST., LONDON E.C.4

QC1
A36

FOR USERS OF CALCULATORS

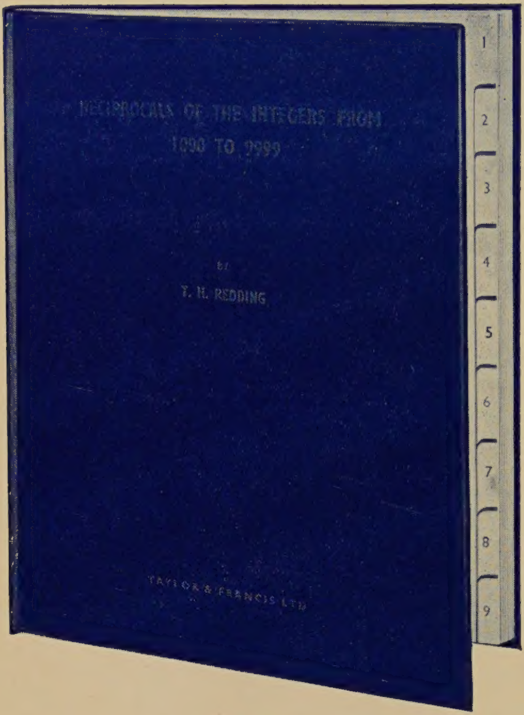

RECIPROCALS OF THE INTEGERS FROM 1000 TO 9999

By T. H. Redding
M.Sc.(Lond.), A.M.I.Mech.E., A.F.R.Ae.S.

Arranged for use with mechanical calculating machines to facilitate the evaluation of quotients and compound fractions

With an Appendix on mechanical barrel-setting calculators

These tables list the 10^6 multiples of the reciprocals of the integers 1000 to 9999 and are displayed as 1000 entries on each of nine double-page spreads which are thumb-indexed (1000 . . . , 2000 . . . , 3000 . . . , . . . etc) to facilitate rapid manipulation with one hand only. The entries are direct reading and are correct to the nearest integer in the third place of decimals.

Although suitable for general use, the tables have been prepared and arranged in a manner particularly suitable for use in conjunction with mechanical computing machines of the " barrel-setting " type in the evaluation of quotients and compound fractions. Equally the tables find application in effecting the evaluation of quotients on adding and listing machines when these incorporate a mechanism for automatically evaluating simple products.

In the first instance it was anticipated that an Appendix dealing with the advantages to be gained by the use of the reciprocal function in conjunction with such machines—and particularly with barrel-setting machines—would suffice to ensure the best use being made of the tables. The present 22-page *Appendix*, however, goes further than this, since the discussion of the tables is prefaced by a description of barrel-setting machines and their (simplest) method of operation in the evaluation of products, quotients and compound fractions. Thus, the description of each calculating procedure is followed by a numerical example with accompanying diagrams to illustrate the keyboard-displays at the beginning, the end, and at intermediate stages in the calculation. The machine-evaluation of series comprising the sum of a number of product or quotient-terms is also discussed. Generally it is hoped that the Appendix will serve as an introduction to mechanical methods of computation and that it will materially assist prospective purchasers in the choice of a machine.

A valuable guide to all users of Computers. Bound in blue publishers case, lettered on the front, with an 18 page table index. Printed on good quality paper for constant use.

Size 10 in. × 8 in. *Price* 18s. 6d. *plus postage and packing* 1s. 3d.

Printed and Published by
TAYLOR & FRANCIS LTD
RED LION COURT, FLEET STREET, LONDON, E.C.4

CONTENTS

Dislocation Damping in Metals. By D. H. Niblett and J. Wilks, Clarendon Laboratory, Oxford. 1

The Rotation of Liquid Helium II. By H. E. Hall, The Physical Laboratories, University of Manchester. 89

5856-2

ADVANCES IN PHYSICS
A QUARTERLY SUPPLEMENT
of the
PHILOSOPHICAL MAGAZINE

VOLUME 9 JANUARY 1960 NUMBER 33

Dislocation Damping in Metals

By D. H. NIBLETT† and J. WILKS
Clarendon Laboratory, Oxford

CONTENTS

§ 1. INTRODUCTION. 2
- 1.1. Internal Friction in Metals. 3
- 1.2. Some General Relations. 3
- 1.3. Methods of Measurement. 4
    - 1.3.1. The torsion pendulum method. 5
    - 1.3.2. The resonant bar method. 5
    - 1.3.3. The ultrasonic pulse method. 7
- 1.4. Some Sources of Internal Friction. 8
    - 1.4.1. Thermoelastic effect. 8
    - 1.4.2. Grain boundary viscosity. 10
    - 1.4.3. Stress-induced ordering. 10
    - 1.4.4. Electronic damping. 13
    - 1.4.5. Miscellaneous. 14

§ 2. THE BORDONI PEAK. 14
- 2.1. Introduction. 14
    - 2.1.1. Measurements of Bordoni. 14
    - 2.1.2. Principal experimental facts. 15
- 2.2. Theory. 16
    - 2.2.1. Seeger's theory. 17
- 2.3. Experimental Details. 22
    - 2.3.1. Dependence on strain amplitude. 22
    - 2.3.2. The effect of cold work. 23
    - 2.3.3. The effect of purity. 25
    - 2.3.4. The effect of neutron irradiation. 26
    - 2.3.5. The effect of frequency. 26
    - 2.3.6. The effect of annealing. 29
    - 2.3.7. The subsidiary peak. 29
    - 2.3.8. Structure of the Bordoni peak. 32
- 2.4. Discussion. 33

---

† Present address: Department of Engineering Physics, Cornell University, Ithaca, N.Y.

§ 3. AMPLITUDE-DEPENDENT INTERNAL FRICTION AT LOW AND MEDIUM TEMPERATURES. 38
3.1. Introduction. 38
3.2. Theory of Granato and Lücke. 40
3.3. Experimental Observations. 42
 3.3.1. Time-dependent effects. 42
 3.3.2. The effect of cold work. 45
 3.3.3. The effect of purity. 47
 3.3.4. The effect of frequency. 48
 3.3.5. The modulus defect. 50
 3.3.6. The effect of temperature. 51
 3.3.7. The effects of quenching and irradiation, and the Köster effect. 55
3.4. Discussion. 58
63
§ 4. INTERNAL FRICTION AT HIGH TEMPERATURES 63
4.1. Introduction. 63
4.2. Experimental Observations. 63
 4.2.1. The activation energy. 65
 4.2.2. Dependence on frequency. 67
 4.2.3. The modulus defect. 67
4.3. Theories and discussion. 68
§ 5. AMPLITUDE-INDEPENDENT INTERNAL FRICTION AT LOW STRAIN AMPLITUDES. 69
5.1. Experimental Observations. 70
 5.1.1. The effect of temperature. 70
 5.1.2. The effect of frequency. 71
 5.1.3. The effect of cold work. 73
 5.1.4. The effect of purity. 73
 5.1.5. The effects of irradiation and quenching. 74
5.2. Theories of the Internal Friction. 74
5.3. The Vibrating String Model. 77
 5.3.1. Dependence on loop length. 77
 5.3.2. Dependence on temperature. 79
 5.3.3. Dependence on frequency. 81
 5.3.4. Summary. 82
5.4. Miscellaneous Peaks. 84

---

§ 1. INTRODUCTION

THE mechanical energy of a vibrating solid is converted quite rapidly into heat, even if the body is completely isolated from its surroundings. This energy transfer, together with the consequent damping of the vibrations, is said to arise because of the presence of *internal friction*. Measurements of internal friction provide valuable information about the structure of the solid state and a wide variety of work has been reported in the last twenty years. Several sources of internal friction in metals have been well understood for some time (Zener 1948), but it is only recently that much information has become available on what is often the principal source of damping in metals, namely the motion of dislocations. In this article we review the various experimental results and consider to what extent they can be explained by current theories. Earlier reviews have been given by Nowick (1953), by Lücke and Granato (1957) and by Mason (1958). For a discussion of the properties of dislocations the reader is referred to books by Cottrell (1953), W. T. Read (1953) and Friedel (1956).

1.1. *Internal Friction in Metals*

The internal friction of metals, particularly pure metals, is very sensitive to cold work. Even very slight handling of a pure annealed single crystal may increase the friction several times. Profound changes in the damping are also produced by annealing. These facts seem to imply that dislocations are responsible for at least part of the friction in metals, as was first suggested by T. A. Read (1940). In addition, neutron or gamma-ray irradiation reduces the friction considerably; this follows naturally if we assume that point defects created by the irradiation diffuse to the dislocations and impede their motion. Impurity atoms also tend to cluster round dislocations (Cottrell 1948), and we find that the friction of impure metals is generally considerably less than that of pure material. Finally, we note that dislocations only move freely in their slip plane, and experiments by Alers (1955) and Waterman (1958) show that the friction is much greater when the oscillating stress has a component in slip plane.

There is now a large amount of experimental information on damping phenomena in metals, but its interpretation is complicated because the friction may arise in quite a large number of different ways. We therefore first indicate briefly the principal sources of friction in metals not associated with dislocations. The damping due to dislocations may arise by several mechanisms and it is necessary to distinguish carefully between the various possibilities. We first deal with the very characteristic peak which occurs in the friction versus temperature curve at low temperatures, and which was first observed by Bordoni (1949). Apart from the Bordoni peak, the internal friction associated with the motion of dislocations usually depends on the strain amplitude except at very small strains, and it is convenient to separate the decrement into amplitude-dependent and amplitude-independent components which we examine in the last three sections.

1.2. *Some General Relations*

The fundamental measure of internal friction is the ratio $\Delta W/W$ where W is the vibrational energy and ΔW is the loss of vibrational energy per cycle. Internal friction is usually measured by observing the decrement (δ) of free vibrations, or the width of the resonance peak for a specimen driven in forced vibration. In the latter case the friction is expressed in terms of a Q factor such that

$$\frac{1}{Q}=\frac{\omega_2-\omega_1}{\omega_r} \qquad . \quad . \quad . \quad . \quad . \quad . \quad . \quad . \quad . \quad (1)$$

where ω_r is the resonant frequency in forced vibration, and ω_1 and ω_2 are the frequencies at which the amplitude of oscillation has fallen to $1/\sqrt{2}$ of its maximum value. For a specimen in which the strain is homogeneous, and the friction small and independent of the amplitude of the oscillations, it may be shown (see for example, Nowick 1953), that

$$\frac{1}{Q}=\frac{\delta}{\pi}=\frac{\Delta W}{2\pi W}. \qquad (2)$$

These expressions are valid provided that $(1/Q) \ll 1$, as is usually the case. Although they are only strictly true if the friction is independent of the amplitude of the oscillations, they may be used as a first approximation provided the amplitude dependence is not very great. Sometimes the friction is measured by observing the attenuation of a sound wave passing through the material; in this case

$$\delta=\alpha\lambda \qquad (3)$$

where α is the attenuation constant and λ the wavelength of the sound wave.

It is often instructive to consider internal friction by way of a stress–strain diagram. In perfectly elastic material the stress–strain curve is a straight line, but the presence of internal friction implies that the curve forms a hysteresis loop whose area is the energy loss per unit volume per cycle. (As the frictional loss is usually quite small $[(1/Q) < 10^{-2}]$ the hysteresis curve only departs very slightly from a straight line.) As is usual with hysteresis mechanisms, the phase of the strain will lag behind the oscillating stress by an angle ϕ, which is related to the decrement of the system so that

$$\phi \simeq \tan\phi=\frac{1}{Q}=\frac{\delta}{\pi}; \qquad (4)$$

ϕ is sometimes used as a measure of internal friction.

If a metal exhibits internal friction, its behaviour is not truly elastic and the total strain at any instant is the sum of an elastic and a plastic strain. (Of course, the plastic strain is usually very much smaller than the elastic component.) Thus for a given stress, the strain is greater than it would be in an elastic solid by an amount equal to the plastic strain, so that the apparent value of the modulus is reduced. The amount ΔE by which the modulus E is reduced below the elastic value is known as the modulus defect, and its value depends on the kind of mechanism responsible for the friction. Theories of internal friction also lead to expressions for the modulus defect; it is therefore highly desirable when investigating internal friction to make simultaneous measurements of the modulus.

1.3. *Methods of Measurement*

The methods of measurement of internal friction fall into three main groups: (*a*) torsion pendulum methods, (*b*) resonant bar methods, and (*c*) ultrasonic pulse methods. We now outline the chief features and variations of each method. It is to be noted that each method is usually only suitable for making measurements over a comparatively small range of frequencies, and this considerably restricts the amount of information which can be obtained from a given specimen. Also, if the specimen is in the form of a bar vibrating in a longitudinal, transverse or torsional mode, the strain is not homogeneous and the measured value of the internal friction is a weighted average of the values corresponding to the strains at different parts of the specimen (see for example, Nowick 1953).

1.3.1. *The torsion pendulum method*

The earliest measurements of internal friction were made by means of a torsion pendulum, and this method has been described in detail by Kê (1947 a). The specimen is in the form of a wire, to which an inertia member is attached so as to give a period of oscillation of the order of a second. Part of the inertia member may be made from ferromagnetic material, and the vibrations excited electromagnetically. The internal friction is usually measured by the damping of free vibrations, successive amplitudes being observed by means of either a mirror, lamp and scale or some automatic arrangement. Sometimes it is convenient to invert the pendulum by clamping the specimen rigidly at its lower end and attaching its upper end to an inertia bar supported by some damping-free suspension (see Norton 1939); in this arrangement the inertia bar does not load the wire. Unless care is taken, the torsion pendulum is unsuitable for measuring specimens with very low internal friction, since the background damping of the apparatus can be of the order of 10^{-4}. It is also difficult to make measurements at low strain amplitudes, the strain usually varying from zero at the cylinder axis to about 10^{-5} at the surface.

The method may be conveniently adapted to measure the internal friction of a wire specimen while it is undergoing tensile deformation, as has been done by Maringer (1953). This author attached an inertia bar and mirror to the centre of the specimen to measure its internal friction while it was being deformed in a tensile machine.

The method of Chang and Gensamer (1953), though not strictly a torsion pendulum, may be mentioned here, since it uses an inertia member and frequencies between 2 and 20 cycles per second. The specimen is a short cylindrical rod, its lower end being rigidly fixed and its upper end attached to a mass of brass. A soft iron rod attached to this mass is used to excite the specimen electromagnetically into *flexural* vibration, and the internal friction is measured by an automatic recorder. Another variant of the torsion pendulum, used to measure the friction at frequencies of the order of 1 cycle *per hour*, has been described by Boulanger (1951) and used by Friedel *et al.* (1955).

1.3.2. *The resonant bar method*

The most frequent method of measuring internal friction has been to excite a specimen, in the form of a rod, in one of its normal modes of vibration, without using an auxiliary inertia member. In this case the frequency depends on the dimensions of the specimen, and is usually of the order of 1 kc/s for flexural vibrations and 30 kc/s for longitudinal vibrations.

Various electrical and magnetic methods have been employed to excite the vibrations. In the piezoelectric method, first introduced by Quimby (1925), the specimen is cemented to a quartz crystal, and the application of a potential difference across the quartz causes the two to vibrate as a single resonant body. The method was improved by Balamuth (1934), who matched the fundamental frequency of the quartz to that of the specimen, and Cooke (1936) has discussed methods of evaluating the data. The three-component piezoelectric resonator was introduced by Marx (1951). An additional quartz crystal (the 'gauge') is attached to the free end of the first crystal and gives a signal which measures the vibrational strain amplitude of the specimen, the ratio of the driving e.m.f. to the gauge signal at resonance being proportional to the logarithmic decrement.

In the electrostatic method, the specimen is set into vibration by applying an alternating potential difference between it and an adjacent fixed electrode. The vibrations are usually detected by measuring the changes in capacity they produce in a condenser formed by the specimen and a second adjacent electrode. Bordoni (1947) used a single electrode placed adjacent to one end of the specimen, both to excite the specimen into longitudinal vibrations and to detect them (using frequency modulation).

Wegel and Walther (1935) attached ferromagnetic pole-pieces to the specimen, and excited vibrations by means of the alternating magnetic field in a coil connected to an oscillator. The vibrations were detected by means of a second coil.

Randall *et al.* (1939) placed a permanent magnet near one end of the specimen, which was surrounded by a coil connected to an oscillator. Eddy currents induced in the specimen interacted with the magnetic field to produce vibrations which were detected by means of a similar coil and magnet at the other end of the specimen. This method has been modified by Thompson and Holmes (1956 b), who used an eddy-current drive but detected the vibrations by means of frequency modulation, using the gap between the end of the specimen and an adjacent electrode as the frequency-determining condenser. The apparatus of Thompson and Holmes (1959) was so constructed as to give automatic and almost continuous readings of internal friction.

Sometimes the specimen has been excited through its supports. Förster (1937) used a magnetic drive and transmitted the vibrations to the specimen by means of its supporting wires, thus eliminating the necessity for attaching pole-pieces. A rather similar arrangement was used by Berry (1955 a) with a piezoelectric drive. In both cases the supports were used as part of the detecting system.

The resonant bar method may be used with specimens of high damping, by measuring the width of the resonance curve in forced vibrations, and with specimens of low damping, by measuring the decay of free vibrations. Care must be taken in the method of supporting the specimens at the vibrational nodes, as has been discussed for example by Kamentsky (1956), but the background losses due to the supports may usually be made relatively unimportant. The method may be used over a wide range of strain amplitudes, strains greater than 10^{-3} having been obtained by Mason (1956) by means of a barium titanate transducer coupled to an exponential horn.

A disadvantage of the method is that the frequencies at which the internal friction of a specimen may be measured are normally limited to the fundamental resonant frequency and perhaps one or two harmonics. Berry (1955 a) has attempted to overcome this limitation by varying the resonant frequency of a specimen vibrating transversely, by loading it with appropriate weights at its centre and ends. Recently however Bordoni *et al.* (1959) have extended the method to cover a range of frequency from 13 kc/s to 6·5 Mc/s. These authors used a specimen in the form of a thin circular plate which could be driven in either flexural or longitudinal vibrations by means of the electrostatic force between it and a small electrode opposite the centre of one of its faces. For flexural vibrations the plate was supported by three needle points located in small holes on a nodal circle; for longitudinal vibration it was clamped by a ring round its circumference in the plane midway between its faces.

1.3.3. *The ultrasonic pulse method*

Internal friction may be measured at megacycle frequencies by the ultrasonic pulse method. A short ultrasonic pulse is introduced into one end of the specimen by means of a piezoelectric crystal, and the attenuation in the specimen is measured by observing the amplitude of the pulse transmitted through it to a second crystal, or reflected back to the transmitting crystal. This method was developed by Huntington (1947), Mason and McSkimin (1947) and Roth (1948); Huntington (1947) has pointed out that care is needed in the interpretation of the attenuation results, owing to the effects of scattering.

Roderick and Truell (1952) examined this method in detail, and obtained attenuation measurements over a frequency range from 5 to 50 Mc/s. They describe two methods of measuring the attenuation. In the first method a quartz crystal is mounted directly on one face of the specimen, and the pulse is reflected from the opposite face, which is accurately parallel to the first. The specimen dimensions are such that reflections from the sides do not interfere with the main echoes. In the second, or water-buffer method, the pulse is passed through a layer of water between the transducer and the specimen. This arrangement makes it possible to measure the reflection loss at the surface of the specimen, which cannot be done when the transmitter is cemented directly to the specimen. Roderick and Truell show that curvature of the wave front in the specimen may account for a considerable fraction of the measured attenuation, and a correction must be applied to obtain the true attenuation of the material.

The strain amplitudes used in the ultrasonic pulse method are usually too small for the method to be used for measuring amplitude-dependent effects. It has, however, proved useful for making measurements of frequency dependence over a relatively wide range, and for the investigation of electronic effects at low temperatures.

1.4. *Some Sources of Internal Friction*

Although this review is concerned primarily with the damping associated with dislocations, it is important to recognize that in a given specimen internal friction may arise in several different and independent ways. Therefore, when investigating dislocation damping it is desirable to make measurements under conditions such that other contributions are small or negligible. In this section we enumerate some of the principal ways in which damping may arise in a metal independently of the presence of dislocations. We do not describe these mechanisms in any detail except in so far as they are similar to those we shall meet when discussing the friction associated with dislocations. The first three mechanisms are ones in which the magnitude of the friction depends critically on the frequency of the vibrations, because the system takes a certain time to respond to an applied stress. Such mechanisms are known by the general term of relaxation processes, and the decrement is generally independent of the strain amplitude.

1.4.1. *Thermoelastic effect*

If an element of material is suddenly subjected to a stress the resulting strain is in general accompanied by a change in temperature. If the stress is homogeneous throughout a specimen, the same temperature change will occur at every point, but if the stress is not homogeneous, as is often the case, temperature gradients will be set up in the material. Consequently, there will be a flow of heat, which is accompanied by an increase of entropy and a dissipation of energy which gives rise to internal friction. Zener (1937) has calculated the magnitude of this effect for the case of a reed in flexural vibration. In each half cycle the convex side is stretched and therefore cooled, while the concave side is compressed and therefore heated. Hence there is a periodic flow of heat back and forth across the reed. At very high frequencies there is insufficient time for appreciable heat flow to take place during a cycle, and so the process is virtually adiabatic and no damping occurs. At very low frequencies the specimen remains always in thermal equilibrium, and the process is isothermal and reversible; again, there is no damping. If, however, the period of the applied stress is comparable with the time taken for heat to flow across the reed, there will be an irreversible conversion of mechanical energy into heat, the thermoelastic internal friction being given by

$$\frac{1}{Q}=\frac{1-2\sigma}{3}\cdot\frac{C_{\mathrm{P}}-C_{\mathrm{V}}}{C_{\mathrm{V}}}\cdot\frac{\omega\mu}{\omega^2+\mu^2} \quad . \quad . \quad . \quad . \quad . \quad . \quad (5)$$

where σ is Poisson's ratio for the material; C_p and C_V are its specific heats at constant pressure and constant volume; ω is the angular frequency of vibration; $\mu = (\pi/a)^2 D$, where D is the thermal diffusivity of the material and a is the thickness of the reed. Zener (1938) also gives a similar type of expression for the thermoelastic damping of a beam of circular cross section in transverse vibration. The theory has been verified by measurements of the frequency dependence of internal friction in transverse vibration by Zener *et al.* (1938) for copper, and by Bennewitz and Rötger (1936, 1938) for German silver and other materials. The precise and detailed investigation on α-brass by Berry (1955 b) shows that Zener's formula agrees extremely well with the measured damping (fig. 1). It usually turns out that thermoelastic damping is small in bars vibrating longitudinally or torsionally, but may become very large for flexural vibrations unless care is taken in selecting the size of the specimens.

Fig. 1

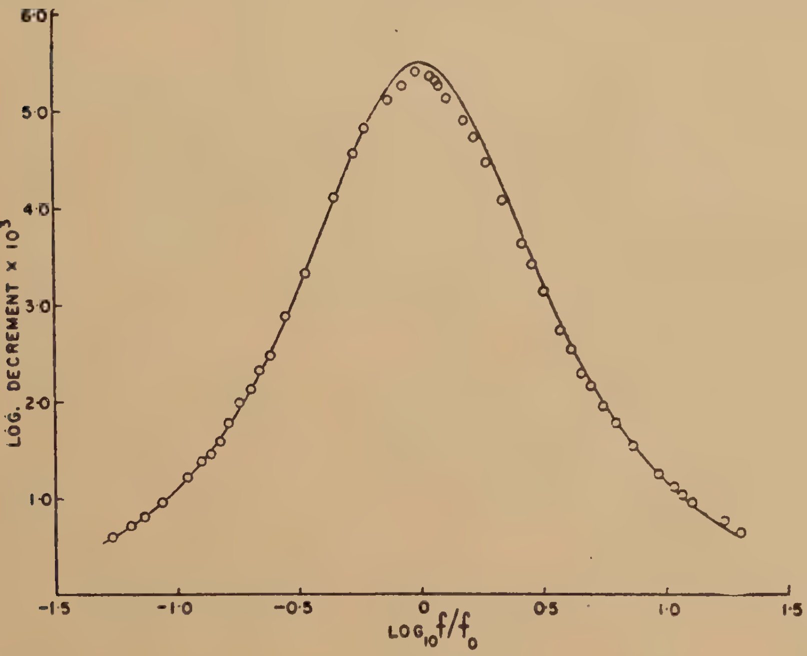

The frequency dependence of the internal friction of four reeds of annealed α brass. Actual frequencies f are divided by the frequency of maximum damping, f_0. The curve is given by theory with no adjustable parameters (Berry 1955 b).

Polycrystalline material also exhibits a further thermoelastic effect. Neighbouring grains have different orientations, so that an applied stress produces different temperature changes in each grain. Hence thermal currents flow across the grain boundaries, giving rise to an internal friction which is a function of the grain size. An expression for this friction, given by Zener (1938), has been verified by Randall *et al.* (1939) using brass with a wide range of grain sizes at 6, 12 and 36 kc/s.

Calculations of the magnitude of the attenuation of ultrasonic waves due to the thermoelastic effect have been made by Lücke (1956). Experiments in the megacycle region suggest that the attenuation due to heat flow between adjacent grains of a polycrystalline specimen or between regions of compression and rarefaction is usually masked by scattering at the grain boundaries. For single crystals, however, the computed and measured values have the same order of magnitude, as shown for example by the measurements of Waterman (1958) for zinc at frequencies from 5 to 200 Mc/s.

1.4.2. *Grain boundary viscosity*

Relative motion of the grains of polycrystalline material at relatively high temperatures gives rise to a viscous-like dissipation of energy at the grain boundaries, and hence an internal friction (Kê 1947 a, b, 1949 a). The energy dissipated is proportional to the product of the relative displacement of adjacent grains and the shear stress responsible for this displacement; it is small at low temperatures where the movement is small, and at high temperatures where the shear stress is small, but is appreciable at an intermediate temperature. This behaviour, typical of a relaxation process, has been observed by Kê (1947 a), and fig. 2 shows a large peak at about 300°c in the internal friction of polycrystalline 99·991% aluminium which was absent in a single crystal of commercially pure aluminium. Kê (1947 b) also measured specimens of aluminium with different grain sizes at frequencies between 0·6 and 2·2 cycles per second, and showed that the internal friction may be expressed as a function of the parameter [grain size × frequency × exp (H/kT)], where $H \sim 1{\cdot}5$ ev. The height of the peak was not affected by the changes in frequency or grain size.

A grain boundary relaxation peak has been observed in copper by Kê (1949 a, b), and by Rotherham and Pearson (1956) who deduced an activation energy of 1·5 ev. Alloying the copper with zinc, gallium, germanium, arsenic or silicon suppressed the peak but produced another with an activation energy of 2·0 ev; the addition of small amounts of oxygen to pure copper reduced the height of the grain boundary peak and lowered its temperature. Similar results were obtained for silver and silver alloys by Pearson and Rotherham (1956). Postnikov (1957) has measured the internal friction of aluminium, copper, nickel, cobalt, iron, titanium, molybdenum and tungsten as a function of temperature from 20°c to 700°c; all these metals show a broad viscous grain boundary peak. He attributes the breadth of the peak to the distribution of grain sizes in a specimen.

1.4.3. *Stress-induced ordering*

The presence of dissolved interstitial atoms in metals with a body-centred cubic lattice often gives rise to a characteristic relaxation peak. The interstitial atoms are located at the centre of one of the cube edges, i.e.

a $(\frac{1}{2}, 0, 0)$ position; they have two close neighbours in the direction of one of the cube axes and thus produce most distortion in this direction. In an unstressed crystal the interstitial atoms will be randomly distributed, but on applying a tensile stress, the energy of an interstitial atom will be less in certain sites because of the distortion produced by the applied stress. Hence the stress produces a redistribution of the interstitial atoms so that some sites are occupied preferentially. This process of redistribution gives rise to an internal friction peak which was first observed by Snoek (1941) in iron containing carbon or nitrogen (fig. 3). For a full account of this mechanism see Zener (1948).

Fig. 2

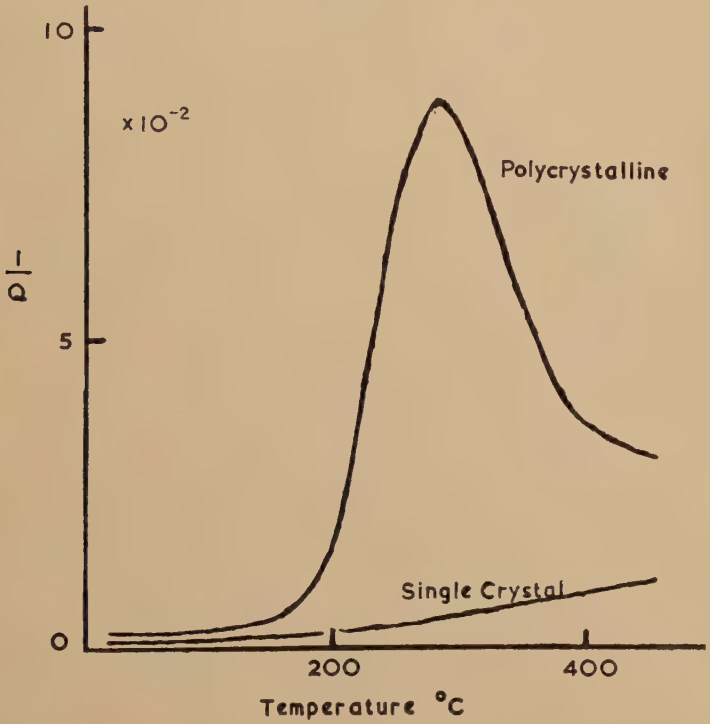

The internal friction of aluminium showing the effect of grain boundary viscosity in polycrystalline material. Measured at 0·8 c/s (Kê 1947 a).

Similar peaks have been observed due to the presence of interstitial oxygen and nitrogen in tantalum by Kê (1948 a, b) and by Marx *et al.* (1953). These were examined in detail by Powers and Doyle (1956), who showed that, in addition to the main peaks, the heights of which were proportional to the concentrations of oxygen and nitrogen respectively, there were other smaller peaks with heights proportional to the squares of the respective concentrations and to their product. They attributed these to interaction of the diffusing atoms with neighbouring interstitial atoms. Powers and Doyle (1957 a) also showed that the diffusion of interstitial carbon in tantalum involved a higher activation energy than that suggested by Kê (1948 a). Interstitial peaks have been observed in columbium by Marx *et. al.* (1953) and by Powers and Doyle (1957 b), and in molybdenum by Maringer and Muehlenkamp (1952). Weiner and Gensamer (1957) have attributed an internal friction peak they observed in hydrogen-charged steel at about 50°K to stress-induced diffusion of the interstitial hydrogen.

Stress-induced ordering also arises in substitutional solutions, such as brass. The mechanism involved is somewhat different from that in interstitial solutions, because the substitution of one type of atom for another leaves the lattice with the same cubic symmetry. However, a pair of solute atoms in nearest neighbour positions will produce distortion along the axis joining them, so that an applied stress will induce a preferential orientation of pairs of solute atoms (Zener 1947). The effect was first observed by Zener (1943) in a single crystal of α-brass, and similar peaks have been observed in β-brass by Artman (1952) and in silver–zinc alloys by Nowick (1952).

Fig. 3

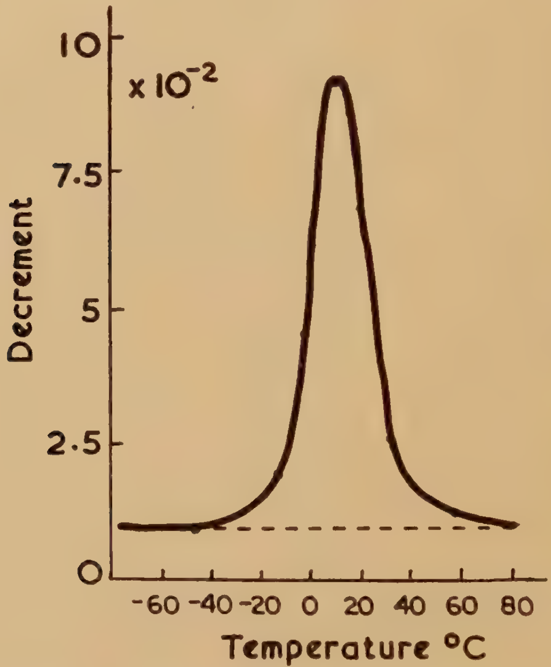

The internal friction of iron loaded with about 0·06% nitrogen by annealing at 600°C in an atmosphere of hydrogen containing 4% ammonia. Broken curve shows the internal friction of iron free from nitrogen and carbon. (Snoek 1941).

1.4.4. *Electronic damping*

At temperatures below about 20°K the attenuation of sound in the megacycle range of frequency increases considerably as the temperature falls. It has been shown by Bömmel (1954) that the attenuation in lead single crystals is much reduced when the metal passes from the normal to the superconducting state (fig. 4). Hence a large contribution to the attenuation is associated with the free electrons. This attenuation, which is proportional to the square of the frequency (Mason and Bömmel 1956), has also been studied in tin by Bömmel (1955), Mackinnon (1955, 1957) and Morse and Bohm (1957); in indium by Morse *et al.* (1956) and Morse and Bohm (1957); in aluminium by Chopra and Hutchison (1958); in copper by Morse *et al.* (1958); and in mercury by Mackinnon and Myers (1959) and Chopra and Hutchison (1959).

Fig. 4

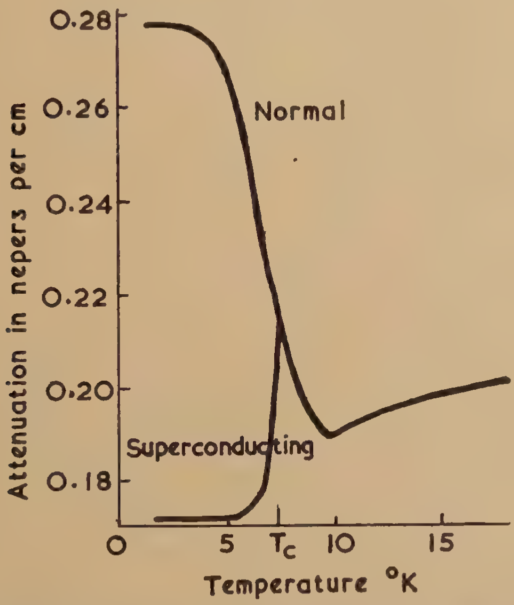

The attenuation of 27 Mc/s longitudinal sound waves in normal and superconducting lead (Bömmel 1954).

A simple explanation of this attenuation (Mason 1955 a) supposes that in the normal state lattice vibrations give energy to the electron gas by a viscous-like reaction. The attenuation is calculated in terms of the viscosity of the electron gas, which is determined from the electrical conductivity; good agreement is found with the observed shape of the graph of attenuation against temperature. More complete treatments, in which the energy transition is associated with distortions of the Fermi surface by the sound wave, have been given by Morse (1955) and Pippard (1955).

In the superconducting state the attenuation decreases very rapidly as the temperature is lowered below the transition temperature. Morse and Bohm (1957) have shown that the rate at which the attenuation decreases in superconducting tin gives some support for the energy gap theory of superconductivity of Bardeen *et al.* (1957). However, there is considerable uncertainty regarding the magnitude of the background losses in the experiments, and further investigations are required before any definite conclusions can be reached.

The attenuation due to lattice-electron interaction has recently been reviewed by Mason (1958).

1.4.5. *Miscellaneous*

There are additional contributions to the internal friction in ferromagnetic materials arising both from mechanical hysteresis when the domains are subjected to a stress, and from eddy current losses associated with magnetostrictive effects. (Similar damping is also observed in ferroelectric material.) The internal friction also assumes large values if the metal exhibits an internal transition, as for example in the case of the β–ζ transition in silver–zinc alloys. However, in this review we shall not be concerned with the properties of these rather special materials; for a further account of this friction see Nowick (1953) or Mason (1958).

§ 2. THE BORDONI PEAK

2.1. *Introduction*

As we have already mentioned, a large internal friction peak occurs at low temperatures in cold-worked face-centred cubic metals. This peak was first observed by Bordoni (1949), and has since been studied in detail by several investigators. We now outline the principal experimental facts concerning the Bordoni peak and then go on to discuss theoretical interpretations.

2.1.1. *Measurements of Bordoni*

The first systematic measurements of internal friction at low temperatures were made by Bordoni (1949, 1954), who measured the internal friction of cold-worked copper, lead, aluminium and silver in the temperature range between 4°K and room temperature, using longitudinal vibrations at frequencies between 10 and 40 kc/s. In each case he found that there is a large maximum in the internal friction at a temperature of about one-third of the Debye temperature of the metal (fig. 5). The largest peak occurred in machined chemically pure polycrystalline copper, at a temperature of about 90°K. In aluminium, lead and silver, the peak was much smaller, and in silver much broader, than in copper. Bordoni's results show that, in general, the height of the internal friction peak increases with cold work and decreases with annealing.

Fig. 5

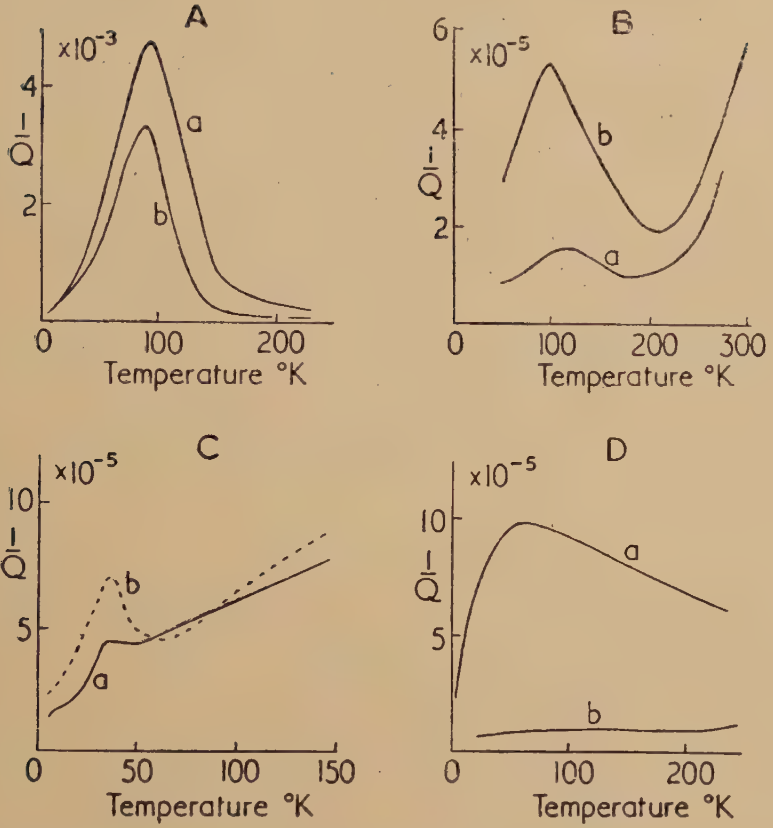

Internal friction in metals (Bordoni 1954).

A. Chemically pure polycrystalline copper, (*a*) machined ; (*b*) after 10 hours' annealing at 150°C.

B. 99·9% pure aluminium, (*a*) after 1 hour's anneal at 140°C ; (*b*) after 2% permanent strain.

C. Lead, (*a*) chemically pure ; (*b*) commercial.

D. Silver, (*a*) machined ; (*b*) after 1½ hours' anneal at 200°C.

2.1.2. *Principal experimental facts*

Extensive measurements on the Bordoni peak in copper have been made on polycrystalline specimens by Niblett and Wilks (1955, 1956, 1957) at about 1 kc/s and by Bordoni *et al*. (1959) between 1·8 kc/s and 6·5 Mc/s; and on single crystals by Caswell (1958) at about 40 kc/s, Paré (1958) at about 5 kc/s, and by Thompson and Holmes (1959) at about 16 kc/s. The principal results of these investigations are as follows :

(*a*) The Bordoni peak appears in both single crystals and polycrystalline specimens.

(*b*) The peak is generally not observed in fully annealed specimens.

(*c*) The height of the peak increases rapidly with increasing amount of cold work for deformations up to about 2%, but for greater deformations there appears to be little change.

(*d*) The height of the peak, and the temperature at which it occurs, are almost independent of the amplitude of the vibrations.

(*e*) In addition to the main peak, a smaller subsidiary peak is generally observed at a lower temperature.

(*f*) Impurities reduce the heights of the peaks.

(*g*) The temperature at which the maximum friction occurs is lower if the friction is measured at a lower frequency.

(*h*) For a given frequency the temperatures at which the peaks occur are only slightly affected by either the amount of cold work or the impurity content of the material.

Peaks have also been observed in aluminium single crystals by Birnbaum and Levy (1956), at frequencies between 30 and 80 kc/s, and by Shibata (1959) at about 3·7 and 40 kc/s; and in polycrystalline aluminium at megacycle frequencies by Hutchison and Filmer (1956). Hutchison and Hutton (1956, 1958), and Einspruch and Truell (1958). Bömmel has observed a peak in lead single crystals at 10·1 and 26·6 Mc/s (Mason 1955 b, c), while Welber and Quimby (1958) have observed one in polycrystalline lead at 45 kc/s. All the above metals have a face-centred cubic structure, but Caswell has reported a large peak at 21°K in a cold-worked specimen of polycrystalline magnesium which has an hexagonal structure. However, it has yet to be confirmed that this is a Bordoni type peak. Measurements on iron (which has a body-centred cubic structure) by Bruner (1959) and by Niblett and Wilks (unpublished) do not show any Bordoni peaks.

Since the most detailed measurements of the Bordoni peak have been on copper, our further discussion of the peak will refer only to this metal, unless otherwise stated.

2.2. *Theory*

The fact that the temperature at which the Bordoni peak occurs is a function of frequency suggests that the internal friction may arise from a relaxation type process. This suggestion is supported by the shape of the peak, which is not unlike that observed for other relaxation processes (see § 1·4), and by the fact that the friction is largely independent of the strain amplitude.

For a simple relaxation process the relaxation time τ depends on the temperature T according to the Arrhenius equation

$$\tau=(1/\omega_0)\exp(Q/kT) \quad . \quad . \quad . \quad . \quad . \quad . \quad . \quad . \quad . \quad (6)$$

where ω_0 is a parameter (the attempt frequency), Q is the activation energy of the process, and k is Boltzmann's constant. The internal friction is a function of the product $\omega\tau$ (where ω is the circular frequency of the applied vibration), and has a maximum value when $\omega\tau=1$. Thus the temperature at which the peak occurs is related to the driving frequency by the equation

$$\omega = \omega_0 \exp(-Q/kT). \qquad (7)$$

Hence the activation energy and attempt frequency can, in principle, be found from the slope and intercept of a graph of the logarithm of the frequency against the reciprocal of the absolute temperature of the peak. It is shown in § 2.3.5 that this leads to an activation energy for copper of the order of 0·1 ev, but that the observed width of the peak is so great that it appears that more than one relaxation time must be involved.

The dependence of the Bordoni peak on the state of cold work of the metal suggests that the activation energy must be associated with the motion of small segments of dislocations. Bordoni (1949) suggested that the sliding of imperfections in a crystal lattice might give rise to a relaxation peak at a low temperature, but did not take into account the specific properties of dislocations. Quantitative theories involving the motion of dislocations were later proposed by Mason (1955 b, c, d) and Seeger (1955, 1956), and these will be discussed in the following sections, together with modifications of Seeger's theory.

2.2.1. *Seeger's theory*

According to Seeger (1955, 1956) the Bordoni peak is due to a relaxation process involving dislocations which run parallel to one of the close-packed directions in the crystal. The energy per unit length of such a dislocation is a periodic function of its position in the crystal lattice (Peierls, 1940). Consider a length of dislocation (AB in fig. 6 *a*) lying in a position of minimum energy along a close-packed direction in a lattice, and suppose that an applied stress is tending to move it in a direction perpendicular to itself. If the dislocation behaves as a rigid rod, a stress equal to the Peierls' stress will be required to move it over the potential barrier to the next equilibrium position CD, but if the line is flexible it is able to move forward much more easily. Thus, if a small bulge (XY in fig. 6 *b*) is formed as the result of thermal fluctuation, a quite small stress will cause it to spread out sideways, as the potential barriers opposing motion in directions parallel to AB and CD are very small. The length of a bulge formed by thermal activation will be determined by the fact that its energy of formation is a minimum; a longer bulge would require more energy to surmount the Peierls' barrier, while a shorter one would involve a greater increase in line length and energy. A bulge of this type may be regarded as a pair of kinks of the kind which arise when a dislocation passes from one lattice row to the next. In the absence of any stress the two kinks will attract and annihilate each other, but an applied stress will tend to move them apart and increase the slipped area. For a given applied force there will be a certain critical separation of the kinks d_{crit} above which they will separate further, and below which they will come together. Internal friction arises because of the formation of these bulges; the motion of the two constituent kinks is approximately reversible for small displacements, but as soon as the critical distance d_{crit} is exceeded they will move apart rapidly and irreversibly.

The internal friction which arises in this way will be of the general form associated with relaxation processes, as for example is the internal friction arising from the stress-induced ordering of solute atoms in solid solutions (see § 1.4.3.). In particular the maximum friction occurs when the rate of formation of bulges is equal to the circular frequency of the oscillations. To calculate the magnitude of the internal friction we must first find the rate of formation ν of the bulges. If this is given by an Arrhenius type of equation, we may write:

$$\nu = A \exp(-H/kT) \qquad \text{. . . . . . . (8)}$$

Fig. 6

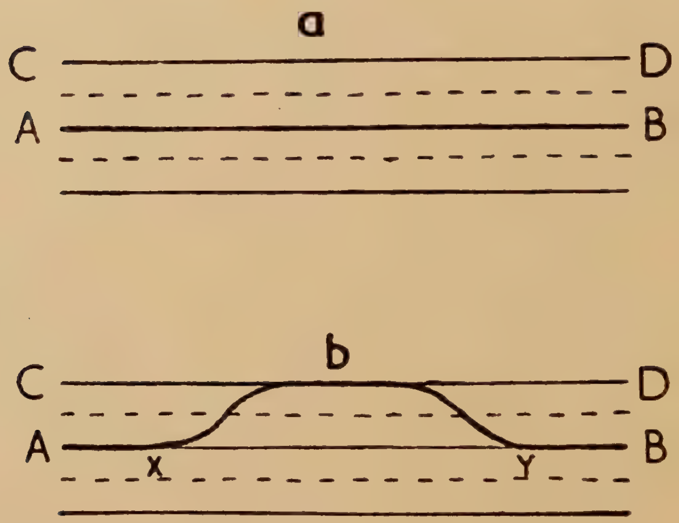

Seeger's dislocation mechanism.
(*a*) Dislocation in position of minimum energy.
(*b*) Bulge in dislocation. (Full straight lines represent positions of minimum energy, broken lines represent positions of maximum energy.)

where H is the activation energy for the formation of a bulge and A is the attempt frequency, that is the number of times per second that the dislocation is in a favourable position to form a bulge. Seeger initially took this rate to be just the frequency of oscillation of the dislocation in the Peierls potential well; in this case

$$A \sim \frac{1}{2\pi a}\sqrt{\frac{2\tau_{\mathrm{p}}}{\rho}} \qquad \text{. . . . . (9)}$$

where τ_{p} is the Peierls stress, ρ the bulk density and a the lattice spacing (see for example Mason 1955 c). In his first treatment, Seeger (1955) also took H to be $2W_{\mathrm{K}}$, where W_{K} is the additional energy associated with a single kink in a dislocation which is otherwise parallel to a lattice direction. In the absence of an applied stress the value of W_K may be estimated by specifying the form of a dislocation at rest by a differential equation of the form

$$E_0 \frac{d^2y}{dx^2} = \mathbf{b}\tau_p \sin\frac{2\pi y}{a} \quad . \quad . \quad . \quad . \quad . \quad . \quad . \quad (10)$$

where E_0 is the energy of unit length of line and a the lattice spacing; hence Seeger obtained

$$H = 2W_K = \frac{4a}{\pi}\sqrt{\left(\frac{2E_0 a\mathbf{b}\tau_p}{\pi}\right)}. \quad . \quad . \quad . \quad . \quad . \quad . \quad (11)$$

Although both the above treatment and a subsequent modification (Seeger 1956) give the right order of magnitude for the values of A and H, they are only approximate because the Arrhenius equation is not applicable to the formation of bulges in dislocation lines. The point is that this equation is derived essentially for the motion of single atoms, whereas the formation of a bulge is a collective process involving the motion of about 100 atoms. Seeger *et al.* (1957) have given a much more complete treatment based on an expression for the rate of formation of kinks derived by Donth (1957) using the theory of stochastic processes. By this treatment, Seeger *et al.* showed that the mean frequency ν with which dislocation bulges are formed, and the activation energy H of the process, could be found from the equations:

$$\log(\nu/B) = F_1(r, \alpha), \quad . \quad . \quad . \quad . \quad . \quad . \quad . \quad . \quad . \quad . \quad (12)$$

$$B = \frac{\pi^2}{32}\frac{G\mathbf{b}^2}{a^2v^2}\frac{kT}{m^{3/2}E_0^{1/2}}, \quad . \quad . \quad . \quad . \quad . \quad . \quad . \quad . \quad (13)$$

$$H \equiv -\frac{d\log\nu}{d(1/kT)} = kT \,.\, F_2(r, \alpha) \quad . \quad . \quad . \quad . \quad . \quad (14)$$

where v is the velocity of sound, G is the shear modulus, m is the mass per unit length of the dislocation, and $F_1(r, \alpha)$ and $F_2(r, \alpha)$ are functions shown in figs. 7 and 8 of the parameters

$$r = \frac{2W_K}{kT} \quad . \quad . \quad . \quad . \quad . \quad . \quad . \quad . \quad . \quad (15)$$

and

$$\alpha = 1 - \frac{\pi\tau}{8\tau_p} \quad . \quad . \quad . \quad . \quad . \quad . \quad . \quad . \quad (16)$$

where τ is the resolved shear stress.

By using rate theory similar to that given by Mason (1955 c), Seeger *et al.* (1957) calculate the maximum value of the internal friction associated with this relaxation process to be

$$\frac{1}{Q} = \frac{p}{2(1+p)^{1/2}} \quad . \quad . \quad . \quad . \quad . \quad . \quad . \quad . \quad (17)$$

where

$$p = \frac{2N_0 a\mathbf{b}^2 sG}{kT}\left(\frac{\pi a E_0}{2\mathbf{b}\tau_p}\right)^{1/2}\left(\frac{1}{3\pi}\log\frac{16\tau_p}{\pi\tau} + 0{\cdot}3\right); \quad . \quad . \quad . \quad (18)$$

N_0 is the number per unit volume of dislocation loops contributing to the process, and s is the mean area swept out by one dislocation loop. A lower limit for the height of the peak is obtained by substituting $s = La$, where L is the average length of the dislocation loops. Some dislocations may however sweep out a larger area whose upper limit is a function of the applied stress and the line tension of the dislocation; in this case

$$\frac{1}{Q} = \frac{\mathbf{b}^2 L^3 N_0 G}{48 E_0} \approx \frac{N_0 L^3}{24} \quad \ldots\ldots\ldots \quad (19)$$

Fig. 7

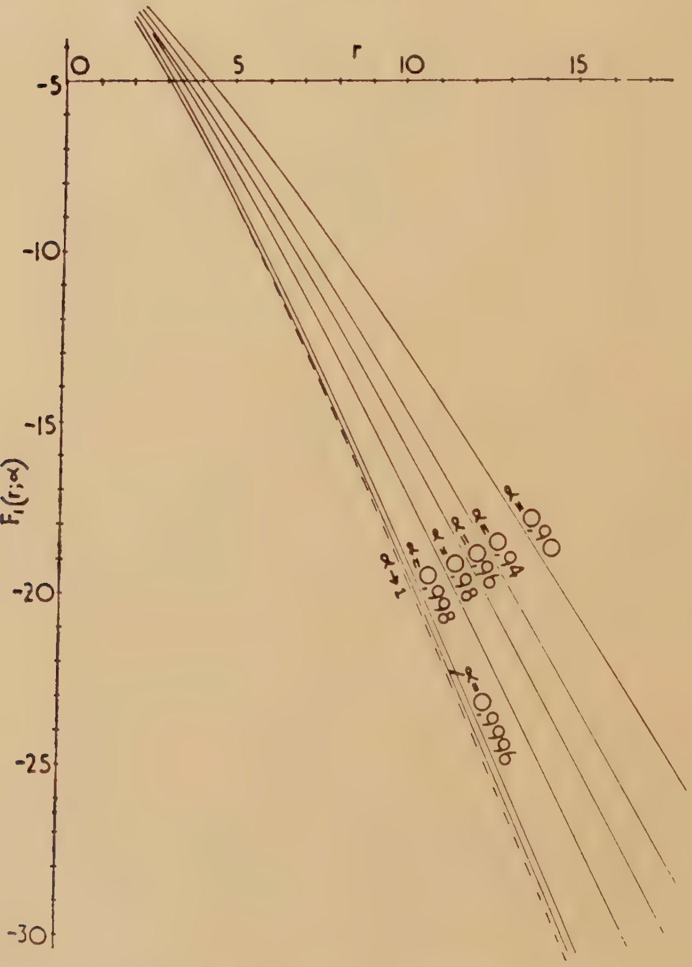

The function $F_1(r;\,\alpha)$ given by Seeger *et al.* (1957).

This theory gives quite a good account of the Bordoni peak, as we shall show after the experimental results have been reviewed in more detail.

It is interesting to note how Seeger's theory differs from a rather similar treatment due to Mason (1955 b, c, d) who proposed that the initial bulge consisted of the whole length of dislocation line between two pinning points as in fig. 9. In this case the activation energy H should be proportional to the distance between pinning points; this does not agree with the observation that the activation energy is substantially independent of both the degree of cold work and the concentration of impurities, (Niblett and

Fig. 8

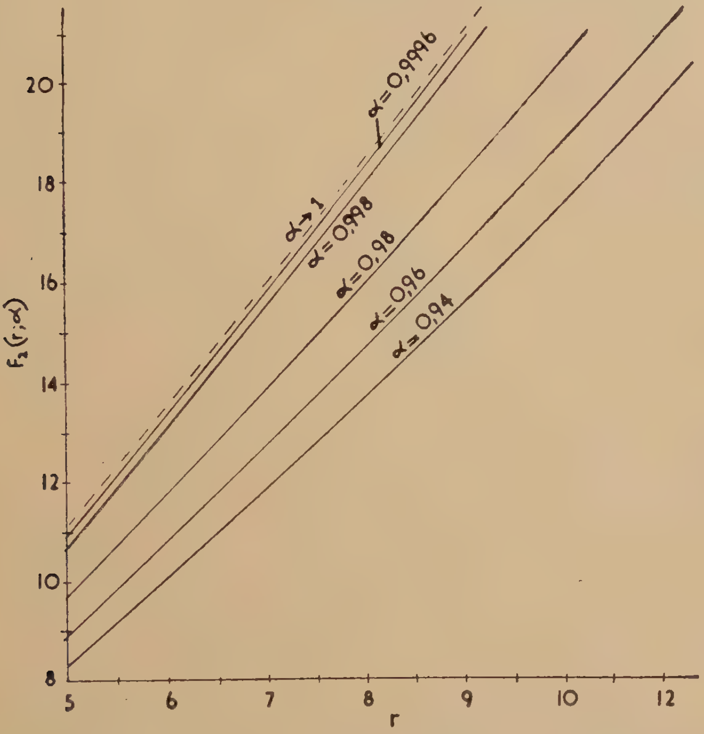

The function $F_2(r;\, \alpha)$ given by Seeger *et al.* (1957).

Fig. 9

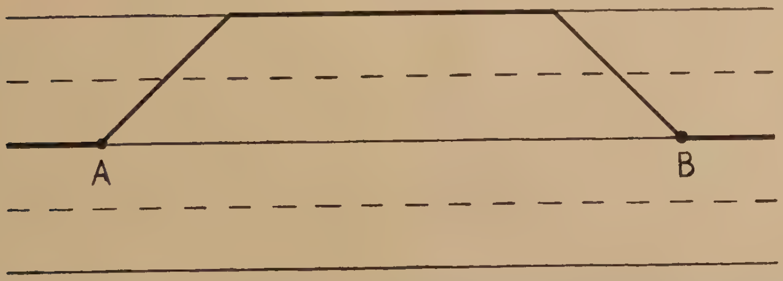

Mason's dislocation mechanism. Full straight lines represent positions of minimum energy, broken lines represent positions of maximum energy. A and B represent pinning points.

Wilks, 1956). In any case, Mason's assumption that the whole length AB of dislocation would move as a rigid rod is untenable (Seeger 1956, Weertman 1956).

2.3. *Experimental Details*

The principal results concerning the Bordoni peak in copper were briefly outlined in § 2.1.2.; we now consider the dependence of the internal friction on various parameters in more detail.

Fig. 10

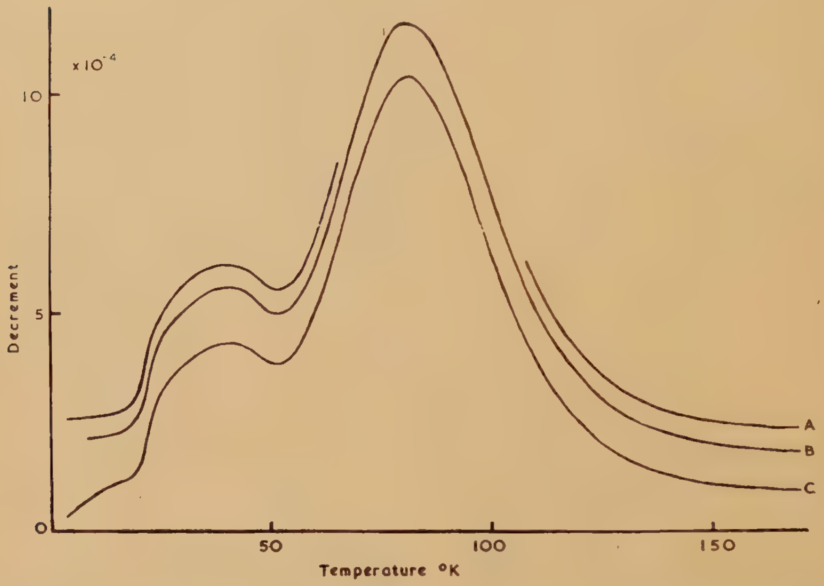

The internal friction of a pure copper single crystal subjected to a reduction by rolling of 5%. Maximum strain amplitudes: A, $3{\cdot}7\times10^{-5}$; B, $2{\cdot}3\times10^{-5}$; C, $9{\cdot}3\times10^{-5}$ (Caswell 1957).

2.3.1. *Dependence on strain amplitude*

The results of Niblett and Wilks (1957), Caswell (1958) and Paré (1958) all show that the internal friction associated with the Bordoni peak is approximately independent of the strain amplitude. The greatest range of strain amplitudes has been investigated by Caswell, who used values ranging from $9{\cdot}3\times10^{-9}$ to $3{\cdot}7\times10^{-5}$ in a specimen which had been deformed 5% by rolling (fig. 10). The Bordoni peak is superposed on a background of internal friction which increases with increasing strain amplitude; if the background component is estimated from the results at higher temperatures it seems that most of the slight amplitude dependence observed in the region of the Bordoni peak can be attributed to the background rather than to the peak itself.

2.3.2. *The effect of cold work*

The internal friction of annealed copper increases monotonically with increasing temperature from 4 °K to room temperature, and depends strongly on the strain amplitude. The peak is either completely absent, or very small, as is shown by the measurements of Briggs (1955) and Caswell (1958) on single crystals and of Niblett and Wilks (1957, 1959 a) on polycrystalline material.

Fig. 11

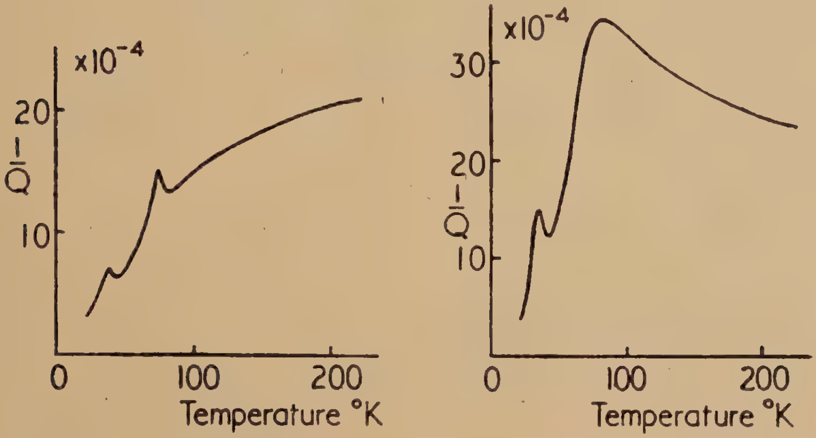

(*a*) (*b*)

The internal friction of polycrystalline copper (Niblett and Wilks 1957). (*a*) Strained 0·1%. (*b*) Strained 0·5%.

Small amounts of plastic deformation produce a small peak superposed on a background of internal friction similar to that observed in the annealed material. Peaks of this type have been observed by Niblett and Wilks (1955) with a polycrystalline specimen extended 0·1% (fig. 11*a*), and by Thompson and Holmes (1959) for a single crystal extended 3·25%. Niblett and Wilks showed that a deformation of 0·5% increased the size of the Bordoni peak and gave it a broad asymmetric shape (fig. 11*b*) similar to that observed by Bordoni (1949, 1954) in machined polycrystalline silver. It thus appears that much of the variation in the shape of Bordoni's curves may arise from the metals being subjected to different amounts of cold work, rather than from the difference in materials.

Further cold work increases the height of the Bordoni peak, and at the same time the background friction is greatly reduced, so that the peak attains its characteristic shape. The growth of the peak is illustrated in measurements of Caswell (1958) on a single crystal which was rolled to produce successive reductions of 1·35%, 3·0% and 4·8% (fig. 12); the reduction to 4·8% did not produce an appreciable increase in the height of the peak. Evidence that the height ceases to increase for deformations greater than about 2% was also obtained by Niblett (1956), who found that three specimens made from the same polycrystalline material and deformed in tension by 2·2%, 5·8% and 8·4% exhibited Bordoni peaks of very similar heights.

Although one cannot increase the height of the peak by continued deformation of the same type, Caswell (1958) has shown that it may be increased by cross-rolling. The specimen of figure 12 was rolled until its width was reduced by 10% and then rotated through an angle of 90° about the axis parallel to its length and rolled again. The height of the peak was then about three times greater than that produced by a single reduction of 4·8% (figure 12). The height of the peak has also been increased by irradiating the specimen prior to the deformation. Niblett and Wilks (1957) observed that for specimens of polycrystalline copper which were subjected to an integrated neutron flux of 5×10^{18} n.v.t. and subsequently strained 2·0%, 5·1% and 8·0% respectively, the Bordoni peaks were considerably larger than for similar un-irradiated material at these deformations. There is also some evidence that deformation by tension produces a larger peak than rolling (Paré 1958).

Fig. 12

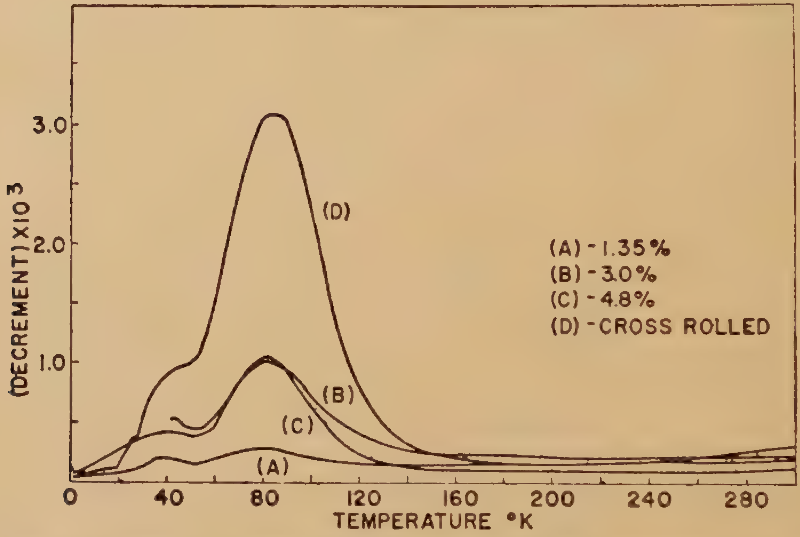

The internal friction of a copper single crystal subject to deformations of 1·35, 3·0 and 4·8% by rolling, and cross-rolling (Caswell 1958).

The results of Caswell (1958) on the specimen deformed successively by 1·35%, 3·0%, 4·8% and cross rolling, suggest that cold work moves the position of the Bordoni peak to a slightly higher temperature. This shift was not observed by Niblett and Wilks, but their measurements were made on different specimens so that the effect may have been hidden by slight differences in purity, etc., from specimen to specimen. Neither Niblett and Wilks nor Caswell have observed any systematic dependence of the peak width on cold work.

2.3.3. *The effect of purity*

The presence of impurities greatly reduces the height of the Bordoni peak. This is illustrated by the measurements of Caswell (1958) on similarly cross-rolled samples of copper doped respectively with 0·065, 0·25 and 0·50% of gold (fig. 13). Caswell also showed that the addition of 0·56% of nickel reduced the height of the peak, but to a much smaller extent than a similar amount of gold, presumably due to the fact that the atomic radius of nickel differs by only 2·5% from that of copper whereas that of gold is 11% larger. The effect of adding gold has also been studied by Paré (1958). According to Niblett and Wilks (1956), as little as 0·0026% bismuth and 0·032% phosphorus were sufficient to reduce the height of the peak by a factor of about 10 relative to that in pure copper.

Fig. 13

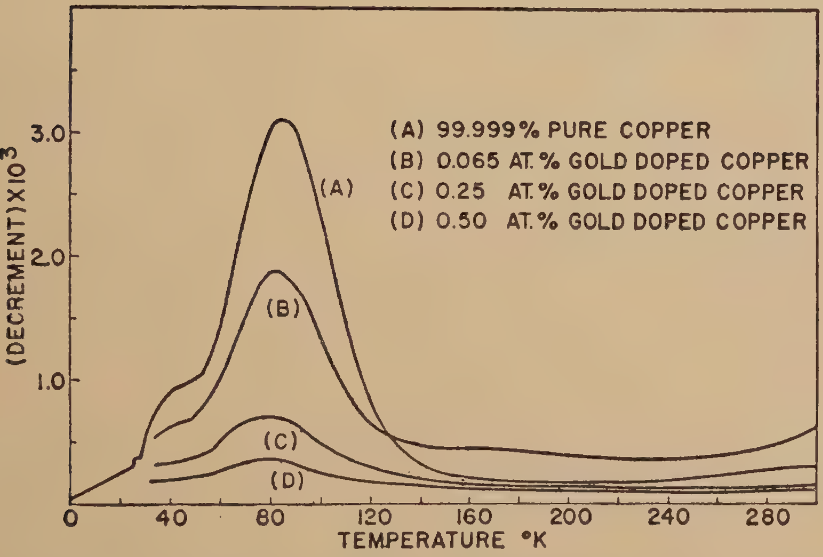

The internal friction of similarly cross-rolled copper single crystals containing different concentrations of gold (Caswell 1958).

Niblett and Wilks (1957), Caswell (1958) and Paré (1958) have all observed that the presence of impurities moves the Bordoni peak to a slightly lower temperature than that at which it occurs in pure copper. The magnitude of this shift varies from about two to six degrees. The peak also appears to be somewhat broader in the impure specimens.

2.3.4. *The effect of neutron irradiation*

Neutron irradiation appears to have a very similar effect on the Bordoni peak in cold-worked copper as the presence of impurities. Thompson and Holmes (1959) showed that irradiating a cold-drawn specimen of commercial polycrystalline copper to an integrated flux of 5×10^{17} n.v.t. reduced the height of the peak by about 15%, while Niblett and Wilks (1957) found that an irradiation of 5×10^{18} n.v.t. reduced the peak damping by a factor of about six for a specimen of pure polycrystalline copper pre-strained 6·6%. Niblett and Wilks also observed that this irradiation lowered the temperature at which the peak occurred by about four degrees. Thompson and Holmes reported that the temperature and shape of the peak were not changed by the irradiation, but with their small neutron flux one would expect the temperature shift to be less than one degree and thus not readily observable. It has been suggested that these effects are due to annealing during the irradiation, rather than to the irradiation itself, since the pile temperature is of the order of 50°C. However, annealing studies by Niblett and Wilks (1959 b) (see § 2.3.6.) suggest that this is rather unlikely.

A small Bordoni peak may be visible after annealed copper is subjected to neutron irradiation as has been observed by Niblett (1956), using polycrystalline copper and an irradiation of $4{\cdot}5 \times 10^{18}$ n.v.t., and by Thompson and Holmes (1959), who irradiated a single crystal to an integrated flux of 2×10^{12} n.v.t. Later measurements (Niblett and Wilks (1959 a)) on annealed copper suggest that this small peak is present all the time, but prior to irradiation is masked by the background friction which is relatively much larger. It is noticeable that this peak appears at a slightly higher temperature than the Bordoni peak in cold-worked material.

2.3.5. *The effect of frequency*

Measurements of the Bordoni peak in copper have been made at the following frequencies: 380 and about 1000 c/s by Niblett and Wilks (1955, 1956, 1957); 3·7 to 5·6 kc/s by Paré (1958); about 16 kc/s by Thompson and Holmes (1959); 28 to 31 kc/s by Bordoni (1949, 1954); 38 to 41 kc/s by Caswell (1958); and various frequencies between 1·8 kc/s and 6·5 Mc/s by Bordoni *et al.* (1959). If a simple relaxation process is involved, a graph of the logarithm of the frequency against the reciprocal of the absolute temperature at which the peak occurs should give a straight line whose slope is equal to the activation energy of the process. Since the temperature of the peak depends to some extent on the degree of cold work and the purity of the material, it is desirable to make measurements over as wide a frequency range as possible on the same specimen. Almost the only work of this nature is that of Bordoni *et al.* (1959) who used relatively impure copper (containing 0·12% of lead) cold-worked by 'machining'. The frequencies and temperatures observed by these authors fit quite closely on to a straight line corresponding to an activation energy of 0·122 ev. Their results also correspond to an attempt frequency of $2{\cdot}4 \times 10^{12}$.

As we have already indicated, the temperature at which the peak occurs seems to depend on several factors. Thus in fig. 14 we plot the temperature of the peak against frequency for all the available experiments on nominally pure copper deformed by a comparable amount (a few parts per cent).

Fig. 14

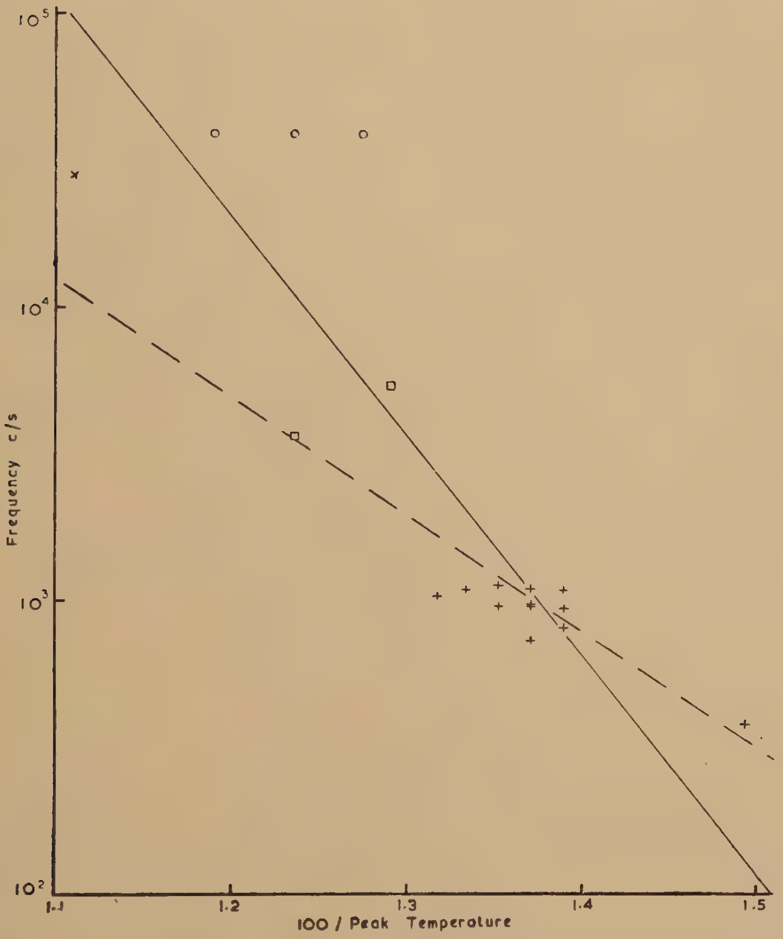

The frequency dependence of the temperature of the Bordoni peak in cold-worked pure copper. Measurements by Bordoni ×; Niblett and Wilks +; Caswell ○; and Paré □.

The results show considerable scatter: the points do not lie on one line. (There is similar scatter in the frequency dependence of the Bordoni peak in aluminium reported by different authors. For instance, Einspruch and Truell (1958) determined an activation energy of about 0·11 ev from their measurements at 10, 30 and 60 Mc/s, while Shibata (1959) found a value of about 0·19 ev from measurements at 3·7 and 40 kc/s.) There are several different ways in which this scatter may arise; (*a*) variations in the impurity content, (*b*) variations in the degree of deformation, (*c*) different methods of deformation, (*d*) different modes of vibration, (*e*) errors in measuring the temperature of the specimen, especially if measurements are not made under steady conditions. In order to eliminate some of these sources of error Paré (1958) and Caswell (1958) measured the friction of the same single crystal (pre-strained 10% by rolling) at frequencies of 5·56 and 39·6 kc/s. However, the temperature shift they observed was only one degree, which corresponds to an activation energy well outside the range suggested by other measurements. Paré attributed this to the non-uniformity of the deformation produced by rolling, and the difference in the stress distribution for flexural and longitudinal vibration. This suggests that a better value for the activation energy might be obtained by using only those results where the specimen was deformed in tension, i.e. those of Niblett and Wilks (1955, 1956, 1957) plus one due to Paré (1958). These give the dashed line in fig. 14 corresponding to an activation energy of about 0·08 ev, whereas if we take all the measured points into consideration we get the full line corresponding to an energy of about 0·15 ev. The intercept on the frequency axis ($1/T=0$) should give the attempt frequency of the relaxation process, but this quantity is extremely sensitive to the choice of line. Thus if we take the activation energy to be 0·08 ev the frequency is of the order of 10^8, while for an energy of 0·15 ev the frequency is about 10^{13}. However, as we now go on to discuss, it seems unlikely that the relaxation process can be described in terms of a single activation energy and attempt frequency.

If the peak arises from a simple relaxation process with a single activation energy H, the friction at a frequency ω is given by

$$\frac{1}{Q}=2\left(\frac{1}{Q}\right)_0\frac{\omega/\omega_0}{1+(\omega/\omega_0)^2} \quad . \quad . \quad . \quad . \quad . \quad . \quad . \qquad (20)$$

where $(1/Q)_0$ is the maximum value of the friction and $\omega_0=A\exp(-H/kT)$. It follows from this expression that a peak with an activation energy of 0·08 ev should have a half-width of about 20°, with a correspondingly smaller value for higher activation energies. In fact the observed peaks are about 40° wide, and this suggests that the relaxation process cannot be characterised by a single energy. Caswell (1958) has shown that a Gaussian distribution of activation energies with a standard deviation of 16° will fit the shape of the observed peaks, while Thompson and Holmes (1959) have introduced a spectrum of discrete activation energies (§ 2.3.8). On the other hand, Bordoni *et al.* (1959) argue that there is a range of attempt frequencies; it is probable that a complete description will have to introduce a range of activation energies and attempt frequencies. In this case the effect of rolling might be to produce a different distribution of energies and frequencies from deformation by tension, and this could account for some of the scatter in fig. 14.

The results of Niblett and Wilks (1957) at frequencies of 380 and 1100 kc/s, and of Bordoni *et al.* over a larger frequency range suggest that the height of the peak is approximately independent of frequency. The latter authors found that the peak was somewhat smaller and considerably broader at megacycle frequencies than that observed in the same specimen at kilocycle frequencies.

2.3.6. *The effect of annealing*

The Bordoni peak in cold-worked copper is not removed by annealing at room temperature. For example, Niblett and Wilks (1957) measured a polycrystalline specimen which had been pre-strained 2·2% both a few days after the deformation and some ten months later, and found little change in the height of the peak.

The peak anneals out in the temperature range from 100°c to 500°c in a rather complex manner. Bordoni (1949, 1954) found that in machined pure polycrystalline copper, the peak height was reduced by about 30% by annealing for ten hours at 150°c, and preliminary results by Niblett and Wilks (1957) showed that the peak in a polycrystalline specimen pre-strained 8·4% was halved in height by annealing for one hour at 180°c but was not eliminated until after one hour at 350°c. Caswell (1958) observed that the peak in a cross-rolled single crystal was reduced by about 40% after two hours at 238°c. More detailed isochronal annealing measurements on polycrystalline copper by Niblett and Wilks (1959 b) have shown that there is a range of annealing temperatures in which the Bordoni peak *increases* in height before it decreases. The temperatures at which the peak height increases and decreases, and the magnitude of the increase, depend quite critically on the grain size of the material.

For example, the maximum $1/Q$ in a specimen with a mean grain size of about 0·3 mm, strained 5·4%, increased from $2{\cdot}9 \times 10^{-3}$ to $4{\cdot}6 \times 10^{-3}$ after a one-hour anneal at 97°c and then fell to $1{\cdot}3 \times 10^{-3}$ after one hour at 181°c (fig. 15). The maximum $1/Q$ for a specimen with a mean grain size about ten times larger (as a result of a prolonged annealing treatment at 1050°c prior to straining it 5·7%) was initially $1{\cdot}9 \times 10^{-3}$, and did not increase until an anneal of one hour at 292°c, when it rose to $6{\cdot}0 \times 10^{-3}$; with further annealing it then decreased as shown in fig. 16.

Measurements by Bordoni (1949, 1954), Bordoni *et al.* (1959), Niblett and Wilks (1957, 1959 b) and Caswell (1958) all show that annealing in the region of 200°c lowers the temperature at which the peak occurs by about five degrees.

2.3.7. *The subsidiary peak*

A smaller internal friction peak occurring in cold-worked copper at a temperature between 30°K and 40°K appears to be associated with the main Bordoni peak (Niblett and Wilks 1955). Its height, and the temperature at which it occurs, are approximately independent of the strain amplitude, and it reacts to annealing treatments in a similar manner as does the main peak. It is visible as a separately resolved peak in all the measurements of Niblett and Wilks, and in some of those of Caswell (1958), Paré (1958) and Thompson and Holmes (1959), but in other measurements by these authors it appears only as a small bump on the low temperature side of the main peak. A quantitative investigation of this subsidiary peak is difficult, because the principal peak gives a considerable contribution to the internal friction at these temperatures.

Fig. 15

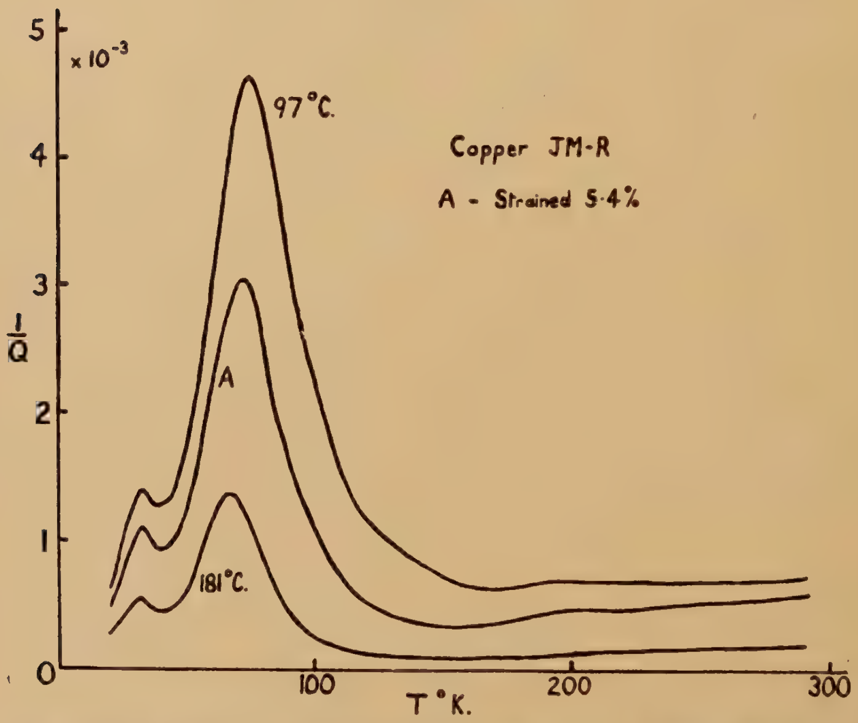

The internal friction of polycrystalline copper with a mean grain size of ~0·3 mm. Initially strained 5·4% and then annealed for one hour at 97°c and 181°c. (Niblett and Wilks.)

In most measurements the temperature of the subsidiary peak cannot be determined with sufficient accuracy to estimate a value of its activation energy from the shift when the frequency is varied. If, however, the same attempt frequency is applicable to the subsidiary peak as to the Bordoni peak, then the activation energies of the two peaks would be in the same ratio as the temperatures at which they occur. This would give an activation energy of the order of 0·04 ev for the subsidiary peak. Bordoni *et al.* (1959) also obtained a value of 0·04 ev for the activation energy of the subsidiary peak from the slope of a graph of the logarithm of the frequency against the reciprocal of the peak temperature. However, in only one specimen did their measurements extend to a sufficiently low temperature to observe this peak clearly; their other points are obtained from the asymmetry of the principal peak.

According to Caswell (1958), rolling a single crystal does not increase the height of the subsidiary peak as rapidly as that of the Bordoni peak; so that it merges into the side of the Bordoni peak at large deformations.

Fig. 16

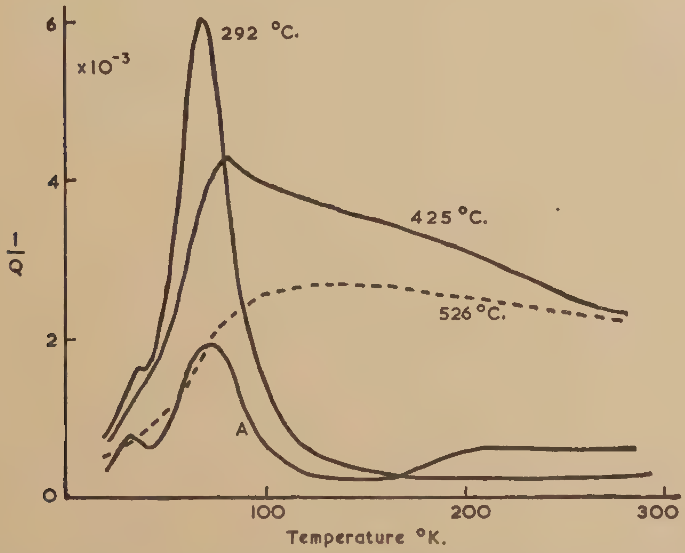

The internal friction of polycrystalline copper (initially annealed at 1050°c) with a mean grain size of ~3 mm. Strained 5·7% (curve A), and then subsequently annealed for one hour at temperatures indicated (Niblett and Wilks 1959 b).

Measurements by Niblett and Wilks (1955, 1956, 1957) show that for polycrystalline specimens deformed in tension, the two peaks have about the same relative sizes for deformations from 2% to 9%. Paré (1958) found that for a single crystal deformed in tension 11·5% the subsidiary peak was relatively larger than for a crystal rolled 10%. This is consistent with the fact that Niblett and Wilks observed relatively larger subsidiary peaks in tensile-deformed specimens than did Caswell (1958) in rolled crystals.

In their measurements on impure specimens, Niblett and Wilks, Caswell, and Paré found that the subsidiary peak occurred at about the same temperature as that in pure copper. Consequently the two peaks are slightly closer together in temperature, and thus tend to merge more into each other, in the impure specimens.

Caswell (1958) observed a very small peak at 44°K in a copper single crystal which had been quenched from 1000°c, and showed no Bordoni peak. He interpreted this as indicating that the presence of vacancies might be instrumental in causing the subsidiary peak. However, the general similarity in behaviour of the Bordoni peak and the subsidiary peak suggests that the two arise from similar mechanisms.

Two peaks have also been observed in cold-worked aluminium (Shibata 1959); these occurred at temperatures of about 90°K and 116°K, when measured at 3·7 kc/s, and at about 100°K and 131°K at 40 kc/s. They are usually of about equal heights, and are very broad, so that it is often difficult to resolve them. However, at present there is not enough evidence to associate these peaks quite definitely with those observed in copper. A further peak has been found at a lower temperature in cold-worked polycrystalline aluminium by Lax and Filson (1959). The temperature of this peak varied from 21°K at a frequency of 25 kc/s to 31°K at 1 Mc/s. It is possible that all these peaks are associated with the structure of the Bordoni peak which is discussed in the following section.

2.3.8. *Structure of the Bordoni peak*

Thompson and Holmes (1959) have made a detailed study of both the friction and modulus defect and deduce that the Bordoni peak is not a single relaxation peak, but a series of simple relaxation peaks which overlap one another. Figure 17 shows their measurements of the internal friction and Young's modulus of a copper single crystal which had been extended 3·25%. The internal friction of this specimen shows at least two small peaks superposed on a large background decrement, and the curve of Young's modulus against temperature is sufficiently detailed to reveal a step-like structure. (Other experimenters have not made their measurements at sufficiently small intervals of temperature, or measured the modulus with sufficient accuracy, to observe these steps.) The authors analyse their curves in some detail by assuming that each step in the modulus-temperature curve corresponds to a simple relaxation process, and that the maximum friction is given by the usual relation

$$\left(\frac{1}{Q}\right)_{\max}=\tfrac{1}{2}\left(\frac{\Delta E}{E}\right) \quad . \quad . \quad . \quad . \quad . \quad . \quad . \quad . \quad (21)$$

where E is Young's modulus, and ΔE is the change in modulus due to the process (see for example Nowick 1953).

Thompson and Holmes conclude that the modulus of fig. 17 indicates a series of internal friction peaks at temperatures of 30°, 40°, 62°, 68°, 75°, 85° and 96°K, that at 85°K being the largest. By making the somewhat doubtful assumption that each process has the same attempt frequency, they deduce an activation energy for each process based on the shift of the main peak with frequency, and then calculate the contribution of each process to the total friction using eqns. (20) and (21). In this way they obtain the curve shown chain-dotted in fig. 18; this curve is quite similar to the friction of a specimen of 'hard drawn' polycrystalline 'commercial' copper. The fact that the *magnitudes* of these two curves are similar is coincidental in view of their different states of cold work, but the fact that the *shape* of the peak has been derived from the modulus measurements gives some support to the author's treatment. (Of course, it would be preferable to compare the friction calculated from the modulus defect with that observed in the *same* crystal; but the structure of the modulus curve is only clearly observed in lightly deformed single crystals, and here the peaks are obscured by the background decrement.)

Fig. 17

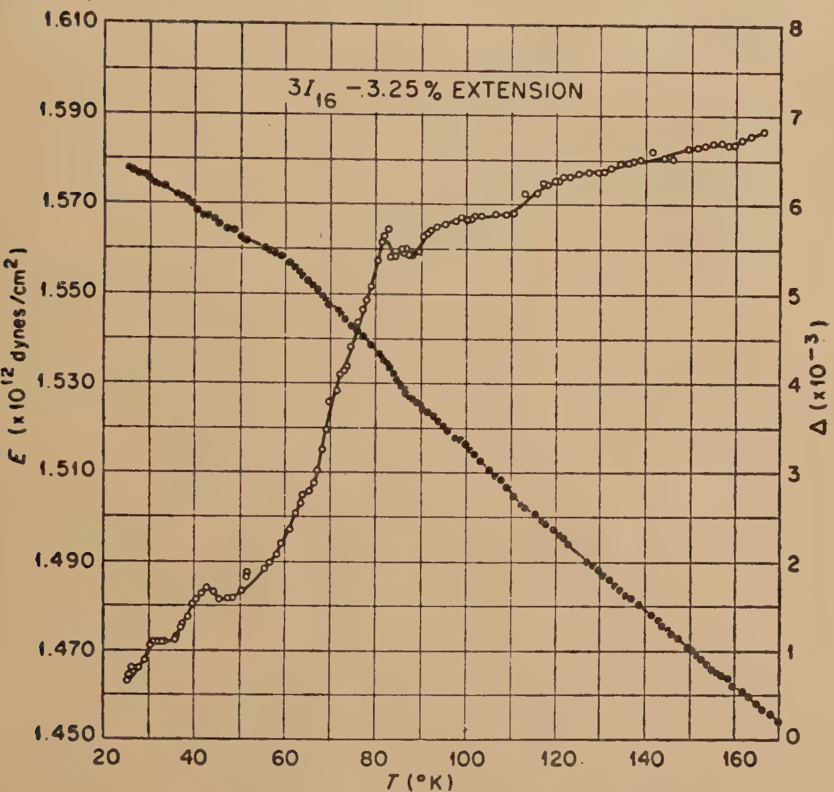

The internal friction and Young's modulus of a copper single crystal deformed 3·25% (Thompson and Holmes 1959).

Thompson and Holmes also analysed the modulus curve for an annealed copper single crystal. This indicated the presence of internal friction peaks at 30°, 40°, 85° and 96°K, with the 85°K peak again being the largest.

2.4. *Discussion*

The theory of Seeger (1956) and of Seeger *et al.* (1957) accounts for nearly all the main features of the Bordoni peak. In particular, it leads to an activation energy which is an intrinsic property of the dislocations, being independent of the separation of any pinning points, so that the temperature at which the peak occurs is approximately independent of both the degree of cold work and the presence of impurities. In Seeger's original treatment, the activation energy was found to vary somewhat with the applied stress, which implied that the temperature of the peak should vary with the strain amplitude. However, the theory of Seeger *et al.* gives an activation energy which is independent of the strain amplitude provided it is not too large. This appears to be in agreement with experiment, although Caswell (1958) states that he observed no shift of the peak at strain amplitudes so high that some might have been expected. According to the theory the height of the peak should be independent of the frequency, and what evidence there is suggests that this is so.

Fig. 18

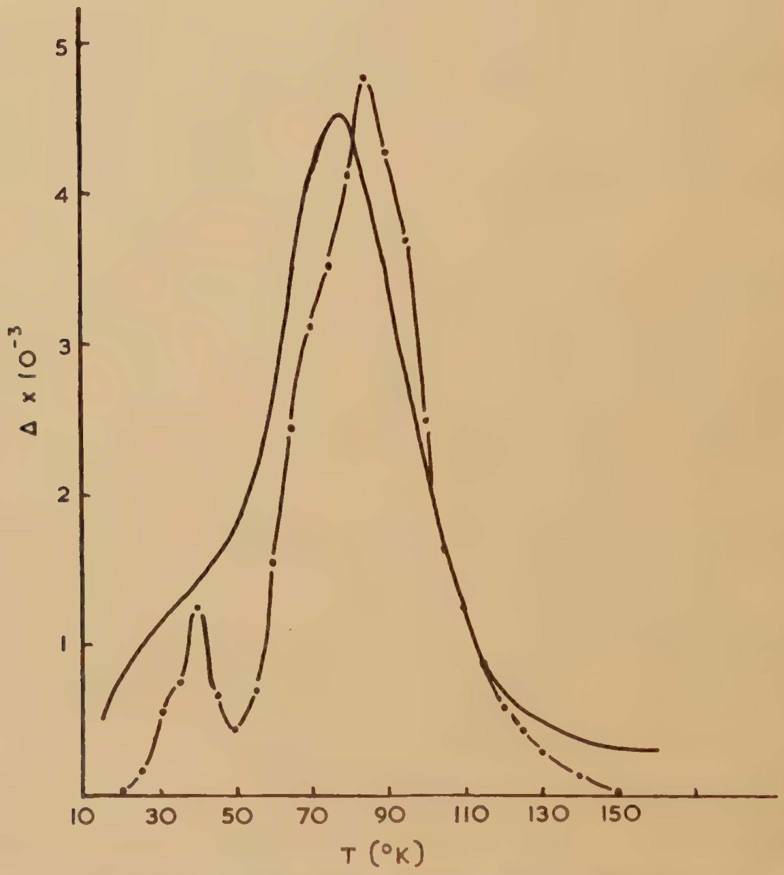

The solid line shows a Bordoni peak observed in polycrystalline copper. The curve with filled points is calculated from observations of the modulus of a lightly cold-worked copper single crystal (Thompson and Holmes 1959).

The only real difficulty with the above theories is that they lead to a peak only about half as wide as that observed. The treatment of Thompson and Holmes (1959) overcomes this difficulty by decomposing the observed peak into an overlapping spectrum of peaks, each with a unique activation energy. Seeger (1956) had previously explained the two internal friction peaks observed by Niblett and Wilks (1955) as being due to dislocations in [110] directions with the Burgers vectors making angles of 0° and 60° with their length. Screw and mixed dislocations would be expected to have different Peierls stresses, and hence to give rise to internal friction peaks with different activation energies. Thompson and Holmes propose that the four peaks present in annealed material are associated with dislocations in [110] and [112] directions, each with two different orientations of the Burgers vector. It is not obvious how one is to account for the additional component peaks in their cold-worked specimens.

The concept of a series of activation energies is in agreement with observations described above that the temperature of the peak is slightly affected by cold work, annealing and irradiation. All these processes may be expected to produce somewhat different effects on dislocations in different orientations. Hence, the total friction compounded of the several individual component peaks may have its maximum at a somewhat different temperature. It is also possible that the activation energy may not be sharply defined even for dislocations in a given orientation. In general, dislocations will be in a considerable stress field, and in such cases the activation energy may be somewhat modified, as is suggested by Thompson and Holmes' remark that the details of the modulus curves of single crystals are destroyed by an increasing amount of cold work (see also Paré 1958). A further point of importance which has also been ignored is that the dislocations in copper are separated into two partial dislocations (Seeger 1954). (All the treatments make the reasonable assumption that both partials behave as if they were rigidly bound together.) It would be of interest, not only in connection with the Bordoni peak, but for all types of internal friction, to pursue this point further.

If one assumes values for the mass per unit length and the line tension of a dislocation, the only unknown parameter in the expression for the activation energy given by Seeger *et al.* is the Peierls stress τ_p. Hence, one can use the experimentally determined value of the activation energy to estimate a value for this force. Seeger *et al.* assumed that the line tension E_0 of the dislocation was equal to $\frac{1}{2}G\mathbf{b}^2$, where G is the shear modulus, and $\mathbf{b}$ is the Burgers vector, and that the effective mass per unit length m is E_0/v^2 where v is the velocity of transverse sound waves. Using the activation energy determined from the measurements of Bordoni (1954) and Niblett and Wilks (1955) they deduced the value of the Peierls stress in copper to be approximately $4 \times 10^{-4} G$. This value is similar to that calculated theoretically by Dietze (1952) and Seeger (1955), but is appreciably higher than values found experimentally for the yield stress in copper single crystals by, for example, Blewitt (1953). Seeger (1956) attributes this difference to the fact that all the dislocations involved in the internal friction mechanism are lying along close-packed directions in the crystal lattice, whereas the crystal will also contain a much larger number of dislocations lying in other directions where they experience a much smaller effective Peierls stress. However, these dislocations cannot contribute appreciably to the total strain before they too become held up at the Peierls barriers. Thus further work is still required on the relation between the Peierls stress and the Bordoni peak and the critical shear stress, possibly taking into account the fact that the dislocations are split into partials (see also Niblett and Wilks 1957).

The theory accounts qualitatively for the observed dependence of the peak height on cold work and annealing and on the impurity content of the material. The initial increase of the internal friction with cold work is associated with an increase in the number of dislocations. For larger amounts of cold work the number of dislocations will continue to increase, but the average lengths of the loops will decrease so that the friction may not rise very rapidly (eqn. 19). Also because of mutual interactions, a smaller fraction of the dislocations may lie along close-packed directions for a sufficient distance to contribute to the friction. The fact that cross rolling increases the friction (§ 2.3.2) follows naturally by assuming that dislocations are being generated on hitherto inoperative slip planes. An anneal at a sufficiently high temperature reduces the number of dislocations present to such an extent that the peak almost completely disappears. The fact that the height of the peak in cold-worked copper may sometimes increase after annealing at a fairly low temperature is to be attributed to a reorientation of the dislocations present. This may result in longer loop lengths, with a larger fraction of them lying along lattice directions and so contributing to the internal friction (Niblett and Wilks 1959 b). Such a reorientation of dislocations may also account for the fact that Clarebrough *et al.* (1955) observed the release of stored energy in cold-worked copper at comparatively low temperatures where measurements of the thermal conductivity (Kemp *et al.* 1959) give no indication of any reduction in the density of the dislocations. That smaller Bordoni peaks are observed in impure material, or after neutron irradiation, can be attributed to pinning of the dislocation segments by impurity atoms and point imperfections respectively, and a consequent reduction in the effective lengths of the dislocation loops.

One cannot make an exact estimate of the height of the peak in any given specimen, for this depends on the dislocation density, the fraction of dislocations lying in favourable orientations, and the distance which the two kinks forming the initial bulge are able to move apart. None of these factors is known with any great accuracy. However, by making reasonable assumptions for the dislocation densities and the distance between pinning points, it appears that between 0·1 and 1·0 parts per cent of the dislocations must lie in favourable orientations, (Seeger *et al.* 1957, Niblett and Wilks 1957). This seems a reasonable figure, particularly as the Peierls stress is quite small compared with the other forces acting on the dislocations. Electron micrographs (see, for example, Hirsch *et al.* 1956) do not show much evidence of dislocations lying parallel to lattice directions, but the critical length of a bulge is about 60 atoms, so that the mechanism should occur if runs of dislocation of the order of a few hundred angstroms lie along close-packed directions. These could well be present and not show up clearly in the existing photographs.

It is to be noted that a very marked feature of the Bordoni peaks is their reproducibility and independence of strain amplitude. In this respect polycrystalline materials are superior to single crystals; although Bordoni peaks are observed in single crystals, they are often superposed on a greater amount of background friction and their analysis is correspondingly more difficult. The peaks give a very definite indication of the state of a system of dislocations, and may be used to follow changes in such a system, as for example, in the annealing studies described in § 2.3.6. Finally, we recall again that most of the work on the peaks has been done on copper, mainly for reasons of convenience, and that more information on other metals would be of interest.

Bruner (1959) has criticized Seeger's theory on the grounds that it should be equally applicable to body-centred cubic metals as to face-centred cubic lattices, whereas his measurements suggest that no Bordoni peak occurs in iron. However, as he himself points out, it is possible that impurities in the iron might have reduced the size of the peak so that it is hidden by the unexplained damping occurring at low temperatures. Measurements on body-centred cubic metals of high purity are required to clarify this point.

In order to account for the fact that he observed no Bordoni peak in iron, Bruner suggested that a rather different relaxation mechanism is responsible for the peaks. In face-centred lattices the dislocations are split into partials, and if there is a point defect situated in a plane adjacent to the slip plane of a dislocation, then the dislocation will tend to take up a position such that one or the other partial is immediately below the point defect. Hence, Bruner proposed that the friction may arise as the dislocation flips from one position to the other under the applied stress, and he calculated values of the activation energy and attempt frequency for the mechanism, which are of the same order of magnitude as those observed for the Bordoni peak. The calculation leads to a peak height which is proportional to the number of point defects per unit length of dislocation, and Bruner suggested that the point defects involved are vacancies. We might then expect the height of the peak to be reduced by an anneal at a comparatively low temperature, whereas in large-grained copper there is (as we mentioned in § 2.3.6) no change until an annealing temperature of about 300 °C. We might also expect that neutron irradiation would (at least on some occasions) increase the size of the peak by producing a greater concentration of vacancies; but this has never been observed. It therefore seems unlikely that the Bordoni peak arises in this way. It is, however, possible that Bruner's mechanism is responsible for the peak observed in copper at about 200 °K which we discuss in § 5.4 This peak has been reduced by an anneal of one hour at 100 °C (Niblett and Wilks 1959b), and on at least one occasion has been produced by neutron irradiation (Thompson and Holmes 1959).

§ 3. AMPLITUDE-DEPENDENT INTERNAL FRICTION AT LOW AND MEDIUM TEMPERATURES

3.1. *Introduction*

We now consider the internal friction which is common to all metals at low and medium temperatures whether or not they exhibit a Bordoni peak. This friction generally increases with increasing temperature, as may be seen in fig. 11 *a*, which shows the damping in lightly cold worked copper; a small Bordoni peak is superposed on a large background of this other friction. In general, this internal friction depends on the amplitude of vibration, and several characteristic types of amplitude dependence have been reported. (It may be useful to note here that it is considerably more

Fig. 19

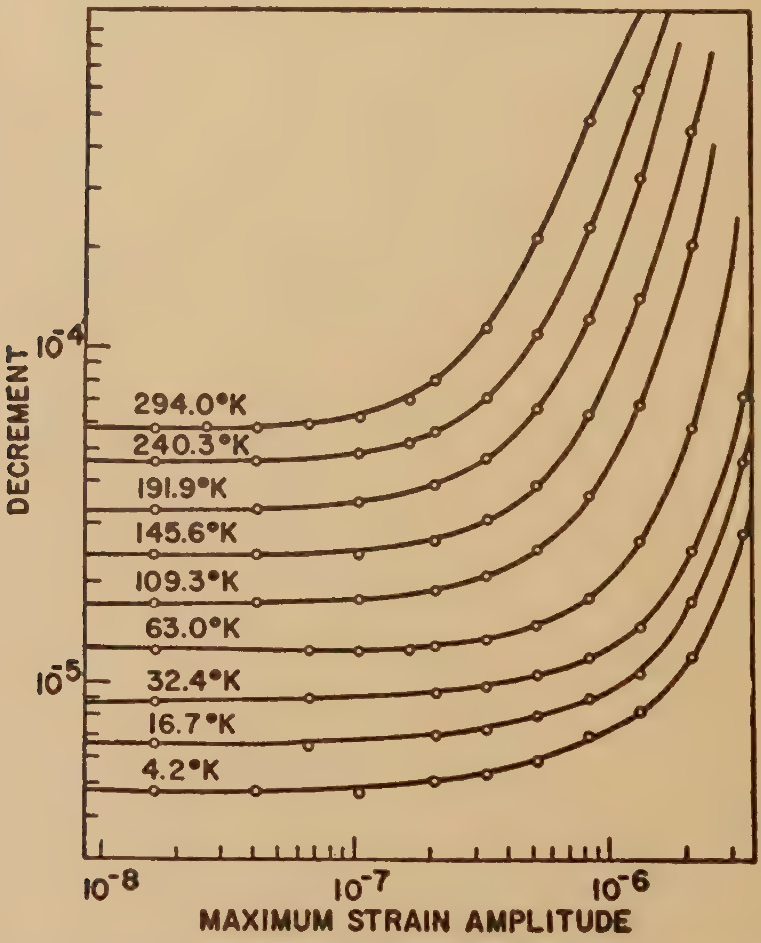

The internal friction of a copper single crystal as a function of strain amplitude and temperature measured at about 40 kc/s (Caswell 1958).

difficult to obtain absolute values of strain amplitude than relative ones; therefore absolute values should always be regarded with a certain amount of reserve.) Figure 19 shows measurements by Caswell (1958) on an annealed pure copper single crystal at various temperatures; these are typical of the kind of amplitude dependence most frequently observed. In other measurements, such as those by Nowick (1950 b) on slightly cold-worked copper single crystals (figure 20) the 'breakpoint' at which the decrement becomes amplitude dependent is somewhat less well defined. The form of these curves suggests that two different mechanisms are responsible for the friction, and it is usual to resolve the total decrement Δ into two components

$$\Delta = \Delta_I + \Delta_H \qquad (22)$$

Fig. 20

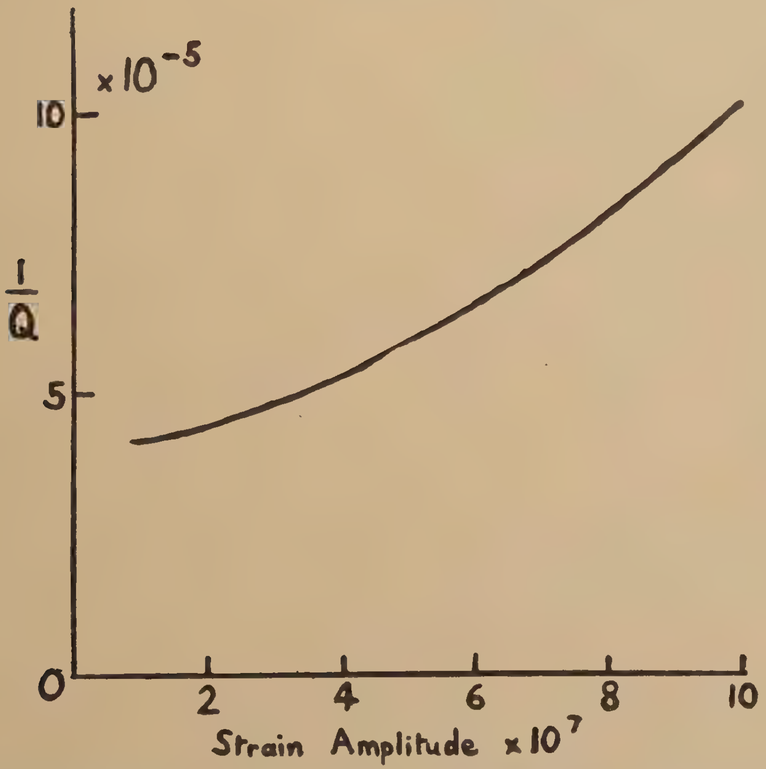

The internal friction of a copper single crystal strained by 190 p.s.i., measured at 39 kc/s (Nowick 1950 b).

where Δ_I is the decrement observed at very small amplitudes, and the remainder Δ_H is the amplitude-dependent component. Although the mechanisms responsible for these components may not be independent of one another (see § 3.4) it is convenient to examine the data by resolving it in this way. In the present chapter we discuss the behaviour of the component Δ_H at temperatures of the order of room temperature and below.

3.2. *Theory of Granato and Lücke*

The only extensive treatment of the amplitude dependent friction is due to Granto and Lücke (1956 a, b). Their theory is based upon an earlier idea of Koehler (1952) who pointed out that the dislocations in a metal will oscillate under the influence of an applied stress in the manner of a stretched string. As previously, it is assumed that if a dislocation is split into partials, both partials will move together so that we have to deal with effectively only one dislocation. The dislocations will be pinned down by impurity atoms and by the nodes of the dislocation network; in most cases impurities will pin the dislocations at more frequent intervals than the network nodes. Thus at low stresses the lengths of dislocation between impurity atoms (of average length L_c) will vibrate, as shown in fig. 21 (*a*).

Fig. 21

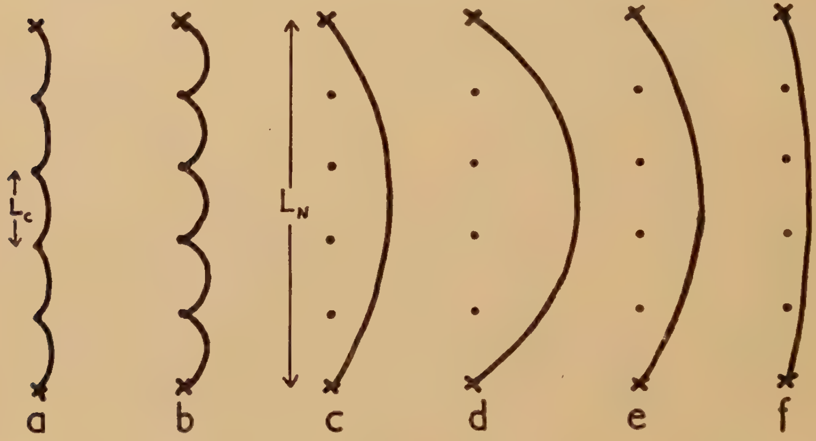

Schematic representation of the bowing out and unpinning of dislocation loops by an increasing and decreasing applied stress. Dots represent impurity pinning points, crosses represent network pinning points (after Granato and Lücke 1956 a.).

However, if the applied stress is increased sufficiently, the dislocations are pulled away from the impurity atoms, and are only pinned at the nodes of the dislocation network (fig. 21 (*c*)), which are separated by a mean distance of L_N. Two types of internal friction result from this model. The first, a dynamic loss due to the damping of the vibrating dislocation segments, is independent of the strain amplitude, and will be discussed in § 5. The second loss arises from the unpinning of the dislocations from the impurity atoms, and gives rise to the amplitude-dependent friction.

Figure 21 (*a*), (*b*), (*c*), (*d*) shows the motion of a dislocation under the action of an increasing stress sufficient to unpin all the impurity atoms, and fig. 21 (*d*), (*e*), (*f*) shows the motion as the stress is decreased. (The unpinning process as the stress increases is a catastrophic one, since the longest segments between impurity atoms can be unpinned most easily. The first unpinning occurs when the stress is sufficient to unpin the longest segment; this creates a longer free length and the unpinning continues.) The stress–strain curve (fig. 22) follows different paths for increasing and decreasing applied stress, giving rise to a hysteresis loss whose magnitude is equal to the shaded area in the figure. The internal friction is given by the relation

$$\Delta = \frac{\Delta W}{2W} = \frac{\Delta W}{\sigma_0{}^2/G} \quad . \quad . \quad . \quad . \quad . \quad . \quad . \quad . \quad . \qquad (23)$$

where σ_0 is the maximum amplitude of the oscillating stress, G the shear modulus, and ΔW the area of the hysteresis loop.

Fig. 22

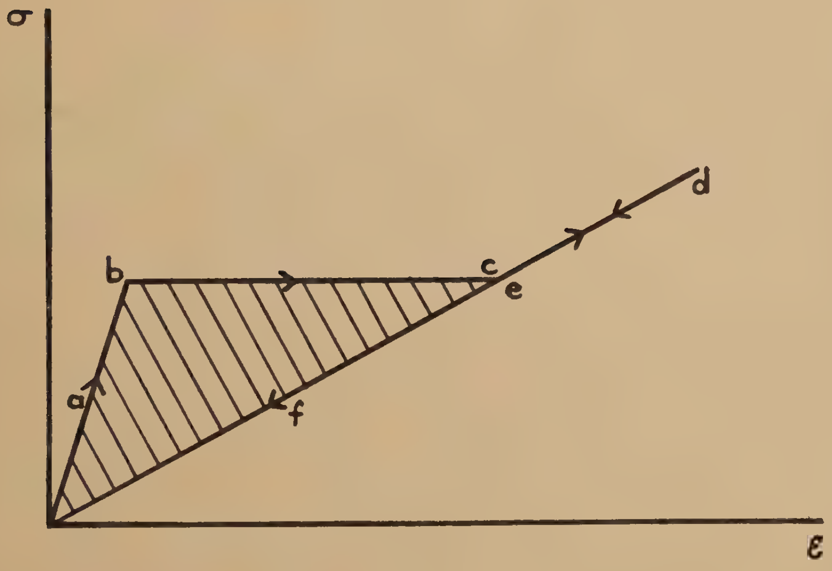

The stress–strain law resulting from the model shown in fig. 21. The elastic strain has been subtracted out so that only the dislocation strain is shown (after Granato and Lücke 1956 a).

In order to calculate the mean area of the loop for the random distributions of dislocations and impurities in a real crystal, Granato and Lücke make two simplifying assumptions. Firstly, that the distance L_N between network nodes is constant for a given specimen, and secondly, that the distribution of the impurities along the dislocations follows an exponential law such that the number of dislocation segments with length between l and $l+dl$ is given by

$$N(l)dl = \frac{\Lambda}{L^2} \, . \exp\left(-\frac{l}{L}\right) . \, dl \quad . \quad . \quad . \quad . \quad . \quad . \qquad (24)$$

where Λ is the dislocation density and L the mean length of a segment.

Using these assumptions Granato and Lücke calculated the internal friction to be

$$\Delta_H = \frac{\Omega\Lambda L_N{}^3}{\pi^2 L_c}\frac{K\eta a}{L_c\epsilon_0}\exp\left(\frac{-K\eta a}{L_c\epsilon_0}\right) \quad . \quad . \quad . \quad . \quad . \quad (25)$$

where the symbols have the following meaning: Ω is an orientation factor which takes into account the fact that the resolved shear stress on the slip planes is less than the applied stress, K is a factor (also dependent on orientation) connected with the stress required to produce unpinning, η is Cottrell's misfit parameter, a the atomic spacing, L_c the mean distance between impurity atoms pinned to dislocations, and ϵ_0 the maximum value of the oscillating strain. The modulus change is found to be given by

$$r\left(\frac{\Delta E}{E}\right)_H = \Delta_H . \quad . \quad . \quad . \quad . \quad . \quad . \quad . \quad . \quad . \quad (26)$$

where r is a constant of order unity.

As we discuss in the subsequent paragraphs, this theory gives quite a good account of the amplitude-dependent friction in many specimens. In view of the large number of parameters in the theory, some of which can only be roughly estimated, it is difficult to make a firm comparison between the predicted and observed *magnitudes* of the friction. However, the estimated values are generally reasonable. Much more stringent tests of the theory are obtained by seeing how the friction varies when the various parameters in the theory are changed, and we now go on to consider this point. First, however, we note that, according to eqn. (25), a graph of $\ln(\Delta_H\epsilon_0)$ against $1/\epsilon_0$ should give a straight line if the theory is applicable; hence, such a plot provides a convenient means of examining the data. (Actually, if the maximum strain amplitude, ϵ_0, varies over the length of a specimen, a further integration must be performed to find the effective value of Δ_H. Thus, for a strain which is produced by a standing wave along the length of a specimen, we should plot $\ln(\Delta_H\epsilon_0{}^{1/2})$ against $1/\epsilon_0$ (Granato and Lücke 1956 b). Although this point is often overlooked, it fortunately does not make much difference in practice.)

3.3. *Experimental Observations*

In this section the experimental data on amplitude-dependent internal friction will be examined in terms of the various parameters involved, and the results discussed according to the theory of Granato and Lücke.

3.3.1. *Time-dependent effects*

Before giving the experimental results, it is necessary to point out that considerable care must always be observed in measuring amplitude-dependent friction because the condition of the material is often modified by the measurement itself. Not infrequently the shape of the graph of decrement against amplitude above the breakaway amplitude is not reversible; the damping observed while decreasing the amplitude being greater than that when the amplitude is being increased. Amplitude dependence of this type has been observed in single crystals of zinc by Read (1940), Read and Tyndall (1946) and Swift and Richardson (1947). A particularly good example of irreversibility is shown in figure 23, in which the sequence of measurements is shown by the letters and the arrows on the curves (Wert 1949). Read also showed that initial measurements could only be repeated if the specimen were allowed to rest for several days.

Fig. 23

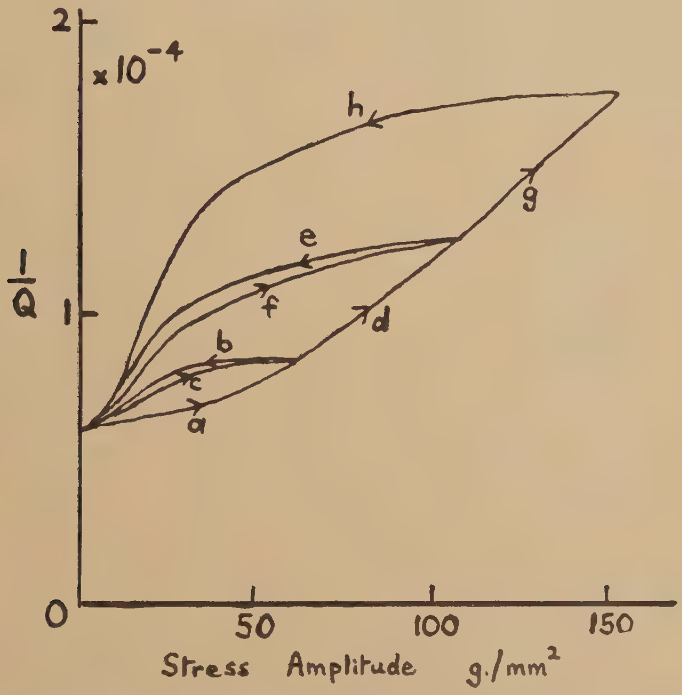

Irreversible amplitude dependence of the internal friction of a zinc single crystal. The letters and arrows indicate the order of measurement (Wert 1949).

A detailed study of time-dependent effects has been made by Chambers (1957) on single crystals of aluminium and magnesium. He showed that the state of a crystal was changed if it was vibrated for a considerable time at strain amplitudes at which the decrement was amplitude-dependent. However, reproducible amplitude-dependence curves were obtained if the measurements at high strain amplitudes did not involve vibrating the specimen for longer than one or two seconds. Chambers also showed that the increase in damping caused by the high-amplitude vibrations disappeared fairly rapidly after these vibrations were stopped, and the initial amplitude-dependence curve could be reproduced a few hours later. Figure 24 shows the damping of an aluminium single crystal excited for various times at a constant strain amplitude at 60°c, and the subsequent decay of the decrement at the end of the excitation periods. (All the internal friction measurements were made very rapidly at the same strain amplitude as the excitation amplitude.) The decrement Δ decayed according to a law of the form

$$\Delta-\Delta_0=(\Delta_1-\Delta_0)\exp(-\beta t^n) \quad . \quad . \quad . \quad . \quad . \quad . \quad . \quad (27)$$

where Δ_0 is the initial decrement, Δ_1 is the maximum decrement at the end of the excitation period, and t is the time after the end of the excitation period. The power of the time dependence, n, was found to be a function of the length of the excitation period, ranging from about $\frac{1}{3}$ for short excitations to about $\frac{2}{3}$ for long periods. The value of β is inversely proportional to the strain amplitude and is a function of the temperature. We return

Fig. 24

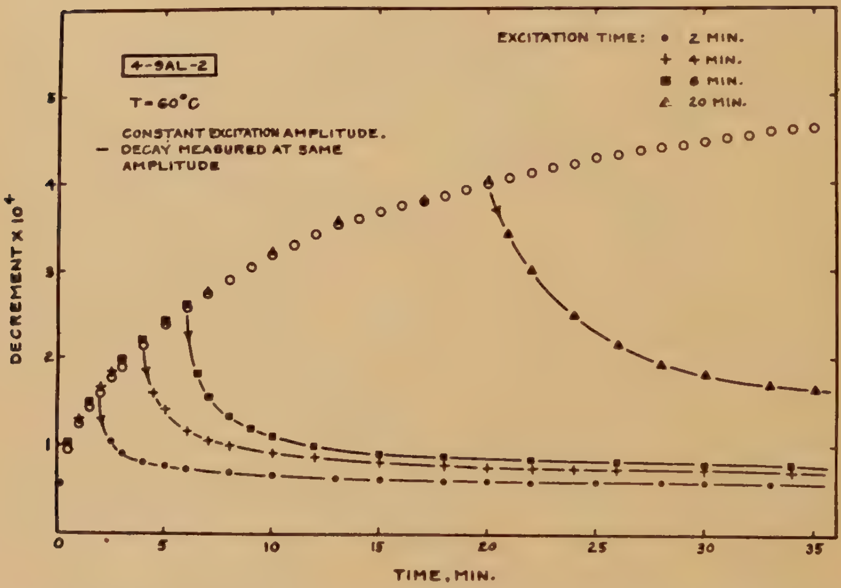

The internal friction of an aluminium single crystal, excited at a constant strain amplitude for 2, 4, 6 and 20 min, as a function of time. Measured at ~ 15 kc/s (Chambers 1957).

to this result in § 3.4, and only note here that time-dependent effects of this type have also been observed in copper single crystals by Kamentsky (1956) and by Beshers (1959). The latter author found that the amplitude-dependent decrement of pure copper crystals at temperatures above 150°c decayed with time after excitation according to a law of the form of equation 27, with a value of $\frac{2}{3}$ for n. Thus the amplitude-dependent friction is a function of the time for which the specimen has been vibrated at a high strain amplitude and of the time elapsed since previous high-amplitude vibration. Hence it is evident that any measurements of the amplitude-dependent internal friction must be treated with suspicion unless the possible existence of time-dependent effects has been investigated.

Finally, we mention that other complicated effects have been reported. Thus, fig. 25 shows the behaviour of an aluminium single crystal in which the friction may have either of two values at the same strain (Birnbaum 1955). This comes about because on increasing the drive voltage there is such a large increase in damping that the amplitude of the vibration is actually reduced.

Fig. 25

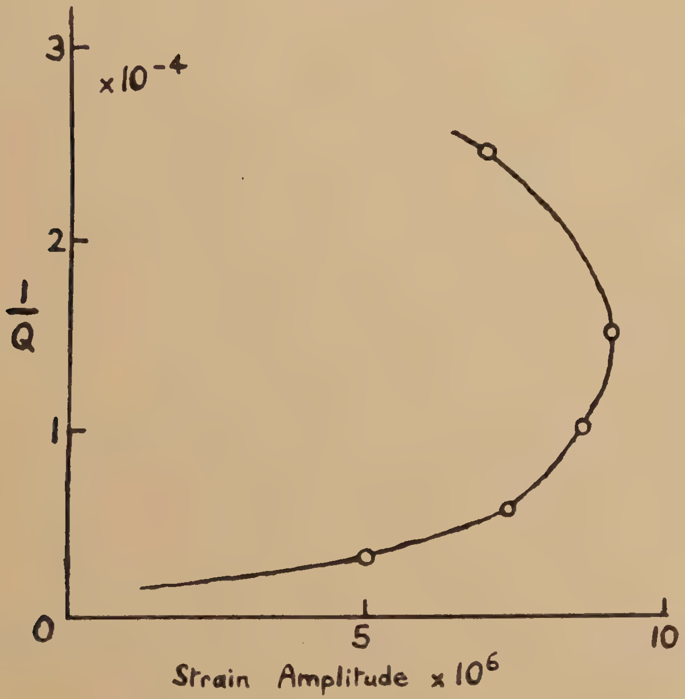

The internal friction of an aluminium single crystal at 126°K. As the force driving the crystal was increased, the friction rose so much that the strain amplitude fell (Birnbaum 1955).

3.3.2. *The effect of cold work*

Measurements by Read (1941) on copper single crystals show that small amounts of cold work cause an increase in the amplitude-dependent internal friction, this increase being monotonic for compressive loads up to 150 p.s.i. Read's results have been plotted by Granato and Lücke (1956 b) in the form of ln $(\Delta_H \epsilon_0)$ against $1/\epsilon_0$, and are shown in fig. 26. They are seen to give a series of approximately parallel straight lines, deviating from linearity at the lower amplitudes. These results have been interpreted by Granato and Lücke in the following way. The intercepts on the axis $1/\epsilon_0 = 0$ are proportional to $(\Lambda L_N{}^3/L_c{}^2)$, where Λ is the dislocation density, and L_N and L_c are defined in § 3.2 As all the lines have the same slope the value of L_c appears to be independent of the degree of cold work. One would expect that small amounts of cold work would create new dislocations rather than change the size of the existing net, so that L_N probably remains

Fig. 26

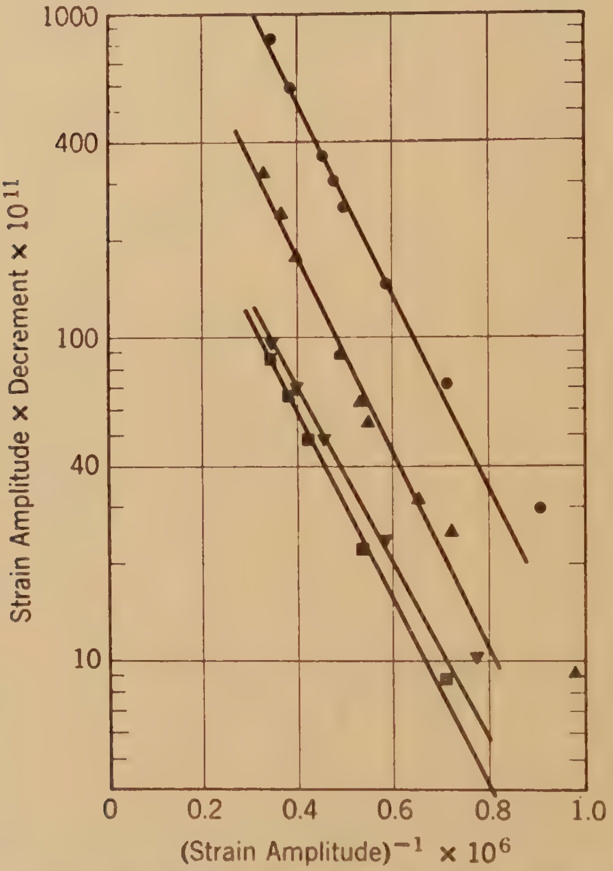

Granato and Lücke plots of the internal friction of a copper single crystal measured by Read (1941). The lowest curve is for the undeformed crystal, and the higher curves are for successive applications of compressive loads of 60, 120 and 150 p.s.i. (Granato and Lücke 1956 b).

fairly constant. Hence the value of the intercepts should increase with the increasing dislocation density consequent on cold work, as is observed.

Nowick (1950 a, b) has also shown that the amplitude-dependent internal friction of copper is steadily increased by the prior application of compressive stresses up to 365 p.s.i. Similar effects have been observed in zinc single crystals by Read and Tyndall (1946) and by Wert (1949).

Measurements by Weertman and Koehler (1953) on copper single crystals showed that, after an initial increase with small amounts of cold work, the amplitude-dependent internal friction went through a maximum value and then decreased with further deformation. After deformations of the order of 3000 p.s.i. the damping was practically independent of the strain amplitude for strains up to 10^{-5}. A similar decrease in the amplitude-dependent internal friction with increasing cold work has been observed by Caswell (1958) for a copper single crystal rolled by various amounts up to 4·8%. Niblett (1956), Caswell (1958) and Paré (1958) also report that the internal friction of strongly cold-worked copper shows very little amplitude dependence.

The fact that the amplitude-dependent internal friction goes through a maximum value as a function of cold work is in agreement with the theory. According to Granato and Lücke (1956 a) the decrement should be proportional to $\Lambda L_N{}^3$. The initial increase in decrement associated with the increase in dislocation density is offset when the density becomes so high that the mean network length L_N is reduced by further cold work. Since the cube of this term is involved, the decrement will eventually decrease with increasing cold work. Finally, when the dislocation density becomes so great that the mean network length becomes shorter than the mean separation of impurity atoms the unpinning process is no longer possible and no amplitude dependence is observed.

3.3.3. *The effect of purity*

The presence of impurities reduces the amplitude-dependent internal friction, as was shown by Read and Tyndall (1946) for zinc single crystals, and by Marx and Koehler (1950) for copper single crystals. Weertman and Salkovitz (1955) investigated this effect in detail in single crystals of lead containing up to one per cent of bismuth, tin or cadmium. Figure 27 shows their results for the lead-bismuth alloys at room temperature, as plotted by Granato and Lücke (1956 b) in the form of graphs of $\ln(\Delta_H \epsilon_0)$ against $1/\epsilon_0$. These plots give straight lines over the limited range of strain amplitudes involved, the slopes of the lines varying with the concentration of impurities. According to equation 25, the slope of this graph is $(-K\eta a/L_c)$, and therefore proportional to the concentration of impurity atoms on the dislocations. The slopes of the lines in fig. 27 are in fair agreement with this requirement.

The reduction of the amplitude-dependent internal friction of copper with increasing impurity concentration has also been observed by Weinig and Machlin (1956), Takahashi (1956), Caswell (1958) and Beshers (1959). Weinig and Machlin (1956) used polycrystalline copper wires containing up to 1% of aluminium or silicon; when plotted in the form of $\ln(\Delta_H \epsilon_0)$ against $1/\epsilon_0$ their results give quite good straight lines, but the slopes of these lines do not change much as the impurity concentration is varied, in contrast to those of Weertman and Salkovitz (1955). Takahashi (1956) has made measurements on polycrystalline copper containing small quantities of aluminium, zinc or phosphorus. He found that the amplitude-dependent internal friction could be represented by a relation of the form

$$\Delta_H = \beta \epsilon_0^{\alpha} \quad . \ . \ . \ . \ . \ . \ . \ . \ . \quad (28)$$

where the value of α increased with the concentration of impurity atoms, varying from approximately unity for pure copper to about 2·5 for copper containing 1% of zinc or phosphorus. Caswell's (1958) results for copper single crystals containing up to 0·5% gold give curved plots of $\ln(\Delta_H\, \epsilon_0)$ against $1/\epsilon_0$, and so the effect of the impurity concentration on the slope cannot easily be judged.

Fig. 27

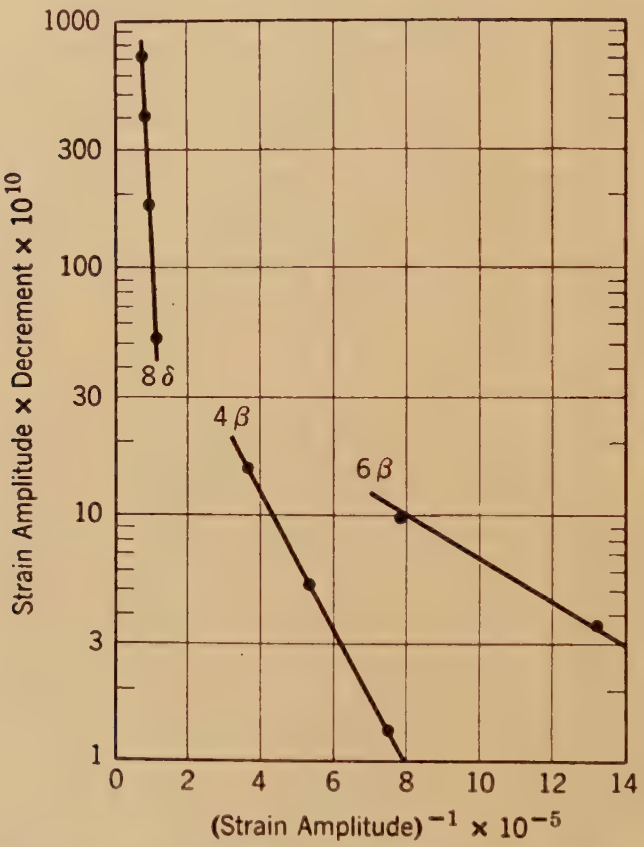

Granato and Lücke plots of the internal friction of lead single crystals with varying concentrations of bismuth measured by Weertman and Salkovitz (1955). The concentrations of bismuth are 0·035, 0·053 and 0·65% for the samples 6β, 4β and 8δ respectively (Granato and Lücke 1956 b).

3.3.4. *The effect of frequency*

There is not much information available concerning the frequency dependence of the amplitude-dependent internal friction. Read (1940) measured the amplitude-dependent damping of a zinc single crystal at 38 and 76 kc/s and found an approximately inverse frequency dependence. Nowick (1950 a) measured the amplitude-dependent internal friction of several copper single crystals at their fundamental frequencies (39 kc/s) and second harmonics; there is considerable scatter from specimen to specimen, but the results suggest that the damping may be independent of frequency. Measurements by Kamentsky (1956) on copper single crystals at various harmonics in the kilocycle frequency range are also somewhat scattered, but appear to show a tendency for the amplitude-dependent component of the internal friction to increase with increasing frequency. Hiki (1958) measured the internal friction of annealed single crystals of lead at their fundamental frequency (64 kc/s) and third harmonic, and found no frequency dependence in the amplitude-dependent component (fig. 28).

Fig. 28

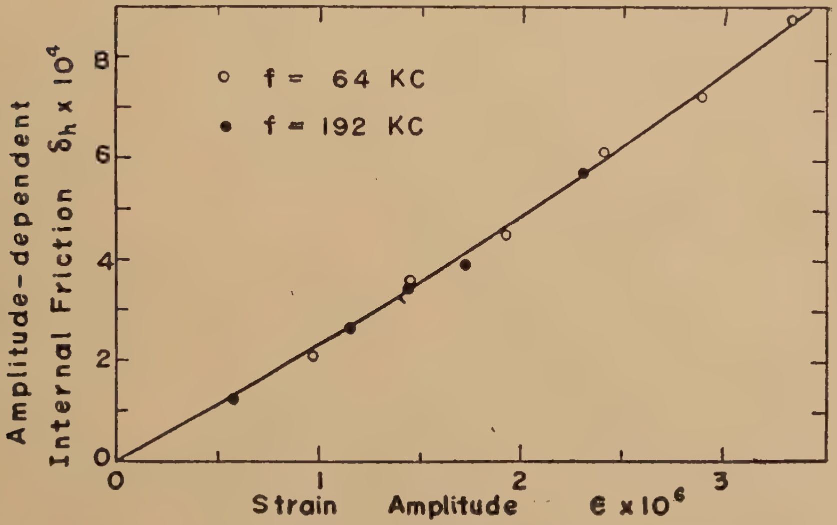

The amplitude-dependent friction of a lead single crystal at room temperature measured at two frequencies (Hiki 1958).

According to Granato and Lücke (1956 a) the amplitude-dependent internal friction should be independent of frequency. The experimental information is insufficient and too scattered either to verify or disprove this. The most satisfactory evidence in its support comes from the results of Hiki (1958). However, in his case the nature of the amplitude dependence observed does not agree very well with the theory of Granato and Lücke, a plot of ln $(\Delta_H \epsilon_0)$ against $1/\epsilon_0$ curving appreciably at the lower amplitudes. This discrepancy may be due to the fact that his decrement *decreases* with increasing amplitude at very low amplitudes, causing uncertainty in estimating a value for the amplitude-independent damping.

3.3.5. *The modulus defect*

The modulus defect associated with amplitude-dependent friction is readily obtained by observing the change in modulus with amplitude. (If a resonant bar method is used, the modulus defect is related to the change in frequency by $\Delta E/E = 2\Delta f/f$.) Information is available for single crystals of zinc (Read 1940), aluminium (Chambers 1957) and copper (Kamentsky 1956), and for dilute copper alloys (Takahashi 1956). The characteristic feature of each set of results is that the modulus defect associated with the amplitude-dependent damping is related to the damping so that

$$\Delta_H \simeq r\left(\frac{\Delta E}{E}\right)_H . \qquad (29)$$

Fig. 29

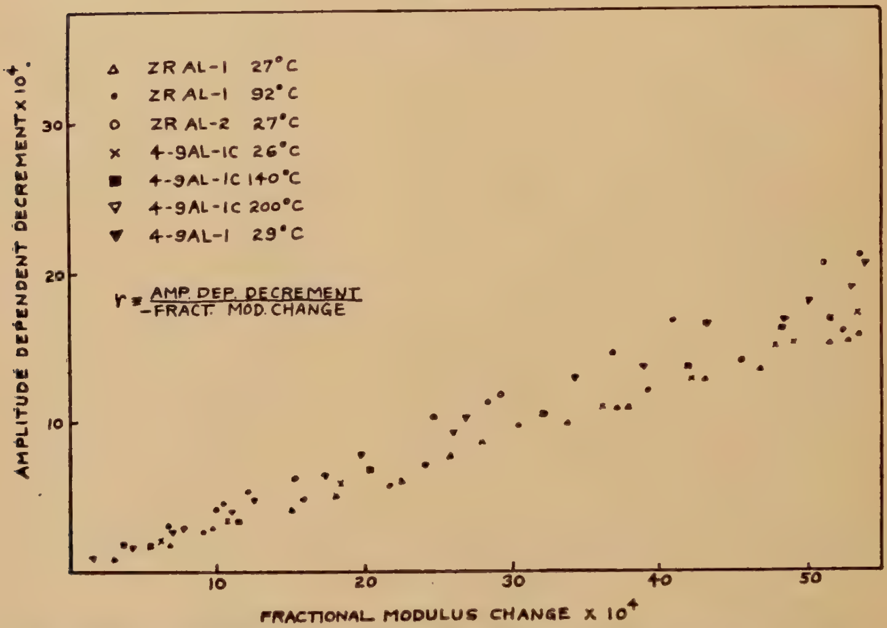

The change in modulus associated with the amplitude-dependent friction in several single crystals of aluminium (Chambers 1957).

where r is a constant. Figure 29 shows measurements of modulus defect and decrement for different aluminium single crystals at various temperatures. The two functions are quite closely proportional with the factor r having a value of about 0·4. Takahashi gives values for r of the order of unity, while Kamentsky reports various values between 0·15 and 6. According to Granato and Lücke (1956 a) the calculation of the modulus change in a particular specimen is quite complicated, but leads to the conclusion that $\Delta E/E$ should be proportional to Δ_H, with a value of r of the order of unity. This relation is probably typical of all types of friction arising from hysteresis loops in the static stress strain curve. (We note also that there is some evidence that the value of r depends on the orientation of the crystal, although this is not predicted (Granato and Lücke 1956 b).)

Fig. 30

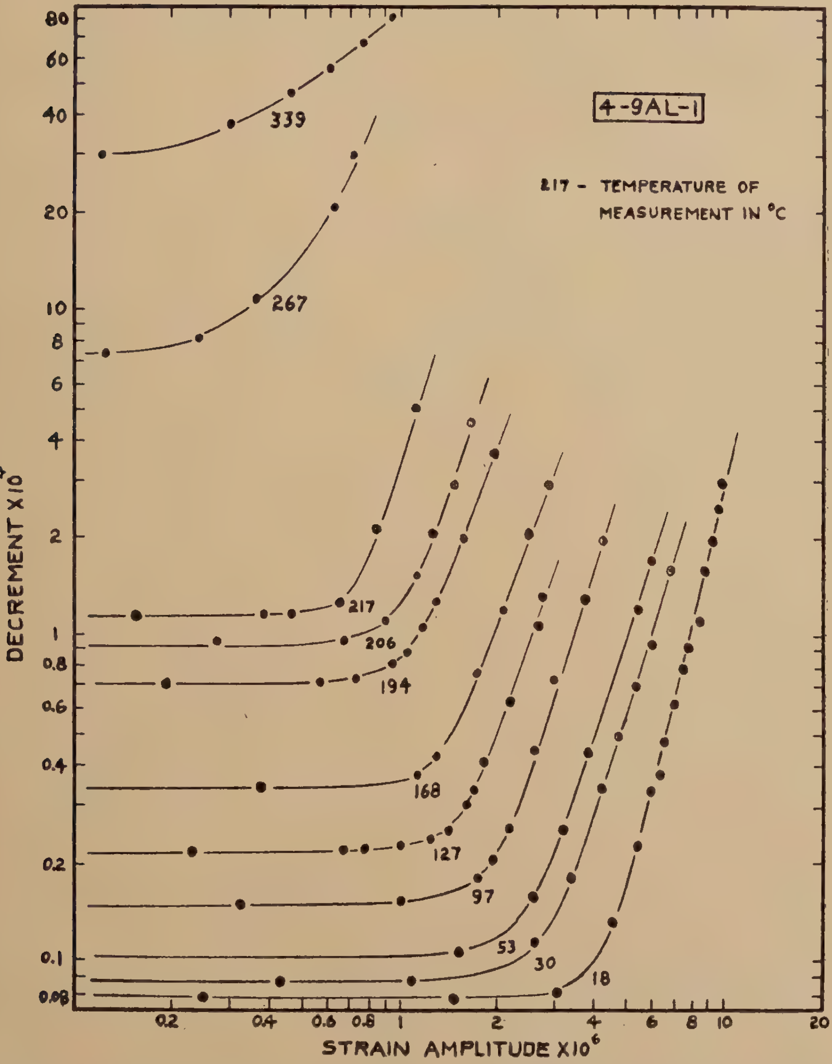

The internal friction of an aluminium single crystal measured at different temperatures and at ~15 kc/s (Chambers 1957).

3.3.6. *The effect of temperature*

There are two effects of temperature on the Granato and Lücke model. Firstly, the thermal energy at higher temperatures will aid the dislocation as it attempts to break away from pinning points. Thus, the breakpoint in the decrement-amplitude curve occurs at lower strain amplitudes with increase of temperature as may be seen, for example, in Chambers' (1957) results on aluminium (fig. 30). From this shift it follows that the activation energy associated with the unpinning process is about 0·1 ev. However, the detailed effect of thermal activation on the amplitude-dependent decrement is difficult to calculate and is ignored by Granato and Lücke.

The second effect of temperature will be to change the equilibrium concentration of impurity atoms on the dislocations according to the relation, given by Cottrell (1948),

$$C = C_0 \exp(Q/kT) \quad . \quad . \quad . \quad . \quad . \quad . \quad . \quad . \quad (30)$$

where C_0 is the mean concentration of impurities in the lattice, and Q is the interaction energy between a dislocation and an impurity atom. Since the value of L_c is inversely proportional to C, the slopes of the lines obtained when plotting $\ln(\Delta_H \epsilon_0)$ against $1/\epsilon_0$ should decrease with increasing temperature. Also, since this slope is proportional to the concentration of impurity atoms on the dislocations, a plot of the logarithm of the slope against the inverse temperature should give a straight line of slope Q/k if the Cottrell pinning mechanism is operative. Figure 31 shows Chambers' plot of $\ln(\Delta_H \epsilon_0)$ against $1/\epsilon_0$ for a series of temperatures from 18°c to 339°c. For temperatures below 200°c, the logarithms of the slopes of the lines plotted against the reciprocal of the absolute temperature give a straight line corresponding to an interaction energy of about 0·12 ev in reasonable agreement with the value deduced from the shift of the breakpoint.

Similarly, Weertman and Salkovitz (1955) have made measurements at 25°c, 152°c and 306°c on a single crystal of lead containing 0·058% tin. An examination of the temperature dependence of the breakpoint leads to an activation energy of 0·10 ev, while Granato and Lücke plots give a value of 0·11 ev (Granato and Lücke 1956 b). These values may be compared with the value of 0·044 ev from the Cottrell misfit formula. Other measurements above room temperature have been made by Wert (1949) on zinc and by Kamentsky (1956) on copper.

Almost all observations of amplitude-dependent friction arising from the unpinning processes show that the damping increases with increasing strain amplitude and temperature; however, the theory implies that eventually the friction must decrease again. As the amplitude is increased the value of ΔW in eqn. (23) will approach a limiting value corresponding to the unpinning of all the dislocations, while σ_0 will continue to increase. Also at sufficiently high temperatures so much thermal energy is available that the dislocations are virtually free of the pinning points all the time. Often this decrease in the friction will be obscured by other types of friction which occur at high stresses (§ 3.4) and high temperatures (§ 4). However, Hiki (1958) has observed that, while below room temperature the internal friction of a lead single crystal increased with increasing amplitude, at higher temperatures it decreased with increasing amplitude (fig. 32). A similar temperature dependence has also been observed by Niblett and

Wilks (1959 b) in a specimen of polycrystalline copper which had been extended 5·7% and then annealed for one hour at 475°C. The friction for three values of strain amplitude is shown in fig. 33; Δ_H again decreases with increasing temperature at the higher temperatures.

Fig. 31

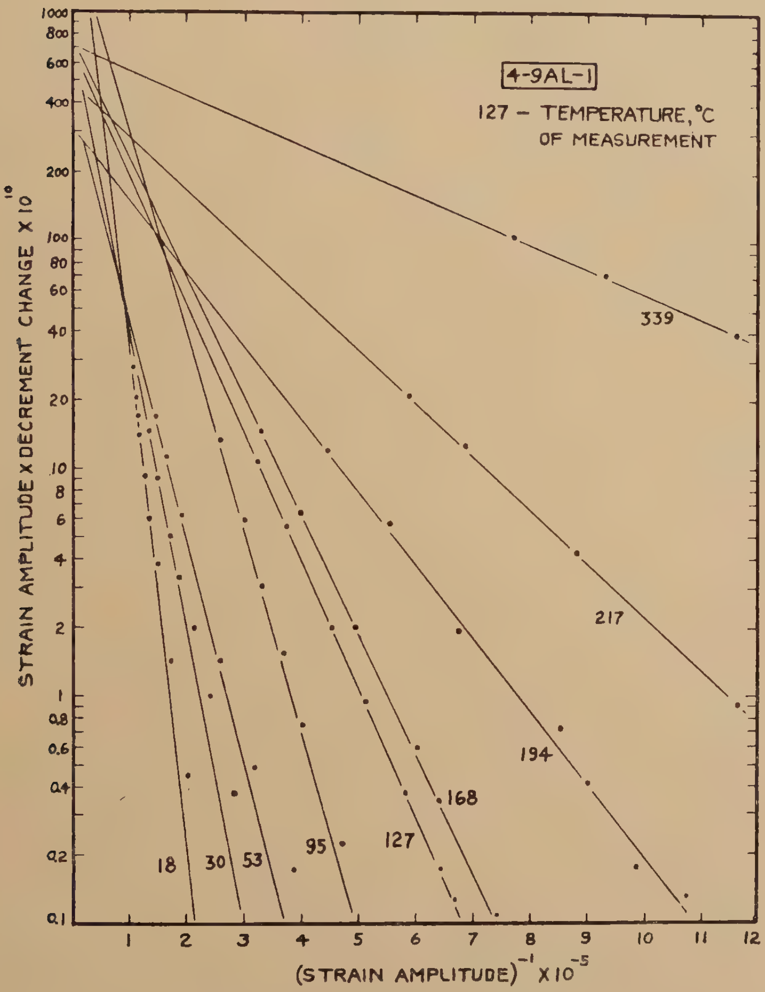

Granato and Lücke plots of the internal friction of the aluminium single crystal shown in fig. 30 (Chambers 1957).

At lower temperatures, Caswell (1958) has measured the internal friction of annealed copper single crystals from room temperature down to 4°K, and his results are shown as a function of strain amplitude in fig. 19. When these results are plotted in the form of $\ln(\Delta_H \epsilon_0)$ against $1/\epsilon_0$ they differ quite appreciably from straight lines, as shown in fig. 34. Although these curves are steeper at the lower temperatures, in agreement with the theory, it is not possible to obtain quantitative data from them on account of their curvature. Curves of a similar type were obtained by Niblett and

Fig. 32

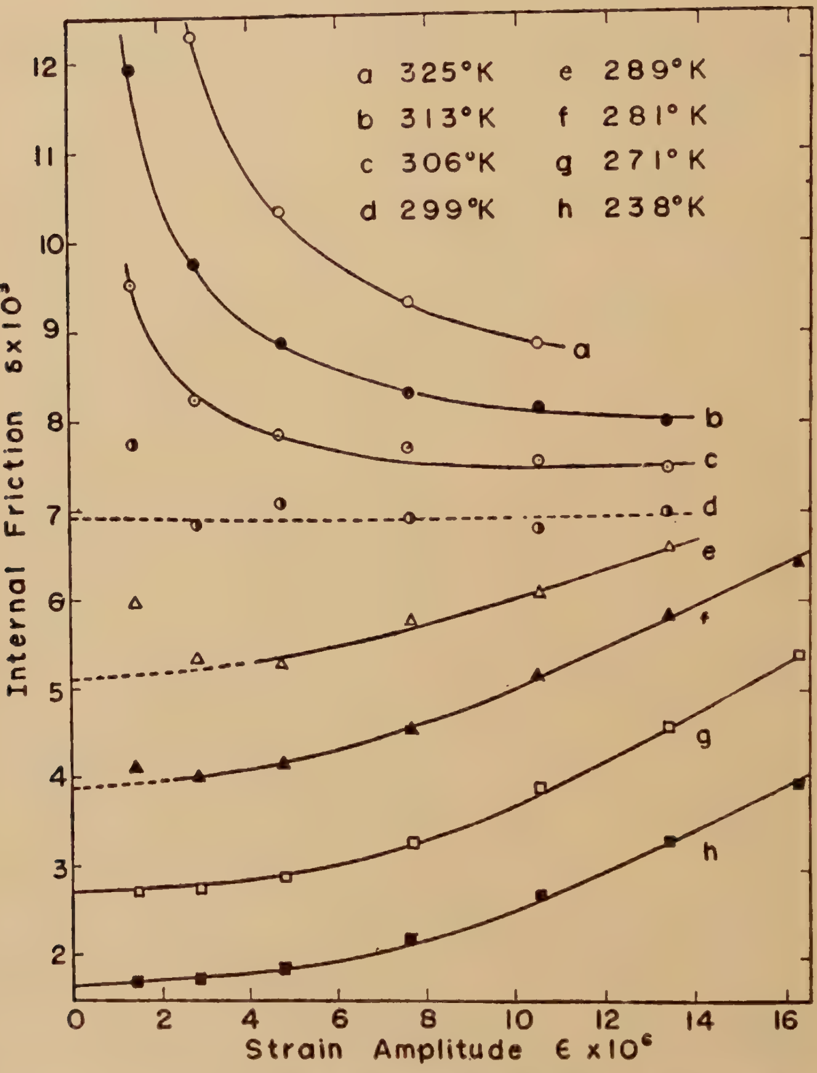

The internal friction of a lead single crystal at various temperatures as a function of strain amplitude, measured at 64 kc/s (Hiki 1958).

Wilks (1959 a) for polycrystalline copper between 20°K and room temperature. Nowick (1950 a) also observed that the amplitude-dependent internal friction of copper single crystals increased with increasing temperature in the range from −49°C to 33°C, but his results also give curved plots of ln ($\Delta_H \epsilon_0$) against $1/\epsilon_0$. (Similar curved plots are obtained from values for copper at room temperature reported by Barnes *et al.* (1958) and Thompson and Holmes (1956 b).)

Fig. 33

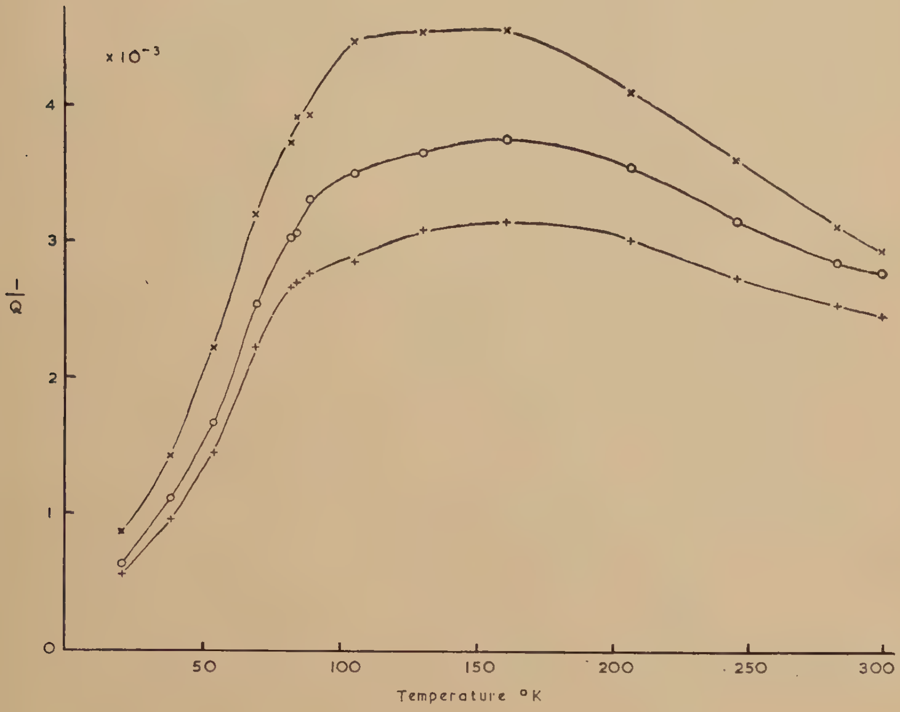

The internal friction of a specimen of polycrystalline copper, extended 5·7% and subsequently annealed for one hour at 475°c. Strain amplitudes; $\times\, 9\times10^{-7}$; $\circ\, 4{\cdot}5\times10^{-7}$; $+\, 2{\cdot}2\times10^{-7}$.

3.3.7. *The effects of quenching and irradiation and the Köster effect*

Both the amplitude-dependent and amplitude-independent damping of metals are reduced by quenching from a high temperature, and usually the faster the quenching the greater the reduction. This behaviour is illustrated by the results of Levy and Metzger (1955) in fig. 35, which shows the friction of a single crystal of aluminium annealed for one day at 640°c and then brought down to room temperature at various rates of cooling. (The decrement was measured after one to three days at room temperature to avoid certain time-dependent effects which we discuss later in this section.) The amplitude-dependent damping was considerably lower in air-cooled specimens than in furnace-cooled ones, while the damping of water-quenched specimens was practically independent of the strain amplitude.

Rather similar results have been obtained by Roswell and Nowick (1957) for polycrystalline gold cooled at various rates from 900°c, while measurements on copper have been reported by Barnes *et al.* (1958).

Fig. 34

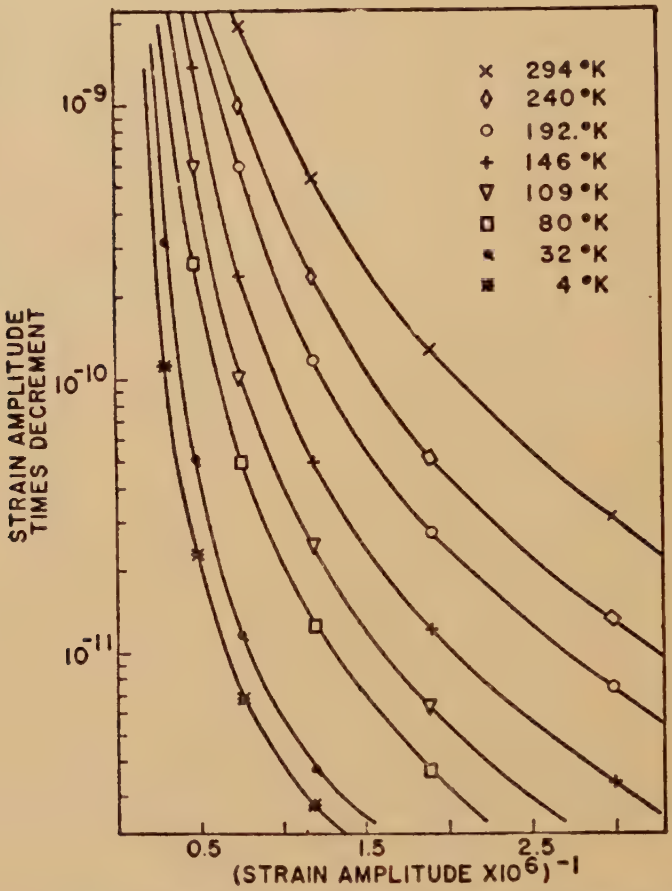

Granato and Lücke plots for the internal friction of an annealed single crystal of copper (Caswell 1958).

The main change of state produced by quenching a metal is to introduce vacancies, the concentration being greater the higher the initial temperature and the faster the rate of quenching. Therefore, the reduction in Δ_H appears to be due to quenched-in vacancies condensing on dislocations, as was suggested by Maddin and Cottrell (1955) to explain hardening consequent on quenching. These vacancies pin the dislocations and thus reduce the loop length and the internal friction. Although the results of Levy and Metzger give curved plots of ln $(\Delta_H \epsilon_0)$ against $1/\epsilon_0$, the slopes of these curves suggest that L_c has been reduced by the quenching.

The amplitude-dependent friction is also reduced by irradiation with either neutrons or γ-rays. Measurements on copper with neutrons have been made by Thompson and Holmes (1956 b), Barnes *et al.* (1958), and Barnes and Hancock (1958), and with γ-rays by Barnes *et al.* (1958). Most of these experiments were carried out at ambient temperature, but Barnes and Hancock also observed that when a copper single crystal was irradiated at 78°K, there was no decrease in the friction until the specimen was allowed to rest for several hours at room temperature. All these results may be explained if we assume that the decrease of friction is due to vacancies produced by the irradiation, which diffuse to the dislocations and pin them. Measurements of electrical resistance (see, for example, Broom and Ham 1957) suggest that vacancies are not mobile until about room temperature, hence irradiation at 78°K produces no effect unless followed by annealing.

Fig. 35

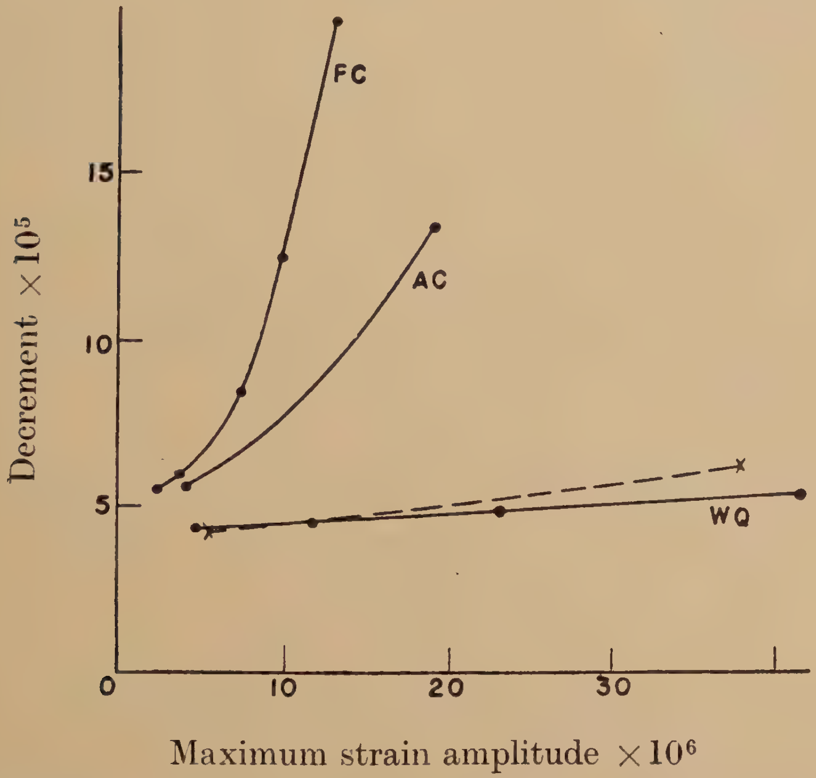

The decrement of an aluminium single crystal after various rates of cooling following anneals of one day at 640°C: FC, furnace cooled at 50°C hr^{-1}; AC, cooled in still air; WQ, two specimens quenched in water (Levy and Metzger 1955).

The diffusion of vacancies also seems to be responsible for the behaviour of the internal friction of metals subsequent to quenching. We have already mentioned that the values of the internal friction of quenched aluminium shown in fig. 35 were taken more than a day after the quenching, because at first the friction decreased with time and only slowly approached a steady value. Similar behaviour has been observed in quenched gold by Roswell and Nowick (1957). Immediately after the quenching the vacancies are distributed uniformly throughout the material and some time must elapse before they diffuse to the dislocations and reduce the friction.

A somewhat related phenomenon concerns the behaviour of the internal friction of metals immediately after plastic deformation. In general, deformation increases the friction, but subsequently the friction falls somewhat and does not reach its equilibrium value until after about a day (Köster 1940). This effect is observed in both the amplitude-dependent and amplitude-independent friction, and in each case appears to be due to vacancies produced during the plastic deformation diffusing to the dislocations. Granato *et al.* (1958) have calculated how the value of Δ_H should vary with time assuming that the number of vacancies, n, which have diffused to dislocations after time t is given by the relation of Cottrell and Bilby (1949)

$$n = A n_0 \Lambda t^{2/3} \qquad \text{. . . . .} \qquad (31)$$

where n_0 is the total number of vacancies, Λ the density of dislocations, and A a constant depending on the diffusion constant, the temperature and the interaction energy between a vacancy and a dislocation. Using the theory of Granato and Lücke to calculate Δ_H, it is then found that the friction should decrease with time according to the law

$$\ln \Delta_H = a - bt^{2/3} \qquad \text{. . . . .} \qquad (32)$$

where a and b are constants. The only detailed measurements are those of Gordon and Nowick (1956) on sodium chloride (fig. 36). There are often considerable differences in the behaviour of dislocations in ionic crystals and metals (see, for example, Pratt (1957)), but the theory should probably apply. In fact, if one takes Δ_H in Gordon and Nowick's experiment to be the difference of the two curves in figure 36, a plot of $\ln \Delta_H$ against $t^{2/3}$ gives a good straight line.

3.4. *Discussion*

The theory of Granato and Lücke generally gives a fair account of the dependence of Δ_H on strain amplitude, impurity concentration, temperature, frequency, cold work, irradiation and quenching. The modulus defect is also of the predicted order. Thus, there is little doubt that their account of the amplitude-dependent friction is essentially correct. We now briefly discuss its limitations and other difficulties which still remain.

As Granato and Lücke point out, their treatment is only valid for a certain range of impurity concentration. In very pure specimens there are no impurities to pin the dislocations, and there will be no contribution to Δ_H. However, as the length of dislocation line between network nodes is of the order of 10^4 atomic diameters, and as impurities congregate preferentially on dislocations, this limitation will only apply to extremely pure metals. In fact, all annealed metals seem to exhibit an amplitude-dependent friction. For high concentrations of impurities the length L_c becomes small and Δ_H tends exponentially to zero (eqn. (25)), and as is well known the friction of alloys tends to be independent of amplitude.

Fig. 36

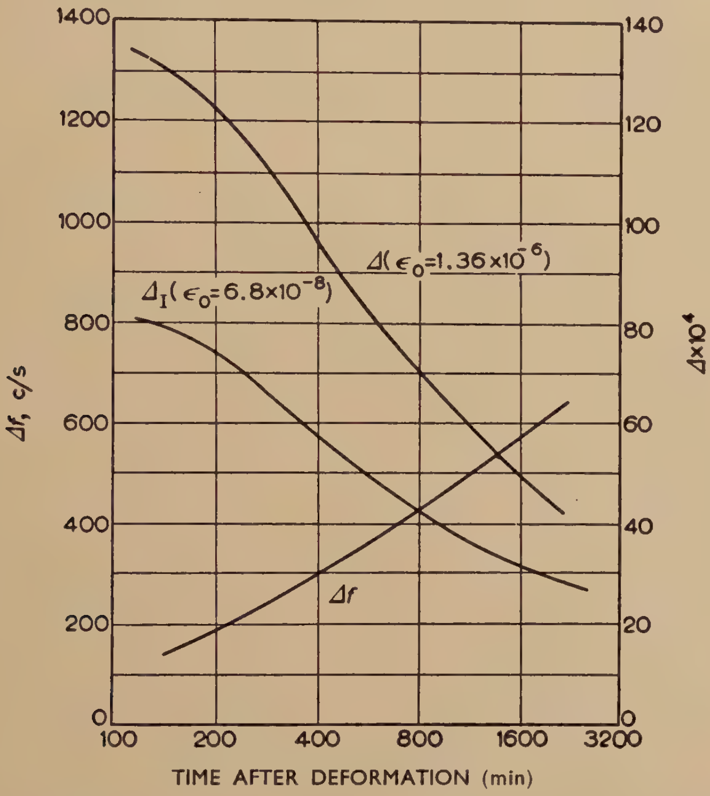

The internal friction and change in resonant frequency of a single crystal of sodium chloride at room temperature as a function of time after a deformation of 4·2% compression. The internal friction is measured at two strain amplitudes at ~85 kc/s (Gordon and Nowick 1956).

The theory is also inapplicable at strain amplitudes sufficiently high to unpin the dislocations from all the impurity atoms each cycle. When this point is reached, increasing the strain amplitude does not affect the area of the hysteresis loop in the stress-strain curve which will remain constant; hence, according to eqn. (23), the decrement will decrease with increasing amplitude, as has been observed by Hiki (1958). Often, however, at high strain amplitudes other forms of dislocation motion are possible, and these give rise to an increasing friction. Thus, Mason (1956) has measured the friction of single crystals and polycrystalline specimens of lead and aluminium of various purities at strain amplitudes in the range from 10^{-6} to 2×10^{-3}. Some typical results, on lead, are given in fig. 37; there appear to be three different amplitude regions: (1) below 10^{-5}, where the decrement is independent of the strain amplitude, (2) between 10^{-5} and about 2×10^{-4}, where the decrement increases with increasing amplitude in a reversible manner, and (3) above about 2×10^{-4}, where the decrement increases very rapidly and irreproducibly, and the metal fatigues in a short time. Mason points out that the rapid increase in internal friction at the highest strain amplitudes is probably due to the dislocation loops cutting through the pinning dislocations and producing jogs, vacancies and Frank–Read loops. There is not much information on internal friction at such high strains, but rather similar behaviour has been observed by Baker (1957).

Fig. 37

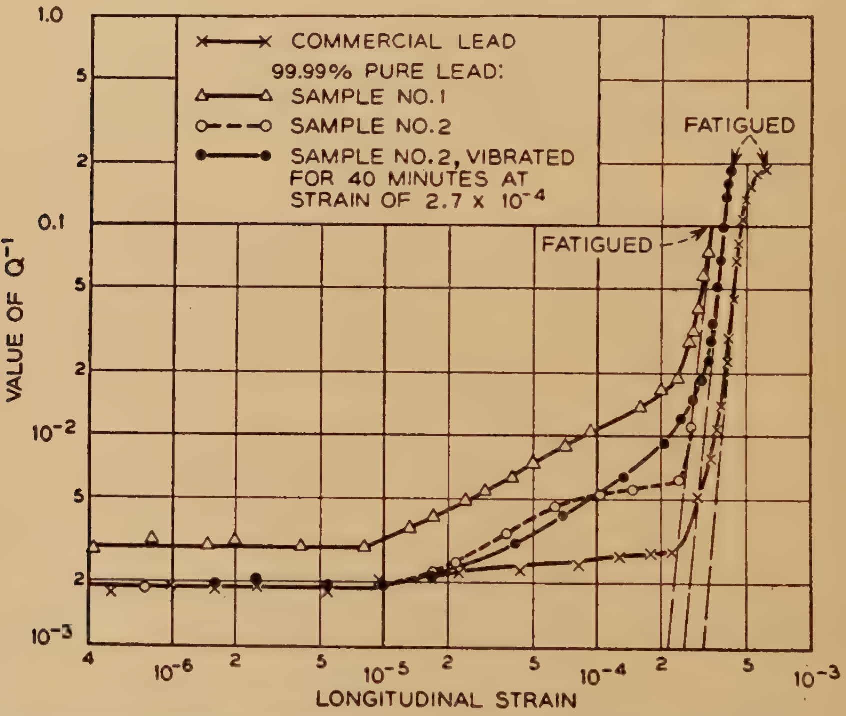

The internal friction of three samples of polycrystalline lead at room temperature as a function of strain amplitude measured at ~ 18 kc/s (Mason 1956).

Perhaps the most extensive discrepancy between theory and experiment concerns the results for copper (§ 3.3.6), where there is considerable evidence that Granato and Lücke plots of $\ln(\Delta_H\epsilon_0)$ against $1/\epsilon_0$ do not give straight lines. Possibly this discrepancy arises when we resolve the observed decrement Δ into two components,

$$\Delta=\Delta_I+\Delta_H \qquad (22)$$

and take Δ_I to be a constant component equal to the total damping at very small strains. It may be that the term Δ_I also increases with strain amplitude on account of the increase in loop lengths, in which case it becomes difficult to resolve the total friction into the two components Δ_I and Δ_H (Niblett and Wilks 1959 a). Filmer *et al.* (1959) have pointed out that some of their measurements on aluminium single crystals at 40 kc/s give decrements which may be resolved into a component of the form $\Delta_I = A + B\epsilon_0$ where ϵ_0 is the strain amplitude, and a second component Δ_H which gives good Granato and Lücke plots. Unfortunately, there does not seem to be any theoretical basis for Δ_I increasing linearly with strain amplitude. It would be particularly useful if this point could be cleared up because the temperature dependence of Δ_H is a matter of some interest, and the only extensive information on its behaviour at low temperatures is for copper.

The only effect of temperature considered by Granato and Lücke is that of changing the concentration of impurities clustered round dislocations, and this accounts quite well for the temperature dependence observed in aluminium and lead above room temperature. However, there is the further effect that the thermal energy assists the applied stress and produces more unpinning. At the higher temperatures, this is probably masked by the changing distribution of the impurities, but at sufficiently low temperatures the impurities will be immobile. In this case the temperature dependence of the friction should be quite different, and be determined only by the effect of the thermal energy on the unpinning process. There is as yet no treatment of this problem, which involves the same sort of difficulties as we referred to in § 2.2.1.

Granato and Lücke predict the absolute value of the friction (eqn. (25)) but it is difficult to verify this experimentally as the expression contains several quantities that can only be estimated. The extent of the agreement has been discussed by Granato and Lücke (1956 a, b, 1957) and by Granato *et al.* (1958); we refer the reader to the original papers for details of the discussion. It seems that by making reasonable estimates of the various parameters, one obtains a friction of the correct order. Experimental results on the Köster effect permit a rather complete analysis for sodium chloride (Granato *et al.* 1958) and similar data would be welcome in the case of metals.

In spite of these uncertainties it is clear that the distance between pinning points must be quite long. Thus, the radius of curvature of a dislocation with a line tension T and Burgers vector $\mathbf{b}$ under an applied stress σ, is readily shown to be $T/\sigma\mathbf{b}$. If we now take $T = \frac{1}{2}G\mathbf{b}^2$, it follows by simple geometry that the maximum displacement of a loop of length L is $L^2\epsilon/4\mathbf{b}$ where ϵ is the strain. Hence, for a loop 10^{-4} cm long and a strain amplitude of 10^{-6} the maximum displacement is ~ 10 Å, and for a loop 10^{-5} cm long the displacement becomes 0.1 Å. In order for Granato and Lücke's theory to be applicable this displacement must be at least equal to the atomic spacing, which implies that there are dislocation loops in the crystals free of pinning points for distances of the order of 10^{-4} cm.

Finally, without going into details, we note that Granato and Lücke's treatment provides a basis for explaining many of the time-dependent effects observed when measuring amplitude-dependent friction (§ 3.3.1.). For example, Chambers observed that the friction increased when an aluminium single crystal was vibrated for several minutes at a constant strain amplitude, and that the friction subsequently assumed its original

Fig. 38

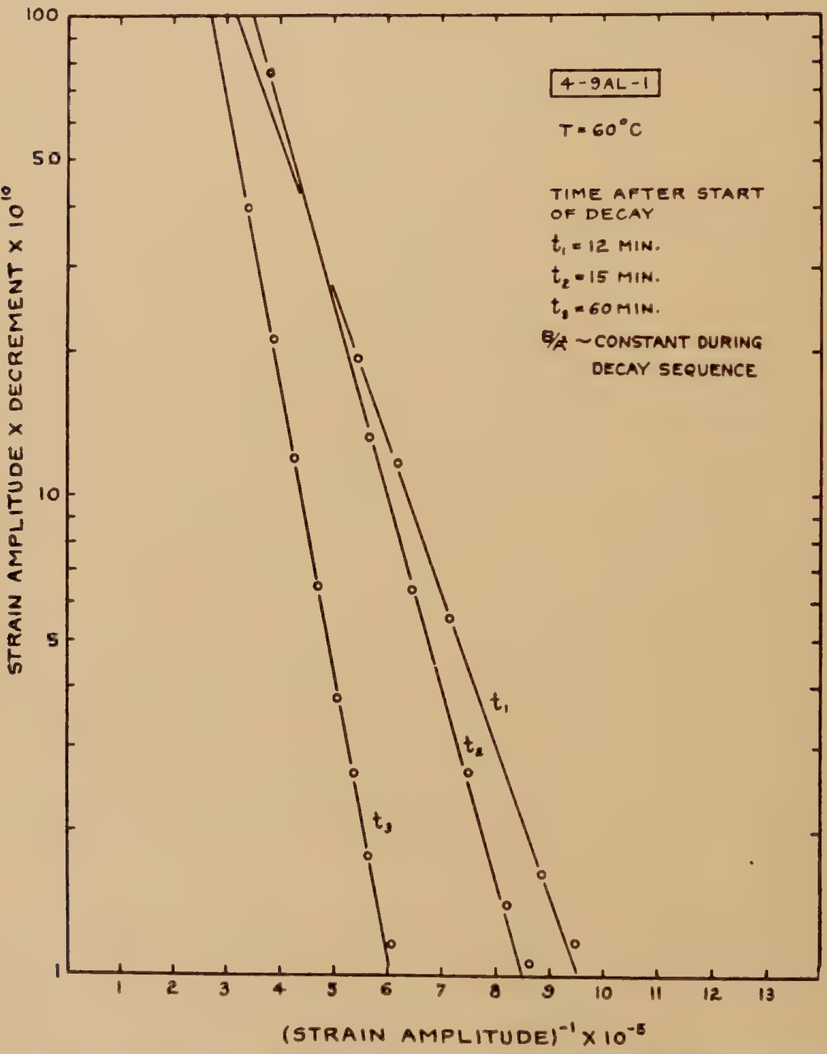

Granato and Lücke plots of the internal friction at 60°C of an aluminium single crystal which had been vibrated at a comparatively high strain amplitude ($\sim 10^{-5}$) for 20 min. The curves correspond to the friction observed 12, 15 and 60 min after the high amplitude vibration ceased (Chambers 1957). (Both scales should be divided by 3.)

value after resting for a few hours. Figure 38 shows Granato and Lücke plots for the friction as measured at various times during the recovery process. The increasing slopes of the lines as recovery proceeds indicate an increasing concentration of pinning points. During the initial excitation many of the dislocations are torn some distance away from pinning points (either impurity atoms or vacancies), and are subsequently repinned by the diffusion of the pinning points to the new positions of the dislocations. In addition the recovery often follows the course specified by eqn. (32) of § 3.3.7, derived by Granato *et al.* (1958) for recovery after plastic deformation.

§ 4. INTERNAL FRICTION AT HIGH TEMPERATURES

4.1. *Introduction*

In the next two chapters we consider the friction which is independent of the strain amplitude. This type of friction may arise in several different ways, and considerable care is necessary in order to resolve a measured friction into its various components. Therefore we begin by considering a very characteristic form of friction observed at the higher temperatures. At sufficiently high temperatures, the amplitude-independent friction Δ_I begins to rise very rapidly with increasing temperature and follows a law of the type

$$\Delta_I = A \exp(-Q/kT) \quad . \quad . \quad . \quad . \quad . \quad . \quad . \quad . \quad (33)$$

so that a plot of ln Δ_I against $1/T$ gives a straight line whose slope gives a value of the activation energy Q. A typical result for aluminium obtained by Chambers (1957) is shown in fig. 39 ; the exponential relation sets in quite sharply at about 200°C.

4.2. *Experimental Observations*

Although an exponentially rising type of friction occurs in both single crystals and polycrystalline material, in the latter it is obscured by grain boundary relaxation (see § 1.4.2.). Therefore, we only consider measurements on single crystals. The most extensive investigation is that of Kamentsky (1956), who made measurements on 99·999% copper up to 750°C. His values of the friction as a function of strain amplitude are shown in fig. 40 ; at low amplitudes the friction is either almost constant or decreases slightly with increasing strain amplitude. (It may be noted that such a decrease was not observed by Chambers (1957) in apparently comparable experiments on aluminium.) For the moment we only consider the friction for values of strain less than ϵ_c, the value above which the friction begins to rise with increasing amplitude.

Kamentsky emphasizes the need for care if one is to obtain reproducible results. Thus, while investigating the effect of temperature on the friction, the strain was never increased above the value ϵ_c, and the specimen was allowed to rest for two hours at each new temperature before taking a reading. In this way, Kamentsky claimed to obtain reproducible results above 500°c, although at lower temperatures his values show considerable scatter. Some typical results of his are shown in fig. 41 as a plot of $\ln \Delta$ against $1/T$. The exponential region sets in at about 400°c, and on some curves there is a suggestion of a small peak at the highest temperatures at

Fig. 39

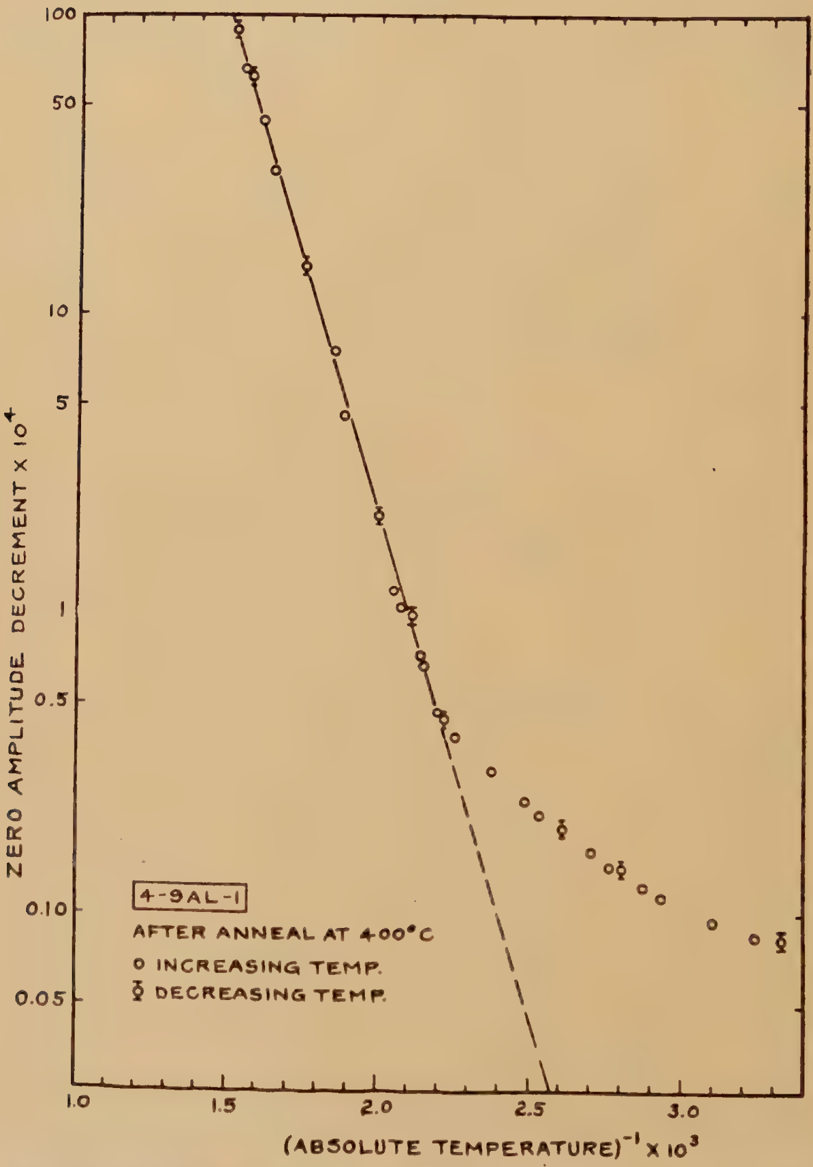

The amplitude-independent internal friction of an aluminium single crystal as a function of temperature (Chambers 1957).

about 700°C. Below 400°C the decrement is much less temperature-dependent and does not appear to arise from a thermally-activated process with a unique activation energy.

Fig. 40

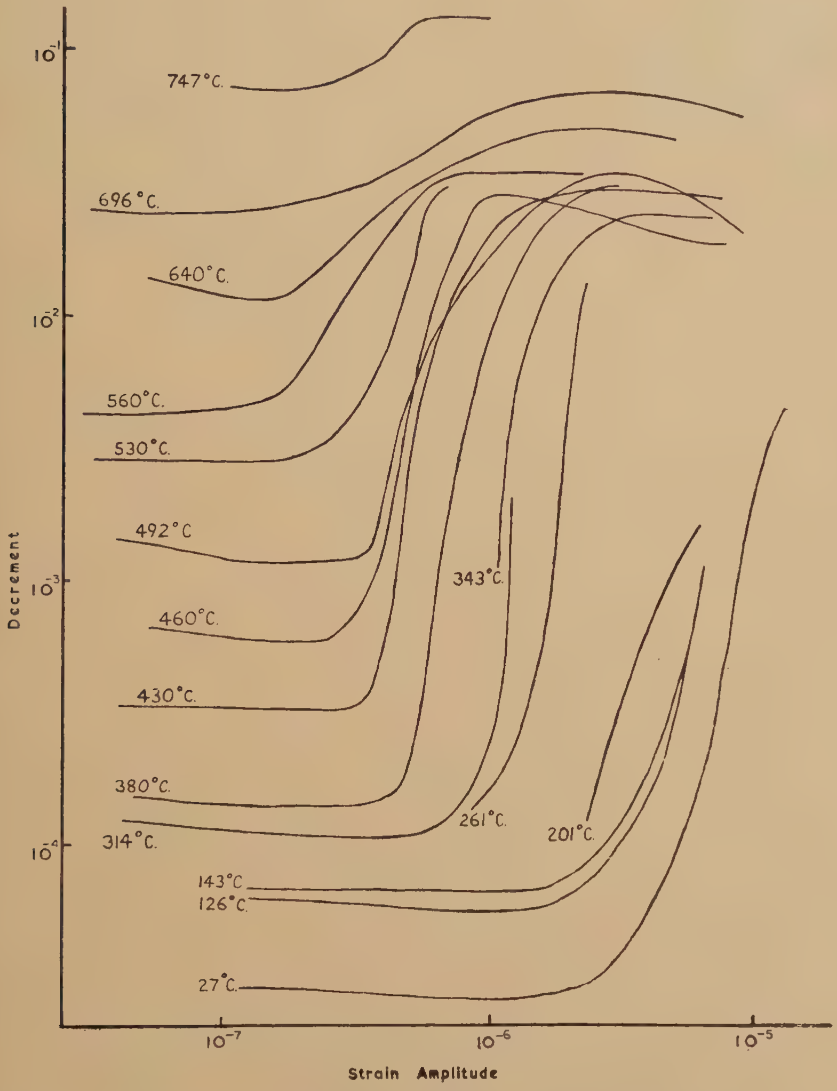

The internal friction of a copper single crystal as a function of strain amplitude at various temperatures measured at ~1450 c/s (Kamentsky 1956).

4.2.1. *The activation energy*

The activation energy associated with the friction is given by the slope of curves such as those in figs. 39 and 41. Kamentsky (1956) quotes energies for single crystals of pure copper ranging from 0·5 to 2 ev, although most of his values are grouped around 0·9 ev. Unfortunately, some of his data is rather scattered, and it is difficult to decide how much weight should be placed on the lowest and highest values. Beshers (1959), using similar material, has given values of about 1 ev below 500°c and 0·8 ev at higher temperatures. Both Beshers (1959) and Stevens (1957) doped copper single crystals with gold and nickel and found that although the friction at higher temperatures was reduced, the activation energy remained unchanged. (At lower temperatures, below 400°c, the impurities appeared to be responsible for a peak in the friction-temperature curve which we discuss in § 5.4).

Fig. 41

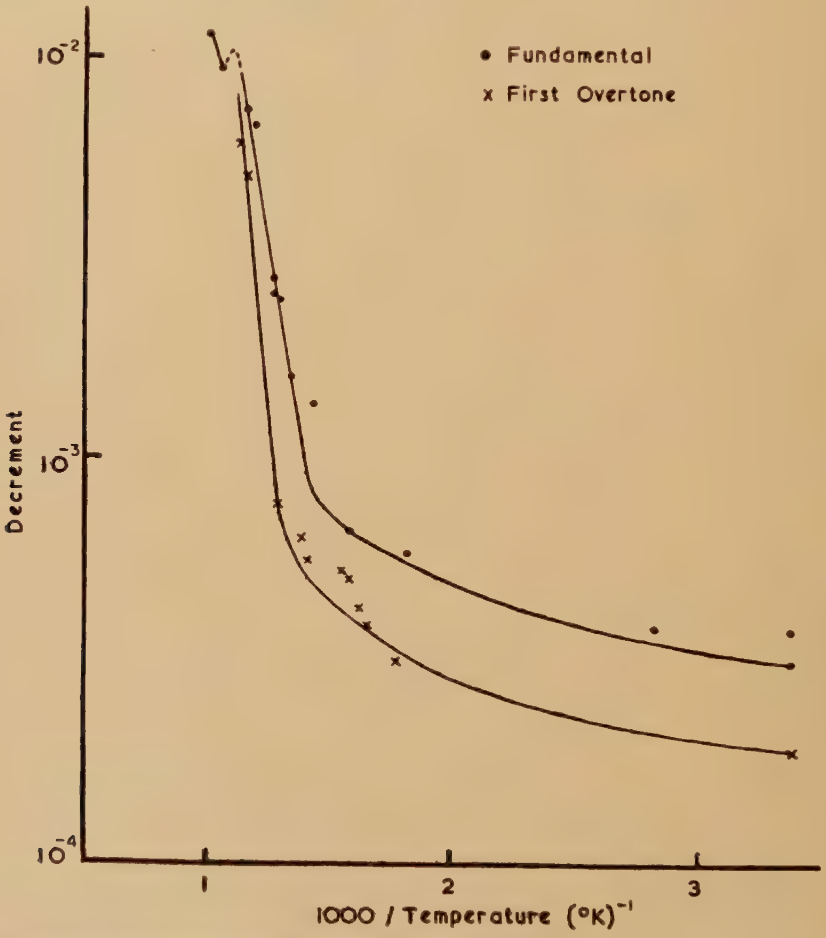

The amplitude-independent internal friction of a copper single crystal as a function of temperature. ● fundamental frequency (~1200 c/s); × first overtone (~3200 c/s) (Kamentsky 1956).

An apparently similar type of friction has been observed in aluminium by Chambers (1957) and by Birnbaum and Levy (1956), who reported energies of about 0·7 ev. Friedel *et al.* (1955) working with polygonised aluminium at frequencies of the order of 1 cycle *per hour* obtained values of about 1·6 ev. For magnesium Chambers gives a value of 0·7 ev, and for lead Weertman and Salkovitz (1955) quote 0·3 ev.

4.2.2. *Dependence on frequency*

Measurements of the friction as a function of frequency have been made by Kamentsky (1956) and by Friedel *et al.* (1955). Kamentsky vibrated copper single crystals at their fundamental frequency and their second and third harmonics. Although his results are rather scattered (fig. 41), the friction appears to decrease with increasing frequency at a rate somewhat less rapid than the reciprocal of the frequency. Friedel *et al.*, working with aluminium at extremely low frequencies, also found that the friction decreased with increasing frequency in a rather similar way. In addition the absolute values obtained by Friedel *et al.* are very large.

Fig. 42

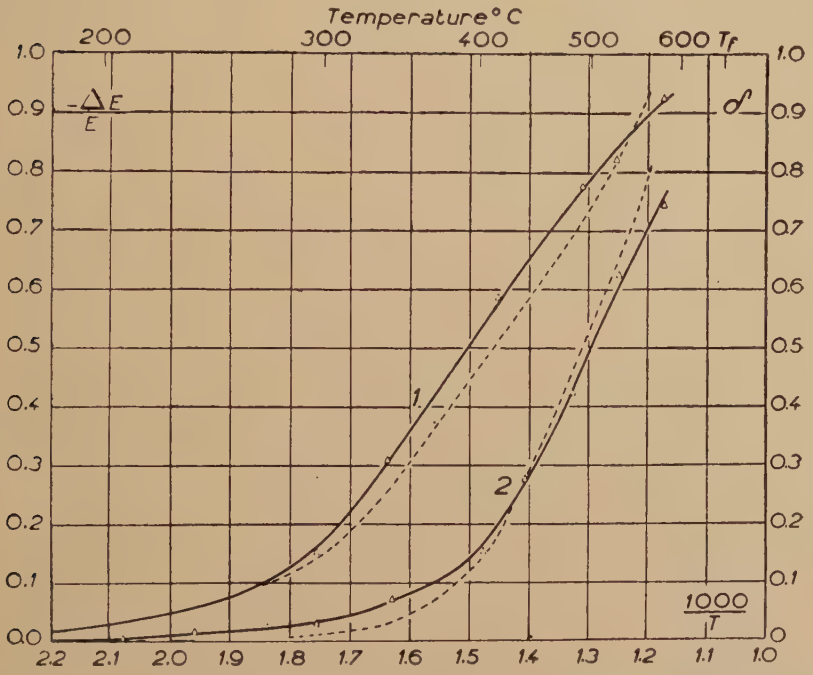

The amplitude-independent internal friction (dotted line) and modulus defect (full line) of polygonised aluminium. Curves 1 measured at a frequency of 1 cycle in 48 min, curves 2 at 1 cycle in 15 sec (Friedel *et al.* 1955).

4.2.3. *The modulus defect*

The modulus defect at high temperatures has been estimated by noting that in the absence of a large internal friction, Young's modulus is expected to vary linearly with temperature, (see for example Ludloff 1940). In the high temperature region a marked and increasing departure from linearity sets in as the friction increases, and this deviation is used as a measure of the modulus defect. The results of Friedel *et al.* on aluminium (fig. 42) show that the modulus defect has approximately the same temperature dependence as that of the friction. Kamentsky (1956) reports that for copper the variation of the defect with temperature may be characterized by an activation energy whose value, depending on the specimen, varies from 0·4 to 1·2 ev. This corresponds to a lesser dependence on temperature than is shown by the friction, but the scatter is rather large. Chambers (1957) characterises the temperature dependence of the modulus defect in aluminium by an activation energy of about 0·25 ev, which is again much less than that associated with the friction.

4.3. *Theories and Discussion*

The experimental observations of the amplitude-independent friction at high temperatures clearly suggest that in this region the mechanism responsible for the friction is characterized by an activation energy, which for copper is about 0·9 ev. Most of the theoretical treatments assume that the friction arises because the dislocations, oscillating under the influence of the applied stress, create defects in the lattice. The decrement will be proportional to the number of defects created, and as thermal activation will play a large part in their creation it follows that the decrement should rise exponentially in the observed manner. There are various possibilities concerning the nature of these defects. They may be jogs formed when two dislocations cut through each other, or they may be vacancies formed by the motion of jogged dislocations (Birnbaum and Levy 1956, Kamentsky 1956, Weertman 1957). On the above picture the friction arises by what is essentially a relaxation process. At low temperatures there is no probability of creating defects and therefore no friction; at the highest temperatures the defects will be created by thermal energy alone and again there will be no friction. Such a relaxation model accounts at least approximately for the observed amplitude independence, the observed frequency dependence, the temperature dependence, and the possibility of a maximum in the friction at high temperatures.

Friedel *et al.* (1955) have pointed out that the temperature dependence of the friction often implies (particularly in their own experiments) that more than one activation energy is involved. They also suggest that an additional loss of energy may arise if a dislocation has to move an atmosphere of impurity atoms along with it through the lattice. Kamentsky (1956) has considered the amplitude dependence of the friction in some detail and suggests that the friction rises at the higher strain amplitudes because the applied stress aids the unpinning of dislocations from jogs or other pinning points. This author also accounts for the initial decrease of the decrement with increasing strain shown in fig. 40. If we write $\Delta = \Delta W/2W$ (see eqn. (2)), then the total energy W increases as the square of the strain amplitude, and the energy loss per cycle, ΔW, depends on the strain σ through an exponential term of the form $A \exp\{-(Q-\alpha\sigma)/kT\}$, where α is some constant. At sufficiently low strains this term will not vary much with strain, so that the net result is that initially the decrement decreases with increasing strain.

Rather different accounts of the friction have been given by Weertman and by Mason. According to Weertman (1957) the essential feature of the situation is that the vibrating loops of dislocation move in the stress field of randomly distributed impurity atoms (Mott and Nabarro 1948). As the temperature rises, thermal activation permits the dislocations to move more rapidly through the stress field; their velocity depends exponentially on the temperature, and decreases with impurity concentration. The viscous damping of the vibrating dislocations is proportional to their velocity (see § 5.2), and the decrement rises rapidly with increasing temperature, and varies inversely with the applied frequency. As we discuss in more detail in § 5.2, such a treatment is only applicable to not too pure material, for the maximum displacements of the dislocations need to be considerably greater than the wavelength of the stress field. Mason (1958) has proposed that the energy loss associated with the friction comes about when two adjacent vibrating loops of dislocation break away from their common pinning point. The consequent exchange of energy between the two loops takes place irreversibly and gives rise to damping. However, any such mechanism should give an activation energy similar to that involved when dislocations are unpinned by an applied stress, and as we saw in § 3 this is of the order of only 0·1 ev.

At present the most satisfying explanation of the high temperature friction is that the moving dislocations create defects in the lattice. However, more work is needed in order to establish the precise nature of the defects. It is quite probable that more that one type of defect is involved, but this can only be resolved by more detailed measurements. There is also a further point of difficulty in that on such a theory one would expect the activation energy associated with the modulus defect to be the same as that associated with the friction. Although this is observed by Friedel *et al.*, Kamentsky and Chambers report activation energies for the modulus defect considerably lower than for the friction. As the measurements are somewhat difficult ones, further experimental information would be of interest.

§ 5. AMPLITUDE-INDEPENDENT INTERNAL FRICTION AT LOW STRAIN AMPLITUDES

We now discuss the amplitude-independent internal friction which is observed at low strain amplitudes and not too high temperatures. That is, we consider temperatures below about 400°K where the contribution from the thermally-activated processes discussed in the previous chapter should be negligible. In the majority of cases, the friction increases with rising temperature, but occasionally peaks are observed in the friction–temperature curve. It appears probable that these peaks are due to different mechanisms from those responsible for the friction which varies monotonically with temperature. In the next three sections we consider the latter friction in some detail, and finally discuss the peaks more briefly in § 5.4.

5.1. *Experimental Observations*

The experimental facts regarding the strain-independent friction at moderate temperatures are probably less well established than is the case with the previous types of friction, particularly the evidence concerning the dependence of the friction on frequency. This uncertainty arises in part because many of the early investigators did not indicate whether the observed decrement contained any amplitude-dependent component. If the measured decrement is small, there is always a serious possibility that background losses in the apparatus may be significant, and there may be appreciable contributions to the damping from the thermoelastic effect and other processes mentioned in § 1.4. Therefore, we consider only those measurements in which the friction has been demonstrated to be independent of strain amplitude, and has a value sufficiently large ($\Delta \sim 10^{-4}$ or greater) that it probably exceeds losses from other causes.

5.1.1. *The effect of temperature*

We consider only experiments on annealed metals, as the low amplitude decrement in cold-worked metals is strongly affected by the presence of the Bordoni peak (see chapter 2). We also ignore the grain-boundary relaxation peak observed in polycrystalline metals in the range between 200°C and 500°C (see § 1.4.2). Figure 41, taken from Kamentsky (1956), shows values of Δ_I plotted as the logarithm of the decrement against the inverse temperature. It is seen that the exponential region ceases at about 400°C, and that at lower temperatures the friction is much less dependent on the temperature. Below 400°C the graph does not seem to be straight enough to determine an activation energy, but Kamentsky concluded that if such an energy existed it was less than 0·05 ev.

Kamentsky's measurements extend down to room temperature and measurements at lower temperatures have been made on annealed copper by Caswell (1958), by Niblett and Wilks (1959 a) and by Thompson and Holmes (1959). Caswell (1958) measured pure annealed copper single crystals from 4°K to room temperature, and found that the low amplitude decrement increased monotonically with increasing temperature over the whole range. The decrement did not appear to be a simple function of temperature; the graph of decrement against temperature was in general concave upwards, approaching a linear form at the lower temperatures. Thompson and Holmes (1959) have also obtained rather similar results in an annealed single crystal (fig. 43). Niblett and Wilks (1959 a), working with polycrystalline material, found the friction to be roughly proportional to the temperature between 20°K and room temperature.

An increase of Δ_I with increasing temperature has also been observed in copper single crystals between −49°C and 33°C by Nowick (1950a), in zinc single crystals between −76°C and 145°C by Wert (1949), and in lead single crystals between 200°K and 330°K by Hiki (1958). (Hiki also observed that below 200°K the decrement was almost independent of the temperature.) Finally, we mention that dilute alloys sometimes exhibit peaks in the curves of friction versus temperature in the region of 100° or 200°C, and we return to these in § 5.4.

Fig. 43

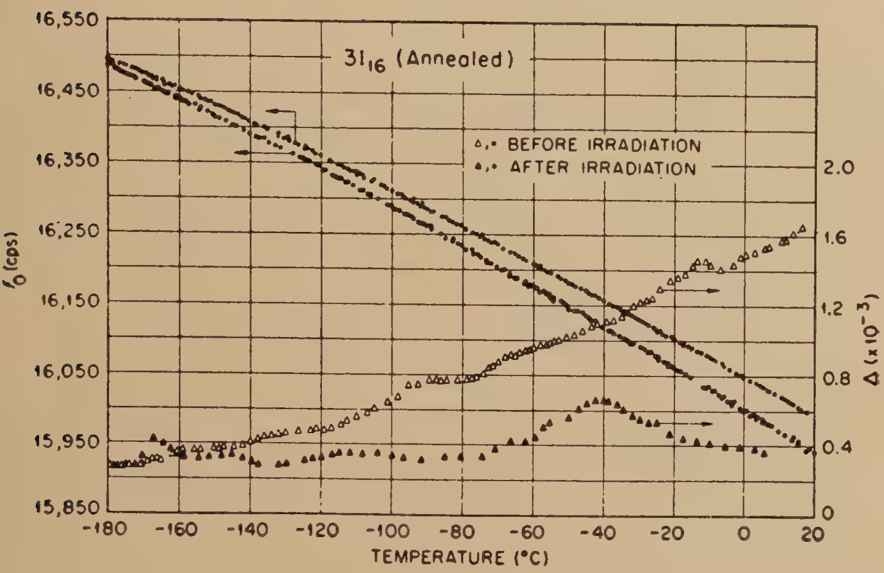

The amplitude-independent internal friction and resonant frequency of a copper single crystal before and after neutron irradiation at room temperature (Thompson and Holmes 1959).

5.1.2. *The effect of frequency*

There is not a great deal of experimental evidence on the frequency dependence of the amplitude-independent friction, and what there is appears at first sight to be somewhat inconsistent. Hiki (1958) measured the friction of two lead single crystals at their fundamental frequency (64 kc/s) and third harmonic (192 kc/s), and found that the amplitude-independent component of the decrement was directly proportional to the frequency in the temperature range from 140°K to about 220°K (fig. 44). Hikata and Truell (1957) report that the internal friction of aluminium is approximately proportional to the frequency at 5 and 10 Mc/s. On the other hand, Nowick (1950a) measured the amplitude-independent decrement of copper single crystals at their fundamental frequency (39 kc/s) and second harmonic (78 kc/s). His results were scattered, but showed no significant variation with frequency. Takahashi (1956) measured polycrystalline copper at room temperature at various frequencies between 1 and 10 kc/s, and found that the amplitude-independent internal friction was practically independent of frequency.

Fig. 44

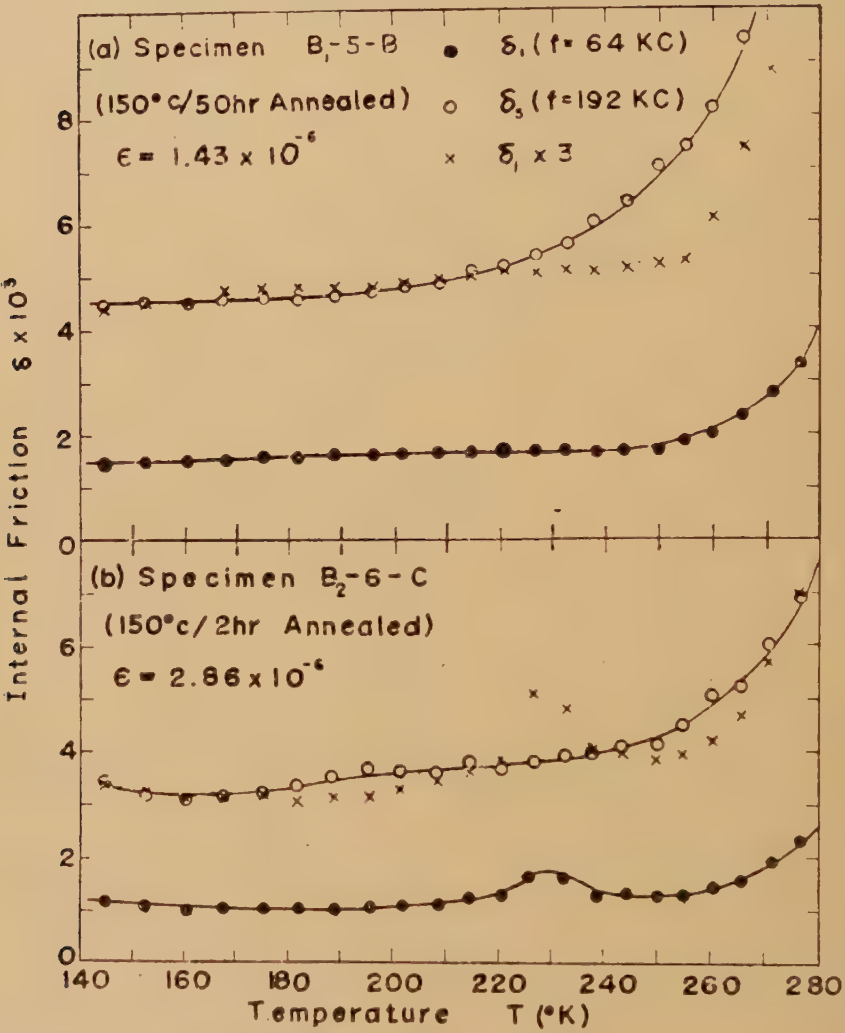

The amplitude-independent internal friction of two lead single crystals as a function of temperature at two frequencies (Hiki 1958).

Bordoni *et al.* (1959) observed little change for polycrystalline copper between 1·8 kc/s and 6·5 Mc/s. Again, the magnitude of the friction observed by Weinig and Machlin (1956) in polycrystalline 99·999% copper at a frequency of about one cycle per second is as great as many values of the friction obtained in the kilocycle range. It is difficult to obtain absolute values of the damping in the megacycle region where measurements are generally made using a pulse technique, but what evidence there is (Mason 1958) suggests that the friction is of the same order as at lower frequencies. Thus it seems that the low amplitude damping either increases slightly with increasing frequency or is frequency-independent. We also mention measurements by Granato and Truell (1956) on germanium single crystals at frequencies from 5 to 300 Mc/s in which the internal friction is approximately proportional to the frequency. However, germanium is a semi-conductor, and these results may not be typical of metals.

5.1.3. *The effect of cold work*

Small amounts of plastic deformation increase the amplitude-independent internal friction of copper single crystals at room temperature (Nowick 1950 a, b, Thompson and Holmes 1959). Caswell (1958) has shown that cold work increases the decrement over the entire temperature range from 4° to 300°K. The measurements of Weertman and Koehler (1953) on copper single crystals and of Niblett (1956) on polycrystalline copper indicate that the friction goes through a maximum value with increasing cold work. Other investigators, e.g. Hirone *et al.* (1955), have also observed such a maximum, but do not give sufficient information to show whether their results are for amplitude-independent or amplitude-dependent damping. It has also been found that the order of a few parts per cent deformation of copper introduces a peak in the friction-temperature curve at about 200°K (see § 5.4).

After plastic deformation it is generally found that the amplitude-independent friction decays somewhat over a period of a few hours, before taking up a steady value. This is the so-called Köster effect which is also exhibited by the amplitude-dependent friction as discussed in § 3.3.7. The effect has been observed in brass and steel by Förster and Köster (1937), in brass by Köster and Rosenthal (1938), in aluminium by Köster (1940), and in iron by Köster (1940–41). More recently, measurements have been made on zinc by Alers (1955), on aluminium by Hikata *et al.* (1956) and on sodium chloride by Gordon and Nowick (1956).

5.1.4. *The effect of purity*

In general the addition of small amounts of impurity reduces the low-amplitude internal friction. For example, Marx and Koehler (1950) showed that annealing a copper single crystal for 20 hours in hydrogen at 1000°C caused the amplitude-independent decrement to be an order of magnitude smaller than in a vacuum-annealed crystal. Similarly the addition of small amounts of gold to copper single crystals considerably reduces the friction, both in the annealed state (Beshers 1959) and when plastically deformed (Paré 1958). Takahashi (1956) has reported that the amplitude-independent friction of polycrystalline copper containing small quantities of aluminium, zinc or phosphorus decreases as a power function of the concentration of the solute atoms.

In some cases, other investigators have found no systematic dependence of the friction on impurity concentration. For example, Weertman and Salkovitz (1955) observed that the amplitude-independent internal friction of lead single crystals containing up to one per cent of bismuth, tin or cadmium varied with the impurity concentration in an apparently random manner. However, this scatter may be due to differences in the previous history of the specimens, for Kamentsky (1956) and others have noted that Δ_I is very sensitive to small amounts of cold work caused by handling the specimens. Caswell (1958) found no systematic dependence of the decrement on impurity concentration in copper single crystals containing up to 0·5% gold, but the interpretation of these results is difficult as the gold-bearing specimens exhibit a broad peak in the friction–temperature curve at about 180°K.

5.1.5. *The effects of irradiation and quenching*

Neutron irradiation reduces the amplitude-independent friction in copper single crystals (Thompson and Holmes 1956a, b, 1959, Barnes and Hancock 1958), and in polycrystalline copper (Barnes *et al.* 1958). The latter authors observed similar reductions in the decrement after irradiation with γ-rays or quenching. Roswell and Nowick (1957) found that the friction of polycrystalline gold was much lower after quenching from 900°C than after cooling slowly from this temperature. (On the other hand, Caswell (1958) found that quenching a copper single crystal from 1000°C increased the friction at room temperature by a factor 5.)

The most detailed studies of the effect of neutron irradiation are those of Thompson and Holmes, and figure 43 shows values of the decrement and resonant frequency of a copper single crystal before and after irradiation. These authors also observed the friction of copper single crystals in situ in a nuclear reactor while undergoing neutron irradiation. In this way, they obtained curves of the friction as a function of total neutron flux (fig. 45), which we discuss later in § 5.3.1. All these experiments are of particular interest in that they yield information as to the modulus defect associated with the friction, which is otherwise rather difficult to obtain. The large reduction in the friction produced by neutron irradiation is accompanied by an increase in Young's modulus; and one can associate the decrease in friction with the change in modulus.

5.2. *Theories of the Internal Friction*

We now briefly review the various theories which have been put forward to account for the amplitude-independent friction at low and medium temperatures. Most of these treatments regard the friction as arising from a viscous-like damping of dislocations set in motion by the oscillating stress. According to Koehler (1952) lengths of dislocation between two pinning points (either impurity atoms or nodes in the dislocation network) vibrate with the applied stress in the manner of a stretched string. The equation of motion of such a line is of the form

$$A\frac{\partial^2 y}{\partial t^2}+B\frac{\partial y}{\partial t}-C\frac{\partial^2 y}{\partial x^2}=\mathbf{b}\sigma_0\sin\omega t \quad . \quad . \quad . \quad . \quad (34)$$

Fig. 45

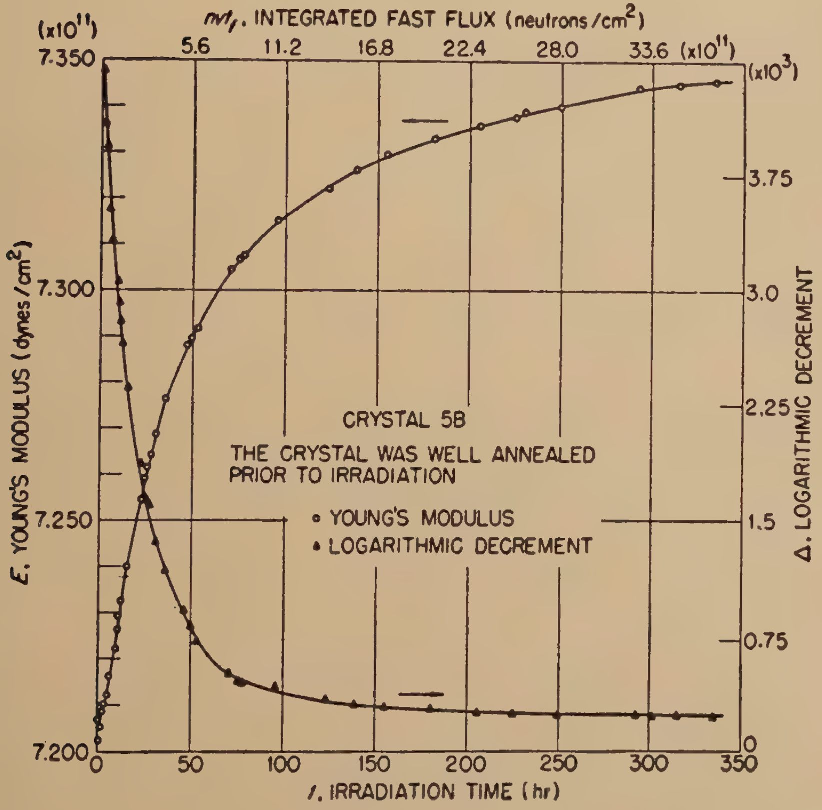

The internal friction and Young's modulus of a copper single crystal as a function of the time of neutron irradiation in a pile at ambient temperature (Thompson and Holmes 1956 b).

where y is the lateral displacement at a position x along the length, A the effective mass per unit length, B the damping force per unit length, C the line tension associated with the dislocation, $\mathbf{b}$ the Burgers vector, and $\sigma_0 \sin\omega t$ the resolved component of the applied stress in the glide plane of the dislocation. The resonant frequency usually is of the order of

100 Mc/s, and for all frequencies with which we are concerned the damping is proportional to the frequency. In this case, Granato and Lücke (1956 a) show that

$$\Delta_I = \frac{\Omega \Lambda L^4 B \omega t_1}{\pi^3 C} \quad . \quad . \quad . \quad . \quad . \quad . \quad . \quad . \quad (35)$$

and

$$\left(\frac{\Delta E}{E}\right)_I = \frac{\Omega \Lambda L^2 t_2}{\pi^2} \quad . \quad . \quad . \quad . \quad . \quad . \quad . \quad . \quad (36)$$

where Ω is an orientation factor, Λ the dislocation density, L the mean length of a vibrating loop and ω the frequency. t_1 and t_2 are constants which take account of the fact that there is a distribution of loop lengths, and that the longer lengths contribute disproportionately to the friction. Thus, for a delta function distribution, t_1 and t_2 are both unity, but for an exponential distribution corresponding to a random distribution of pinning points $t_1=120$ and $t_2=6$.

The damping constant B was first estimated by Eshelby (1949), who showed that a dislocation oscillating under an applied stress sets up temperature gradients which are responsible for an irreversible flow of heat. Another calculation by Leibfried (1950) estimated the loss associated with the interaction between a moving dislocation and the thermal vibrations of the crystal lattice. The damping given by Leibfried's mechanism is considerably greater than that given by Eshelby's; Granato and Lücke (1956 b) quote values of B of the order of 10^{-4} and 10^{-6} c.g.s. units for the two treatments. Nabarro (1951) has also investigated the problem in some detail and concludes that while Leibfried's result is correct in form, it is numerically somewhat high. The dissipation of energy by moving dislocations has also been treated by Seitz (1950) and Hart (1955).

Other mechanisms to account for the amplitude-independent friction have been proposed by Eshelby and by Weertman. Eshelby (1949) regards the dislocations as oscillating in the potential wells associated with the Peierls force, and being damped by a similar viscous-like reaction to that discussed above. However, the displacements of the dislocations on this model are much smaller than on the string model, and the friction correspondingly less. A quite different approach has been given by Weertman (1955) and Weertman and Salkovitz (1955); these authors assume that the only restraint on a dislocation in a crystal is the stress field associated with impurity atoms. Consider a dislocation lying at the bottom of a potential trough in the stress field. On applying a stress the dislocation will move reversibly up to the crest of a potential hill, but on reaching the top will rush down the other side irreversibly. The stress–strain curve will show a hysteresis loop because each potential gradient is traversed reversibly in one direction and irreversibly in the other. The resulting friction and modulus defect are given by

$$\Delta \sim 10^{-2} \Lambda \lambda G \mathbf{b} / \sigma_m \quad . \quad . \quad . \quad . \quad . \quad . \quad . \quad . \quad (37)$$

and

$$\left(\frac{\Delta E}{E}\right) = \Delta \quad . \quad . \quad . \quad . \quad . \quad . \quad . \quad . \quad (38)$$

where λ is the wavelength of the stress field, and σ_m the average height of the stress barriers, as given by Mott (1952). Although this is a possible mechanism, it has two serious limitations. Firstly, the displacement of the dislocations must be greater than the wavelength of the stress field, which in 99·999% pure material will be of the order of 50 atomic diameters. In fact, the displacements of the dislocations are limited by their line tensions, and for strains of the order of 10^{-6} are probably equal to only a few atomic diameters (see § 3.4.). Thus, the present mechanism is not applicable to high purity material, nor to measurements at low oscillating strains (Granato and Lücke 1956 a, Weertman and Salkovitz 1956). A second criticism is that while the amplitude-independence of the friction arises quite naturally on the string model, we should in general expect a hysteresis mechanism to lead to an amplitude-dependent friction. In Weertman's theory this is avoided as a result of an integration over a statistical distribution of dislocations all with different positions (and energies) in the stress field. However, slightly different distributions would probably lead to a friction which is a function of strain amplitude.

5.3. *The Vibrating String Model*

In this section we consider to what extent the amplitude-independent friction may be accounted for by the vibrating string model.

5.3.1. *Dependence on loop length*

A characteristic feature of the vibrating string model is that if all the loops have the same length, l, then the modulus defect is proportional to l^2 and the decrement to l^5. In fact, the loop lengths will have some sort of random distribution and most authors assume that the number of loops with length between l and $l+dl$ is given by

$$N(l)dl=\frac{\Lambda}{L^2}\exp(-l/L)dl \qquad . \; . \; . \; . \; . \quad (24)$$

where Λ is the density of dislocations and L the average length. To obtain values for the decrement and modulus defect, it is necessary to integrate over all loop lengths; one then finds that the modulus defect is proportional to L^2 and the decrement to L^4 as in eqns. (35) and (36). We now describe several experiments which suggest that the friction and modulus defect often depend on the loop lengths in this way.

Thompson and Holmes (1956 a, b) have analysed their experiments in which the friction of copper single crystals was reduced by neutron irradiation (§ 5.1.5) by assuming that the neutrons produce point defects which diffuse to the dislocations and shorten the loop lengths. By assuming that all neutron collisions are equally likely to produce pinning, and an initial distribution of loop lengths given by eqn. (24), they show that the measured modulus, E_{M}, after a time of irradiation t should be given by

$$\frac{E_{\mathrm{E}}-E_{\mathrm{M}}}{E_{\mathrm{M}}}=\frac{E_{\mathrm{E}}-E_0}{E_0}\frac{1}{(1+\gamma nvt)^2} \qquad . \; . \; . \; . \quad (39)$$

where E_E is the purely elastic part of the modulus, E_0 is the value of the modulus at $t=0$, γ is a constant and nvt the integrated neutron flux. Equation (39) is a relation between E_M and t containing effectively three constants, E_E, E_0 and γnv, which may be determined by solving for three spot values of E_E and t taken from experimental results such as those in fig. 45. The relation (39) may now be verified by plotting

$$\left[\ln\left(\frac{E_E-E_M}{E_M}\right)-\ln\left(\frac{E_E-E_0}{E_0}\right)\right]$$

against $\ln(1+\gamma nvt)$, and such a plot is shown in fig. 46. Over a large part of the experiment, the points lie on a line with the expected slope of -2.

Thompson and Holmes also show that if the friction arising from a single loop of length l is proportional to l^m, then the decrement, Δ, after time t is given by

$$\frac{\Delta-\Delta_1}{\Delta_1}=\frac{\Delta_0-\Delta_1}{\Delta_1}\cdot\frac{1}{(1+\gamma nvt)^{m-1}} \quad . \quad . \quad . \quad . \quad . \quad (40)$$

where Δ_0 is the friction at $t=0$, and Δ_1 is the value to which the friction tends for an infinitely long irradiation. Δ_0 and Δ_1 are determined experimentally and γnv is known from the measurements of the modulus defect; therefore eqn. (40) is a relation between Δ and t in terms of only one unknown m, which may be found by plotting

$$\left[\ln\left(\frac{\Delta-\Delta_1}{\Delta_1}\right)-\ln\left(\frac{\Delta_0-\Delta_1}{\Delta_1}\right)\right]$$

against $\ln(1+\gamma nvt)$. Such a plot is shown in fig. 46; it is quite a good straight line with a slope of -4 corresponding to the expected value of $m=5$. Thus, these results are quite consistent with the dependence of the modulus defect and friction predicted by the vibrating string model. (However, it must be remembered that the analysis has to assume an expression for the initial distribution of lengths, and, as Thompson and Holmes (1956 b) point out, slightly different interpretations are possible.)

A rather similar type of analysis has been made by Granato *et al.* (1958) of the decrease in the amplitude-independent friction during the first few hours after a specimen has been plastically deformed. This behaviour is another example of the so-called Köster effect which we described in § 3.3.7 in connection with the amplitude-dependent damping. Granato *et al.* assume that the friction Δ_I arises from a vibrating string mechanism and that the decrease is due to point defects, such as vacancies, produced during the deformation. Subsequently, the defects diffuse to the dislocations where they shorten the loop lengths and thus reduce the friction. By assuming that the defects diffuse according to the Cottrell–Bilby (1949) relation given in eqn. (31), Granato *et al.* derive expressions for the consequent decrease in loop lengths and hence for the friction and modulus defect as a function of time. Their results are shown in arbitrary units by the full lines in fig. 47.

It is a little difficult to compare these curves with the experimental results, because the friction and modulus defect change rapidly immediately after deformation; also the absolute magnitudes involved depend on parameters such as the dislocation density and impurity concentration which are not at all well-known. Measurements of this effect have been made on zinc by Alers (1955), on copper by Smith (1953), on aluminium by Hikata *et al.* (1956), and Köster (1940), and on sodium chloride by Gordon and Nowick (1956). Figure 47, taken from Granato *et al.* (1958) shows that all these results may be normalized so that they exhibit the predicted dependence on time shown by the full curves in the diagram. Granato *et al.* also analyse the results of Gordon and Nowick on sodium chloride and of Smith on the modulus of copper in more detail; again there is quite good agreement with the theory.

Fig. 46

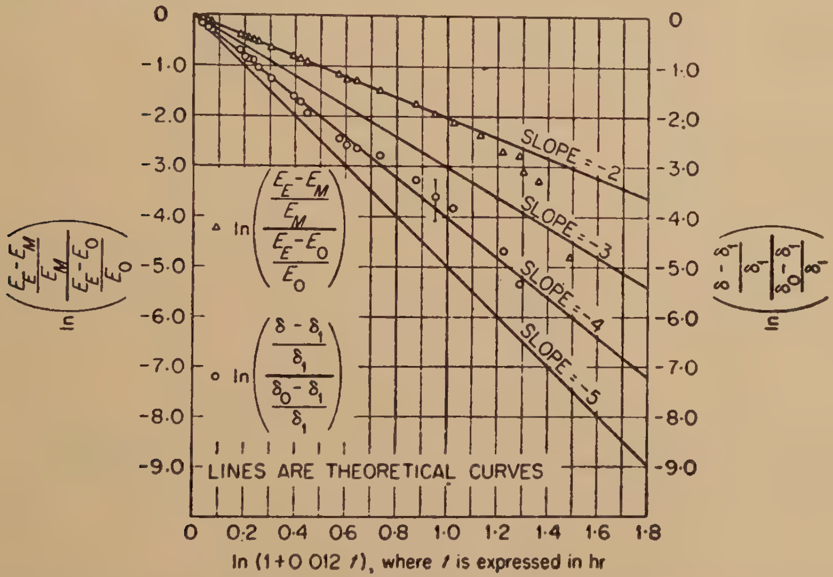

Comparison of the theoretical and experimental dependence of the internal friction and Young's modulus of a copper single crystal on the time of neutron irradiation; see text (Thompson and Holmes 1956 a).

5.3.2. *Dependence on temperature*

There is not a great deal of either experimental or theoretical information as to how the amplitude-independent friction behaves as a function of temperature; in particular there is little experimental evidence as to how the viscous damping constant B in the equation of motion of a dislocation depends on temperature. Thompson and Holmes (1959) have analysed their results on a copper single crystal shown in fig. 43 by assuming that the changes in modulus and decrement (ΔE_{i} and Δ_{i}) on irradiation are due to a suppression of the motion of dislocations. As is shown in fig. 48 it appears that between 100° and 300°K these quantities increase rapidly and are so related that

$$(\Delta E_{\mathrm{i}}/E)^2 \propto \Delta_{\mathrm{i}} \quad . \quad . \quad . \quad . \quad . \quad . \quad . \quad . \quad . \quad . \quad (41)$$

Fig. 47

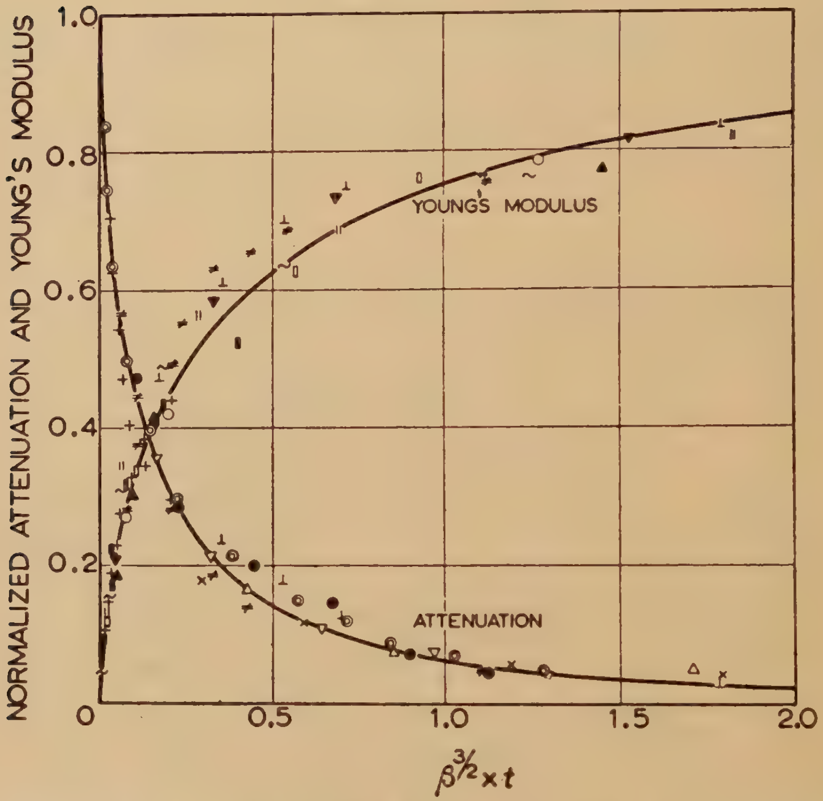

The changes in internal friction and Young's modulus as a function of time following plastic deformation. The full lines are theoretical curves as described in text. The points correspond to various measurements on copper, zinc, aluminium and sodium chloride. Both the horizontal and vertical scales have been normalized for each specimen. (β is a parameter determining the recovery.) (Granato *et al.* 1958).

(This nomenclature differs slightly from that used by Thompson and Holmes which is rather confusing.) These authors suggest that the friction increases with rising temperature because the thermal energy is able to free the dislocations from more pinning points and thus increase the effective lengths of the loops. The relation between the modulus defect and the friction follows naturally as $(\Delta E/E)_l \propto L^2$ and $\Delta_l \propto L^4$. Such a correlation is difficult to explain otherwise; for example, it could not arise solely from the temperature dependence of the viscous damping coefficient, for this coefficient affects only the friction and not the modulus defect. (In addition Thompson and Holmes deduce a T^2 temperature dependence for this friction which is close to their experimental values, but the exact form of this dependence will depend on the distribution of the pinning points.)

Fig. 48

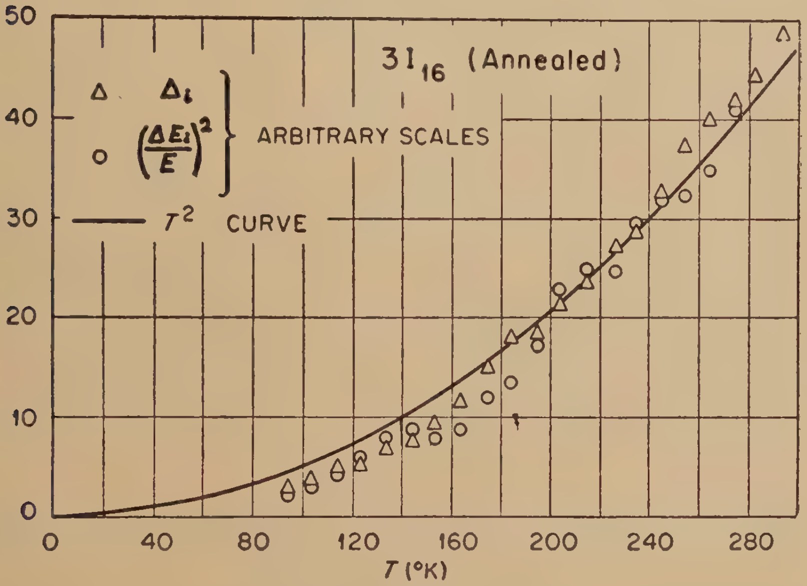

The change in modulus and internal friction (ΔE_i and Δ_i) of a copper single crystal after neutron irradiation, plotted as $(\Delta E_i/E)^2$ and Δ_i in arbitrary units against absolute temperature (see text). The solid line is a T^2 curve (Thompson and Holmes 1959).

5.3.3. *Dependence on frequency*

The vibrating string model leads to the conclusion that, except at very high frequencies of the order of 100 Mc/s, the damping should be proportional to the frequency. However, such a dependence has only been observed in two sets of experiments, those of Hiki (1958) and of Hikata and Truell (1957), and the results discussed in § 5.1.2 show that the observed dependence is often much weaker. There are, of course, difficulties in determining damping over a wide range of frequencies, as a given specimen can usually only be vibrated over a small range of harmonics. (Also if a specimen vibrates at a different harmonic, the maximum strain occurs at different parts of the specimen which may not have an entirely homogeneous distribution of dislocations.) In addition

Granato and Lücke (1957) have drawn attention to an effect of orientation which might reduce the dependence for frequencies of the order of 100 kc/s. Even allowing for all this, it seems that the amplitude-independent friction in many metals varies much less rapidly than the first power of the frequency.

A possible explanation of this discrepancy arises from the fact that the treatments of the string model ignore the effects of thermal fluctuations (Wilks 1959). As discussed in § 5.3.2 there is evidence that Δ_I may increase with rising temperature because the increasing thermal energy is able to free the dislocations from more pinning points and thus increase the effective lengths of the loops (Thompson and Holmes 1959). The number of thermal fluctuations per second sufficient to free a dislocation from a given pinning point will be independent of the frequency of the applied stress. Therefore the probability of a dislocation being unpinned from this point in a given cycle is inversely proportional to the applied frequency. Hence the effective value of the term L^4 may decrease with increasing frequency, so that Δ_I varies less rapidly than the first power of the frequency. The magnitude of this unpinning effect will depend quite critically on the state of the specimen, particularly on the nature and amount of the impurities, and for a complete discussion one needs measurements of both Δ_I and Δ_H together with the modulus defect for the same specimen over fairly wide ranges of temperature and frequency, but no such measurements are yet available.

5.3.4. *Summary*

The amplitude-independent friction depends qualitatively on impurity content and cold work as one would expect from the theory. Impurities reduce the effective loop lengths and hence the friction ; cold work increases the dislocation density Λ rapidly at first, but also reduces the loop length L so that the decrement first increases and then decreases. The apparent dependence of the decrement and modulus defect on loop length is in quite good agreement with the predictions of the model. More information is required about the temperature dependence.

The position regarding the dependence of the friction on frequency is still somewhat obscure. It is possible that the predicted proportionality between decrement and frequency is masked by orientation effects or by a dependence of the effective loop lengths on frequency. More experimental data is required to clarify this position. Finally we note that an important corollary of the string model is that a plot of friction versus frequency in the megacycle region should exhibit a maximum at a frequency comparable with the resonant frequency of the vibrating dislocation, see for example Granato and Lücke (1956 a). These authors estimate that the peak will occur at a frequency of the order of 100 Mc/s, and measurements by Dobbs *et al.* (1959) on germanium give some indication of such a peak at about 500 Mc/s. However, Lamb *et al.* (1959) have found that the ultrasonic absorption of silicon, which varies with frequency in a similar manner to that of germanium, is independent of the dislocation density over a wide range. Thus it is not certain whether dislocations are responsible for the attenuation observed by Dobbs *et al.*

Fig. 49

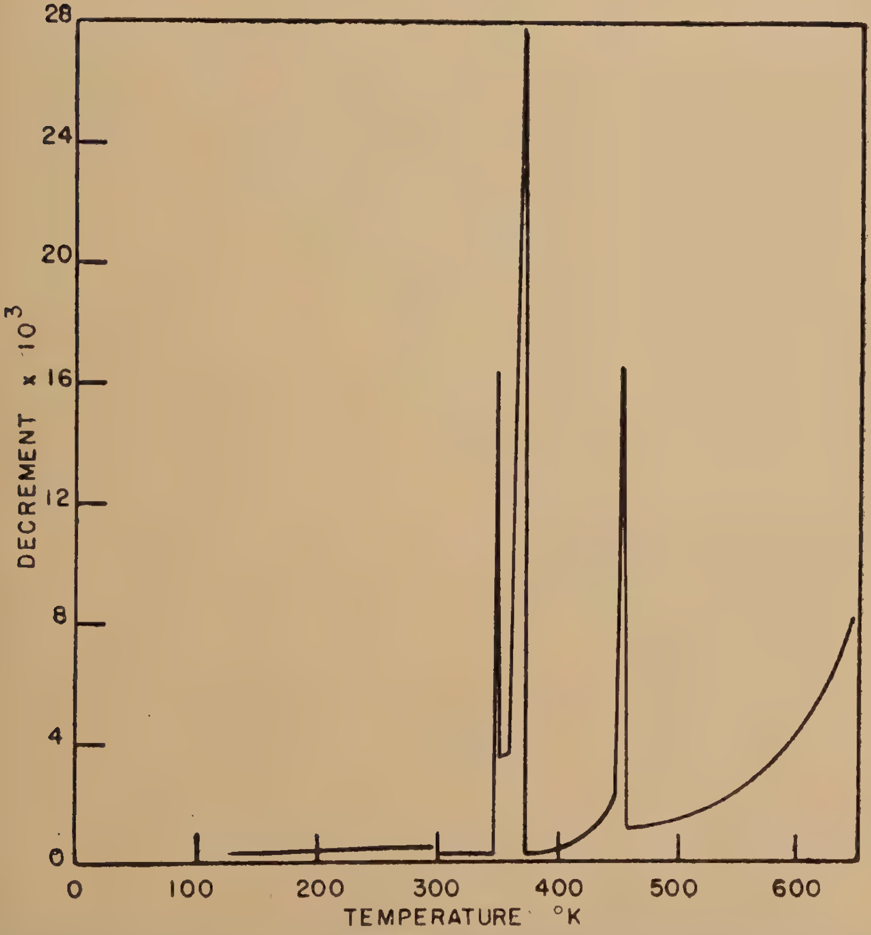

The internal friction of an as-grown single crystal of aluminium measured at steadily increasing temperatures (Birnbaum and Levy 1956).

It is clear that more experiments are needed before one can say definitely if this amplitude-independent friction arises wholly or in part from a vibrating string model, and whether other mechanisms are involved. It is also particularly difficult to make a good estimate of the magnitude of the friction to be expected in any given specimen, because the number and lengths of the dislocation loops are unknown and there is no generally accepted value for the damping constant B. The most complete analysis of this type of friction has been made by Granato *et al.* (1958) using the experimental data of Gordon and Nowick (1956) for both the modulus defect and decrement of sodium chloride, including observations of the Köster effect. These authors showed that the friction could be accounted for by selecting reasonable values for all the parameters, and similar experiments and analyses for the friction of metals would be valuable.

5.4. *Miscellaneous Peaks*

As we mentioned in § 5.1, the friction discussed in the two preceding sections generally rises with increasing temperature, but sometimes the curve of amplitude-independent friction versus temperature exhibits a maximum. This is usually an indication that friction is also arising by some quite different mechanism, and we briefly mention some of the more characteristic features which have been observed.

Fig. 50

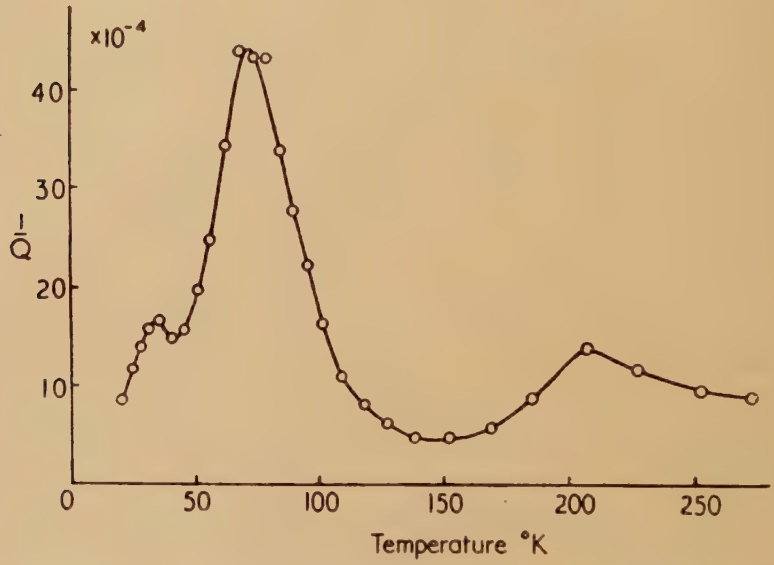

The amplitude-independent internal friction of a polycrystalline specimen strained 5·3% (Niblett and Wilks 1957).

Figure 49, taken from Birnbaum and Levy (1956), shows the decrement of an 'as grown' single crystal of aluminium as a function of temperature, obtained by steadily raising the temperature of the specimen; a series of sharp peaks is superposed on a monotonically rising background. However, on repeating the whole measurement again only the smooth background curve was observed; thus the heating treatment during the first series of measurements was sufficient to anneal out the structure responsible for the peaks. Similar behaviour has been reported in aluminium by Filmer *et al.* (1958) and in copper by Kamentsky (1956), Caswell (1958) and Paré (1958). The fact that these sharp peaks are often removed by annealing suggests that they may be due to an unstable dislocation configuration. However, an explanation is difficult owing to their lack of reproducibility: experiments have so far failed to reveal the conditions necessary for their existence.

Stevens (1957) has shown that the presence of small additions of the order of 0·1 parts per cent of nickel or gold in copper single crystals reduces the friction and also produces a peak in the decrement versus temperature curve at a temperature of about 200°C. There is not at present very much information on these peaks, although Stevens' results suggest that the friction decreases with increasing frequency. Quite possibly the peak arises from a relaxation process of the type suggested by Friedel *et al.* (1955) in which the motion of the dislocations is impeded by impurity atoms condensed on to them, as discussed in § 4.3.

Several authors working at kilocycle frequencies have observed a peak in the friction versus temperature curve of cold-worked copper in the region of 200°K as shown in fig. 50 (Niblett and Wilks 1957, Paré 1958, Thompson and Holmes 1959, Bruner 1959). Measurements by Baxter and Wilks (unpublished) at about 1 c/s show that at this frequency the peak is shifted to about 150°K. If we plot all these results in the form of $\ln f$ against $1/T_m$, where f is the frequency of the oscillations and T_m the temperature of the peak, we obtain quite a good straight line, whose slope corresponds to an activation energy of 0·3 ev.

As we mentioned in § 2.4, the peak in large-grained copper is removed by an anneal at 100°C, whereas the Bordoni peak only anneals at temperatures of the order of 300°C. Therefore this peak must arise by a different mechanism, and a possible one is that put forward by Bruner (1959) to account (incorrectly as we believe) for the Bordoni peaks. This mechanism was described in § 2.4; the essential idea is that if a vacancy is situated in a plane lying immediately above or below a dislocation extended into partials, there will be two equilibrium positions of the dislocation with the vacancy above one or the other partial. The friction then arises from a relaxation mechanism in which the dislocation is displaced from one equilibrium position to the other. Such a mechanism would account for the peak, and also for the fact that it anneals out at about 100°C as the vacancies would then be mobile and diffuse out. One would also expect that the peak could be produced by introducing vacancies either by neutron irradiation or quenching. In fact Thompson and Holmes (1959) have given results for the friction of an irradiated single crystal in which the peak is only obviously present after the irradiation (fig. 43).

ACKNOWLEDGMENTS

We wish to thank Professor J. A. Sauer, Dr. J. Weertman and Mr. W. J. Baxter for their assistance and helpful comments. We also gratefully acknowledge permission to reproduce diagrams given by the authors concerned and the following journals: *Acta Metallurgica*, *Faraday Society Discussions*, *Journal of the Acoustical Society of America*, *Journal of Applied Physics*, *Journal of the Physical Society of Japan*.

REFERENCES

ALERS, G. A., 1955, *Phys. Rev.*, **97,** 863.

ARTMAN, R. A., 1952, *J. appl. Phys.*, **23,** 475.

BAKER, G. S., 1957, *J. appl. Phys.*, **28,** 734.

BALAMUTH, L., 1934, *Phys. Rev.*, **45,** 715.

BARDEEN, J., COOPER, L. N., and SCHRIEFFER, J. R., 1957, *Phys. Rev.*, **108,** 1175.

BARNES, R. S., and HANCOCK, N. H., 1958, *Phil. Mag.*, **3,** 527.

BARNES, R. S., HANCOCK, N. H., and SILK, E. C. H., 1958, *Phil. Mag.*, **3,** 519.

BENNEWITZ, K., and RÖTGER, H., 1936, *Phys. Z.*, **37,** 578 ; 1938, *Z. tech. Phys.*, **19,** 521.

BERRY, B. S., 1955 a, *Rev. sci. Instrum.*, **26,** 884 ; 1955 b, *J. appl. Phys.*, **26,** 1221.

BESHERS, D. N., 1959, *J. appl. Phys.*, **30,** 252.

BIRNBAUM, H. K., 1955, *Acta Met.*, **3,** 297.

BIRNBAUM, H. K., and LEVY, M., 1956, *Acta Met.*, **4,** 84.

BLEWITT, T. H., 1953, *Phys. Rev.*, **91,** 1115.

BÖMMEL, H. E., 1954, *Phys. Rev.*, **96,** 220 ; 1955, *Phys. Rev.*, **100,** 758.

BORDONI, P. G., 1947, *Nuovo Cim.*, **4,** 177 ; 1949, *Ric. Sci.*, **19,** 851 ; 1954, *J. acoust. Soc. Amer.*, **26,** 495.

BORDONI, P. G., NUOVO, M., and VERDINI, L., 1959, *Nuovo Cim.*, **14,** 273.

BOULANGER, C., 1951, *C. R. Acad. Sci., Paris*, **233,** 722.

BRIGGS, N. W., 1955, Thesis, Cornell University.

BROOM, T., and HAM, R. K., 1957, *Symposium on Vacancies and other Point Defects in Metals and Alloys* (London : Institute of Metals), 41.

BRUNER, L. J., 1959, *Phys. Rev. Letters*, **3,** 411.

CASWELL, H. L., 1958, *J. appl. Phys.*, **29,** 1210 (see also Thesis, Cornell University, AFOSR-TR-57-69, 1957).

CHAMBERS, R. H., 1957, Carnegie Inst. of Tech. Report, AT(30-1)-1193 (see also Chambers, R. H., and Smoluchowski, R., 1960, *Phys Rev.*, **117,** 725).

CHANG, L. C., and GENSAMER, M., 1953, *Acta Met.*, **1,** 483.

CHOPRA, K. L., and HUTCHISON, T. S., 1958, *Canad. J. Phys.*, **36,** 805 ; 1959, *Ibid.*, **37,** 1100.

CLAREBROUGH, L. M., HARGREAVES, M. E., and WEST, G. W., 1955, *Proc. roy. Soc.* A, **232,** 252.

COOKE, W. T., 1936, *Phys. Rev.*, **50,** 1158.

COTTRELL, A. H., 1948, *Report of a Conference on the Strength of Solids* (London : Physical Society), p. 30 ; 1953, *Dislocations and Plastic Flow in Crystals* (Oxford).

COTTRELL, A. H., and BILBY, B. A., 1949, *Proc. phys. Soc., London.* A, **62,** 49.

DIETZE, H. D., 1952, *Z. Phys.*, **131,** 156.

DOBBS, E. R., CHICK, B. B., and TRUELL, R., 1959, *Phys. Rev. Letters*, **3,** 332.

DONTH, H., 1957, *Z. Phys.*, **149,** 111.

EINSPRUCH, N. G., and TRUELL, R., 1958, *Phys. Rev.*, **109,** 652.

ESHELBY, J. D., 1949, *Proc. roy. Soc.* A, **197,** 396.

FILMER, A. J., ROGERS, D. H., and HUTCHISON, T. S., 1959, *Proc. of Inter. Cong. of Refrig.* (Copenhagen).

FILMER, A. J., HUTTON, G. J., and HUTCHISON, T. S., 1958, *J. appl. Phys.*, **29** 146.

FÖRSTER, F., 1937, *Z. Metallk.*, **29,** 109.

FÖRSTER, F., and KÖSTER, W., 1937, *Z. Metallk.*, **29,** 116.

FRIEDEL, J., 1956, *Les Dislocations* (Paris).

FRIEDEL, J., BOULANGER, C., and CRUSSARD, C., 1955, *Acta Met.*, **3,** 380.

GORDON, R. B., and NOWICK, A. S., 1956, *Acta Met.*, **4,** 514.

GRANATO, A., HIKATA, A., and LÜCKE, K., 1958, *Acta Met.*, **6,** 470.

Granato, A., and Lücke, K., 1956 a, *J. appl. Phys.*, **27,** 583 ; 1956 b, *Ibid.*, **27,** 789 ; 1957, *Ibid.*, **28,** 635.

Granato, A., and Truell, R., 1956, *J. appl. Phys.*, **27,** 1219.

Hart, E. W., 1955, *Phys. Rev.*, **98,** 1775.

Hikata, A., and Truell, R., 1957, *J. appl. Phys.*, **28,** 522.

Hikata, A., Truell, R., Granato, A., Chick, B., and Lücke, K., 1956, *J. appl. Phys.*, **27,** 396.

Hiki, Y., 1958, *J. phys. Soc., Japan*, **13,** 1138.

Hirone, T., Kunitomi, N., and Abe, M., 1955, *J. phys. Soc., Japan*, **10,** 960.

Hirsch, P. B., Horne, R. W., and Whelan, M. J., 1956, *Phil. Mag.*, **1,** 677.

Huntington, H. B., 1947, *Phys. Rev.*, **72,** 321.

Hutchison, T. S., and Filmer, A. J., 1956, *Canad. J. Phys.*, **34,** 159.

Hutchison, T. S., and Hutton, G. J., 1956, *Canad. J. Phys.*, **34,** 1498 ; 1958, *Ibid.*, **36,** 82.

Kamentsky, L. A., 1956, Thesis, Cornell University, AFOSR–TN–56–425.

Kê, T. S., 1947 a, *Phys. Rev.*, **71,** 533 ; 1947 b, *Ibid.*, **72,** 41 ; 1948 a, *Ibid.*, **74,** 9 ; 1948 b, *Ibid.*, **74,** 914 ; 1949 a, *J. appl. Phys.*, **20,** 274 ; 1949 b, *Ibid.*, **20,** 1226.

Kemp, W. R. G., Klemens, P. G., and Tainsh, R. J., 1959, *Phil. Mag.*, **4,** 845.

Koehler, J. S., 1952, *Imperfections in Nearly Perfect Crystals* (Wiley), Ch. VII, p. 197.

Köster, W., 1940, *Z. Metallk.*, **32,** 282 ; 1940–41, *Arch. Eisenhüttenw.*, **14,** 271.

Köster, W., and Rosenthal, K., 1938, *Z. Metallk.*, **30,** 345.

Lamb, J., Redwood, M., and Shteinshleifer, Z., 1959, *Phys. Rev. Letters*, **3,** 28.

Lax, E., and Filson, D. H., 1959, *Phys. Rev.*, **114,** 1273.

Leibfried, G., 1950, *Z. Phys.*, **127,** 344.

Levy, M., and Metzger, M., 1955, *Phil. Mag.*, **46,** 1021.

Lücke, K., 1956, *J. appl. Phys.*, **27,** 1433.

Lücke, K., and Granato, A., 1957, *Dislocations and Mechanical Properties of Crystals* (Wiley), p. 425.

Ludloff, H. F., 1940, *J. acoust. Soc. Amer.*, **12,** 193.

Mackinnon, L., 1955, *Phys. Rev.*, **100,** 655 ; 1957, *Ibid.*, **106,** 70.

Mackinnon, L., and Myers, A., 1959, *Proc. phys. Soc. Lond.*, **73,** 291.

Maddin, R., and Cottrell, A. H., 1955, *Phil. Mag.*, **46,** 735.

Maringer, R. E., 1953, *J. appl. Phys.*, **24,** 1525.

Maringer, R., and Muehlenkamp, G. T., 1952, *J. Metals, N.Y.*, **4,** 149.

Marx, J., 1951, *Rev. Sci. Instrum.*, **22,** 503.

Marx, J. W., Baker, G. S., and Sivertsen, J. M., 1953, *Acta Met.*, **1,** 193.

Marx, J., and Koehler, J. S., 1950, *Carnegie Inst. of Tech. Symp. on the Plastic Deformation of Crystalline Solids* (Office of Naval Research).

Mason, W. P., 1955 a, *Phys. Rev.*, **97,** 557 ; 1955 b, *Ibid.*, **98,** 1136 ; 1955 c, *J. acoust. Soc. Amer.*, **27,** 643 ; 1955 d, *Bell tech. J.*, **34,** 903 ; 1956, *J. acoust. Soc. Amer.*, **28,** 1207 ; 1958, *Physical Acoustics and the Properties of Solids* (van Nostrand).

Mason, W. P., and Bömmel, H. E., 1956, *J. acoust. Soc. Amer.*, **28,** 930.

Mason, W. P., and McSkimin, H. J., 1947, *J. acoust. Soc. Amer.*, **19,** 464.

Morse, R. W., 1955, *Phys. Rev.*, **97,** 1716.

Morse, R. W., and Bohm, H. V., 1957, *Phys. Rev.*, **108,** 1094.

Morse, R. W., Bohm, H. V., and Gavenda, J. D., 1958, *Phys. Rev.*, **109,** 1394.

Morse, R. W., Tamarkin, P., and Bohm, H. V., 1956, *Phys. Rev.*, **101,** 1610.

Mott, N. F., 1952, *Imperfections in Nearly Perfect Crystals* (Wiley), Chap. VI, p. 173.

Mott, N. F., and Nabarro, F. R. N., 1948, *Report of a Conference on the Strength of Solids* (London : Physical Society), p. 1.

Nabarro, F. R. N., 1951, *Proc. roy. Soc.* A, **209,** 278.

Niblett, D. H., 1956, Thesis, Oxford University.

Niblett, D. H., and Wilks, J., 1955, *Conf. Phys. Basses Temp., Paris*, p. 484; 1956, *Phil. Mag.*, **1,** 415 ; 1957, *Ibid.*, **2,** 1427 ; 1959 a, *Proc. phys. Soc., Lond.*, **73,** 95 ; 1959 b, *Proc. of Inter. Cong. of Refrig.* (Copenhagen).

Norton, J. T., 1939, *Rev. sci. Instrum.*, **10,** 77.

Nowick, A. S., 1950 a, *Phys. Rev.*, **80,** 249 ; 1950 b, *Carnegie Inst. of Tech. Symp. on the Plastic Deformation of Crystalline Solids* (Office of Naval Research) ; 1952, *Phys. Rev.*, **88,** 925 ; 1953, *Prog. Metal Phys.*, **4,** 1.

Paré, V. K., 1958, Thesis, Cornell University, AFOSR–TR–58–92.

Pearson, S., and Rotherham, L., 1956, *J. Metals, N.Y.*, **8,** 894.

Peierls, R. E., 1940, *Proc. phys. Soc., Lond.*, **52,** 34.

Pippard, A. B., 1955, *Phil. Mag.*, **46,** 1104.

Postnikov, V. S., 1957, *Fiz. Met. i Metalloved.*, **4,** 344.

Powers, R. W., and Doyle, M. V., 1956, *Acta Met.*, **4,** 233 ; 1957 a, *J. appl. Phys.*, **28,** 255 ; 1957 b, *J. Metals, N.Y.*, **9,** 1285.

Pratt, P. L., 1957, *Symposium on Vacancies and other Point Defects in Metals and Alloys* (London: Institute of Metals).

Quimby, S. L., 1925, *Phys. Rev.*, **25,** 558.

Randall, R. H., Rose, F. C., and Zener, C., 1939, *Phys. Rev.*, **56,** 343.

Read, T. A., 1940, *Phys. Rev.*, **58,** 371 ; 1941, *Trans. A.I.M.E.*, **143,** 30.

Read, T. A., and Tyndall, E. P. T., 1946, *J. appl. Phys.*, **17,** 713.

Read, W. T., 1953, *Dislocations in Crystals* (McGraw-Hill).

Roderick, R. L., and Truell, R., 1952, *J. appl. Phys.*, **23,** 267.

Roswell, A. E., and Nowick, A. S., 1957, *Acta Met.*, **5,** 228.

Roth, W., 1948, *J. appl. Phys.*, **19,** 901.

Rotherham, L., and Pearson, S., 1956, *J. Metals, N.Y.*, **8,** 881.

Seeger, A., 1954, *Z. Naturf.*, **9a,** 870 ; 1955, *Handb. Phys.*, **7/1,** 383 ; 1956, *Phil. Mag.*, **1,** 651.

Seeger, A., Donth, H., and Pfaff, F., 1957, *Disc. Faraday Soc.*, **23,** 19.

Seitz., F., 1950, *Carnegie Inst. of Tech. Symp. on the Plastic Deformation of Crystalline Solids* (Office of Naval Research).

Shibata, A., 1959, Thesis, Cornell University.

Smith, A. D. N., 1953, *Phil. Mag.*, **44,** 453.

Snoek, J. L., 1941, *Physica*, **8,** 711.

Stevens, R. R., 1957, Thesis, Cornell University, AFOSR–TR–57–11.

Swift, I. H., and Richardson, J. E., 1947, *J. appl. Phys.*, **18,** 417.

Takahashi, S., 1956, *J. phys. Soc., Japan*, **11,** 1253.

Thompson, D. O., and Holmes, D. K., 1956 a, *J. appl. Phys.*, **27,** 191 ; 1956 b, *Ibid.*, **27,** 713 ; 1959, *Ibid.*, **30,** 525.

Waterman, P. C., 1958, *J. appl. Phys.*, **29,** 1190.

Weertman, J., 1955, *J. appl. Phys.*, **26,** 202 ; 1956, *Phys. Rev.*, **101,** 1429 ; 1957, *J. appl. Phys.*, **28,** 193 and 636.

Weertman, J., and Koehler, J. S., 1953, *J. appl. Phys.*, **24,** 624.

Weertman, J., and Salkovitz, E. I., 1955, *Acta Met.*, **3,** 1 ; 1956, *J. appl. Phys.*, **27,** 1251.

Wegel, R. L., and Walther, H., 1935, *Physics*, **6,** 141.

Weiner, L. C., and Gensamer, M., 1957, *Acta Met.*, **5,** 692.

Weinig, S., and Machlin, E. S., 1956, *J. appl. Phys.*, **27,** 734.

Welber, B., and Quimby, S. L., 1958, *Acta Met.*, **6,** 351.

Wert, C. A., 1949, *J. appl. Phys.*, **20,** 29.

Wilks, J., 1959, *Phil. Mag.*, **4,** 1379.

Zener, C., 1937, *Phys. Rev.*, **52,** 230 ; 1938, *Ibid.*, **53,** 90 ; 1943, *Trans. A.I.M.E.*, **152,** 122 ; 1947, *Phys. Rev.*, **71,** 34 ; 1948, *Elasticity and Anelasticity of Metals* (Chicago).

Zener, C., Otis, W., and Nuckolls, R., 1938, *Phys. Rev.*, **53,** 100.

The Rotation of Liquid Helium II

By H. E. HALL
The Physical Laboratories, University of Manchester

CONTENTS

§ 1. INTRODUCTION. 89

§ 2. THE QUANTIZATION OF CIRCULATION. 92
  2.1. Feynman's Circulation Theorem. 92
  2.2. Experimental Evidence for the Quantization of Circulation. 96

§ 3. UNIFORMLY ROTATING HELIUM II. 100
  3.1. The Equilibrium State of Rotating Helium II. 100
  3.2. The Attenuation of Second Sound. 104
  3.3. The Theory of the Mutual Friction. 107
  3.4. Torsional Oscillations: Vortex Waves. 111
  3.5. Vortex Waves and Mutual Friction. 117

§ 4. THE OBSERVABLE PROPERTIES OF VORTEX LINES. 125
  4.1. The Collision Diameters. 126
  4.2. The Effective Core Radius. 129

§ 5. SUPERFLUID TURBULENCE. 131
  5.1. Mutual Friction and Turbulence. 131
  5.2. Dimensional Analysis of Homogeneous Turbulence. 133
  5.3. Wall Effects. 138
  5.4. Boundary Layer Experiments. 142
  5.5. Eddy Viscosity. 144

§ 6. CONCLUSION. 145

---

§ 1. INTRODUCTION

WHEN the flow properties and theory of liquid helium II were last reviewed in this journal (Atkins 1952, Dingle 1952), wave propagation and reversible flow phenomena had already found a satisfactory explanation in Landau's (1941, 1947) theory. According to this theory superfluidity is essentially a property of the quantum-mechanical ground state of liquid helium; and at any finite temperature below the λ-point the liquid differs from its ground state only by the presence of a number of thermal excitations. Landau postulated two types of thermal excitation, phonons and rotons. The phonons are quanta of sound vibration, as in a solid, except that only longitudinal modes are present, and the energy E is related to the momentum p by

$$E=cp, \qquad (1)$$

where c is the velocity of sound. The rotons Landau considered to be the excitation of some form of vortex motion in the liquid. From an analogy between the commutation relations for angular momentum and the commutation relations for curl $\mathbf{v}$ he argued that a minimum energy Δ would be necessary to excite this type of motion, and he therefore suggested for rotons the dispersion relation

$$E=\Delta+\frac{(p-p_0)^2}{2\mu}. \qquad (2)$$

These thermal excitations can move freely through the background fluid, and thus behave very like a gas of free particles. In particular the whole excitation gas can drift with velocity $\mathbf{u}$ relative to the background fluid, but straightforward statistical mechanical arguments show that the momentum carried is only $\rho_n\mathbf{u}$, where $\rho_n<\rho$. Landau's theory therefore leads in a natural way to the phenomenological two-fluid model. The normal fluid can be identified with the excitation gas, with velocity $\mathbf{v}_n$ and density ρ_n, and the total entropy S of the liquid will naturally be carried along with the excitations. The remaining superfluid part of the liquid, with velocity $\mathbf{v}_s$ and density $\rho_s=\rho-\rho_n$ can be identified with what remains of the ground state, and the velocity $\mathbf{u}$ is clearly $(\mathbf{v}_n-\mathbf{v}_s)$. These considerations lead to the equations of motion

$$\rho_n\frac{D\mathbf{v}_n}{Dt}=-\frac{\rho_n}{\rho}\operatorname{grad}p-\rho_sS\operatorname{grad}T+\eta_n(\nabla^2\mathbf{v}_n+\tfrac{1}{3}\operatorname{grad}\operatorname{div}\mathbf{v}_n), \qquad (3)$$

and

$$\rho_s\frac{D\mathbf{v}_s}{Dt}=-\frac{\rho_s}{\rho}\operatorname{grad}p+\rho_sS\operatorname{grad}T.\dagger \qquad (4)$$

The viscosity term in eqn. (3) arises from collisions between the excitations, as in a gas; there is no such term in eqn. (4) for the superfluid, since this represents the ground state of the liquid, and flows as a classical perfect fluid, without dissipation. The hydrodynamics is completely specified if we add to eqns. (3) and (4) the equations of conservation of mass

$$\frac{\partial\rho}{\partial t}+\operatorname{div}(\rho_n\mathbf{v}_n+\rho_s\mathbf{v}_s)=0 \qquad (5)$$

and of entropy

$$\frac{\partial(\rho S)}{\partial t}+\operatorname{div}(\rho S\mathbf{v}_n)=0. \qquad (6)$$

It is an essential feature of Landau's theory that with suitable boundary conditions a non-zero value of $(\mathbf{v}_n-\mathbf{v}_s)$ can exist *in thermal equilibrium*; superfluidity is not due to scarcity of collisions, but is rather the equilibrium state which the collisions tend to produce; the friction between normal fluid and superfluid is identically zero. This is essentially the

---

† Second-order terms, other than those implied by the convective derivatives D/Dt, have been omitted from these equations of motion, since they do not affect the phenomena discussed in this article.

consequence of an additional restrictive condition obtained by Landau, namely

$$\operatorname{curl} \mathbf{v}_s = 0 ; \qquad (7)$$

from this it follows that the flowing superfluid can lose energy only by the creation of excitations, and this process can only occur with conservation of energy and momentum if the velocity exceeds

$$v_c = \left(\frac{E(p)}{p}\right)_{\min} \approx \frac{\Delta}{p_0} \doteqdot 70 \text{ m/sec.} \qquad (8)$$

Equations (3)–(6) should therefore be valid for all velocities less than v_c.

Two important predictions follow from eqns. (3)–(6). First, there should exist two modes of wave motion in the liquid: pressure oscillations at almost constant temperature (first sound); and temperature oscillations at almost constant pressure (second sound). Second sound was first observed by Peshkov (1944, 1946), and the measured velocity was in very good agreement with Landau's theory. The second prediction was that the moment of inertia of the liquid should correspond to density ρ_n rather than ρ; Andronikashvili (1946) checked this by measuring the period of torsional oscillations of a pile of closely spaced disks, and likewise found results in good quantitative agreement with theory. The theory was also successful in accounting for other reversible effects, and for various dissipative effects, such as the viscosity of the normal fluid, arising from collisions between the excitations (see Khalatnikov 1956).

However, many non-linear dissipative processes were also observed (see Atkins 1952). These effects occur even at velocities of the order of 1 cm/sec, very much less than the critical velocity given by eqn. (8), and so cannot be explained by Landau's theory. For many years it was not at all clear whether frictional forces existed between normal fluid and superfluid. The mutual friction force introduced by Gorter and Mellink (1949) gave a fairly successful phenomenological description of a number of steady flows; but it appeared not to be present in a second sound wave, and on the other hand, some experiments seemed to require the existence of yet more frictional forces. And whatever the phenomenological successes of such a friction force, there was no theoretical explanation of its existence. Another difficulty of the Landau theory was that observations of the free surface of helium II in a rotating vessel (Osborne 1950) showed that the superfluid could be made to rotate quite easily, thereby violating the condition $\operatorname{curl} \mathbf{v}_s = 0$ (eqn. (7)). We shall see in the course of this article that these two failures of the original Landau theory—the existence of non-linear dissipative processes and violation of the condition $\operatorname{curl} \mathbf{v}_s = 0$—are in fact intimately connected.

Since 1952 the foundations of Landau's theory have been considerably strengthened by Feynman's (1954, Feynman and Cohen 1956) deduction of the phonon-roton excitation spectrum from atomistic considerations of the form of the wave function of liquid helium, and by the experimental verification of that spectrum by the inelastic scattering of cold neutrons

(Yarnell *et al.* 1959). We shall not be concerned with these developments here. A development of far greater value for the interpretation of experimental results is Feynman's (1955) replacement of the condition curl $\mathbf{v}_s = 0$ by the rather less restrictive condition

$$\oint \mathbf{v}_s \,.\, d\mathbf{l} = n\frac{h}{m}, \qquad . \;.\;.\;.\;.\;.\;.\;.\;.\;.\; (9)$$

where n is an integer. Feynman interprets this equation as meaning that curl $\mathbf{v}_s = 0$ almost everywhere in the liquid, but there may be certain lines in the liquid on which the velocity is singular. These are quantized vortex lines, and the circulation round them is an integral multiple of h/m. Our principal object in this article will be the exploration of the consequences of this idea; we interpret 'rotation' as meaning any flow in which circulation of the superfluid exists. We shall not attempt to follow Dingle (1952) in discussing all theoretical attempts to explain the behaviour of liquid helium II. Instead we shall adopt a definite theoretical viewpoint, essentially that of Landau as modified and extended by Feynman, and attempt to use it to give a unified coherent account of as many experimental facts as possible. We shall discuss the various types of flow in order of increasing complexity, proceeding from irrotational circulation through macroscopically uniform rotation to turbulence. This is an almost complete reversal of the historical order of development, for the connection between rotation and mutual friction was in fact first conjectured by Vinen as a result of his discovery that mutual friction in a heat current was associated with turbulence; the reader interested in the genesis of the ideas discussed in this article may consult a note (Hall and Vinen 1955) written shortly before the publication of Feynman's ideas on superfluid rotation.

§ 2. The Quantization of Circulation

From time to time a number of authors (H. London 1946, Onsager 1949, F. London 1954, Landau and Lifshitz 1955) have suggested that macroscopic rotation of the superfluid could be achieved despite the condition curl $\mathbf{v}_s = 0$ if a few small regions of concentrated vorticity (either vortex sheets or vortex lines) were permitted; the quantization condition (9) was also conjectured by some of these authors. Equation (9) is formally similar to a Bohr quantization condition for each atom; but in liquid helium the atoms are interacting and the velocity of a single atom cannot be defined; only the velocity $\mathbf{v}_s$ has meaning at absolute zero. The advances made by Feynman (1955) were, first, a satisfactory theoretical argument for the validity of eqn. (9) in liquid helium, and secondly, a fairly detailed qualitative exploration of the possible observable consequences of quantized circulation.

2.1. *Feynman's Circulation Theorem.*

We now give Feynman's proof of the quantization of circulation; this is the basic theoretical result for the whole problem of rotating helium.

Consider the liquid at abolute zero in its ground state. Since ^{4}He atoms are bosons the wave function $\Phi(\mathbf{r}_1, \mathbf{r}_2 \ldots \mathbf{r}_N)$ is a symmetric function of the atomic coordinates $(\mathbf{r}_1, \mathbf{r}_2, \ldots \mathbf{r}_N)$. In considering the way in which the wave function depends on the atomic coordinates we shall speak of the changes in the wave function as the atoms are moved about; but it cannot be too strongly emphasized that this is merely a pictorial language to describe the dependence of Φ on the coordinates $(\mathbf{r}_1, \mathbf{r}_2 \ldots \mathbf{r}_N)$, and does not refer to any real physical motion of the atoms. Indeed, an attempt to consider individual atomic motions would soon lead into conflict with the uncertainty principle. We know that in the ground state Φ is real and for a system of bosons contains no nodes; it may therefore be taken as a positive number. Since the atoms form a liquid, Φ will be near its maximum value for all configurations in which the atoms are fairly evenly spaced at about the equilibrium density, but will fall rapidly if a hole develops in the liquid or if any two atoms approach so closely as to repel each other strongly. Because of the rather low density of liquid helium, atoms can move freely between each other without causing a serious decrease in the amplitude Φ. The importance of this result is that it enables us to follow changes in phase of the wave function as the atoms are moved about; if there are no nodes for any intermediate configuration the phase changes will be continuous.

Now consider the effect on the wave function if the whole liquid is set in motion with a uniform velocity $\mathbf{v}_S$. The centre of gravity coordinate separates out from the Schrödinger equation, so the new wave function is

$$\begin{aligned}\Psi &= \Phi \exp\left[i\,\frac{Nm\mathbf{v}_S}{\hbar} \cdot \frac{\sum_i \mathbf{r}_i}{N} \right] \\ &= \Phi \exp\left[i(m/\hbar)\mathbf{v}_S \cdot \sum_i \mathbf{r}_i \right]. \qquad (10)\end{aligned}$$

This wave function is exact. We now try to extend it to situations in which $\mathbf{v}_S$ is not uniform but varies from point to point in the liquid. Provided the velocity variations are very gradual on an atomic scale, we may expect that (10) is still a good wave function locally, in the sense that the change in phase produced by local displacements of the atoms (over distances too small for appreciable velocity variation) will be the same as that given by (10), except that $\mathbf{v}_S$ is now a function of position. Thus the total phase change $\Delta\phi$ due to a displacement of atoms is given by

$$\Delta\phi = (m/\hbar) \sum_i \mathbf{v}_S \cdot \Delta\mathbf{r}_i, \qquad (11)$$

where $\mathbf{v}_S$ is the velocity at position $\mathbf{r}_i$, provided that all the displacements $\Delta\mathbf{r}_i$ are small compared with the scale of velocity variation. Consider in particular a large ring of atoms (say at least 100) and let $\mathbf{v}_S$ be slowly varying at each atomic position. Now slide the whole ring along itself until each atom occupies the position formerly occupied by the one next in line, if necessary giving other atoms small temporary displacements so as to keep Φ large. All the atomic displacements are small (about an atomic spacing) so according to our previous result the phase change is

$$\frac{m}{\hbar}\sum_i \mathbf{v}_s \,.\, \Delta\mathbf{r}_i = \frac{m}{\hbar}\oint \mathbf{v}_s \,.\, \mathbf{dl} \quad . \quad . \quad . \quad . \quad . \quad . \quad . \quad (12)$$

if the sum is smoothed out to a line integral round the ring. But the special displacement we have considered is just a permutation of atoms, and must therefore leave the wave function unchanged, because of the Bose statistics. The phase change must therefore be an integral multiple of 2π, i.e.

$$\oint \mathbf{v}_s \,.\, \mathbf{dl} = n\frac{h}{m}, \quad . \quad . \quad . \quad . \quad . \quad . \quad . \quad . \quad . \quad (9)$$

where n is an integer.

If the velocity is slowly varying at every point in the liquid, eqn. (9) will be valid for all circuits of integration and we have

$$\operatorname{curl} \mathbf{v}_s = 0 ; \quad . \quad . \quad . \quad . \quad . \quad . \quad . \quad . \quad (7)$$

in a simply connected vessel this implies $\mathbf{v}_s = 0$, but in a multiply connected vessel there may be a quantized circulation. But if eqn. (9) is only valid for *almost* all circuits it is possible to have $n \neq 0$ for some circuits even in a simply connected vessel. Suppose we take a circuit for which $n=1$ in a simply connected vessel and gradually shrink it. As the circuit shrinks $\mathbf{v}_s$ rises and becomes more rapidly varying until the assumptions used in deriving eqn. (9) are no longer valid; we are approaching a node in the wave function where the velocity is singular and the phase indeterminate. It can be seen from the fact that eqn. (9) is valid unless the path of integration passes near to such a node that these nodes must form lines in the liquid which either close on themselves or end on the boundaries. They are in fact the vortex lines of classical hydrodynamics, and eqn. (9) is the quantum mechanical form of Kelvin's circulation theorem. In the classical hydrodynamics of an inviscid fluid the circulation round a path moving with the fluid is conserved; in the quantum hydrodynamics of superfluid helium the same quantity is quantized.

Our conclusion, then, is that eqn. (9) should be valid for almost all sufficiently large circuits, i.e. for all circuits which nowhere approach too close to a vortex line. It is difficult to say how close one can approach to a vortex line before eqn. (9) fails. The critical distance can hardly be smaller than an atomic spacing, but might be considerably larger. For a classical vortex line of circulation κ on the axis of a cylinder of radius b in a liquid of density ρ_s the energy per unit length is

$$\epsilon = \frac{\rho_s \kappa^2}{4\pi} \ln(b/a_0), \quad . \quad . \quad . \quad . \quad . \quad . \quad . \quad . \quad (13)$$

where a_0 is the radius of the hole in the centre of the line. This calculation will apply to liquid helium in the region where eqn. (9) is valid, so that the logarithmic dependence on b should be preserved; but the contribution to the energy from the core of the vortex can only be obtained from an accurate wave function for the line. This contribution will be partly kinetic energy, and partly potential energy required to reduce the density of the liquid near the node in the wave function. At any rate we may expect the core of the vortex to give an additive contribution to the energy, independently of the boundary conditions, so that eqn. (13) with a suitable value of a_0 can still be used to represent the energy of unit length of line, which is, as we shall see, an experimentally observable quantity. But it must be stressed that the effective core radius a_0 does not correspond to the radius of any real hole in the liquid; it is simply a characteristic length defined by eqn. (13).

So far our considerations have been confined to absolute zero. At a finite temperature the wave function (11) will be multiplied by a number of factors like $\sum_i \exp(i\mathbf{k}\,.\,\mathbf{r}_i)$ representing the presence of excitations. The change in phase of the wave function therefore separates into a contribution from each excitation and a contribution from the velocity field $\mathbf{v}_S$, so that eqn. (9) is still valid. If we use a more accurate wave function in which the excitations are localized wave packets this conclusion still holds provided that the path of integration used in evaluating the circulation does not pass too close to an excitation. The energy of a vortex line will be independent of temperature to the same approximation that the energy of an excitation is independent of the presence of other excitations. In fact it is easy to obtain a rather better approximation to the energy; for the velocity field of a vortex line polarizes the rotons in its vicinity (compare Feynman 1954) with the result that the momentum density becomes $\rho_S\mathbf{v}_S$ rather than $\rho\mathbf{v}_S$, and the energy density becomes $\frac{1}{2}\rho_S v_S^2$; it is therefore reasonable to write ρ_S rather than ρ in eqn. (13).

We may thus expect the concept of quantized vortex lines to be a useful one until the density of excitations becomes very great or until considerable quantities of vortex line are excited thermally. It is not easy to give a theoretical estimate of the amount of vortex line excited thermally; the energy is known, but there is no reliable estimate of the statistical weight factor due to the various configurations available for a given length of line. But it is known (Feynman and Cohen 1956) that rotons may be thought of as the smallest possible vortex rings (about one atomic spacing in diameter) and thus represent a form of thermally excited vortex line. Feynman (1955) has suggested that at the λ-point it suddenly becomes possible to excite thermally very large vortex rings, or long lengths of line. On this view the λ-point marks a change in topology of the thermally excited vortex line from a set of disconnected rings to a single curve winding continuously back and forth through the liquid. The suggestion is an attractive one, but has not been proved. If it is correct the idea of vortex lines should be a useful one almost up the λ-point. We shall see later that experimental evidence suggests that vortex lines are indeed a useful concept to within at least a few tenths of a degree of the λ-point.

2.2. *Experimental Evidence for the Quantization of Circulation*

The first experiment to be reported which was relevant to the question of quantization of circulation was that of Craig and Pellam (1957), who measured the lift force on an airfoil in helium II. For irrotational flow of a fluid of density ρ about an airfoil (or other cylindrical object) the lift force per unit length of airfoil is given by

$$\mathbf{f}=\rho\mathbf{v}\times\boldsymbol{\kappa}, \quad . \quad . \quad . \quad . \quad . \quad . \quad . \quad . \quad . \quad . \quad (14)$$

where $\mathbf{v}$ is the free stream velocity and $\boldsymbol{\kappa}$ is the circulation round the airfoil; this phenomenon is known as the Magnus effect. In an ordinary fluid $\boldsymbol{\kappa}$ is determined by the condition that fluid should not have to flow round the sharp trailing edge of the airfoil, so that $\kappa \propto v$ and $f \propto v^2$. This result will clearly be modified if κ is quantized.

In Craig and Pellam's experiment two airfoils were used, arranged with opposite angles of attack like a small propeller, and hung from a torsion fibre in a vertical tube, so that the lift force could be deduced from the twist of the fibre. The working section of the tube was closed at both ends with plugs of fine powder, and superfluid was drawn up the tube past the airfoils by means of a heater placed above the upper powder plug; the two powder plugs served to prevent flow of the normal fluid, and the flow rate was measured by means of a venturi tube. The experiments were done at 1·3°K, where the superfluid density is 95% of the total.

For flow velocities below 0·3 cm sec^{-1} the lift was exactly zero within the accuracy of the experiment (i.e. less than 1/1000 of the value expected for an ordinary liquid). This is clear evidence for a certain stability of the flow with curl $\mathbf{v}_s=0$, and for the absence of any mechanism (such as a viscous boundary layer) capable of starting a circulation round the airfoil at these low velocities. From 0·3 to 0·6 cm sec^{-1} a very small *negative* lift was observed, possibly due to a secondary flow of normal fluid between the powder plugs. Above 0·6 cm sec^{-1} the lift was positive and proportional to $v\,(v-0{\cdot}6)$; there was no sign of a stepwise increase in lift, such as might be expected if circulation is quantized. But this negative result is not conclusive. Strong fluctuations were found both in the venturi flow meter and in the deflection of the airfoils, which necessitated strong electromagnetic damping of the airfoils to make observations possible, so that only a time averaged lift was measured. These irregularities suggest several possibilities for explaining the results in terms of quantized vortex lines:

(i) Circulation round the airfoil requires that a free vortex line should leave from the ends; the force exerted by such a free vortex line at its point of attachment will depend on its inclination relative to the airfoil.

(ii) A free vortex line need not leave at the end of an airfoil, but could leave from a point on the trailing edge, giving different circulations round different parts of the airfoil. Fluctuations of lift would arise if the point of attachment ran back and forth along the trailing edge.

(iii) These effects could be further complicated by turbulence in the flowing superfluid, which other experiments (§ 5) suggest would probably occur at the flow velocities concerned.

(iv) The measurement of pressure in a venturi flow meter depends on the existence of vorticity at the entrance of the side tube used for pressure measurement. Quantized circulation could thus lead to irregularities in the measured pressure.

This experiment therefore provides no conclusive evidence for or against quantized circulation; but it does provide conclusive evidence of the stability of irrotational superfluid flow.

The difficulties of the airfoil experiment were ingeniously avoided by Vinen (1958 b). His apparatus consisted essentially of a closed cylindrical vessel (5 mm diameter, 5 cm long) with a fine wire (0·001 in. diameter) stretched along the axis. The circulation round the wire could be deduced from a study of its transverse vibrations, for the Magnus effect (eqn. (14)) gives a force on the wire proportional to its velocity and perpendicular to its direction of motion, and thus causes a precession of the plane of vibration. In other words the presence of a circulation κ round the wire removes the degeneracy of transverse vibrations, so that the normal modes become two circularly polarized vibrations with opposite directions of rotation, differing in frequency by an amount $\rho_s\kappa/2\pi w$ where w is the mass of unit length of wire. This frequency difference was measured as the frequency of beats superposed on the freely decaying vibrations of the wire. The vibrations were detected by observing the voltage generated between the ends of the wire when it was placed in a magnetic field, and were started by passing a pulse of current through the wire.

It can be seen that this arrangement avoids the difficulty due to free ends of the airfoil, and also reduces the risk of turbulence, since only the wire moves. To minimise the risk of turbulence, or of otherwise disturbing the flow, the amplitude of vibration was normally kept extremely small, less than the radius of the wire, and also the product of velocity and radius was kept less than h/m.

Circulation round the wire was initially generated by rotating the whole apparatus. Calculations of the type given in the next section (§ 3.1) show that if circulation is quantized the thermodynamic equilibrium state of the superfluid consists of one or more quanta of circulation round the wire, and possibly a number of free vortex lines, for all angular velocities greater than $[(h/m)\ln(b/a)]/(b^2-a^2)$, where b is the radius of the vessel and a is the radius of the wire. To encourage formation of this equilibrium state the apparatus was first rotated above the λ-point at an angular velocity greater than this critical value (about 7·5 rev/hr) for a sufficient time to achieve equilibrium. It was then slowly cooled to 1·3°K, still rotating, and the circulation was measured (unfortunately the viscous damping of the wire was too great to permit circulation measurements above 1·4°K). Finally, rotation was stopped and further measurements of circulation made; it might be expected that any circulation round the wire would persist in metastable equilibrium for a considerable time.

Some typical experimental results of circulation as a function of time are shown in fig. 1†. The small arrows on the figure indicate times at which the wire was given a large amplitude vibration, in an attempt to disrupt any non equilibrium state. It can be seen that when the apparatus is rotating the apparent circulation round the wire, though of the expected order of magnitude, is not an integral multiple of h/m; it varies with time in a somewhat irregular way, and large amplitude vibrations have no definite effect. But after rotation is stopped large amplitude vibrations always reduce the apparent circulation, until a value of exactly h/m (within the experimental accuracy of 2%) is reached. Thereafter the circulation is remarkably stable; it is difficult to produce any alteration, and if a reduction is produced it is only temporary. Once a circulation of exactly h/m is produced, small alterations from this flow tend to eliminate themselves. This result provides the best experimental evidence to date for a true persistent current in helium II, with identically zero dissipation; the circulation has been observed to stay constant within the experimental error for as long as 100 min. Indeed, once the circulation has been created, the only way that has been found to destroy it is to heat the liquid above the λ-point.

Fig. 1

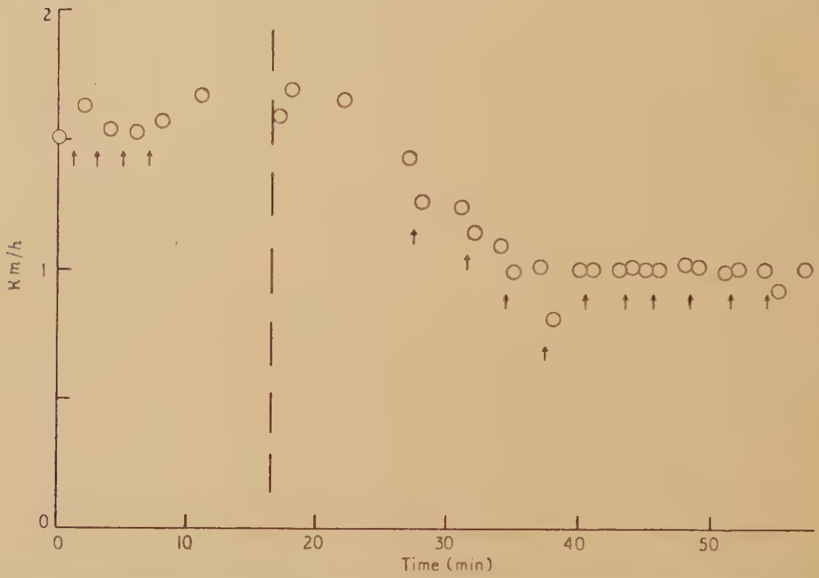

Circulation round the vibrating wire as a function of time. The small arrows indicate times at which the wire was given a large amplitude vibration, and the broken line marks the time at which rotation was stopped.

---

† I am grateful to Dr. Vinen for allowing me to make use of figs. 1 and 2 before publication.

The stability of a circulation of h/m is illustrated in another way in fig. 2, which is a histogram of those values of circulation which were not changed by more than 4% by a large amplitude vibration of the wire, and were thus particularly stable. The peak at h/m is convincing evidence of the stability of this value of circulation.

It thus appears that quantized circulation, though exceptionally stable, is not the only possible value. But it must be remembered that this experiment does not measure the circulation round a single path in the liquid, but rather the average circulation along the length of the wire. Thus, if a free vortex line finishes at a point on the wire we can have, for example, one quantum of circulation above that point and two below it, so that the measured average circulation is intermediate between one and two quanta; this is analogous to one of the difficulties considered in connection with the airfoil experiment. It might be expected that such a free vortex line could be removed from the wire by large vibrations, whereas circulation without such a free line would be more stable; this is in agreement with the experimental results. The results obtained when the apparatus is rotating suggest that although large vibrations can move the point of attachment of a free vortex line, the equilibrium is almost neutral, and there is no marked preference for either one or two quanta of circulation round the wire. This result is significant in relation to the energy of a free vortex line, and will be considered further in § 4.

Fig. 2

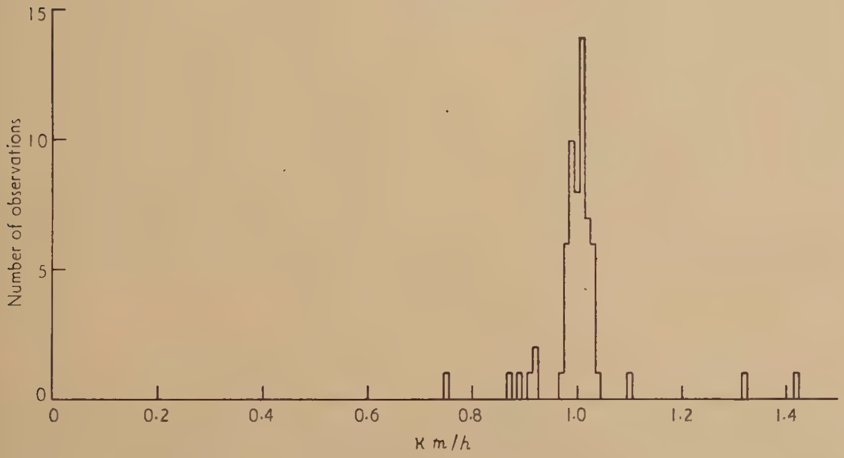

Histogram showing the distribution of stable values of the circulation.

This experiment thus provides clear evidence for the exceptional stability of a circulation of precisely h/m, and the less stable apparent circulations of other values can also be explained in terms of free quantized vortex lines. In principle, the detailed distribution of circulation along the wire could be deduced from measurements of the apparent circulation for all its harmonic vibrations, but this is hardly practicable experimentally.

§ 3. UNIFORMLY ROTATING HELIUM II

3.1. *The Equilibrium State of Rotating Helium II*

For any substance the state of thermodynamic equilibrium with a closed vessel rotating uniformly with angular velocity ω_0 is obtained by minimizing the quantity $(F-M\omega_0)$, where F is the free energy and M the angular momentum (Landau and Lifshitz 1958). For an ordinary liquid, in which any velocity distribution is possible, the equilibrium state turns out to be rotation as a solid body with angular velocity ω_0, but in helium II such a velocity distribution is not allowed for the superfluid, because of the quantization of circulation. The free energy of helium II can be written in the form $(F_0+\frac{1}{2}\rho_s v_s^2+\frac{1}{2}\rho_n v_n^2)$ where F_0 is the free energy of the stationary liquid. It is therefore sufficient to minimize the quantity

$$F'=E-M\omega_0, \quad . \quad . \quad . \quad . \quad . \quad . \quad . \quad . \quad . \quad (15)$$

where E is the kinetic energy, for each fluid separately. The normal fluid clearly rotates as solid-body with angular velocity ω_0, like any other liquid; the superfluid requires a more detailed calculation, but it will be convenient to preface this with some general qualitative considerations. It is fairly clear that the quantity F' will be lower the more nearly we can imitate solid-body rotation, despite the quantization of circulation. Now solid body rotation is characterized by a uniform vorticity $2\omega_0$; this can be imitated on a macroscopic scale if the superfluid contains a number of vortex lines running parallel to the axis of rotation and uniformly spaced at a density n_0 per unit area normal to the axis of rotation given by

$$n_0=\frac{2\omega_0}{\kappa}, \quad . \quad . \quad . \quad . \quad . \quad . \quad . \quad . \quad . \quad . \quad (16)$$

since this ensures that the circulation round a circuit embracing many vortex lines has the same value as for solid-body rotation. The smaller the circulation κ round individual lines, the nearer the flow is to uniform rotation, so we may expect κ to have the smallest allowed value, h/m. Figure 3 is a schematic drawing of this flow, viewed from a coordinate system rotating with angular velocity ω_0, so as to exhibit the departure from uniform rotation. It can be seen that each vortex line is surrounded by a set of closed streamlines, with the velocity rising to high values at the vortex core, but on the network represented by dotted lines in the figure the total velocity due to all the vortex lines is exactly the same as for uniform rotation. Since each vortex line moves with the velocity created in its vicinity by the others, the whole array of vortex lines rotates with angular velocity ω_0. To give an idea of the scale of the flow shown in fig. 3, we remark that for $\omega_0=1\,\mathrm{rad\,sec^{-1}}$ and $\kappa=h/m$ the vortex lines are about 0·2 mm apart.

We now proceed to calculate the free energy F' for an arrangement of vortex lines of this type. For a correct quantum mechanical calculation the quantities E and M in eqn. (15) should be replaced by the Hamiltonian and angular momentum operators respectively, but we shall continue to use the semi-classical model of a vortex line introduced in § 2.1. This should be quite adequate except near the core of a vortex, and quantum mechanical contributions to the energy from the core of the vortex can be taken into account by means of the effective core radius a_0 (eqn. (13)); the corresponding contributions to the angular momentum should be quite negligible. Our calculation will necessarily be somewhat approximate, because a detailed calculation of the flow due to very many vortex lines (say about 1000) is hardly practicable.

Fig. 3

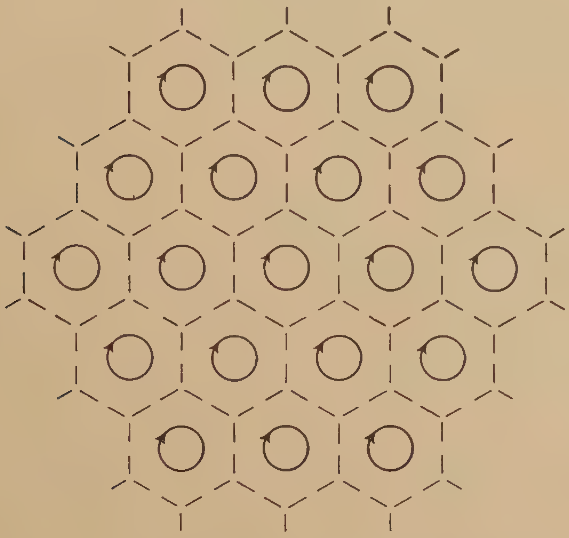

Schematic drawing of part of the flow due to a close-packed array of vortex lines, viewed from a coordinate system rotating with angular velocity $\omega_0 = n_0\kappa/2$ where n_0 is the number of lines per unit area. The solid lines are streamlines, and the broken lines are lines of zero velocity, i.e. lines on which the flow due to the vortex lines corresponds exactly to uniform rotation with angular velocity ω_0.

Consider a cylindrical vessel of liquid of radius R and unit height, rotating about its axis with angular velocity ω_0, and suppose that the superfluid contains N vortex lines of circulation κ running parallel to the axis of rotation. We shall first arrange these N lines to minimize the free energy F' and then find the most favourable value of N. For simplicity we do not consider a completely general arrangement of lines, but suppose that they are packed uniformly so as to simulate solid-body rotation with angular velocity ω (not necessarily equal to ω_0); the lines will then be contained within a radius r given by

$$r^2 = \frac{N\kappa}{2\pi\omega}, \qquad \qquad (17)$$

and beyond this radius the flow will be very nearly a simple irrotational flow with circulation $N\kappa$. The energy and angular momentum are then given by

$$E=\frac{\rho_s\pi}{4}\left(\frac{N\kappa}{2\pi\omega}\right)^2\omega^2+\frac{\rho_s N\kappa^2}{4\pi}\ln(b/a_0)+\frac{\rho_s N^2\kappa^2}{4\pi}\ln(R/r) \quad . \quad (18)$$

and

$$M=\frac{\rho_s\pi}{2}\left(\frac{N\kappa}{2\pi\omega}\right)^2\omega+\frac{\rho_s\kappa}{4}\left(\frac{N\kappa}{2\pi\omega}\right)+\frac{\rho_s N\kappa}{2}\left(R^2-\frac{N\kappa}{2\pi\omega}\right), \quad . \quad (19)$$

where b is a distance of the order of the line spacing. The first term in eqns. (18) and (19) is the contribution from solid body rotation within the radius r; the second term is the correction to this for the small eddies illustrated in fig. 3; and the third term is the contribution from irrotational flow outside the radius r. Differentiating with respect to ω, and remembering that $b\propto\omega^{-1/2}$, we find that

$$\frac{\partial F'}{\partial\omega}=\frac{\rho_s N(N-1)\kappa^2}{8\pi\omega}\left(1-\frac{\omega_0}{\omega}\right), \quad . \quad . \quad . \quad . \quad . \quad . \quad (20)$$

so that in equilibrium $\omega=\omega_0$. This means that the vortex lines rotate with the containing vessel; the above argument cannot be regarded as proving that this result is *exactly* true, because of our approximations, but there are strong reasons for believing that this is in fact the case. Vinen (private communication) has made exact free energy calculations for the vibrating wire apparatus described in § 2.2, for up to two quanta of circulation round the wire and up to six free vortex lines around it, and finds that in the state of lowest free energy the lines always rotate at exactly the same speed as the vessel. If this result were not generally true the theory would contain an internal inconsistency; for we shall see in § 3.3 that relative motion of vortex lines and normal fluid leads to energy dissipation, and thus the state of lowest free energy would not correspond to zero entropy production.

We now set $\omega=\omega_0$ and minimize F' with respect to N; the result is that in equilibrium

$$N=\frac{2\pi R^2\omega_0}{\kappa}-n, \quad . \quad . \quad . \quad . \quad . \quad . \quad . \quad . \quad (21)$$

where n, neglecting terms of relative order $N^{-1/2}$, is given by

$$n^2=\frac{4\pi R^2\omega_0}{\kappa}(\ln(b/a_0)-\tfrac{1}{2}). \quad . \quad . \quad . \quad . \quad . \quad . \quad . \quad (22)$$

The first term in eqn. (21) is the number of lines required to fill the vessel; eqn. (22) shows that $n\sim N^{1/2}$, so that about one layer of vortex lines is missing at the edge of the vessel. The physical reason for this behaviour is easily understood; near to the wall 'image' vortex lines contribute to the velocity field, and this reduces the number of real vortex lines required to simulate solid-body rotation. The value of the free energy in equilibrium is

$$F'_{\min}=-\tfrac{1}{4}\rho_s\pi R^4\omega_0{}^2+\tfrac{1}{2}\rho_s\kappa R^2\omega_0(\ln(b/a_0)-\tfrac{1}{2}); \quad . \quad . \quad (23)$$

the first term is the value for solid-body rotation, and the second the correction due to the presence of vortex lines (higher order corrections have been neglected). It is clear that F' is least for the smallest possible value of κ, namely h/m. Henceforth we shall use the term 'vortex lines' to mean lines of unit circulation, unless explicitly stated otherwise.

Equation (23) shows that the arrangement of vortex lines we have been considering, corresponding to the flow illustrated in fig. 3 except near the edge of the vessel, gives a fractional excess free energy of order $(h/m)R^{-2}\omega_0^{-1}$. But quite different ways of imitating solid-body rotation are possible; for example the arrangement of concentric cylindrical vortex sheets considered by London (1954) and Landau and Lifshitz (1955). Such vortex sheets would have a surface energy associated with them, and for dimensional reasons this would have to be of order $h^2/m\,d^4$, where d is the atomic spacing (Mott 1949, Ginsburg 1955). This surface energy leads to a fractional excess free energy for the model of order

$$(h/m)^{4/3}\,d^{-2/3}R^{-2}\omega_0^{-4/3}$$

(Hall and Vinen 1956 b); this is much larger than the excess free energy for the vortex line model for all angular velocities less than about 10^9 rad sec^{-1}. The reason for this preference for vortex lines is the association of an energy $h^2/m\,d^2$ per atom with regions of concentrated vorticity, due to the node in the wave function. It is therefore energetically favourable to have curl $\mathbf{v}_s \neq 0$ in as small a volume as possible, and this is achieved with vortex lines; if a vortex sheet were formed it would tend to split into a row of lines (Feynman 1957).

We thus conclude that at all angular velocities for which the spacing of the vortex lines given by eqn. (16) is small compared with the dimensions of the vessel perpendicular to the axis of rotation the superfluid should rotate almost as a solid body. This condition is valid for almost all experimental situations; even the rotation of the earth should produce about one vortex line per 7 cm^2. The most direct experimental evidence for the theory given above comes from observations of the free surface of the liquid in a rotating vessel (Osborne 1950, Andronikashvili and Kaverkin 1955), which is found to have the same parabolic form as for an ordinary liquid rotating at the same angular velocity. In fact, if the vortex lines are strictly localized, there should be a depression in the surface near each line. But even if surface tension is neglected this depression should only be $10\,\mu$ deep at a radius of $1\,\mu$ from the centre; it is difficult to calculate the effect of surface tension precisely, but it probably flattens the depression to a maximum depth of the order of 10 Å.

However, free surface observations can only be used at rather large angular velocities ($\gtrsim 10$ rad sec^{-1}). At lower angular velocities the only evidence comes from measurements of the torque exerted by the liquid on its containing vessel as it slows down from a state of rotational equilibrium (Hall 1957, Walmsley and Lane 1958); this torque can be integrated with respect to time to give the change of angular momentum. It is found that at angular velocities of about 0·1 rad sec^{-1} the amount of angular momentum collected is considerably less than the classical solid body value, in contradiction to the theory given above. But the measured angular momenta are strictly only lower limits, for the possibility cannot be excluded that the final stages of retardation are produced by a torque too small to be detected experimentally acting for a very long time. There is indeed some evidence from these experiments (Hall 1957) which suggests that a persistent current of long lifetime is generated, at any rate in a multiply connected vessel; but Walmsley and Lane used a simply connected vessel, and for this arrangement there is no direct evidence for or against the existence of a persistent current of long lifetime. These experiments therefore suggest that the theory given here *may* be wrong at low angular velocities, but do not disprove it. However, we shall see in § 3.4 that rather less direct experimental evidence does in fact indicate that even at 0·1 rad sec^{-1} rotating helium II contains the number of vortex lines predicted here.

3.2. *The Attenuation of Second Sound*

In a second sound wave the normal fluid and superfluid oscillate in antiphase, so that there is no transport of matter and the temperature oscillates at constant pressure. Therefore the propagation of second sound in rotating helium will cause relative motion of the excitations constituting the normal fluid and the vortex lines. Because of collisions between the thermal excitations and the vortex lines this relative motion will give rise to a force of mutual friction tending to annul the relative motion, and thus causing dissipation of energy and an additional attenuation of second sound. In this section we shall consider the experimental evidence (Hall and Vinen 1956 a) for the existence of such an effect, and in § 3.3 we shall give the theory of the effect (Hall and Vinen 1956 b).

Fig. 4

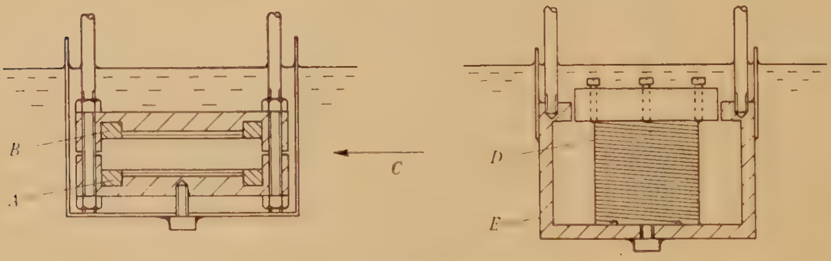

(*a*) (*b*)

The resonators. The heater and thermometer are wound across the rings A and B in the axial mode resonator (*a*). In the radial mode resonator (*b*) they are wound on the cylinder D.

Changes in attenuation were deduced from the changes in amplitude of a half-wave resonance when a resonator was fed with a constant signal at the resonant frequency. The two resonators used are shown in fig. 4;

in the axial mode resonator (fig. 4 (*a*)) the second sound is propagated parallel to the axis of rotation, and in the radial mode resonator (fig. 4 (*b*)) propagation is perpendicular to the axis of rotation; the axial mode resonator can also be used for propagation perpendicular to the axis of rotation by rotating it about the axis indicated by the arrow C in the figure. Each resonator is placed in a can which rotates with it and the whole assembly is situated in a chamber containing a constant amount of liquid helium, so that the liquid level is as shown in fig. 4. Thus, when the resonator assembly is rotated the uniformly rotating liquid within the resonator is effectively isolated from liquid that is not rotating uniformly, since the only contact is via vapour and the film.

It is found that rotation at speeds from 3 to 7·5 rad sec^{-1} does not change the velocity of second sound by more than 0·1 %; therefore, if the resonator is set on resonance it remains on resonance during rotation, and changes of attenuation with time can be followed by recording the amplitude of the received second sound signal. Figure 5 is a tracing of a typical record for the radial mode resonator. It can be seen that when rotation is started a considerable attenuation rapidly develops; most of this attenuation disappears after about 30 sec, but the second sound amplitude never regains its original value, i.e. there is a steady excess attenuation in the uniformly rotating liquid. When rotation is stopped there is again a transient attenuation, but after about 3 min the second sound recovers its original amplitude characteristic of stationary helium. These transient attenuations are of the same order as the steady attenuations observed by Wheeler *et al.* (1955) between concentric cylinders rotating at different speeds; both effects are almost certainly the result of turbulence (compare § 5), and we shall not consider them further. The quantity of interest is the steady attenuation in the uniformly rotating liquid; except near the λ-point it is found to be accurately proportional to angular velocity ω, independent of second sound amplitude, and independent of second sound frequency. It is therefore convenient to write the excess attenuation α in the form

Fig. 5

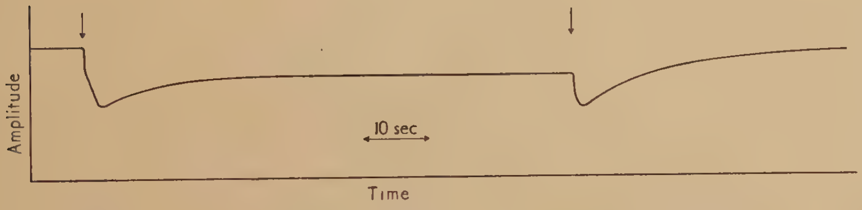

The effect of rotation on the amplitude of a second sound resonance. The arrows indicate when rotation was started and stopped.

$$\alpha = B\omega/2u_2, \qquad (24)$$

where u_2 is the velocity of second sound, thereby defining a dimensionless constant B; experimental values of B are shown in fig. 6. Near the λ-point (above 2·0°K) the experimental values of B are somewhat dependent on second sound amplitude and angular velocity. These non-linear effects are not understood and have not yet been fully investigated; the points above 2°K in fig. 6 represent an extrapolation to zero second sound amplitude.

The axial mode resonator gives a very much smaller steady attenuation, although the transients are similar to those for the radial mode resonator. The effect is so small that it is impossible to check the constancy of B in eqn. (24), or even to be sure that $B \neq 0$; the single point shown in figure 6 was obtained at the highest speed of rotation (7·5 rad sec^{-1}). However, when the axial mode resonator is turned on its side (see fig. 4), so that the

Fig. 6

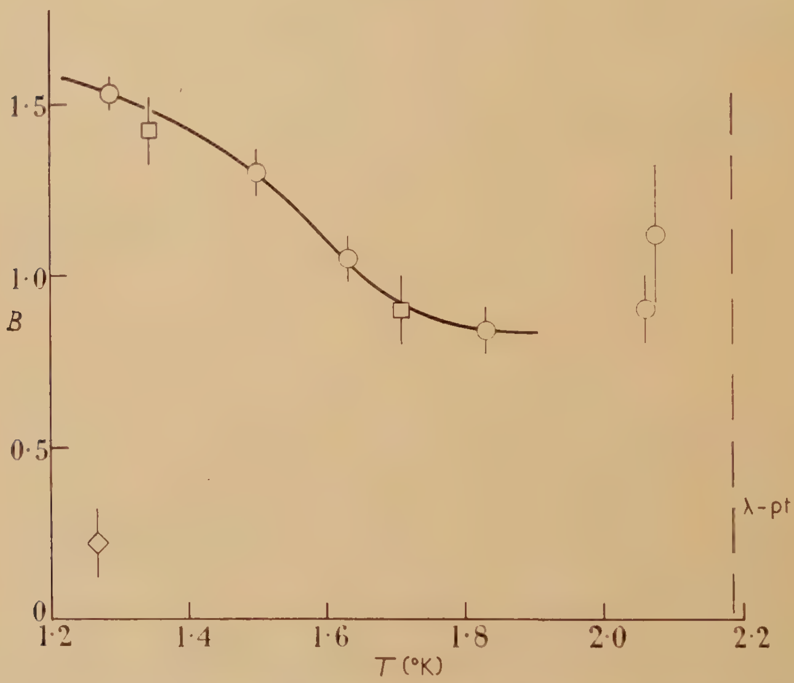

The mutual friction constant B, deduced from second sound attenuation. ○, radial mode resonator; ◇, axial mode resonator; □, axial mode resonator on its side (rotation about the axis C in fig. 4).

second sound is propagated perpendicular to the axis of rotation, values of B equal to those for the radial mode resonator are obtained. It thus appears that B is of order unity for second sound propagated in any direction perpendicular to the axis of rotation, but is much smaller for propagation parallel to the axis of rotation. It is noteworthy that this anisotropy is the same as that of a uniform array of vortex lines, as considered in § 3.1, but is different from the anisotropy of an array of concentric vortex sheets, for which the r and θ directions in cylindrical coordinates are not equivalent. The anisotropy of the observed attenuation by itself therefore provides experimental support for the vortex line model of rotating helium.

From a phenomenological point of view the fact that second sound is propagated with unchanged velocity in rotating helium provides evidence that the two fluid model is still applicable with unchanged values of ρ_n and the thermodynamic parameters; this conclusion also follows from the unchanged fountain pressure in rotating helium (Andronikashvili and Kaverkin 1955). We are therefore justified in attempting to describe the observed attenuation of second sound by the addition of extra terms to the equations of motion of the two fluid model (eqns. (3) and (4)). To give an attenuation independent of frequency, proportional to ω and independent of second sound amplitude, the extra term must be independent of velocity gradients and proportional to both ω and $(v_{\mathrm{s}}-v_{\mathrm{n}})$. Equation (24) for the attenuation results if we add to eqns. (3) and (4) a force of mutual friction between the two fluids which for unit volume of normal fluid is given by

$$F_{\mathrm{sn}}=B\frac{\rho_{\mathrm{s}}\rho_{\mathrm{n}}}{\rho}\,\omega\,(v_{\mathrm{s}}-v_{\mathrm{n}}). \qquad (25)$$

In the next section we shall see how a uniform volume force of this type results from the collision of thermal excitations with vortex lines.

3.3. *The Theory of the Mutual Friction*

It may be seen at once, from qualitative arguments, that eqn. (25) is of the form to be expected from the vortex line model. For if vortex lines act as scattering centres for the excitations they will produce a resisting force proportional to the mean drift velocity of the excitations; furthermore, the magnitude of this force will be proportional to the density of scattering centres and therefore, from eqn. (16), to ω.

We begin by considering the case in which $(\mathbf{v}_{\mathrm{s}}-\mathbf{v}_{\mathrm{n}})$ is perpendicular to $\boldsymbol{\omega}$ and assume that the wavelength of the second sound is large compared with the spacing between vortex lines. $\mathbf{v}_{\mathrm{s}}$ and $\mathbf{v}_{\mathrm{n}}$ are used to denote average values of these velocities over a region containing many vortex lines, and further notation is as follows :

$\mathbf{v}_L$ is the velocity of the vortex lines;

$\mathbf{v}_R$ is the average drift velocity of rotons that collide with a vortex line (phonons may be neglected above 1°K);

v_G is the average group velocity of rotons in thermal equilibrium at temperature T; it is given by (Landau and Khalatnikov 1949)

$$v_G{}^2=\frac{2kT}{\pi\mu}; \qquad (26)$$

$\bar{\sigma}$, $\bar{\sigma}_\perp$ are total effective collision diameters of a vortex line for momentum exchange parallel and perpendicular to $(\mathbf{v}_R-\mathbf{v}_L)$. A non zero value of $\bar{\sigma}_\perp$ is possible in principle because the symmetry of a vortex line does not demand that scattering of a roton from a vortex line should be symmetrical about the forward direction; discussion of the theoretical values of these collision diameters is deferred to § 4.1; for the moment we content ourselves with expressing the macroscopic mutual friction force in terms of them. The averaging implied in these effective collision diameters is to be done in such a way that the force $\mathbf{f}$ on unit length of vortex line due to collision of rotons with it is given by

$$\mathbf{f}=D(\mathbf{v}_R-\mathbf{v}_L)+D'\boldsymbol{\omega}\times(\mathbf{v}_R-\mathbf{v}_L)/|\boldsymbol{\omega}|, \tag{27}$$

with

$$D=\rho_n\bar{\sigma}v_G, \tag{28}$$

and

$$D'=\rho_n\bar{\sigma}_\perp v_G. \tag{29}$$

In order to express the mutual friction in terms of $(\mathbf{v}_s-\mathbf{v}_n)$ it is necessary to relate $(\mathbf{v}_R-\mathbf{v}_L)$ to $(\mathbf{v}_s-\mathbf{v}_n)$. The difference between $\mathbf{v}_R$ and $\mathbf{v}_n$ arises because a vortex line tends to drag the normal fluid in its vicinity; this happens because the spacing between vortex lines ($\sim 10^{-2}$ cm) is very much greater than the roton–roton mean free path ($\sim 10^{-6}$ cm). It may be shown by a simple extension of some calculations by Sewell (1910) that

$$(\mathbf{v}_n-\mathbf{v}_R)=\mathbf{f}/E, \tag{30}$$

where to a good approximation

$$E=\frac{-4\pi\eta_n(\ln\frac{1}{2}\lambda L+1)}{(\ln\frac{1}{2}\lambda L+1)^2+\frac{1}{16}\pi^2}; \tag{31}$$

here $\lambda(=(\rho\omega_0/\eta_n)^{1/2}$, where ω_0 is the angular frequency of the second sound) is the reciprocal penetration depth of viscous waves in the normal fluid, and $L(=3\eta_n/\rho_n v_G$ with adequate accuracy) is the roton–roton mean free path. Eliminating $\mathbf{v}_R$ between eqns. (27) and (30) we find that the force $\mathbf{F}_{Ln}(=(2\omega/\kappa)\mathbf{f})$ on the lines in unit volume of superfluid is given by

$$\mathbf{F}_{Ln}=B_L\frac{\rho_s\rho_n}{\rho}\frac{\boldsymbol{\omega}\times[\boldsymbol{\omega}\times(\mathbf{v}_L-\mathbf{v}_n)]}{|\boldsymbol{\omega}|}+B_L{}'\frac{\rho_s\rho_n}{\rho}\boldsymbol{\omega}\times(\mathbf{v}_L-\mathbf{v}_n), \tag{32}$$

where

$$B_L=\frac{2\rho}{\rho_s\rho_n\kappa}\frac{X}{X^2+Y^2}, \tag{33}$$

and

$$B'_L=\frac{2\rho}{\rho_s\rho_n\kappa}\frac{Y}{X^2+Y^2}, \tag{34}$$

in which

$$X=\frac{1}{E}+\frac{D}{D^2+D'^2} \tag{35}$$

and

$$Y=\frac{-D'}{D^2+D'^2}. \tag{36†}$$

These equations would be our final result for the mutual friction if the vortex lines were fixed in the superfluid so that $\mathbf{v}_L=\mathbf{v}_s$. In fact, however, under the action of a force $\mathbf{f}$ the vortex lines may be expected to move according to the Magnus effect equation

$$\mathbf{f}=\rho_s(\mathbf{v}_L-\mathbf{v}_s)\times\boldsymbol{\kappa}; \tag{37}$$

---

† We have retained the notation introduced by Lifshitz and Pitaevsky (1957), in which D' and B'_L have opposite signs, but D and B_L have the same sign.

the validity of this equation for a free vortex line is not absolutely certain, because the concepts of the two fluid model become invalid near the vortex core; but it seems probable that eqn. (37) in fact only demands obedience to the laws of classical hydrodynamics away from the core. In fact, eqn. (37) provides the mechanism by which force is transmitted to the superfluid; the transverse movement of the vortex lines under an applied force produces acceleration of the liquid in the direction of that force. Our final expression for the force $\mathbf{F}_{\mathrm{sn}}$ on unit volume of normal fluid is therefore obtained by eliminating $\mathbf{v}_L$ between eqns. (32) and (37), with the result:

$$\mathbf{F}_{\mathrm{sn}}=-B\frac{\rho_{\mathrm{s}}\rho_{\mathrm{n}}}{\rho}\frac{\boldsymbol{\omega}\times[\boldsymbol{\omega}\times(\mathbf{v}_{\mathrm{s}}-\mathbf{v}_{\mathrm{n}})]}{|\boldsymbol{\omega}|}-B'\frac{\rho_{\mathrm{s}}\rho_{\mathrm{n}}}{\rho}\boldsymbol{\omega}\times(\mathbf{v}_{\mathrm{s}}-\mathbf{v}_{\mathrm{n}}), \quad . \quad (38)$$

where

$$B=\frac{2\rho}{\rho_{\mathrm{s}}\rho_{\mathrm{n}}\kappa}\,\frac{X}{X^2+(Y+1/\rho_{\mathrm{s}}\kappa)^2}, \quad . \quad . \quad . \quad . \quad . \quad . \quad (39)$$

and

$$B'=\frac{2\rho}{\rho_{\mathrm{s}}\rho_{\mathrm{n}}\kappa}\,\frac{Y+1/\rho_{\mathrm{s}}\kappa}{X^2+(Y+1/\rho_{\mathrm{s}}\kappa)^2}. \quad . \quad . \quad . \quad . \quad . \quad . \quad (40)$$

The above results have been derived on the assumption that $(\mathbf{v}_{\mathrm{s}}-\mathbf{v}_{\mathrm{n}})$ is perpendicular to $\boldsymbol{\omega}$. Now if the vortex lines are straight the effective scattering potential presented to a roton cannot vary parallel to the axis of rotation, and therefore there can be no momentum exchange in this direction. The mutual friction force must therefore be perpendicular to $\boldsymbol{\omega}$ and proportional to the component of $(\mathbf{v}_{\mathrm{s}}-\mathbf{v}_{\mathrm{n}})$ perpendicular to $\boldsymbol{\omega}$; this property is shown by eqns. (32) and (38), and they are therefore true for any orientation of $(\mathbf{v}_{\mathrm{s}}-\mathbf{v}_{\mathrm{n}})$ with respect to $\boldsymbol{\omega}$. We thus see that according to this theory there should be no attenuation of second sound propagated parallel to the axis of rotation, in approximate agreement with experiment; the extent to which this conclusion may be modified by thermal vibration of the vortex lines will be discussed later (§ 4.1).

The second term in eqn. (38) represents a force perpendicular to $(\mathbf{v}_{\mathrm{s}}-\mathbf{v}_{\mathrm{n}})$, and is therefore not dissipative; it is analogous to a Coriolis force. Ordinary Coriolis forces on the two fluids will also be present; the effect of these for a second sound wave (in which $\rho_{\mathrm{s}}\mathbf{v}_{\mathrm{s}}+\rho_{\mathrm{n}}\mathbf{v}_{\mathrm{n}}=0$) is to replace B' by $(B'-2)$ in eqn. (38). The effect of this transverse force will be to tend to excite second sound vibrations in the transverse direction, but for the experiments described in § 3.2 this effect should be unobservably small, because there is no possibility of resonance in the transverse direction. However, if the geometry of the resonator were chosen so that transverse resonances were possible, observable effects should be produced which could be used to determine B' experimentally (Hall and Vinen 1956 a); this experiment has not yet been tried.

At low temperatures the value of B is principally controlled by $\bar{\sigma}$, and that of B' by $\bar{\sigma}_{\perp}$. In order to compare theory and experiment we assume for simplicity that $\bar{\sigma}_\perp = 0$ and $\bar{\sigma} \propto 1/T$, which is the result obtained when the scattering is calculated in Born approximation (§ 4.1); but the theoretical result for B is not much affected by any value of $\bar{\sigma}_\perp < \bar{\sigma}$ nor by the substitution of any other relatively weak temperature dependence for $\bar{\sigma}$.

Fig. 7

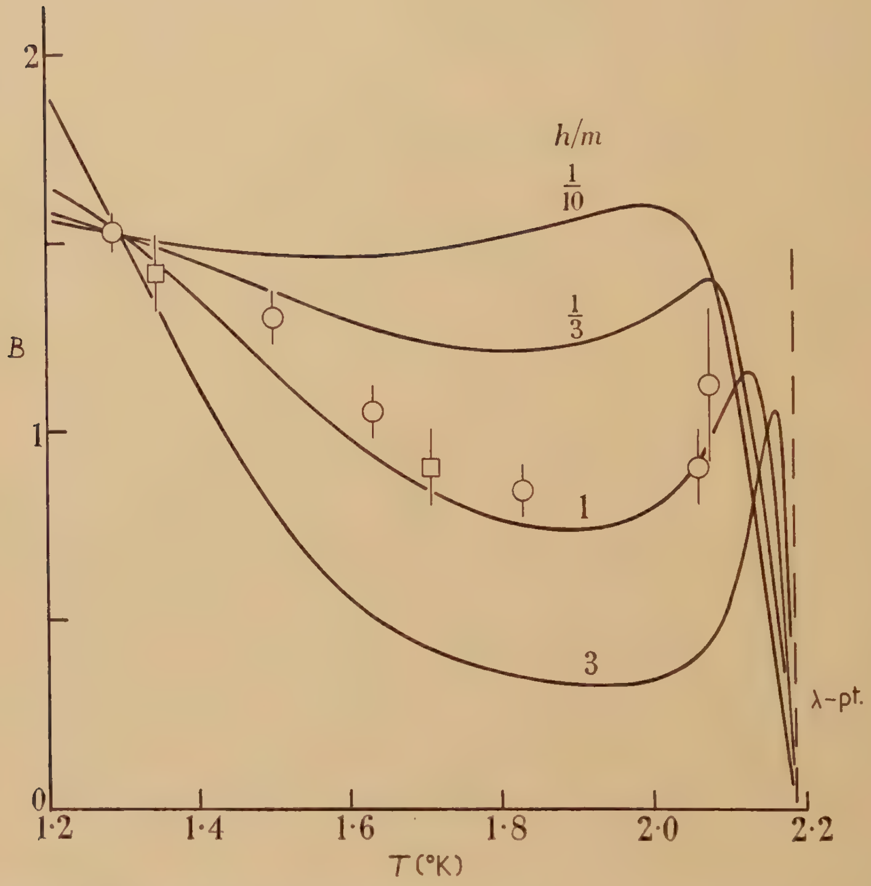

Comparison of the theoretical and experimental temperature dependence of B. The curves are calculated assuming the values of κ marked on them, with the absolute value of $\bar{\sigma}$ adjusted so as to agree with experiment at 1·3°K. The experimental points are as in fig. 6.

We note that the theoretical value of B depends slightly on the second sound frequency, through the logarithmic frequency dependence of E (eqn. (31)). The reason for this is that the dragging of the normal fluid by a vortex line involves velocity gradients; but this theoretical frequency dependence is too weak to have been detected in the experiments described in § 3.2.

Figure 7 shows some theoretical curves for the temperature dependence of B, calculated for various assumed values of κ, together with the experimental points; for each curve the absolute value of $\bar{\sigma}$ has been chosen so as to agree with experiment at 1·3°K. It is clear that much the best agreement between theory and experiment is obtained for $\kappa = h/m$. The effect of κ on the temperature dependence of B is due to the dragging of the normal fluid by a vortex line, which is responsible for the low value of B near 1·8°K; for a larger value of κ the lines have to be more widely spaced and this effect is more marked. We may therefore conclude from the temperature dependence and absolute magnitude of the experimental values of B that rotating superfluid helium contains an array of linear scattering centres at about the spacing predicted for vortex lines and with a collision diameter of about 10 Å ($\bar{\sigma} = (14{\cdot}8/T)$ Å for the curve with $\kappa = h/m$ in fig. 7). To this extent the experiments on second sound attenuation support the vortex line model. They do not provide any evidence for or against the Magnus effect (eqn. (37)), since B and B_L are appreciably different only near the λ point ($B \to 0$ and $B_L \to \infty$) where no experiments have yet been done. Nor do they provide any information about $\bar{\sigma}_\perp$, except that it cannot be appreciably greater than $\bar{\sigma}$, because of the insensitivity of B to $\bar{\sigma}_\perp$.

3.4. *Torsional Oscillations: Vortex Waves*

The experiments described in § 3.2 were essentially a repetition of Peshkov's (1944, 1946) second sound experiments in the uniformly rotating liquid. In this section we consider the information that can be obtained from a similar extension of Andronikashvili's (1946) experiments on the torsional oscillations of a pile of closely spaced disks (Hall 1958). In the non-rotating liquid the close spacing of the disks forces the normal fluid to follow their motion (by reason of its viscosity) but the superfluid remains at rest, provided that the oscillation amplitude is not too large; Andronikashvili was thus able to deduce values for the density ρ_n of the normal fluid from measurements of the period of free oscillations. If these small torsional oscillations are superposed on a uniform rotation it might be expected that the mutual friction discussed in §§ 3.2 and 3.3 would cause both an increase in period due to dragging of the superfluid and an increase in damping due to the work done against mutual friction. In fact, however, these expectations are not fulfilled, because of a tendency of the ends of the vortex lines to become attached to a sufficiently rough surface. In these circumstances mutual friction plays only a minor part, and the motion is controlled by a balance between the tension in a curved vortex line and the Magnus effect force due to motion of the line through the superfluid. This balance of forces leads to the propagation of circularly polarized transverse waves on the vortex lines (Thomson 1880); we shall see below that an experimental study of this wave motion enables us to deduce a value for the energy of unit length of vortex line.

In the actual experiment the pile of disks was clamped in a thin walled aluminium can; the whole disk assembly could then be filled with liquid and suspended in vapour. In this way the experimental helium was effectively isolated from non-rotating helium and edge effects were avoided. The torsion head from which the disk system was suspended could be rotated uniformly by a synchronous motor, and oscillations relative to the rotating torsion head were observed photoelectrically.

The experiments were made at a temperature of 1·27°K, low enough for effects due to the inertia of the normal fluid to be negligible. It is convenient to express the effect of rotation on the period of oscillation in terms of an effective density ρ', defined as that density which, filling the space between the disks and moving with them, would produce the observed change in period. The experimental values of ρ' show two different types of behaviour, depending on whether the angular velocity of rotation ω_0 is large or small compared with the angular frequency of oscillation $(\Omega = 2\pi/T)$.

Fig. 8

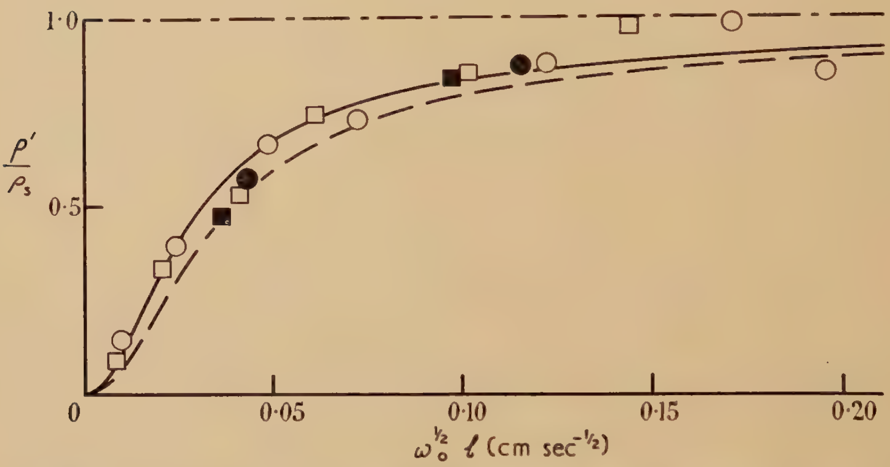

Dragging of the superfluid by oscillating disks for rapid rotation $(\omega_0 \gg \Omega)$. Period about 25 sec; open points for smooth surfaces and solid points for rough surfaces; ○ ●, $\omega_0 = 1{\cdot}100$ rad sec^{-1}; □ ■, $\omega_0 = 0{\cdot}785$ rad sec^{-1} Theoretical curves for $\nu = 8{\cdot}5 \times 10^{-4}$ cm^2 sec^{-1}: broken curve, eqn. (45); solid curve, eqn. (48) with $\gamma_1 = \frac{1}{2}$.

Figure 8 shows the results for fast rotation and slow oscillation $(\omega_0 \gg \Omega)$. It can be seen that for given values of ω_0 and Ω, ρ'/ρ_s *increases* monotonically from 0 to 1 as the disk separation $2l$ is increased—a rather surprising result; for one would normally expect the disks to become less effective in dragging liquid as their separation was increased. Figure 8 also shows that by plotting ρ'/ρ_s against $\omega_0^{1/2} l$ the results for two different angular velocities are brought into coincidence; the theoretical reason for this will become apparent shortly. Measurements were made using smooth mica disks, and also with disks artificially roughened on a scale of about 50 μ; the figure shows no appreciable effect of surface roughness on the results. Only very rough measurements of damping were possible, but it can be said that if the extra damping is expressed as an imaginary component of density ρ'', then $\rho'' \ll \rho'$.

In the case of slow rotation and fast oscillation ($\omega_0 \ll \Omega$) there is no significant change in period due to rotation if smooth mica disks are used, but with rough disks the results shown in fig. 9 are obtained. Figure 9 essentially shows the variation of ρ'/ρ_s with disk separation when $\omega_0 \ll \Omega$, as does fig. 8 when $\omega_0 \gg \Omega$. The scaling factors used to bring results for different periods and angular velocities into coincidence on fig. 9 are theoretical, and will be derived below. The most striking feature of fig. 9 is that ρ' can be negative. For the results illustrated $|\rho'/\rho_s| \lesssim 1/10$, but negative values of ρ' as large as half the total density of the liquid have been observed when $2\omega_0 \sim \Omega$. The shape of fig. 9 strongly suggests that it is the dispersion curve associated with a resonance effect; there seems to be a main resonance when $(\Omega - 2\omega_0)^{1/2} l \approx 0{\cdot}04$ cm sec$^{-1/2}$ and a subsidiary one when $(\Omega - 2\omega_0)^{1/2} l \approx 0{\cdot}14$ cm sec$^{-1/2}$. This interpretation is supported by some very rough observations of the damping; the imaginary density ρ'' is small except near the centre of a resonance, where it rises to a value

Fig. 9

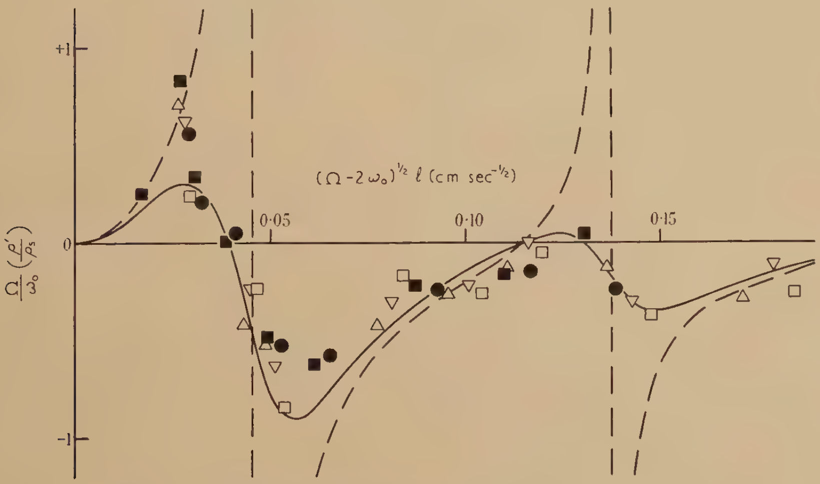

Dragging of the superfluid by oscillating disks with rough surfaces for slow rotation ($\omega_0 \ll \Omega$). Open points for period about 3 sec and solid points for period about 7 sec. ●, $\omega_0 = 0{\cdot}098$ rad sec^{-1}; □ ■, $\omega_0 = 0{\cdot}140$ rad sec^{-1}; ▽, $\omega_0 = 0{\cdot}196$ rad sec^{-1}; △, $\omega_0 = 0{\cdot}275$ rad sec^{-1}. Theoretical curves for $\nu = 8{\cdot}5 \times 10^{-4}$ cm^2 sec^{-1}; broken curve, eqn. (46); solid curve, eqn. (49) with $\gamma_2 = \frac{1}{2}$.

of the same order as the dispersion in ρ'. Qualitatively, therefore, the damping shows the corresponding resonance absorption behaviour.

It is easily seen that neither an increase in ρ' with increasing disk spacing, as in fig. 8, nor negative values of ρ', as in fig. 9, can be explained by a simple dragging of the superfluid by mutual friction. Negative values of ρ' can only occur if the superfluid moves in antiphase with the disks, and this implies some form of elastic coupling between the superfluid and the disks. The existence of a subsidiary resonance at about three times the disk separation for the main resonance suggests that this elastic coupling takes the form of a wave motion in the liquid, with resonance occurring for an odd number of half-wavelengths between the disks. Now it is known (Thomson 1880) that classical vortex lines are capable of vibration, and also that they tend to stick to surface protuberances, because of the Bernoulli pressure drop near the centre of a line. It therefore seems reasonable to suppose that the ends of the vortex lines in uniformly rotating helium will stick to a sufficiently rough surface. Oscillation of the disks will then excite waves on the vortex lines. Since these waves are circularly polarized there will be a radial component of line motion giving rise to oscillations in the density of vortex lines, and thus to oscillations in the angular velocity of the superfluid. It is therefore clear that the hypothesis that the ends of the vortex lines are attached to a sufficiently rough surface offers some hope of accounting for the results described above; it is evident from the results shown in fig. 8 that in this case even a 'smooth' surface is sufficiently rough.

We now give the theory of the collective vibrations of a uniform array of vortex lines, which we shall refer to as vortex waves. For the present we neglect mutual friction, and consider only the equation of motion of the superfluid. We shall not be concerned with the detailed velocity field, which has singularities at the vortex lines, as shown in fig. 3, but rather with the average flow $\mathbf{v}_S$ defined by equating $\bar{\boldsymbol{\omega}} = \operatorname{curl} \mathbf{v}_S$ to the number of vortex lines per unit area (a smooth function of position) multiplied by the circulation round a single line. The equation of motion for this average flow is

$$\frac{\partial \mathbf{v}_S}{\partial t} = \mathbf{v}_L \times \bar{\boldsymbol{\omega}} + \operatorname{grad} \phi \quad . \quad . \quad . \quad . \quad . \quad . \quad . \quad (41)$$

where $\mathbf{v}_L$ is the velocity of the vortex lines. The first term on the right-hand side of eqn. (41) gives the change in $\mathbf{v}_S$ at a point due to flow of vortex lines past the point, and the second term represents acceleration due to pressure and temperature gradients.

In addition to $\mathbf{v}_S$ there is a local velocity field in the vicinity of each vortex line. We shall take this into account by introducing the concept of the tension in a vortex line. Between any pair of adjacent lines there is a surface on which the *total* superfluid velocity is $\mathbf{v}_S$, and these surfaces form a net of tubes surrounding the vortex lines; a cross-section of this net is shown by the dotted lines in fig. 3. It can be seen from fig. 3 that the local velocity field of a vortex line has closed streamlines contained in the tube which surrounds it; it is the Bernoulli pressure drop due to this velocity field which, classically, produces a tension within the tube. But other, non-classical contributions to the energy from the core of a vortex may also be expected to contribute to the tension; for the tension in a vortex line is equal to the free energy of unit length and thus, at absolute zero, to the energy. The tension can therefore be written as

$$\epsilon = \frac{\rho_S \kappa^2}{4\pi} \ln (b/a_0), \quad . \; . \; . \; . \; . \; . \; . \; . \; . \; . \quad (13)$$

where b is a distance of the order of the line spacing and a_0 is the effective core radius of a vortex line (§ 2.1). If we assume for simplicity that the tubes shown in fig. 3 are circles of the same area, $b = (\hbar / 7{\cdot}39\, m\omega_0)^{1/2}$. Now if the tube surrounding a vortex line has a radius of curvature R it will experience a transverse force ϵ/R per unit length due to the tension within it, and this must be balanced by a Magnus effect force due to motion of the tube through the liquid. The equation expressing this balance of forces is thus

$$\frac{\epsilon}{R} = \epsilon \frac{(\boldsymbol{\kappa} \,.\, \nabla)\boldsymbol{\kappa}}{\kappa^2} = \rho_S(\mathbf{v}_L - \mathbf{v}_S) \times \boldsymbol{\kappa}. \quad . \; . \; . \; . \; . \; . \quad (42)$$

Since $\bar{\boldsymbol{\omega}}$ is parallel to $\boldsymbol{\kappa}$ eqns. (41) and (42) give

$$\frac{\partial \mathbf{v}_S}{\partial t} = \mathbf{v}_S \times \bar{\boldsymbol{\omega}} + \nu(\bar{\boldsymbol{\omega}} \,.\, \nabla)\left(\frac{\bar{\boldsymbol{\omega}}}{|\bar{\boldsymbol{\omega}}|}\right) + \operatorname{grad} \phi, \quad . \; . \; . \; . \quad (43)$$

where $\nu = \epsilon / \rho_S \kappa$; this is the required equation of motion.

It should be stressed that eqn. (43) is an equation of motion for the average superfluid velocity, and is therefore only valid if such a velocity can be defined, i.e. if

(i) the fractional change in $\mathbf{v}_S$ across the tube surrounding a vortex line is small;
(ii) the radius of curvature of a tube is large compared with its diameter;
(iii) the radius of curvature does not change appreciably in a distance equal to the tube diameter.

In the experiments described above conditions (i) and (ii) are always satisfied, but condition (iii) is not. Failure of condition (iii) means that the radius of curvature of a vortex line is not precisely equal to that of the tube surrounding it, so that the transverse force is not precisely ϵ/R. However, we shall see later that Thomson's (1880) calculations enable us to allow for this by choosing a slightly different value for b in eqn. (13), giving a slightly different value of ϵ.

The correct boundary condition for the flow is that the total superfluid velocity should have no component normal to the actual, rough, disk surface. For the average flow considered here we assume that $\mathbf{v}_S$ has no component normal to an effective plane disk surface, and incorporate our physical idea of vortex lines attached to surface protuberances by imposing the additional boundary condition that $\mathbf{v}_L$ is equal to the disk velocity.

This idealized boundary condition may not be an accurate representation of the physical situation, but it should be sufficiently realistic to give the main qualitative features correctly.

When eqn. (43) is linearized for a small departure from uniform rotation and solved for oscillatory motion with these boundary conditions we find that (ignoring edge effects that are only important when $2\omega_0 \sim \Omega$) the possible wave numbers of the motion are given by

$$k_{\pm}{}^2 = -\frac{2\omega_0 \pm \Omega}{\nu}. \quad \ldots \ldots \ldots \quad (44)$$

The normal modes corresponding to these wave numbers are circularly polarized transverse vibrations of the vortex lines. k_+ corresponds to a vibration in the same sense as the rotation and is always an evanescent wave; k_- corresponds to a vibration in the opposite sense and is an undamped wave for $2\omega_0 < \Omega$, equivalent to the vibrations of a single vortex considered by Thomson (1880) as $\omega_0 \to 0$. When these motions are combined to fit the boundary conditions we find that for $\omega_0 \gg \Omega$

$$\frac{\rho'}{\rho_s} = 1 - \frac{\tanh k_1 l}{k_1 l}, \quad \ldots \ldots \ldots \quad (45)$$

with $k_1{}^2 = 2\omega_0/\nu$, and for $\omega_0 \ll \Omega$

$$\frac{\rho'}{\rho_s} = \frac{\omega_0}{\Omega}\left(\frac{\tan k_2 l - \tanh k_2 l}{k_2 l}\right), \quad \ldots \ldots \quad (46)$$

with $k_2{}^2 = \Omega/\nu$. The imaginary density ρ'' is predicted to be zero except for δ-functions at the resonances of eqn. (46). The broken lines in figs. 8 and 9 show eqns. (45) and (46) with $\nu = 8{\cdot}5 \times 10^{-4}\,\mathrm{cm}^2\,\mathrm{sec}^{-1}$ (in fig. 9 the fact that Ω is only about $10\omega_0$ has been allowed for by taking

$$k_2{}^2 = (\Omega - 2\omega_0)/\nu$$

in eqn. (46)). It may be mentioned that this value of ν leads to an effective core radius $a_0 \sim 30\,\text{Å}$ for the vortex lines, which is not unreasonable; but we defer discussion of this until we have considered the more accurate value of ν obtained from later experiments (§ 3.5).

It can be seen that eqns. (45) and (46) describe the main qualitative features of the results very well, but they do not account for the observed width of the resonances; nor do they account for the fact that a smaller value of ν would give a better fit to the data of fig. 8. We shall see in § 3.5 that the effects of mutual friction are inadequate to account for the observed resonance widths. The explanation probably lies in our use of an over-simplified boundary condition. If instead we allow a vortex line to slip somewhat relative to the disk surface by taking the boundary condition

$$\frac{\partial \xi}{\partial t} = -u\frac{\partial \xi}{\partial z}, \quad \ldots \ldots \ldots \ldots \quad (47)$$

where ξ is the displacement of a vortex line relative to the disk surface, the reflection of vortex waves at the boundary is no longer perfect. The constant u controls the amount of slip; $u = 0$ corresponds to the ideally rough surface considered so far, and $u=\infty$ to an ideally smooth surface. With this more general boundary condition eqn. (45) is replaced by

$$\frac{\rho'}{\rho_s}=1-\frac{(\tanh k_1l)/k_1l}{1+\gamma_1{}^2\tanh^2 k_1l}, \quad . \; . \; . \; . \; . \; . \; . \; . \qquad (48)$$

where $\gamma_1=uk_1/\Omega$, and eqn. (46) becomes

$$\frac{\rho'}{\rho_s}=\frac{\omega_0}{\Omega}\left[\frac{(\tan k_2l)/k_2l}{1+\gamma_2{}^2\tan^2 k_2l}-\frac{(\tanh k_2l)/k_2l}{1+\gamma_2{}^2\tanh^2 k_2l}\right], \quad . \; . \; . \; . \qquad (49)$$

where $\gamma_2=uk_2/\Omega$. The full curves in figs. 8 and 9 show eqn. (48) with $\gamma_1=\frac{1}{2}$ and eqn. (49) with $\gamma_2=\frac{1}{2}$. It can be seen that the quantitative agreement with experiment is now very good; the idea of slip accounts for both the broadened resonances and the apparently lower value of ν when $\omega_0\gg\Omega$. It must be admitted, however, that the reason for the observed values of γ is not understood; in particular it is not clear why γ rather than u is roughly constant. An understanding of this problem must await a more detailed consideration of the interaction between a vortex line and a solid boundary. However, it should be stressed that although the precise form of slip boundary condition is not properly understood, there is no reason to doubt that eqn. (43) gives a completely satisfactory description of the propagation of vortex waves in bulk helium.

3.5. *Vortex Waves and Mutual Friction*

We now consider the way in which theory of vortex waves given in the previous section is modified by the presence of the mutual friction discussed in § 3.3. Equation (42) for the balance of forces on a vortex line must now include the force of mutual friction $\mathbf{F}_{Ln}$ given by eqn. (32), so that it is replaced by

$$\rho_s(\mathbf{v}_L-\mathbf{v}_s)\times\bar{\boldsymbol{\omega}}=\rho_s\nu\,(\bar{\boldsymbol{\omega}}\,.\,\nabla)\left(\frac{\bar{\boldsymbol{\omega}}}{|\bar{\boldsymbol{\omega}}|}\right)+\mathbf{F}_{Ln},$$

i.e. by

$$\mathbf{F}_{Ln}=\rho_s\left(\mathbf{v}_L-\mathbf{v}_s-\nu\,\mathrm{curl}\left(\frac{\bar{\boldsymbol{\omega}}}{|\bar{\boldsymbol{\omega}}|}\right)\right)\times\bar{\boldsymbol{\omega}}. \quad . \; . \; . \; . \; . \qquad (50)$$

Thus the only effect on the arguments of § 3.3 is that $\mathbf{v}_s$ is replaced by $\mathbf{v}_s+\nu\,\mathrm{curl}\,(\bar{\boldsymbol{\omega}}/|\bar{\boldsymbol{\omega}}|)$; elimination of $\mathbf{v}_L$ as in § 3.3 therefore gives

$$\begin{aligned}\mathbf{F}_{Ln}&=B\frac{\rho_s\rho_n}{2\rho}\frac{\bar{\boldsymbol{\omega}}\times[\bar{\boldsymbol{\omega}}\times(\mathbf{v}_s+\nu\,\mathrm{curl}\,(\bar{\boldsymbol{\omega}}/|\bar{\boldsymbol{\omega}}|)-\mathbf{v}_n)]}{|\bar{\boldsymbol{\omega}}|}\\&\quad-B'\frac{\rho_s\rho_n}{2\rho}\bar{\boldsymbol{\omega}}\times(\mathbf{v}_s+\nu\,\mathrm{curl}\,(\bar{\boldsymbol{\omega}}/|\bar{\boldsymbol{\omega}}|)-\mathbf{v}_n)\\&=B\frac{\rho_s\rho_n}{2\rho}\frac{\bar{\boldsymbol{\omega}}\times[\bar{\boldsymbol{\omega}}\times(\mathbf{v}_s-\mathbf{v}_n)]}{|\bar{\boldsymbol{\omega}}|}+B'\frac{\rho_s\rho_n}{2\rho}\bar{\boldsymbol{\omega}}\times(\mathbf{v}_s-\mathbf{v}_n)\\&\quad-B\frac{\rho_s\rho_n}{2\rho}\nu|\bar{\boldsymbol{\omega}}|\,\mathrm{curl}\left(\frac{\bar{\boldsymbol{\omega}}}{|\bar{\boldsymbol{\omega}}|}\right)-B'\frac{\rho_s\rho_n}{2\rho}\nu(\bar{\boldsymbol{\omega}}\,.\,\nabla)\left(\frac{\bar{\boldsymbol{\omega}}}{|\bar{\boldsymbol{\omega}}|}\right). \quad . \qquad (51)\dagger\end{aligned}$$

---

† Note that we are now using $\bar{\boldsymbol{\omega}}=\mathrm{curl}\,\mathbf{v}_s$, instead of $\boldsymbol{\omega}=\frac{1}{2}\,\mathrm{curl}\,\mathbf{v}_s$, as in § 3.3.

Combining eqns. (50) and (51) with eqn. (41) and writing the potential ϕ explicitly we have for the equation of motion of the superfluid

$$\begin{aligned}\rho_s\frac{D\mathbf{v}_s}{Dt} = &-\frac{\rho_s}{\rho}\operatorname{grad}p+\rho_s S\operatorname{grad}T\\ &+B\frac{\rho_s\rho_n}{2\rho}\frac{\bar{\boldsymbol{\omega}}\times[\bar{\boldsymbol{\omega}}\times(\mathbf{v}_s-\mathbf{v}_n)]}{\bar{\boldsymbol{\omega}}}+B'\frac{\rho_s\rho_n}{2\rho}\bar{\boldsymbol{\omega}}\times(\mathbf{v}_s-\mathbf{v}_n)\\ &-B\frac{\rho_s\rho_n}{2\rho}\nu|\bar{\boldsymbol{\omega}}|\operatorname{curl}\left(\frac{\bar{\boldsymbol{\omega}}}{|\bar{\boldsymbol{\omega}}|}\right)+\rho_s\nu\left(1-B'\frac{\rho_n}{2\rho}\right)(\bar{\boldsymbol{\omega}}\,.\,\nabla)\left(\frac{\bar{\boldsymbol{\omega}}}{|\bar{\boldsymbol{\omega}}|}\right),\end{aligned} \quad . \quad . \quad (52)$$

where the term $\mathbf{v}_s\times\bar{\boldsymbol{\omega}}$ in eqn. (43) has been absorbed in $D\mathbf{v}_s/Dt$. Addition of $\mathbf{F}_{Ln}$ to eqn. (3) gives for the equation of motion of the normal fluid

$$\begin{aligned}\rho_n\frac{D\mathbf{v}_n}{Dt} = &-\frac{\rho_n}{\rho}\operatorname{grad}p-\rho_s S\operatorname{grad}T+\eta_n(\nabla^2\mathbf{v}_n+\tfrac{1}{3}\operatorname{grad}\operatorname{div}\mathbf{v}_n)\\ &-B\frac{\rho_s\rho_n}{2\rho}\frac{\bar{\boldsymbol{\omega}}\times[\bar{\boldsymbol{\omega}}\times(\mathbf{v}_s-\mathbf{v}_n)]}{|\bar{\boldsymbol{\omega}}|}-B'\frac{\rho_s\rho_n}{2\rho}\bar{\boldsymbol{\omega}}\times(\mathbf{v}_s-\mathbf{v}_n)\\ &+B\frac{\rho_s\rho_n}{2\rho}\nu|\bar{\boldsymbol{\omega}}|\operatorname{curl}\left(\frac{\bar{\boldsymbol{\omega}}}{|\bar{\boldsymbol{\omega}}|}\right)+B'\frac{\rho_s\rho_n}{2\rho}\nu(\bar{\boldsymbol{\omega}}\,.\,\nabla)\left(\frac{\bar{\boldsymbol{\omega}}}{|\bar{\boldsymbol{\omega}}|}\right).\end{aligned} \quad . \quad . \quad (53)$$

Equations (52) and (53) are the appropriate generalizations of eqns. (4) and (3) respectively when $\bar{\boldsymbol{\omega}}\neq 0$. They take into account all possible effects of the presence of vortex lines in the superfluid: tension, Magnus effect, and collisions with rotons and phonons. They are not of completely general validity, however: first, they are subject to the same restriction of slowly varying $\mathbf{v}_s$ as eqn. (43); and secondly, as we have seen, the 'constants' B, B', and ν have a slight (logarithmic) dependence on some characteristic length such as the spacing between vortex lines. Equations (52) and (53) will not therefore, for example, be expected to apply to turbulence, and for this problem it is probably necessary to consider the interactions of individual vortex lines. Nevertheless, eqns. (52) and (53) are the most general truly macroscopic equations of motion we can write down for helium II.

To calculate the effect of mutual friction on vortex waves we note that for $\rho_n/\rho\ll 1$ and $\omega_0\ll\Omega$ the terms in B and B' are a small perturbation coupling the two fluids together. In these circumstances it is permissible to calculate the perturbed superfluid flow by setting $\mathbf{v}_n=0$ in eqn. (52), and to ignore the effect of rotation on the normal fluid, since its contribution to the inertia is proportional to ρ_n. Equation (52) with $\mathbf{v}_n=0$ leads to the replacement of eqn. (44) for the wave numbers $k_\pm$ of superfluid motion by

$$(k_\pm{}^2\nu+2\omega_0)(1-B'\rho_n/2\rho\pm iB\rho_n/2\rho)=\mp\,\Omega. \quad . \quad . \quad . \quad (54)$$

We are principally interested in the wave number k_- which, for $\Omega>2\omega_0$, corresponds to undamped wave motion in the absence of mutual friction. Setting $k_-=k+i\alpha$, we find that

$$[(k^2-\alpha^2)\nu+2\omega_0]=\Omega(1+B'_L\rho_n/2\rho) \quad . \quad . \quad . \quad . \quad . \quad (55)$$

and

$$2\alpha k\nu=\Omega B_L\rho_n/2\rho, \quad . \quad . \quad . \quad . \quad . \quad . \quad . \quad (56)$$

where eqns. (33), (34), (39), and (40) have been used to relate B_L and B'_L to B and B'. When $\rho_n \ll \rho$ and $\omega_0 \ll \Omega$ these equations simplify to

$$k^2 = (\Omega/\nu)(1 + B'_L\rho_n/2\rho) \qquad (57)$$

and

$$\alpha/k = B_L\rho_n/4\rho. \qquad (58)$$

Thus the longitudinal component of mutual friction produces attenuation of the vortex waves, and the transverse component a small change in wavelength. The reappearance of B_L and B'_L in eqns. (57) and (58) in place of B and B' is not surprising; for this limiting case corresponds to the vibrations of a single isolated vortex line, for which B_L and B'_L are the relevant mutual friction constants.

Fig. 10

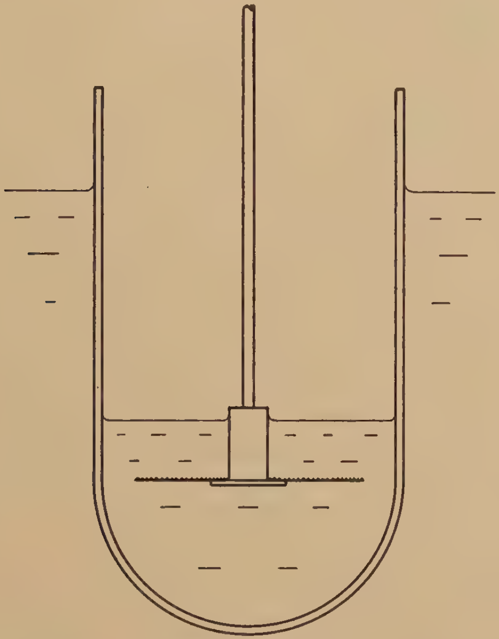

The single disk apparatus. The beaker surrounding the disk is rigidly connected to the torsion head from which the disk is suspended, and rotates with it. Changes in period are measured as the beaker fills with helium by film flow.

Recent experiments by the author were designed to study the effect of mutual friction on vortex waves, discussed above, and to obtain a value of the constant ν sufficiently accurate to give a useful estimate of the effective core radius of a vortex line. The apparatus used is shown in fig. 10. It consists of a single disk, roughened on the upper surface only, hanging in a beaker of helium which rotates at the same speed as the point of suspension of the disk. Vortex waves excited by oscillation of the upper surface of the disk will be reflected at the free surface of the liquid and resonances should occur for suitable values of the distance from disk to liquid surface. One would expect the liquid surface to be ‘ideally smooth’ so that the vortex lines meet it normally; this boundary condition gives resonance for an odd number of quarter wavelengths between disk and liquid surface, which is indeed the result found experimentally.

In an experiment the apparatus shown in fig. 10 is placed in a chamber containing a constant amount of liquid helium, so that the beaker slowly fills with liquid by film flow. The period of oscillation of the disk is measured as a function of time as the beaker fills; some typical results at a temperature of 1·3°K are shown in fig. 11 (*a*). The periodic dependence of oscillation period on liquid level is clearly visible; each sharp drop corresponds to a resonance. The fact that successive resonances diminish very little in strength shows that the attenuation of vortex waves is small, as we should expect from eqn. (58), and confirms that the rather broad resonances are due to imperfect reflection of the waves at a disk surface rather than to attenuation in the liquid. Andronikashvili and Zakadze (1959) have made similar experiments with a rather more massive disk, which enabled them to study the damping; they find a series of peaks in damping as a function of liquid level, corresponding to resonant absorption of energy by vortex waves. By recording the time at which the disk of fig. 10 was just covered with liquid and the time at which the liquid was level with the top of the boss on which the disk was mounted fig. 11 was used to determine the number of wavelengths in a known distance, and hence ν. The best value of ν from the single disk experiments at 1·3°K is $(9{\cdot}7 \pm 0{\cdot}2) \times 10^{-4}\,\mathrm{cm^2\,sec^{-1}}$ for an angular velocity of 0·140 rad $\mathrm{sec^{-1}}$ and a period of about 7 sec; this is consistent with the earlier value of $(8{\cdot}5 \pm 1{\cdot}5) \times 10^{-4}\,\mathrm{cm^2\,sec^{-1}}$ (Hall 1958).

Figure 11 (*b*) shows the effect of raising the temperature to 1·6°K. The higher resonances are now weaker, indicating appreciable attenuation, as would be expected from the factor ρ_n/ρ in eqn. (58). By a simple extension of the theory of § 3.4 it can be shown that the amplitude of period oscillation ΔT at a liquid depth l which is not too small is given by

$$\Delta T = \frac{\rho_s \omega_0 T/\rho\Omega k h_0}{\gamma_2 \cosh 2\alpha l + \frac{1}{2}(1+\gamma_2{}^2)\sinh 2\alpha l}, \quad . \quad . \quad . \quad . \quad (59)$$

where h_0 is the depth of liquid with moment of inertia equal to that of the disk. By fitting eqn. (59) to the observations values of $B_L\rho_n/\rho$ can be deduced, and these are shown in fig. 12 (the value of γ_2 turns out to be slightly smaller than previously, about 0·4). It can be seen that the experimental values of B_L are somewhat smaller than the values of B from second sound experiments (though perhaps not significantly). This is to be expected because of the frequency dependence of E (eqn. (31)); the upper limit to the logarithm is of the order of the spacing between vortex lines for the present experiments.

Experimental detection of the change in wavelength due to B'_L (eqn. (57)) is more difficult; calculation shows that even if D' (eqn. (29)) is of the same order as D the predicted variation in wavelength over the experimentally accessible temperature range is only about 1%. To obtain the necessary sensitivity the single disk of fig. 10 was replaced by a pair of disks about 1 cm apart, roughened on their inner surfaces; the separation of the disks was chosen so that there would be almost exactly 7 half-wavelengths between them. Thus, by working on the steep part of the resonance–dispersion curve, small changes in wavelength were made to yield appreciable changes in period of oscillation. By comparing the experimental results with the theoretical dispersion curve calculated for the known values of γ_2 and α the temperature dependence of the wavelength could be deduced, and hence the temperature dependence of the apparent value ν^* of ν defined by the equation

Fig. 11

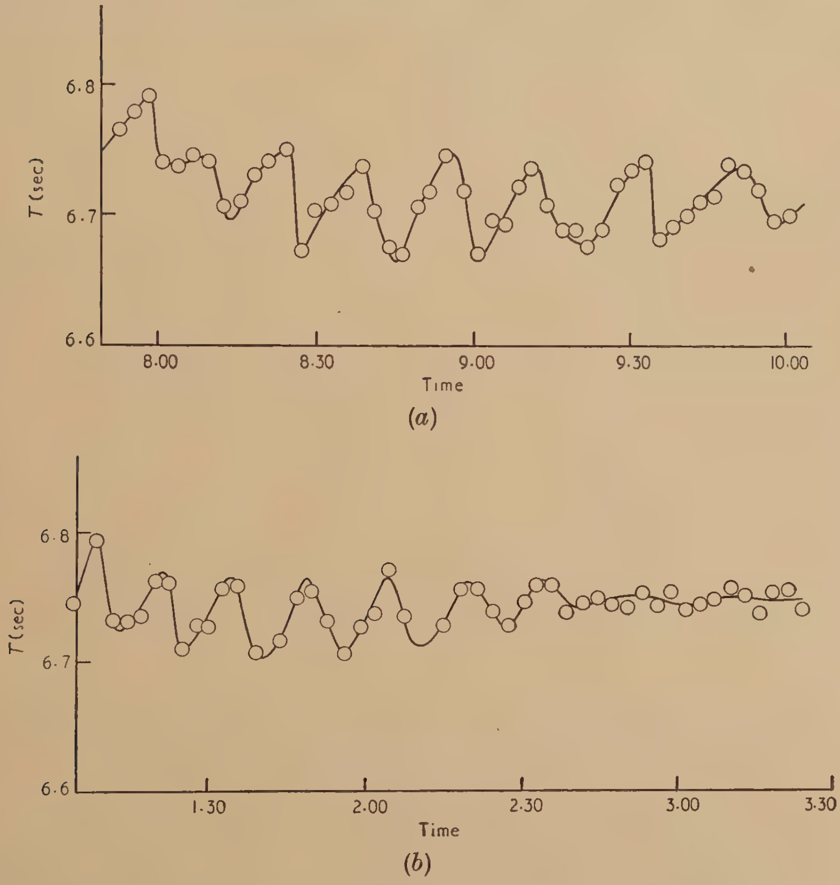

Dependence of the single disk period on time, due to changing liquid level. (*a*) 1·3°K; (*b*) 1·6°K; $\omega_0 = 0{\cdot}140$ rad sec^{-1}. The period axis is placed at the time when the disk surface was just covered by liquid.

$$k^2 = (\Omega - 2\omega_0)/\nu^*. \qquad (60)$$

Figure 13 shows experimental values of the relative change in ν^* with temperature. Equations (55) and (56) show that, to a first order in $B'_L\rho_n/\rho$ we should expect

$$\frac{\delta\nu^*}{\nu^*}=\frac{-\Omega}{\Omega-2\omega_0}B'_L\frac{\rho_n}{2\rho}+\text{const.} \qquad . \quad . \quad . \quad . \quad . \quad . \quad (61)$$

We shall see in § 4.2 that there should also be a small contribution to $\delta\nu^*$ from a genuine temperature dependence of ν arising from the thermal excitation of vortex waves; allowance is made for this in the theoretical curves shown in fig. 13. The solid curve is calculated for $D=0{\cdot}70\kappa\rho_n$ and $D'=0{\cdot}60\kappa\rho_n$; these are of the order of the values predicted by Lifshitz and Pitaevsky (1957); the broken curve is for $D'=0$, as predicted by Hall and Vinen (1956 *b*). It can be seen that the experimental results are barely adequate to distinguish between these possibilities. Above 1·4°K the results are very scattered, and moreover at these temperatures the effect of the normal fluid, which has been ignored, may not be entirely negligible. Below 1·4°K the results are rather more consistent and there does seem to be some evidence that $d\nu^*/dT$ is positive and of the order predicted by Lifshitz and Pitaevsky. On the whole, therefore, the results favour the predictions of Lifshitz and Pitaevsky, but they are insufficiently accurate

Fig. 12

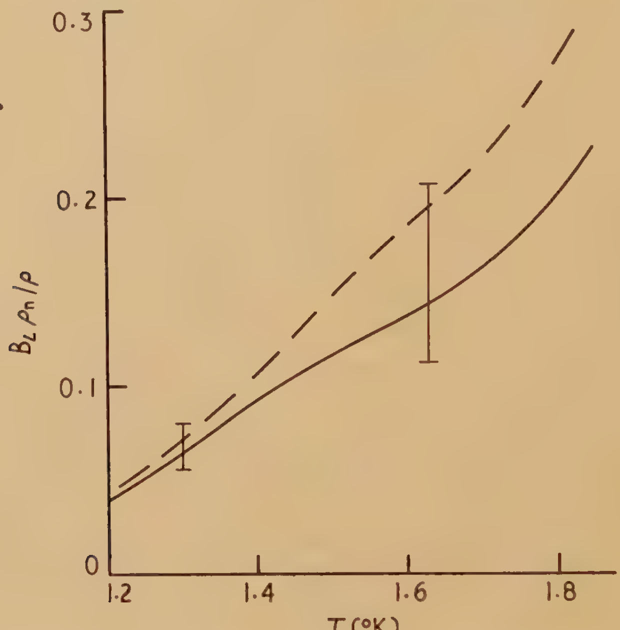

Experimental values of $B_L\rho_n/\rho$ from vortex wave attenuation. Full curve, theoretical for $D=0{\cdot}70\kappa\rho_n$ and $D'=0{\cdot}60\kappa\rho_n$; broken curve, experimental values of $B\rho_n/\rho$ from second sound attenuation.

to make this conclusion certain; there is urgent need for a better determination of B', as could be made from experiments on second sound.

We therefore adopt as the best experimental values $D = 0{\cdot}70\kappa\rho_n$ and $D' = 0{\cdot}60\kappa\rho_n$; these correspond to collision diameters $\bar{\sigma}$, $\bar{\sigma}_\perp$ of about 10Å. Values of B calculated on this basis are compared with the experimental values from second sound measurements in fig. 14, and calculated values of B_L are compared with the experimental values from vortex wave attenuation in fig. 12; for all these curves due allowance has been made for the different values of E (eqn. (31)) for vortex waves and second sound.

Fig. 13

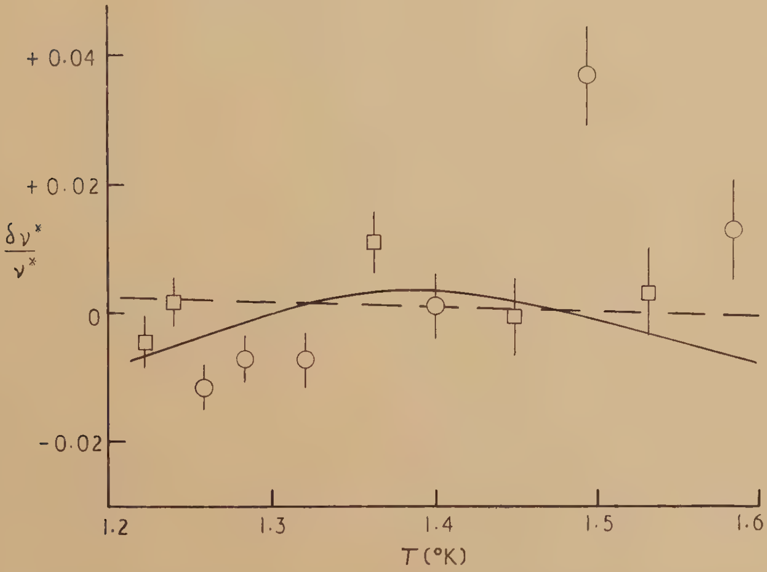

Temperature dependence of ν^* from vortex wave velocity. The squares and circles represent results obtained in two separate helium runs; there may be a constant error of about 1% in ν^* for results from a single run, due to distortion of the disk system in cooling. Full curve, theoretical for $D = 0{\cdot}70\kappa\rho_n$ and $D' = 0{\cdot}60\kappa\rho_n$; broken curve, theoretical for $D' = 0$; the zero of $\delta\nu^*/\nu^*$ for these curves is arbitrary.

It can be seen from figs. (12), (13) and (14) that each type of experiment shows agreement with theory within the experimental error. It is perhaps worth remarking that this overall agreement is good evidence for the validity of eqn. (51) for the mutual friction; for second sound is affected only by the first two terms of this equation, whereas vortex waves are affected primarily by the last two terms.

Equation (13) for the energy of unit length of vortex line shows that

$$\nu = (\kappa/4\pi)\ln(b/a_0), \qquad \text{(62)}$$

so that to determine the effective core radius a_0 from the experimental value of ν we need to know b. We saw in § 3.4 that when the wavelength

$(2\pi/k)$ is large compared with the line spacing $b=(\hbar/7{\cdot}39m\omega_0)^{1/2}$. In the opposite case when the line spacing is much larger than the wavelength, vortex waves reduce to the vibrations of a single line for which $b=1{\cdot}046/k$ (Thomson 1880). The value of b is thus controlled by the smaller of the two characteristic lengths, wavelength and line spacing. In the absence of a complete solution of the problem for the general case it seems reasonable to determine b by means of an interpolation formula with this property, for example

$$1/b^2=0{\cdot}915k^2+7{\cdot}39m\omega_0/\hbar; \quad . \quad . \quad . \quad . \quad . \quad (63)$$

Fig. 14

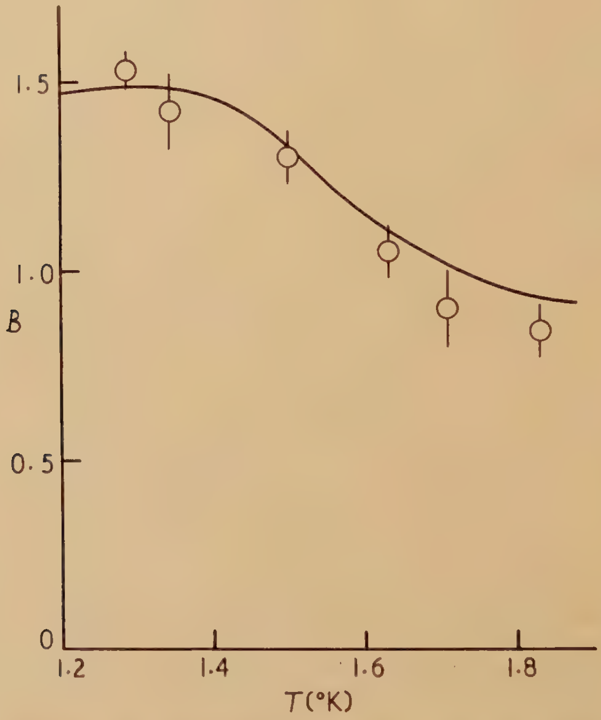

Theoretical temperature dependence of B for $D=0{\cdot}70\kappa\rho_n$ and $D'=0{\cdot}60\kappa\rho_n$ compared with the experimental values from second sound attenuation.

with $k^2=(\Omega+2\omega_0)/\nu$ and the experimental value of $\ln(b/a_0)$ this becomes

$$1/b^2=(0{\cdot}151\Omega+7{\cdot}71\omega_0)m/\hbar. \quad . \quad . \quad . \quad . \quad . \quad (64)$$

For values of $\omega_0 \sim 0{\cdot}1\Omega$, as used in the single disk experiments, the second term is dominant, so errors due to the use of an approximate interpolation formula are unlikely to be serious. Experimental values of ν obtained with the single disk at various angular velocities are plotted in fig. 15 against $\ln b$ calculated from eqn. (64); the straight line has the theoretical slope required by eqn. (62). It can be seen that the experimental results are consistent with the theoretical logarithmic dependence of ν on b. To obtain a meaningful value of a_0 from fig. 15 the experimental values of ν must first be extrapolated to absolute zero with the aid of the full curve of fig. 13. Estimating the uncertainty in this value for ν at absolute zero at 2%, we finally obtain

$$a_0 = 6{\cdot}8 \pm 1{\cdot}6\,\text{Å}.$$

It is gratifying to note that this value is of the order of atomic dimensions, as predicted by Feynman.

Fig. 15

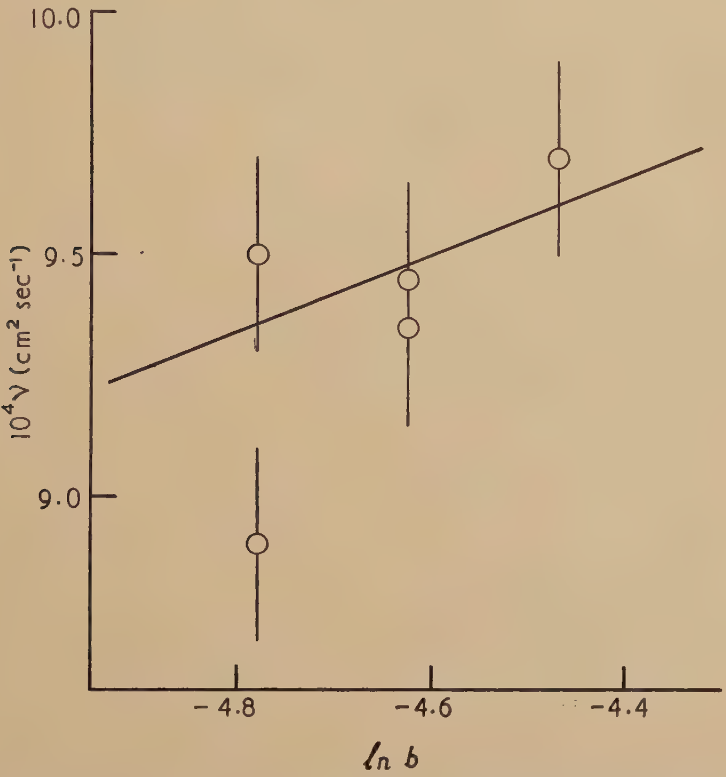

Dependence of ν on the effective spacing between vortex lines. The straight line has the slope predicted theoretically (eqn. (62)).

§ 4. THE OBSERVABLE PROPERTIES OF VORTEX LINES

The experiments so far described provide the most direct evidence at present available for the existence of vortex lines. No single experiment demonstrates all the properties of a vortex line; but taken together they provide a body of experimental evidence that it would be very difficult to explain in any other way. The vibrating wire experiment shows that circulation is quantized; the second sound attenuation shows that the rotating liquid contains linear scattering centres at about the spacing predicted for vortex lines; and the existence of vortex waves shows that these linear scattering centres exhibit the dynamical properties expected of vortex lines—tension and the Magnus effect.

The analysis of these experiments has made it clear that there are four observable constants associated with a vortex line: the circulation; the longitudinal and transverse collision diameters $\bar{\sigma}$, $\bar{\sigma}_{\perp}$; and the effective core radius a_0. These four constants determine the behaviour of the vortex line completely. The circulation requires no further discussion, since its value is unambiguously predicted by theory, and the experimental value is in excellent agreement with this prediction. The three characteristic lengths all turn out experimentally to be of the order of atomic dimensions; this seems intuitively reasonable, but clearly requires further discussion. We therefore now proceed to discuss in the light of experiment the various attempts that have been made to calculate these characteristic lengths theoretically.

4.1. *The Collision Diameters*

In the absence of a satisfactory wave function for the core of a vortex line, all the attempts so far made to calculate its scattering properties have made use of a classical model of the line. The vortex line is regarded simply as creating a velocity field $v_s(=\hbar/mr$ where r is the distance from the line) in the background fluid through which the excitations move; the phonons and rotons are considered simply as particles specified by their energy-momentum relation. In a velocity field v_s the energy of an excitation becomes $E+\mathbf{p}.\mathbf{v}_s$ so that there is an interaction energy $\mathbf{p}.\mathbf{v}_s$ near a vortex line which can produce scattering. The change in density of the liquid near the centre of the vortex due to finite compressibility can also produce an interaction energy, but this effect turns out to be unimportant for rotons.

The first calculation of roton-line scattering (Hall and Vinen 1956 b) was made by means of the first Born approximation, with the results

$$\bar{\sigma} \sim \left(\frac{\mu}{m}\right)^2 \frac{k_0}{(k-k_0)^2}, \quad \bar{\sigma}_{\perp}=0, \qquad \text{. . . . . . (65)}$$

where the momentum of the roton is $\hbar k$ and $k_0=p_0/\hbar$. Since the average value of $(k-k_0)$ in thermal equilibrium is proportional to $T^{1/2}$ and since $D=\rho_n\bar{\sigma}v_G$ eqn. (65) implies that $D/\rho_n \propto T^{-1/2}$. This temperature dependence gives results in fair agreement with experiment (see fig. 7), but the absolute value of the collision diameter is too large unless the interaction is cut off near the vortex core by supposing that the 'effective' velocity determining the interaction is not $\hbar/mr$ but $(\hbar/mr)[1-\exp(-r/a_0)]$. However, we should not expect the Born approximation to give a good answer, since it is only valid if all the phase shifts are small (Mott and Massey 1933), and this implies for rotons that

$$\frac{\mu}{m}\left(\frac{k_0}{k-k_0}\right) \ll 1 \qquad \text{. . . . . (66)}$$

whereas in fact $(\mu/m)k_0/(k-k_0)\sim 1$. It was at first thought that the result $\bar{\sigma}_\perp = 0$ could be regarded as indicating that this quantity was at any rate small, even though the Born approximation is not strictly valid. However, closer consideration shows that the result $\bar{\sigma}_\perp = 0$ is a property of the Born approximation. Although the scattering potential is asymmetric, it differs only in sign on the two sides of the vortex line, and therefore the differential collision diameter $\sigma(\theta)$, which depends on the square of the matrix element, is symmetrical about the forward direction. The Born approximation therefore only tells us that $\bar{\sigma}_\perp$ would vanish if the scattering potential were sufficiently weak.

One might expect the condition for validity of the quasi-classical approximation to be just eqn. (66) with the sign of the inequality reversed, in which case this approximation would be equally invalid. But because of the peculiar energy-momentum relation of rotons the condition for orbit and scattering angle to be well defined is in fact

$$\frac{\mu}{m}\left(\frac{k_0}{k-k_0}\right)^2 \gg 1; \qquad (67)$$

essentially this arises from the large momentum p_0 of a roton at rest. At temperatures of the order of 1°K $(\mu/m)[k_0/(k-k_0)]^2\sim 10$, so the quasi-classical approximation should give fairly good results. Lifshitz and Pitaevsky (1957) have recalculated the scattering of a roton by a vortex line in the quasi-classical approximation and find that

$$\bar{\sigma}\sim\frac{\mu}{mk_0}\dagger, \quad \bar{\sigma}_\perp\sim\frac{\mu}{m(k-k_0)}, \qquad (68)$$

from which

$$D \doteqdot 1{\cdot}2\kappa\rho_n\sqrt{(\mu kT)}/p_0, \quad D'=\kappa\rho_n. \qquad (69)$$

The precise numerical factors in eqns. (69) may however be altered if the distribution function for rotons near a vortex line differs from that for thermal equilibrium. This value of D', calculated before relevant experimental data were available, is of the order of the experimentally determined value. But the value of D is much too small, about $\frac{1}{10}$ of that required to explain the second sound data. Lifshitz and Pitaevsky suggest that this discrepancy is due to some form of 'strong interaction' which can occur if a roton passes close to a vortex line. For example, a roton could be captured into a bound state with the emission of vortex waves, and the inverse process could occur later. This would be a form of inelastic scattering, whereas so far we have only considered elastic scattering. It cannot be calculated without accurate wave functions for the roton and the vortex line, so Lifshitz and Pitaevsky simply add an arbitrary temperature independent collision diameter to $\bar{\sigma}$ so as to obtain agreement with experiment. They also suppose that the region of this 'hard-core' interaction should be excluded from the region of integration for $\mathbf{p}\,.\,\mathbf{v}_s$ scattering,

---

† Note that this agrees with eqn. (65) when $(\mu/m)[k_0/(k-k_0)]^2\sim 1$.

so that $\bar{\sigma}_\perp$ is reduced slightly. It is reasonable to suppose that the hard core itself does not contribute to $\bar{\sigma}_\perp$ if the interaction proceeds through an intermediate state of the type suggested above, since memory of the initial state would be lost and therefore the scattering should be isotropic.

It is clear that this type of inelastic scattering gives rise to exchange of momentum between rotons and vortex wave quanta parallel to the axis of rotation. Lifshitz and Pitaevsky suggest that B_z is zero in spite of this because the vortex wave quanta will form part of the normal fluid; but we shall now see that closer consideration of vortex waves shows that this conclusion may be incorrect. If the displacement of a vortex line running parallel to the z axis is written as $\xi = x + iy$ the equation of motion of the line is (Hall 1958)

$$-\frac{\hbar^2}{2m^*}\frac{\partial^2 \xi}{\partial z^2} = i\hbar \frac{\partial \xi}{\partial t}, \quad . \quad . \quad . \quad . \quad . \quad . \quad . \quad . \quad (70)$$

where $m^* = m/\ln(b/a_0)$. This is analogous to the one dimensional Schrödinger equation of a particle of mass m^* and it follows that the vortex wave quanta have the energy-momentum relation $E = p^2/2m^*$. Now for such an energy spectrum Landau's criterion for superfluidity (eqn. (8)) gives zero critical velocity (strictly a very small critical velocity determined by the length of the vortex line). In other words, superfluidity does not occur and an equilibrium distribution function of vortex wave quanta with a mean drift velocity relative to the superfluid does not exist. The vortex wave quanta cannot therefore move with the normal fluid in the usual sense. Indeed, if thermal equilibrium among vortex wave quanta is rapidly established they must move with the superfluid and we should expect a value of B_z as the same order as B, since comparison of theory and experiment suggests that the roton-vortex wave interaction makes a major contribution to B. It may be, however, that thermal equilibrium is only attained slowly, especially among low energy vortex wave quanta. This is suggested by the idea that at long wavelengths the mean free path of a vortex wave quantum should be equal to the attenuation length for a macroscopic vortex wave; eqn. (58) shows that this gives a long relaxation time at low energies. If these ideas are correct it may be that the high energy, strongly interacting, vortex wave quanta do in fact move approximately with the normal fluid, giving a small value of B_z, at the second sound frequencies hitherto used. Clearly the value of B_z requires further experimental and theoretical investigation.

The scattering of phonons by vortex lines has been calculated by Pitaevsky (1958). He finds that in the temperature region where phonons are dominant

$$B \approx 0{\cdot}42T \qquad B' = 0.$$

Above about 0·6°K the roton contribution to ρ_n is dominant, and the phonons hardly affect the value of B. The long mean free path of phonons below 0·5°K precludes any attempt to verify this result by means of second sound; and the very small value of ρ_n/ρ means that the attenuation of vortex waves would be too small to measure. The experimental verification of this phonon contribution to B therefore constitutes a considerable experimental problem.

4.2. *The Effective Core Radius*

Very little progress has been made with the calculation of the energy of a vortex line since Feynman's original conjecture that the radius a_0 should be of the order of the atomic spacing.

Ginsburg and Pitaevsky (1958) have given a theory of the line energy near the λ-point. They suppose that the free energy of unit volume of liquid can be put in the form

$$F = F_0(p, T, \rho_s) + \tfrac{1}{2}\rho_n v_n^2 + \tfrac{1}{2}\rho_s v_s^2 + \frac{\hbar^2}{8m}\frac{(\nabla\rho_s)^2}{\rho_s}. \quad . \quad . \quad (71)$$

Near the λ-point the first two terms in the expansion of F_0 in powers of ρ_s are adequate, and by treating ρ_s as an order parameter these terms can be deduced from the experimental values of $(\partial\rho_s/\partial T)$ at the λ-point and the discontinuity in specific heat. The last term in eqn. (71) is obtained by treating ρ_s/ρ as the square of an 'effective' wave function, as in the Ginsburg and Landau (1950) theory of surface energy in superconductors. Equation (71) is then used to find the radial variation of ρ_s that gives the minimum free energy for a vortex line. Except very near the core of the vortex the result is that ρ_s has the equilibrium value appropriate to the local value of $(\mathbf{v}_s - \mathbf{v}_n)$; near the centre the last term in eqn. (71) becomes important and makes ρ_s proportional to radius. The final result is that for a line with one quantum of circulation $a_0 \approx 2{\cdot}7/(T_\lambda - T)^{1/2}$ Å; the effective core radius therefore tends to infinity at the λ-point. This result is only valid at temperatures such that a_0 is much larger than an atomic spacing; for eqn. (71) is certainly invalid unless the variations in ρ_s are slow on an atomic scale.

Near absolute zero the temperature dependence of the line energy come from the temperature dependence of ρ_s and from the thermal excitation of vortex waves. Using the relation $E = p^2/2m^*$ for vortex wave quanta, as found in § 4.1, we find that the free energy ϵ of unit length of line is given by

$$\epsilon = \epsilon_0 - \frac{(kT)^{3/2}}{(2\pi\nu h)^{1/2}}\int_0^\infty \frac{x^{1/2}dx}{e^x - 1} \quad . \quad . \quad . \quad . \quad . \quad . \quad (72)$$

where ϵ_0 is the free energy at absolute zero. In deriving eqn. (72) the logarithmic dependence of m^* and ν on wavelength has been neglected; this is justifiable at low temperatures where the long wavelengths are dominant. In the region of 1 °K the variation in ϵ due to eqn. (72) is less than that due to ρ_s. Nevertheless, the corresponding variation in $\nu(=\epsilon/\rho_s\kappa)$ is just significant, and an appropriate correction was therefore applied in the extrapolation of experimental values of ν to absolute zero (§ 3.5).

Neither of these calculations throws any light on the question of the energy of a vortex line at absolute zero, for which a knowledge of the wave function of the liquid containing a vortex line is necessary. Feynman's wave function for a line along the z axis is, in cylindrical polar coordinates (r, θ, z)

$$\psi = \Phi \exp \sum_i i\theta_i \quad . \quad . \quad . \quad . \quad . \quad . \quad . \quad . \quad (73)$$

where θ_i are the angular coordinates of the atoms and Φ is the ground state wave function. This is clearly unrealistic near the axis and so should be multiplied by a factor which becomes small when any atom approaches too close to the axis. Unfortunately, with this modified wave function it has not proved possible to evaluate the integrals required in order to minimise the free energy $(E - M\omega_0)$ (eqn. (15)). Moreover, it is probably incorrect to assume that the line is on the z axis; one should allow a superposition of states with different positions of the line in order to take account of the zero-point motion associated with vortex waves, and this further complicates the problem. Essentially, then, the unsolved problem is to choose a plausible vortex line wave function for which the energy integral can be evaluated and minimized.

Experimentally, it might appear at first sight that the vortex wave experiments (§§ 3.4 and 3.5) give an unambiguous value of the effective core radius a_0 and thus of the line energy. But it must be borne in mind that the line energy may depend on the experimental conditions. Thus, in the vortex wave experiments the lines are forcibly localized because their ends are fixed to the disk surface, and this may prevent a reduction of line energy due to zero point motion. There is indeed some indication of a lower energy for a free vortex line (larger a_0) from Vinen's (1958 b) measurements of the circulation round a fine wire (§ 2.2). He finds that there is a considerable range of angular velocities for which the apparent circulation round the wire is intermediate between one and two quanta. This suggests that there are two quanta round part of the wire, but one of them becomes detached as a free vortex line. If this is so the free energies of the states with one and two quanta round the wire must be nearly equal, and Vinen has shown by calculation that this implies a rather low energy for a free vortex line ($a_0 \sim 10^{-5}$ cm). This conclusion can be criticised on the grounds that the true equilibrium state was not attained. The vortex lines are formed by cooling through the λ-point while rotating, and at the λ-point a_0 is very large, according to Ginsburg and Pitaevsky; the configuration of vortex lines which gives the lowest free energy at the λ-point might therefore persist at lower temperatures. In fact, however, considerable efforts were made to attain true equilibrium, by vibrating the wire strongly. When rotation was stopped these vibrations did reduce the circulation (i.e. produce a tendency to equilibrium); but in the rotating state they had no definite effect (see fig. 1), suggesting that the liquid was already in equilibrium.

It is also worth remembering that the non-resonant vortex wave experiments ($\omega_0 \gg \Omega$, fig. 8) at first suggested a lower value of the line energy.

This discrepancy was later explained in terms of slip of the vortex lines relative to the disk surfaces, when such an effect was found to be necessary to account for the observed resonance widths. But in the absence of a full understanding of the slip effect we cannot be sure that the first explanation, in terms of a low line energy, was not in fact the correct one.

None of these indications of a lower line energy than that deduced from the vortex wave resonances is conclusive; but they do suggest that the definite value of a_0 deduced in § 3.5 should be interpreted with caution. More experimental and theoretical work is required to determine whether the line energy is independent of the experimental conditions.

§ 5. SUPERFLUID TURBULENCE

5.1. *Mutual Friction and Turbulence*

So far in this article we have been entirely concerned with experiments specially designed to demonstrate the existence and properties of vortex lines. We now wish to enquire how far the idea of vortex lines can enable us to understand the many non-linear dissipative effects that have hitherto been unexplained. Gorter and Mellink (1949) showed that the dissipative effects associated with the steady flow of heat and matter in slits and capillaries could be described semi-quantitatively by adding to the equations of motion a phenomenological mutual friction force

$$F_{\mathrm{sn}} = A\rho_{\mathrm{s}}\rho_{\mathrm{n}}(v_{\mathrm{s}} - v_{\mathrm{n}})^3. \qquad \qquad (74)$$

We saw in § 3.2 that the regular array of vortex lines in uniformly rotating helium II gave rise to a force of mutual friction, and it is therefore reasonable to suppose that turbulence in the superfluid, corresponding to an irregular array of vortex lines, will likewise give rise to mutual friction. Vinen (1957 a, b) has made a detailed experimental study of the properties of the Gorter–Mellink force, and these experiments, which we shall now discuss, do indeed provide rather convincing evidence that the Gorter–Mellink force is associated with turbulence.

Vinen studied heat flow in a wide (~ 1 mm) tube of rectangular cross section. The temperature difference between the ends of the tube was proportional to the cube of the heat current, in agreement with eqn. (74), but when second sound was propagated across the tube it did not suffer the severe non-linear attenuation to be expected from eqn. (74). In the absence of a heat current the attenuation was very small and could be attributed to the well understood dissipative processes in the normal fluid; but in the presence of a heat current there was an additional linear attenuation of the second sound proportional to the square of the heat current. These results suggest that eqn. (74) should be modified to

$$\begin{aligned} \mathbf{F}_{\mathrm{sn}} &= A\rho_{\mathrm{s}}\rho_{\mathrm{n}}(V - v_0)^2(\mathbf{v}_{\mathrm{s}} - \mathbf{v}_{\mathrm{n}}) \\ &= G(\mathbf{v}_{\mathrm{s}} - \mathbf{v}_{\mathrm{n}}), \qquad \qquad (75) \end{aligned}$$

where $(\mathbf{v}_{\mathrm{s}} - \mathbf{v}_{\mathrm{n}})$ is the instantaneous value of the relative velocity of the two fluids and V is the time average of this relative velocity, averaged over a time long compared with a second sound period. v_0 is a small constant, empirically necessary to fit the experimental data accurately, which decreases somewhat with increasing tube width; we shall for simplicity ignore it in this section. Equation (75), with $v_0=0$, leads to the same temperature difference in a steady heat flow as eqn. (74), but it also produces an attenuation α of second sound given by

$$\alpha=\frac{A\rho}{2\rho_s{}^2S^2T^2u_2}W^2, \qquad (76)$$

Fig. 16

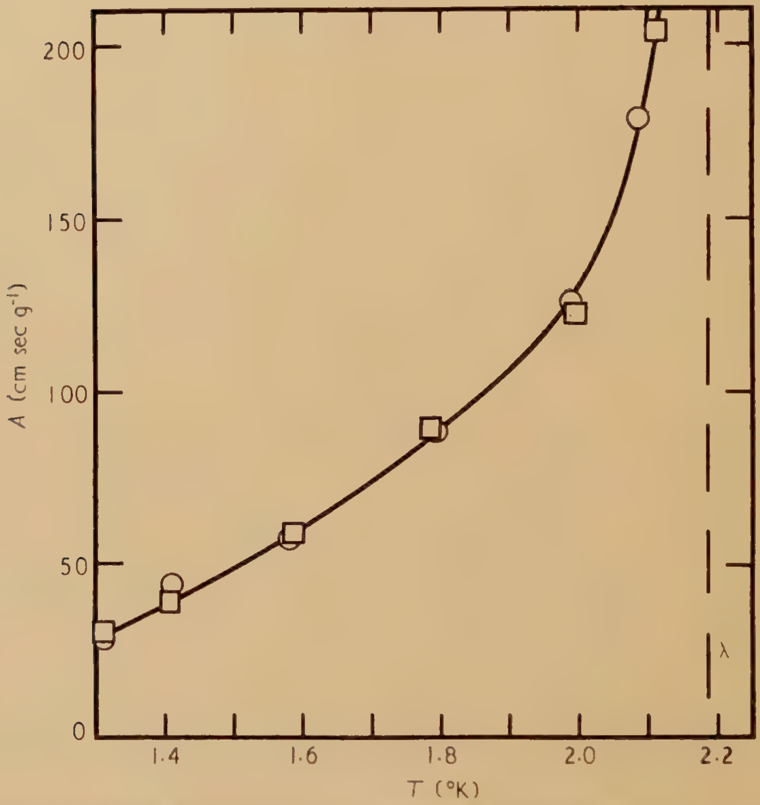

The Gorter–Mellink mutual friction constant A as a function of temperature. □, from temperature gradients; ○, from second sound attenuation.

where W is the heat current density. Figure 16 shows values of A deduced from the temperature gradient and from eqn. (76); the excellent agreement of the two sets of points verifies eqn. (75)†. The form of eqn. (75) indicates that the presence of a steady relative velocity $(\mathbf{v}_s-\mathbf{v}_n)$ causes the helium to become modified in some way, and that an essentially linear mutual friction, the strength of which is represented by the factor G in eqn. (75), is a property of this modified state. The modified state is not affected by the rapidly alternating relative velocity in a second sound wave.

---

† Experiments with comparable relative velocities due to heat flow and second sound proved that the square of the average relative velocity was relevant, rather than the average of the square.

Evidence that this modified state is in fact turbulence of the superfluid comes from observations of transient effects when the heat current is switched on or off. Figure 17 shows the transient behaviour of the amplitude of a second sound resonance. The heat current apparently has no effect for a time of the order of 1 sec after it is switched on; then there is a rapid drop in the resonance amplitude, indicating increased attenuation, as the mutual friction constant G builds up to a new equilibrium value. When the heat current is switched off the decay of mutual friction is at first complex, then steady and rather slow. These rather long delays are very reminiscent of the behaviour of ordinary turbulence: and even the form shown in fig. 17—rapid build up after a waiting period and very slow final decay—is what one would expect for turbulence. The build up can also be observed by means of the temperature difference, and gives results in agreement with those from second sound; but the decay, during which there is no steady heat flow, can only be observed by means of second sound.

Fig. 17

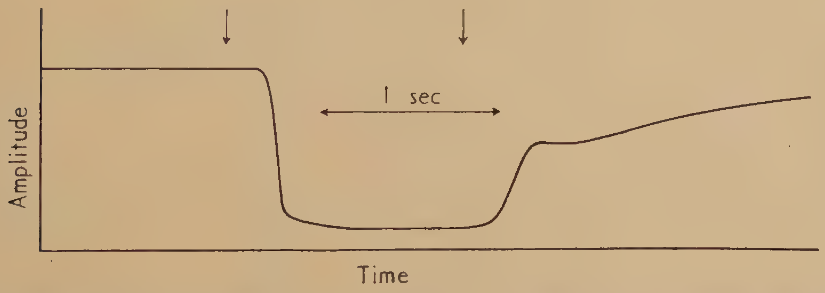

The effect of a heat current on the amplitude of a second sound resonance. The arrows indicate when the heat current was switched on and off.

The delay time τ for G to build up to half its final value is not completely reproducible, but if the helium has been left undisturbed for sufficiently long the scatter is only a few percent about a value τ_f. If the helium has not been left sufficiently long since a heat current was last switched off, the observed value of τ is less than τ_f; this is readily explained as the nucleation of turbulence by residual turbulence from the previous heat current. Except very close to a critical velocity of the same order as v_0 it is found that $\tau_f \propto W^{-3/2}$ and is independent of tube width.

5.2. *Dimensional Analysis of Homogeneous Turbulence*

The fact that the velocity v_0 and anomalies associated with it tend to decrease with increasing channel width suggests that in a channel of infinite width eqn. (75) would hold with $v_0 = 0$. In other words we should expect that in an unbounded volume of helium there should exist an equilibrium turbulent intensity depending only on the average value of $(\mathbf{v}_s - \mathbf{v}_n)$. Such turbulence must be homogeneous, and the equality of the values of A obtained from temperature gradient and second sound measurements (fig. 16) shows that it must also be quite accurately isotropic. This is therefore probably the simplest form of turbulence that can exist in helium; we shall now analyse it by dimensional methods, following Vinen (1957 c).

If a vortex line is perpendicular to a flow of normal fluid the force on unit length of it in the direction of the relative velocity is given by

$$\mathbf{f} = B_L \frac{\rho_s \rho_n}{2\rho} \kappa (\mathbf{v}_n - \mathbf{v}_L); \quad . \quad . \quad . \quad . \quad . \quad . \quad . \quad (77)$$

if the line is not perpendicular to $(\mathbf{v}_n - \mathbf{v}_L)$ this force, as we saw in § 3.3, is multiplied by an angular factor which need not concern us here. There is also a force perpendicular to $(\mathbf{v}_n - \mathbf{v}_L)$ which is proportional to B'_L: it is difficult to take this into account in a dimensional approach since two force constants make the problem indeterminate. We shall therefore use eqn. (77) to give a characteristic magnitude of the force on unit length of line, but bear in mind that the appropriate force constant may not be precisely B_L. The transverse force is perhaps likely to be less important, since it cancels out on the average. We shall also ignore the difference between B and B_L and the dependence of B on the experimental conditions arising from the dragging of the normal fluid by a vortex line; this is justifiable for the range of temperatures, frequencies, and velocities with which we shall be concerned.

To apply dimensional analysis we have to assume that the structure of the turbulence is geometrically similar at all times, i.e. that it depends only on the length of vortex line L in unit volume, or the characteristic spacing of the lines, $l = L^{-1/2}$. This is equivalent to the hypothesis of complete self-preservation, often made in the theory of ordinary turbulence. It is known to be approximately, but not accurately, true; we may reasonably expect our deductions to have a similar degree of accuracy. With this hypothesis, the rate of growth or decay of turbulence can depend only on $\mathbf{f}$, the force on unit length of line, ρ_s, and κ. We must therefore have

$$\frac{dL}{dt} = \kappa L^2 \phi\left(\frac{f}{\rho_s \kappa^2 L^{1/2}}\right), \quad . \quad . \quad . \quad . \quad . \quad . \quad . \quad . \quad (78)$$

where ϕ is an arbitrary function. For a stable turbulent intensity to exist ϕ must be positive for small L and negative for large L. The equilibrium turbulent intensity L_0 (if it exists) is then given by $\phi = 0$, or

$$L_0^{1/2} \propto \frac{f}{\rho_s \kappa^2} = \frac{B\rho_n}{2\rho\kappa}(v_n - v_s), \quad . \quad . \quad . \quad . \quad . \quad . \quad . \quad (79)$$

assuming that on the average $\mathbf{v}_L = \mathbf{v}_s$. The mutual friction force per unit volume is then given by $\frac{2}{3}L_0 f$ (assuming the vortex lines are randomly oriented) so that the Gorter–Mellink law is obeyed with

$$A \propto \frac{B^3}{\kappa}\frac{\rho_n^{\,2}}{\rho^3}\,; \qquad (80)$$

this expression does indeed account for most of the observed temperature dependence of A.

To discuss the growth and decay of turbulence Vinen uses simple physical arguments to justify a particular form for ϕ, namely

$$\phi = \chi_1 \frac{f}{\rho_s \kappa^2 L^{1/2}} - \frac{\chi_2}{2\pi}, \qquad (81)$$

where χ_1 and χ_2 are numerical constants expected to be of order unity; the two terms represent separate growth and decay processes. The prototype of a growth process is probably the expansion or contraction of a large vortex ring which takes place when a stream of normal fluid flows past it; whether expansion or contraction occurs depends on the orientation of the ring relative to the flow. If the plane of the ring is normal to the flow the Magnus effect gives, for a large ring of radius b:

$$\left|\frac{db}{dt}\right| \doteqdot \frac{f}{\rho_s \kappa}. \qquad (82)$$

In homogeneous turbulence the only length that can be substituted for b is the line spacing $l = L^{-1/2}$, and thus we expect

$$\frac{dL}{dt} = \chi_1 \frac{f}{\rho_s \kappa} L^{3/2}, \qquad (83)$$

where χ_1 is a numerical constant of order unity. It is not immediately obvious whether this process gives a net growth or a net decay. But since turbulent flow in general continually increases the length of vortex line, it is reasonable to suppose that eqn. (83) gives a net growth and thus represents the first term of eqn. (82). If turbulent flow continually stretches existing vortex line we may well ask, how can the turbulence finally decay? This stretching of vortex line can be expressed in another way as the tendency of the turbulence to spread over a wider and wider range of wave numbers in the velocity spectrum. In ordinary turbulence viscosity removes energy by damping out the motion at high wave numbers; at high Reynolds numbers the decay time of the turbulence is controlled by the energy containing eddies and viscosity merely produces an energy sink at high wave numbers. This gives the decay law

$$\frac{du^2}{dt} = -\chi_2 \frac{u^3}{l} \qquad (84)$$

(Batchelor 1953), where u is a typical turbulent velocity, l is the length scale of the energy containing eddies, and χ_2 a constant of order unity. In superfluid turbulence motion of high wave number corresponds to oppositely directed lengths of vortex line running close together. If these can mutually annihilate, as Feynman (1955) suggested, we have a process to take the place of viscosity; and if this process is rapid we can expect the energy containing eddies to control the motion and eqn. (84) to be obeyed. A suitable velocity scale for superfluid turbulence is the velocity at distance l from an isolated vortex line, which is $\kappa/2\pi l$; if this is inserted in eqn. (84) we obtain

$$\frac{dL}{dt} = -\chi_2 \frac{\kappa L^2}{2\pi}, \qquad (85)$$

which is the second term in eqn. (83).

If we set $\mathscr{L} = L/L_0$ eqns. (78) and (81) give

$$\frac{d\mathscr{L}}{dt} = \frac{\pi B^2}{2\kappa} \frac{\chi_1^2}{\chi_2} \left(\frac{\rho_n}{\rho}\right)^2 (v_s - v_n)^2 \mathscr{L}^{3/2}(1 - \mathscr{L}^{1/2}), \qquad (86)$$

and the Gorter–Mellink constant A is given by

$$A = \frac{\pi^2 B^3}{3\kappa} \frac{\rho_n^2}{\rho^3} \left(\frac{\chi_1}{\chi_2}\right)^2. \qquad (87)$$

Figure 18 shows the application of eqn. (86) to the build up of turbulence when a heat current is switched on; the dependence of $d\mathscr{L}/dt$ on $\mathscr{L}$ is well verified and the slope of the graph yields a value of χ_1^2/χ_2. Values of $(\chi_1/\chi_2)^2$ can be deduced from eqn. (87), and hence χ_1 and χ_2 deduced separately. χ_1 is found to be equal to $0{\cdot}29 \pm 0{\cdot}015$ at all temperatures; χ_2 is approximately 1, increasing slightly with increasing temperature, presumably because the decay of turbulence is affected by the presence of normal fluid. So far, therefore, the theory is strikingly well verified.

Nevertheless, eqn. (86) is clearly incomplete, since it includes no mechanism for the initial nucleation of turbulence; it predicts an infinite value for the delay time τ_f. Vinen therefore adds to dL/dt an empirical nucleation term. To give the observed result $\tau_f \propto W^{-3/2}$ this term has to have the form

$$\frac{dL}{dt} = \gamma (v_s - v_n)^{5/2}, \qquad (88)$$

where $\gamma \sim T^{11}$. This very rapid temperature dependence suggests at first sight that the nucleation mechanism is essentially thermal in origin; but we shall now suggest a possible nucleation mechanism which indicates that this conclusion may not be valid. In a heat current the superfluid flows with a velocity discontinuity at the wall, and this means that there is a certain length of 'virtual' vortex line at the walls of the tube. The length L' of virtual line per unit volume of liquid is given by

$$L' = \frac{2v_s}{\kappa d} = \frac{2\rho_n}{\rho\kappa d}(v_s - v_n), \qquad (89)$$

where d is the ratio of area to perimeter of the cross-section of the flow tube (the effective width). If we now suppose that this virtual line can be amplified in the same way as real vortex line, substitution in eqn. (83) gives

$$\frac{dL}{dt} = \frac{\sqrt{2}\chi_1 B}{(\kappa d)^{3/2}} \left(\frac{\rho_n}{\rho}\right)^{5/2} (v_s - v_n)^{5/2}. \qquad (90)$$

This accounts for the velocity dependence and most of the temperature dependence of the observed nucleation term; but it predicts a dependence on tube width that is not observed. Equation (90) predicts that the values of τ_f for the two tubes used by Vinen should differ by about 20% whereas they are in fact equal within about 4%. The actual nucleation rates given by eqn. (90) are about 10 times those observed, the precise factor depending somewhat on tube width and temperature. In view of these discrepancies and of the very great difficulty of seeing how 'virtual' vortex line could in fact be amplified, we cannot take eqn. (90) very seriously; but it does serve to illustrate that there may not be any essentially thermal process involved in the nucleation of turbulence.

Fig. 18

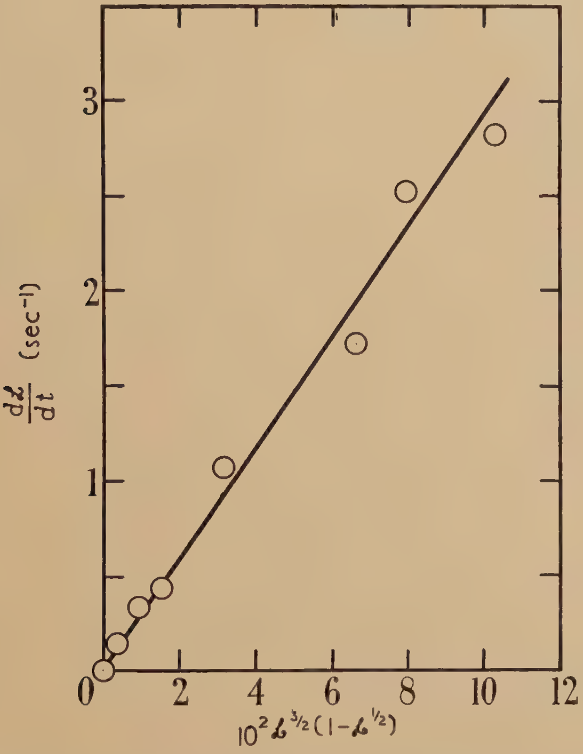

The growth of mutual friction when a heat current is switched on, for $(v_s - v_n) = 3{\cdot}78$ cm sec^{-1} at 1·41°K.

The decay of turbulence can also be observed with $(v_s - v_n) = 0$ by observing the decay of mutual friction after a heat current is switched off; it is easily shown from eqn. (85) that $1/G$ should vary linearly with time. Experimental results on the decay of turbulence are shown in fig. (19); it can be seen that after an initial anomaly depending on the previous heat current (and also on tube width) a linear relation is indeed obeyed, and from this the value of χ_2 can be deduced.

These values of χ_2 are rather smaller than those deduced from the growth of turbulence, about 0·2 decreasing slightly with increasing temperature. This difference suggests that either the separation of dL/dt into separate growth and decay terms is not completely valid, or else the turbulence is not fully self-preserving. Probably there is overall self-preservation during growth and decay, but the self-preserving states are different in the two cases.

Fig. 19

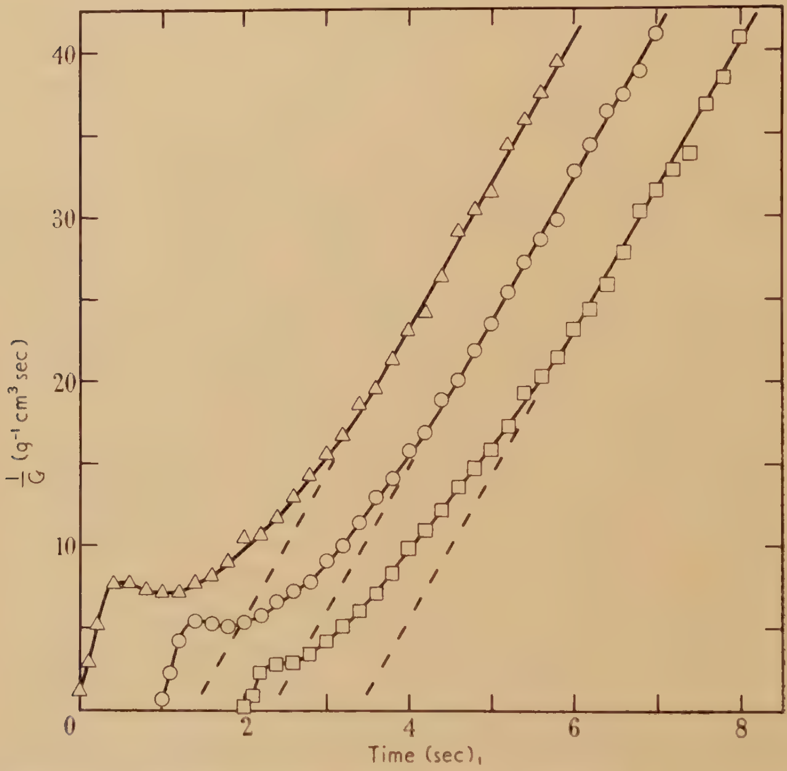

The decay of mutual friction after a heat current is switched off. Temperature $=1{\cdot}41°\text{K}$; △, $9{\cdot}76\times10^{-2}$ w cm^{-2}; ○, 0·139 w cm^{-2}; □, 0·245 w cm^{-2}. The origin of time is displaced to avoid overlap of the curves.

5.3. *Wall Effects*

When the effects of the channel walls become important our analysis becomes much less reliable; for the turbulence is probably no longer homogeneous, and there is now no reason to suppose that it is self-preserving. However, our present ignorance of the fundamental interaction processes between vortex lines and a solid boundary precludes a more satisfactory approach, and we shall therefore pursue our dimensional analysis, remembering that its results can only be expected to have qualitative significance. The presence of solid walls introduces an extra dimensionless parameter, the ratio of line spacing to channel width, l/d, so that eqn. (78) now becomes

$$\frac{dL}{dt} = \kappa L^2 \phi\left(\frac{f}{\rho_s \kappa^2 L^{1/2}}, \frac{l}{d}\right). \qquad (91)$$

We shall for simplicity suppose that dL/dt can still be split into separate growth and decay terms and write

$$\frac{dL}{dt} = \chi_1 B \frac{\rho_n}{2\rho} v L^{3/2} g_1\left(\frac{l}{d}\right) - \frac{\chi_2}{2\pi} \kappa L^2 g_2\left(\frac{l}{d}\right), \qquad (92)$$

where $v = (v_s - v_n)$ and g_1 and g_2 are functions to be determined.

Fig. 20

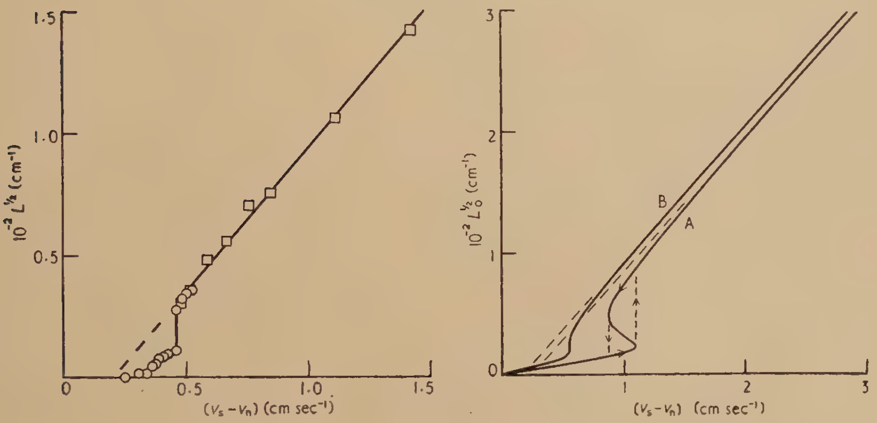

(*a*) (*b*)

The equilibrium turbulent intensity at low velocities at 1·40°K. (*a*) Experimental results for d = 0·1325 cm. □, from second sound attenuation; ○, from delay times. (*b*) Theoretical curves: A, d = 0·0875 cm; B, d = 0·1325 cm.

The simplest results appear to be those of Vinen (1958 a) on heat flow; some typical observations of mutual friction in the region of the critical velocity are shown in fig. 20 (*a*). The lowest values of L were deduced indirectly from their effect on the initial growth of turbulence for a higher heat current. These indirectly deduced values agree with the directly measured ones only if they are multiplied by a scaling factor of order unity which depends somewhat on temperature and channel width; this is probably another symptom of incomplete self-preservation. Vinen finds that his results can be accounted for almost quantitatively by the addition of a single term to dL/dt for an infinite channel, namely

$$\frac{dL}{dt}_{\text{wall}}=-\chi_3 B\frac{\rho_n}{2\rho}v\frac{L}{d}. \qquad (93)$$

This corresponds in eqn. (92) to

$$g_1=1-\frac{\chi_3}{\chi_1}\frac{l}{d}, \quad g_2=1; \qquad (94$$

the extra term can, for example, be considered as representing interference of the wall with the normal growth process for a distance of order l from it. Values of L as a function of v deduced with this extra term in dL/dt are shown in fig. 20 (*b*) (the nucleation term $\gamma(v_s-v_n)^{5/2}$ is also included). The agreement is in general good, except that the predicted critical velocity varies rather too rapidly with channel width, and the hysteresis effects predicted in the narrower channel at low temperatures were not observed. However, in narrower channels ($\sim 100\,\mu$) the predicted hysteresis becomes much more marked; and in such channels marked hysterisis has indeed been observed by Brewer and Edwards (1957).

Isothermal flow of the superfluid with the normal fluid virtually at rest has been observed by measurements of capillary flow (Atkins 1951) and of the angular acceleration of helium contained in a pile of closely spaced disks (Hall 1957). The situation is clearly rather different here, since v_0 (eqn. (75)) turns out to be negative, although A has the same value as for a heat flow. The angular acceleration experiments showed time dependent effects broadly similar to those found for heat flow, and it was therefore possible to deduce values of dL/dt as a function of L and v. These results were originally analysed with the restrictive assumption that only the decay process was affected by the presence of solid boundaries; we now present a revised analysis which avoids this assumption, based on the foregoing dimensional analysis (eqn. (91)). Figure 21 shows empirical contours of constant $(2\pi/\kappa L^2)\,dL/dt$ as a function of $v/L^{1/2}$ and l/d; for the sake of clarity experimental points are shown only on the zero contour. Contours well established by experiment are shown solid; those where the experimental data are scarce or unreliable are shown by broken lines. The intersections of the contours with the $v/L^{1/2}$ axis are chosen so as to give the same results for an infinite channel as those deduced from heat flow experiments, since the two types of flow are then equivalent. It must be remarked that the experimental results suggest that this diagram may not be single valued; but since it is not certain that these deviations are outside the limits of experimental error they have been ignored. Such deviations would represent departures from complete self-preservation; since they may well exist fig. 21 should be regarded as having no more than semi-quantitative significance.

It is clear from the gathering together of the contours at the top of the diagram that when $l/d \gg 1$ the walls assist both the growth and decay processes. But the behaviour of the contours for $v=0$ shows that the decay process is at first hindered, reaching a minimum for $l/d\sim 1$. The parallelism of the contours in the region of small l/d suggests that in this region the growth rate is not much affected. These qualitative features can be reproduced if we choose the functions g_1 and g_2 in eqn. (92) to have some such form as

$$g = \exp(-\alpha l/d) + \beta l/d. \qquad (95)$$

Fig. 21

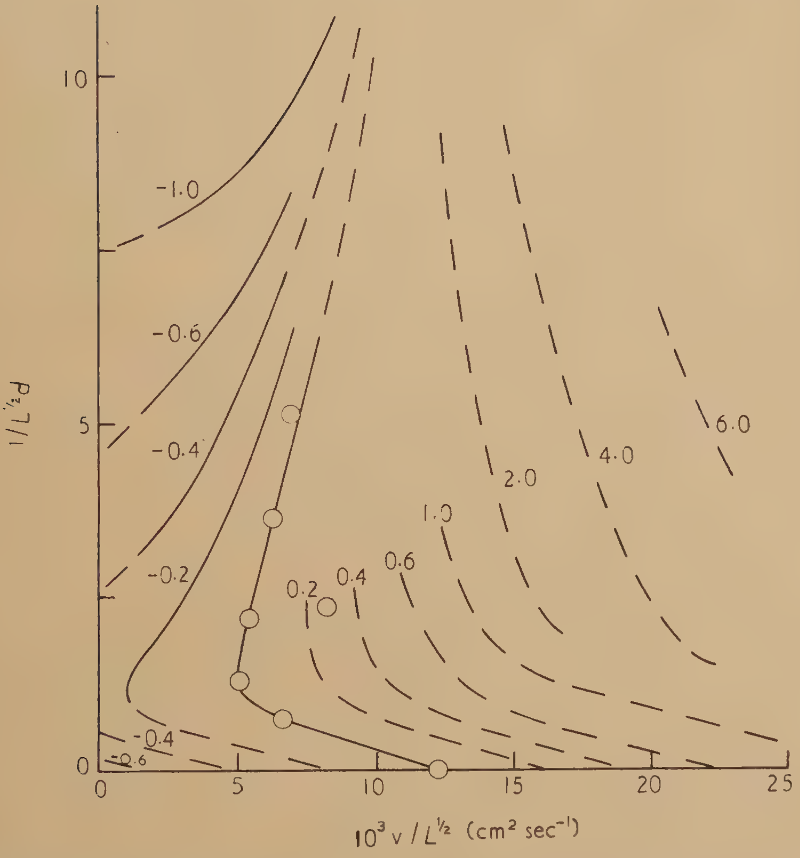

Contours of constant $(2\pi/\kappa L^2)dL/dt$ from angular acceleration experiments; the values of this quantity are marked on the curves. ○, experimental points on the zero contour. The solid curves are fairly well established; the broken curves are more schematic.

Then the observed behaviour shown in fig. 21 is qualitatively reproduced if we choose

$$\alpha_1 \doteqdot \beta_1, \quad \alpha_2 > \beta_2, \qquad (96)$$

$$\text{whence } v_0 < 0.$$

On the other hand, for heat flow we require

$$\alpha_1 > \beta_1, \quad \alpha_2 \div \beta_2, \quad \ldots \ldots \quad (97)$$

$$\text{whence } v_0 > 0;$$

this reduces to eqn. (94) for small l/d. It thus appears that it may be possible to describe the different behaviour of different types of flow solely by variations in the constants α_1, α_2, β_1, β_2. Now the first term of eqn. (95) can be regarded as representing interference of the wall with the normal growth or decay process, and the second term can be interpreted as growth or decay specifically at the wall. It is likely that all these processes depend on the value of v_s at the boundary, as well as $(v_s - v_n)$, and it is therefore reasonable that the constants α_1, α_2, β_1, β_2 should depend on the type of flow. We can therefore say that the observed effects of solid walls on turbulence seem *a priori* reasonable; any deeper consideration of these effects must await an understanding of the fundamental processes by which a vortex line can be created or annihilated at a solid boundary.

5.4. *Boundary Layer Experiments*

A class of experiments rather different from those just considered is the torsional oscillations of a suspended sphere or disk and the oscillations of liquid in a U tube. All these experiments approximate to the flow produced by oscillation of an infinite plane boundary parallel to itself. In such a flow any turbulence is clearly inhomogeneous, and any attempt to apply the foregoing ideas is therefore rather hazardous. We shall content ourselves with a very crude attempt to estimate the critical velocity at which superfluid turbulence, and hence extra dissipation due to mutual friction, becomes apparent.

Donnelly and Hollis-Hallett (1958) have reviewed these experiments, and find empirically that ideal superflow breaks down when a certain number $\mathscr{R}_{\mathrm{ns}}$ exceeds about 30 (the critical value is about 10 for oscillating disks, probably because of the sharp edges). $\mathscr{R}_{\mathrm{ns}}$ is defined by the equation

$$\mathscr{R}_{\mathrm{ns}} = \frac{v\lambda_{\mathrm{n}}}{\nu_{\mathrm{ns}}} \frac{(\rho_s \rho_n)^{1/2}}{\rho}, \quad \ldots \ldots \quad (98)$$

where v is the maximum tangential velocity of the boundary,

$$\lambda_{\mathrm{n}} = (2\eta_{\mathrm{n}}/\rho_{\mathrm{n}}\omega)^{1/2}$$

is the penetration depth of viscous waves in the normal fluid, ω is the angular frequency of oscillation, and ν_{ns} is an empirical kinematic viscosity. At large amplitudes the two fluids are strongly coupled by mutual friction and move together; ν_{ns} is the apparent kinematic viscosity measured under these conditions.

The results of the preceding section suggest that, whatever the precise effect of the walls on the turbulence, some sort of critical velocity occurs when the spacing l beween vortex lines, deduced from the volume growth and decay processes alone, becomes comparable with the channel width. In the boundary layer flow the effective channel width is probably the region over which $(v_s - v_n)$ is appreciable, i.e. λ_n. We should therefore expect the critical condition to be

$$\frac{\lambda_n}{l} = \left(\frac{3A\rho}{B\kappa}\right)^{1/2} \lambda_n v \sim 1 \, ; \qquad (99)$$

combining this with eqn. (98) we have

$$\frac{\lambda_n}{l\mathscr{R}_{ns}} = \left(\frac{3A\rho^3}{B\kappa\rho_s\rho_n}\right)^{1/2} \nu_{ns} \sim \frac{1}{30}. \qquad (100)$$

This quantity has been calculated for the range of temperatures for which experimental values of A, B and ν_{ns} are available, and the results are shown in fig. 22. Below about 2°K, $(\lambda_n/l\mathscr{R}_{ns})$ is indeed almost constant, and implies a critical value of $(\lambda_n/l) = 2{\cdot}0 \pm 0{\cdot}2$, which is very reasonable.

Fig. 22

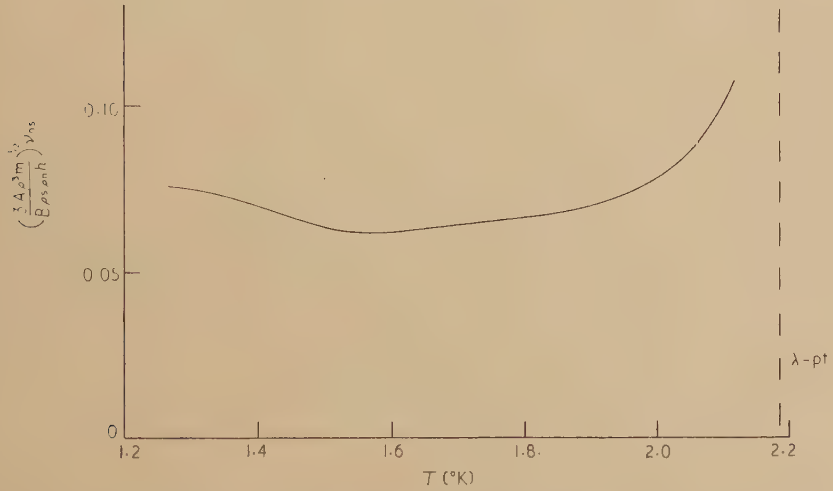

Temperature dependence of $\lambda_n/l\mathscr{R}_{ns} = (3A\rho^3 m/B\rho_s\rho_n h)^{1/2}\nu_{ns}$ for boundary layer flow.

The rather abrupt rise in $(\lambda_n/l\mathscr{R}_{ns})$ near the λ-point is not unduly disquieting, for it is just here that our theory is least reliable, because of our neglect of the difference between B and B_L and our assumption that on the average the vortex lines move with the superfluid. Indeed, it is rather surprising that our very crude theory accounts so well for the observed magnitude and temperature dependence of the critical velocity in boundary layer experiments.

It is pertinent to remark at this point that all the critical velocities we have considered so far have arisen in rather complicated ways, and represent velocities at which the equilibrium turbulent intensity is drastically reduced, rather than velocities below which turbulence is impossible. An estimate of this more fundamental critical velocity may be obtained by applying Landau's criterion (eqn. (8)) for the creation of excitations to large vortex rings of radius R. The result is

$$v_c = \frac{\kappa}{2\pi R}\left(\ln\frac{8R}{a_0} - \frac{5}{4}\right). \qquad (101)$$

Now only vortex rings smaller than the tube can be created, so an estimate of the critical velocity is obtained by setting R equal to the tube radius. Feynman (1955) obtained a similar critical velocity by a slightly different argument: it is likely that several different processes for the creation of vortex line lead to a critical velocity of this order of magnitude. In not too narrow channels eqn. (101) gives a velocity less than or equal to the observed critical velocity, as expected; but in very narrow channels or the film eqn. (101) gives too large a critical velocity unless a_0 is chosen rather large. However, eqn. (101) at least gives a critical velocity of the observed order of magnitude, very much smaller than the critical velocity for the creation of rotons. The complex nature of the observed critical velocities in wide channels should warn us not to expect any very simple explanation of the critical velocities in narrow channels and the film.

5.5. *Eddy Viscosity*

In addition to mutual friction we should expect turbulent superfluid to exhibit an eddy viscosity: the kinematic viscosity should be of the order of the product of the length and velocity scales of the turbulence, i.e. h/m. Some evidence for such an effect is provided by the kinematic viscosity ν_{ns} mentioned in the preceding section. If the superfluid has an eddy viscosity η_s we should expect when both fluids are coupled together by mutual friction to measure a kinematic viscosity

$$\nu_{ns} = (\eta_n + \eta_s)/\rho. \qquad (102)$$

Experimentally, the measured values of ν_{ns} are about 15% greater than η_n/ρ in agreement with this idea.

Further evidence comes from fountain pressure measurements in a heat flow. If mutual friction alone is present the pressure gradient is related to the heat current W in a tube of radius r by

$$\frac{\operatorname{grad} p}{W} = \frac{8\eta_n}{\pi r^4 \rho S T}, \qquad (103)$$

and the ratio is thus independent of the mutual friction. If the superfluid has an eddy viscosity, eqn. (103) is still true when the mutual friction is small, but when the mutual friction is large it is replaced by

$$\frac{\operatorname{grad} p}{W} = \frac{8(\eta_n + \eta_s)}{\pi r^4 \rho S T}, \qquad (104)$$

if it is assumed that the superfluid still slips over the walls and the turbulent intensity is uniform. A transition from eqn. (103) to eqn. (104) can just be detected in some of the early Leiden measurements; but it is most clearly apparent in the more recent work of Brewer and Edwards (1957) with tubes of about 100 μ diameter.

§ 6. CONCLUSION

The general impression left by this survey is one of broad general agreement between the consequences of the vortex line hypothesis and experiment. In the experiments deliberately designed to exhibit the properties of vortex lines in their simplest form—the circulation experiment, the attenuation of second sound in rotating helium, and the propagation of vortex waves—almost complete quantitative agreement is obtained. For the previously unexplained non-linear dissipative processes the agreement is less complete; but it is clear that quantized turbulence is capable of producing all the qualitative effects observed. In the simple examples of turbulence we have analysed, dimensional arguments supplemented by very simple physical ideas have proved surprisingly powerful; the degree of quantitative agreement obtained is as much as we have any right to expect from such crude arguments.

Nevertheless, there do remain a number of serious difficulties, which it is well to summarize here; these may be roughly divided into two classes, mathematical and physical. In the former class fall the finding of a good wave-function for a vortex line, on which depends the proper calculation of the line energy and the scattering properties; and a proper calculation of the dynamics of turbulence. In the second class, where the physical principles involved are not really understood, we have the nucleation of turbulence; the way in which vortex lines are created and annihilated at the walls, and the probably related problem of the slip of vortex lines over a rough surface; and the process by which vortex lines mutually annihilate in the body of the liquid.

But these difficulties, though important and requiring investigation, should not be over emphasized. Though many of the detailed arguments and conclusions presented in this article may subsequently be proved wrong, Feynman's basic idea of quantized vortex lines can explain so many diverse experimental results that we may be confident that it will find a permanent place in the theoretical description of liquid helium II.

ACKNOWLEDGMENTS

I should like to thank Dr. W. F. Vinen for the many benefits of a very happy collaboration during the period when the ideas discussed in this article were being formulated, and Professor B. H. Flowers for helpful comments on the first draft of the article.

REFERENCES

ANDRONIKASHVILI, E. L., 1946, *J. Phys. Moscow*, **10**, 389.

ANDRONIKASHVILI, E. L., and KAVERKIN, I. P., 1955, *J. exp. theor. Phys.*, **28**, 126.

ANDRONIKASHVILI, E. L., and ZAKADZE, D. S., 1959, *J. exp. theor. Phys.*, **37**, 322, 562.

ATKINS, K. R., 1951, *Proc. phys. Soc. Lond.*, A, **64**, 833; 1952, *Advanc. Phys.*, **1**, 169.

Batchelor, G. K., 1953, *The theory of homogeneous turbulence*, Ch. VI (Cambridge : University Press).

Brewer, D. F., and Edwards, D. O., 1957, *Proc. 5th Int. Conf. Low Temp. Phys.*, Madison, Wisconsin, p. 12.

Craig, P. P., and Pellam, J. R., 1957, *Phys. Rev.*, **108,** 1109.

Dingle, R. B., 1952, *Advanc. Phys.*, **1,** 111.

Donnelly, R. J., and Hollis-Hallett, A. C., 1958, *Annals of Phys.*, **3,** 320.

Feynman, R. P., 1954, *Phys. Rev.*, **94,** 262: 1955, *Prog. Low. Temp. Phys.* I, Ch. II (North Holland Publishing Co.): 1957, *Rev. mod. Phys.*, **29,** 205.

Feynman, R. P., and Cohen, M., 1956, *Phys. Rev.*, **102,** 1189.

Ginsburg, V. L., 1955, *J. exp. theor. Phys.*, **29,** 254.

Ginsburg, V. L., and Landau, L. D., 1950, *J. exp. theor. Phys.*, **20,** 1064.

Ginsburg, V. L., and Pitaevsky, L. P., 1958, *J. exp. theor. Phys.*, **34,** 1240 (*Sov. Phys.*, **7,** 858).

Gorter, C. J., and Mellink, J. H., 1949, *Physica*, **15,** 285.

Hall, H. E., 1957, *Phil. Trans.* A, **250,** 359; 1958, *Proc. roy. Soc.* A, **245,** 546.

Hall, H. E., and Vinen, W. F., 1955, *Phil. Mag.* **46,** 546; 1956 a, *Proc. roy. Soc.* A, **238,** 204; 1956 b, *Proc. roy. Soc.* A, **238,** 215.

Khalatnikov, I. M., 1956, *Usp. fiz. Nauk*, **59,** 673.

Landau, L. D., 1941, *J. Phys. Moscow*, **5,** 71; 1947, *Ibid.*, **11,** 91.

Landau, L. D., and Khalatnikov, I. M., 1949, *J. exp. theor. Phys.*, **19,** 637, 709.

Landau, L. D., and Lifshitz, E. M., 1955, *C.R. Acad. Sci. U.R.S.S.*, **100,** 669; 1958, *Statistical Physics* § 26 (Pergamon Press).

Lifshitz, E. M., and Pitaevsky, L. P., 1957, *J. exp. theor. Phys.*, **33,** 535 (*Sov. Phys.*, **6,** 418).

London, F., 1954, *Superfluids II* (Wiley), p. 151.

London, H., 1946, *Phys. Soc. Camb. conf.*, **2,** 48.

Mott, N. F., 1949, *Phil. Mag.*, **40,** 61.

Mott, N. F., and Massey, H. S. W., 1933, *The Theory of Atomic Collisions* (Oxford: University Press).

Onsager, L., 1949, *Nuovo Cim.*, **6,** Suppl., 2,249.

Osborne, D. V., 1950, *Proc. phys. Soc. Lond.*, A, **63,** 909.

Peshkov, V. P., 1944, *J. phys. Moscow*, **8,** 381; 1946, *Ibid.*, **10,** 389.

Pitaevsky, L. P., 1958, *J. exp. theor. Phys.*, *Moscow*, **35,** 1271 (*Sov. Phys.*, **8,** 888).

Sewell, C. J. T., 1910, *Phil. Trans.* A, **210,** 239.

Thomson, Sir W., 1880, *Phil. Mag.*, **10,** 155.

Vinen, W. F., 1957 a, *Proc. roy. Soc.* A, **240,** 114; 1957 b, *Ibid.*, **240,** 128; 1957 c, *Ibid.*, **242,** 493; 1958 a, *Ibid.*, **243,** 400; 1958 b, *Nature, Lond.*, **181,** 1524.

Walmsley, R. H., and Lane, C. T., 1958, *Phys. Rev.*, **112,** 1041.

Wheeler, R. G., Blakewood, C. H., and Lane, C. T., 1955, *Phys. Rev.*, **99,** 1667.

Yarnell, J. L., Arnold, G. P., Bendt, P. J., and Kerr, E. C., 1959, *Phys. Rev.*, **113,** 1379.

ERRATUM

The Structure of Ice–I, as Determined by X-Ray and Neutron Diffraction Analysis: A Correction

By P. G. Owston
Imperial Chemical Industries Ltd., Akers Research Laboratories,
The Frythe, Welwyn, Herts.

In table 1 on page 179 of this paper (Owston 1958) there are a number of errors resulting from the use of an incorrect factor in converting kx to Å units, and from the assumption that Truby's (1955) values were given in Å, though they were probably in kx units. The corrected values are given in the table below, and agree with similar tables given by Gränicher (1958) and Lonsdale (1958). The errors do not affect the discussion, which depended on the ratio c/a rather than on the actual values of a and c.

The author is indebted to Dr. H. Gränicher (private communication) for drawing his attention to these errors.

Table 1. The Cell-Dimensions of Ice (Å)

a	c	c/a	Temp. °C	Reference
H_2O Ice				
4·5227 ± 0·0014	7·3671 ± 0·0012	1·629	0	Megaw (1934)
4·5163 ± 0·0005	7·3477 ± 0·0009	1·627	−46	Truby (1955)
4·5177 ± 0·0014	7·353 ± 0·0035	1·628	−66	Megaw (1934)
4·493 ± 0·004	7·337 ± 0·006	1·633	−110	Blackman and Lisgarten (1957)†
4·479 ± 0·004	7·310 ± 0·002	1·632	−185	Vegard and Hillesund (1942)
D_2O Ice				
4·5267 ± 0·0014	7·3702 ± 0·0012	1·628	4	Megaw (1934)
4·5257 ± 0·0014	7·3687 ± 0·0012	1·628	0	
4·5147 ± 0·0002	7·353 ± 0·0035	1·629	−66	
4·495 ± 0·004	7·335 ± 0·007	1·632	−110	Blackman and Lisgarten (1957)†
4·479	7·316	1·633		Vegard and Hillesund (1942)

† These results are from electron diffraction experiments; all others are from x-ray work.

References

Blackman, M., and Lisgarten, N. D., 1957, *Proc. roy. Soc.*, A, **239,** 93.
Gränicher, H., 1958, *Zeit. Krist.*, **110**, 432.
Lonsdale, K., 1958, *Proc. roy. Soc.* A, **247,** 424.
Megaw, H. D., 1934, *Nature Lond.*, **134,** 900.
Owston, P. G., 1958, *Advanc. Phys.*, **7,** 171.
Truby, F. K., 1955, *Science*, **121,** 404.
Vegard, L., and Hillesund, S., 1942, *Avh. norske VidenskAkad*, No. 8, 1.

nnouncing the new publication

INSTRUMENT CONSTRUCTION

Translated from the Russian

Приборостроение

Editor-in-chief: M. E. Rakovskii. Sub-editor: Yu. I. Shendler

The Russians describe their publication as a ' scientific, technical and production ' journal. It covers industrial instruments and instrumentation, automatic control, and production engineering for precision work. The articles which it presents not only introduce new instruments and techniques, they also afford a valuable insight into current Russian practice.

Subscription £6 yearly post free ($17.10 U.S.A. and Canada). A special rate of £3 yearly post free ($8.55 U.S.A. and Canada) is available to University and Technical College libraries.

Single copies 15*s*. each ($2.15 U.S.A. and Canada) plus postage

Orders should be sent to the Subscription Department, Taylor & Francis Ltd

Produced for the Department of Scientific and Industrial Research by the
British Scientific Instrument Research Association,
' Sira ', South Hill, Chislehurst, Kent

Printed and Published for B.S.I.R.A. by
TAYLOR & FRANCIS LTD
RED LION COURT, FLEET STREET, LONDON, E.C.4

27JUN1960 FILED IN STACKS

The Scientific Work of René Descartes (1596-1650)

By J. F. SCOTT, B.A., M.Sc., Ph.D.

This book puts the chief mathematical and physical discoveries of Descartes in an accessible form, and fills an outstanding gap upon the shelf devoted to the history of philosophy and science. The careful treatment that Dr. Scott has accorded to this work of Descartes is welcome, and will be an asset to all libraries. Publication is recommended and approved by the Publication Fund Committee of the University of London.

212 pages, 7 in. × 10 in. Price 20*s*. net plus postage

Correspondence and Papers of Edmond Halley

Arranged and edited by EUGENE FAIRFIELD MACPIKE

First published on behalf of The History of Science Society by Oxford University Press. Now re-issued by Taylor & Francis Ltd.

Price 21*s*. net plus postage
Limited stock still available

Memoirs of Sir Isaac Newton's Life

By WILLIAM STUKELEY, M.D., F.R.S. (1752)

This work is taken from an original manuscript now in the possession of the Royal Society, London. Price 5*s*. net plus postage

First Published 1936 *Limited stock still available*

Hevelius, Flamsteed and Halley

By EUGENE FAIRFIELD MACPIKE

This work contains an account of three contemporary astronomers and their mutual relations.

Published by arrangement with The History of Science Society

First Published 1937 Price 12*s*. 6*d*. net plus postage
Limited stock still available

Printed and Published by
TAYLOR & FRANCIS LTD
RED LION COURT, FLEET STREET, LONDON, E.C.4